



Department of Electromagnetism and Physics of Matter, and  
Institute *Carlos I* for Theoretical and Computational Physics  
University of Granada, Spain

# Short-Term Synaptic Plasticity: Computational Implications in the Emergent Behavior of Neural Systems

**Jorge F. Mejías Palomino**

Ph.D. Thesis

Advisor: Joaquín J. Torres Agudo

Granada, November 4th 2009

Editor: Editorial de la Universidad de Granada  
Autor: Jorge F. Mejías Palomino  
D.L.: Gr.192-2010  
ISBN: 978-84-692-8368-4

*Dedicated to my family*

# Agradecimientos

Antes de comenzar, me gustaría agradecer a todas aquellas personas que, de un modo u otro, han contribuido a que hoy esté aquí escribiendo estas líneas. Para mí, este es sin duda el capítulo más difícil de escribir, puesto que se me hace imposible mostrar a estas personas la gratitud que merecen en tan sólo unas líneas.

Quiero comenzar por la persona que me ha dirigido estos años con un entusiasmo y buen hacer desbordantes, que no es otro que mi director Joaquín Torres. Gracias a él he aprendido que la paciencia y el rigor son los ingredientes imprescindibles para hacer buena ciencia, y que aunque cueste, tiene su recompensa. Él me ha enseñado todo lo que sé sobre la física de sistemas neuronales, y lo ha hecho, a mi entender, de la mejor manera posible: ayudándome a razonar y descubrir por mí mismo la belleza de esta disciplina. Sin duda, una forma impecable de dirigir a un estudiante de doctorado.

Asimismo he de agradecer a mis otros mentores del grupo de Física Estadística, que me han instruido y orientado en multitud de ocasiones, siempre de una forma amable y con una dedicación digna de elogio, y sin los cuales mi viaje por los tortuosos caminos de la Física Estadística habría sido mucho más complicado. Gracias por tanto a Joaquín Marro, Pedro Garrido, Miguel Ángel Muñoz, Paco de los Santos, Pablo Hurtado y Antonio Lacomba. No voy a olvidarme de mencionar aquí a mis compañeros de trabajo que, compartiendo las interminables horas de depuración de códigos, se han convertido para mí en verdaderos amigos. Gracias a Omar, Juan Antonio, Jose Manuel, Samuel, Sebastiano, Carlos, Clara y Pablo, porque sin vuestra compañía y apoyo (y sin esas cervezas después del trabajo) estos años no hubieran sido lo mismo.

Me gustaría agradecer también a Nicolas Brunel y Gianluigi Mongillo, mis tutores durante mi estancia en París, por el constante apoyo y guía que me han proporcionado durante y tras los meses que estuve allí. También a mis amigos del Colegio de España en París (Luis, Silvia, Lorena, Armando, Laura, Cristina y tantos otros), por compartir conmigo sus penas y alegrías y por esas legendarias veladas en el Bateau Ivre. Gracias a vosotros, estos meses fueron inolvidables.

Si hay algo que he aprendido en estos últimos años, es la importancia de poder

apoyarse en compañeros y amigos cuando las fuerzas flaquean. En este sentido, me considero muy afortunado: Alex, Antonio, Bea, Dani, Jesús, Pablo, Paqui y Sheila siempre han estado ahí cuando los he necesitado, y no han sido pocas veces. Gracias por esas noches de tubos en la Glorieta, los cumpleaños, las quedadas *frikis* y las fiestas pre y post estancia, y tantas otras ocasiones especiales que hemos vivido juntos. Gracias también a Jose, Sara y los demás por contar siempre conmigo para todo, y por los buenos momentos que hemos pasado (y los que nos quedan). Y por supuesto, gracias a Lidia por el apoyo que me ha dado en los buenos y malos momentos, y por conseguir que estos años hayan sido los mejores que he tenido.

Por último, me gustaría terminar este apartado mencionando a aquellos que lo han dado todo por mí de manera incondicional: mi familia. A mis padres, por darme su cariño y su apoyo en todo aquello que he hecho en la vida, y a mi hermano, por estar siempre ahí. Todo lo que soy y pueda llegar a ser se lo deberé siempre a ellos.

A todos vosotros, gracias. Esta tesis es tan mía como vuestra.

# Contents

<b>Agradecimientos</b>	<b>iii</b>
<b>1 General introduction</b>	<b>1</b>
<b>2 Basic biological principles</b>	<b>9</b>
2.1 Introduction . . . . .	9
2.2 The central nervous system . . . . .	10
2.3 The cerebral cortex . . . . .	12
2.4 Neurons . . . . .	14
2.4.1 Classification of neurons . . . . .	15
2.4.2 Generation of neural signals: the action potential . . . . .	17
2.5 Synapses . . . . .	19
2.5.1 Classification of synapses . . . . .	19
2.5.2 Synaptic plasticity . . . . .	22
<b>3 Methods in computational neuroscience</b>	<b>27</b>
3.1 Introduction . . . . .	27
3.2 Neuron models . . . . .	28
3.2.1 The Hodgkin-Huxley model . . . . .	29
3.2.2 The FitzHugh-Nagumo model . . . . .	30
3.2.3 The Izhikevich model . . . . .	31
3.2.4 The integrate and fire model . . . . .	32
3.2.5 The McCulloch-Pitts model . . . . .	33
3.3 Synapse models . . . . .	35
3.3.1 Electrical synapses . . . . .	36
3.3.2 Chemical synapses . . . . .	36
3.3.3 Dynamic synapses . . . . .	39
3.4 Network models . . . . .	43
3.4.1 The rate model . . . . .	44
3.4.2 The spiking network model . . . . .	46
3.4.3 The Hopfield model . . . . .	49

---

3.4.4	The neural field model . . . . .	51
<b>4</b>	<b>Spike coincidence detection</b>	<b>54</b>
4.1	Introduction . . . . .	54
4.2	The model . . . . .	56
4.3	Results . . . . .	58
4.3.1	Mean-field calculations . . . . .	60
4.3.2	Detection of strongly correlated signals . . . . .	63
4.3.3	The effect of jitter and synaptic fluctuations . . . . .	68
4.3.4	Detection of presynaptic firing rate changes . . . . .	74
4.4	Discussion . . . . .	75
<b>5</b>	<b>Bimodal resonances</b>	<b>77</b>
5.1	Introduction . . . . .	77
5.2	Model and methods . . . . .	79
5.3	Results . . . . .	83
5.3.1	Mean-field calculations . . . . .	83
5.3.2	Emergence of bimodal resonances with STD . . . . .	85
5.3.3	Bimodal resonances with STF . . . . .	86
5.3.4	The role of adaptive neuron threshold . . . . .	88
5.3.5	Further analysis with more realistic considerations . . . . .	92
5.3.6	Experimental evidences of bimodal resonances . . . . .	96
5.4	Discussion . . . . .	97
<b>6</b>	<b>Storage capacity of attractor neural networks</b>	<b>99</b>
6.1	Introduction . . . . .	99
6.2	The model . . . . .	101
6.3	Results . . . . .	102
6.3.1	Mean-field analysis . . . . .	102
6.3.2	Maximum storage capacity . . . . .	108
6.3.3	Basins of attraction . . . . .	114
6.4	Discussion . . . . .	116
<b>7</b>	<b>Up and down critical dynamics</b>	<b>119</b>
7.1	Introduction . . . . .	119
7.2	Model . . . . .	121
7.3	Results . . . . .	123
7.3.1	Theoretical analysis . . . . .	123
7.3.2	Statistics of up and down transitions . . . . .	128
7.3.3	Further analysis . . . . .	132

---

7.4 Discussion . . . . .	136
<b>8 Conclusions</b>	<b>139</b>
Appendix	144
A Postsynaptic current with dynamic synapses	144
B Mean firing rate of the IF neuron model	148
C Stochastic ANN with dynamic synapses	152
D Resumen en español	156
Bibliography	164
List of publications	178

# List of Figures

2.1	The seven main structures of the CNS . . . . .	10
2.2	The four lobes of the human cortex . . . . .	13
2.3	A typical scheme of a neuron . . . . .	14
2.4	Morphology of neurons . . . . .	16
2.5	First AP recorded . . . . .	18
2.6	Biophysical mechanisms of synapses . . . . .	20
2.7	Types of synapses according to involved structures . . . . .	21
2.8	Scheme of the biophysical mechanism of STD . . . . .	24
2.9	Scheme of the biophysical mechanism of STF . . . . .	25
3.1	An AP generated by the Hodgkin-Huxley neuron model . . . . .	31
3.2	Spiking of different neuron models . . . . .	34
3.3	Effect of STD on the EPSC . . . . .	40
3.4	Effect of STF on the EPSC . . . . .	40
3.5	Dynamics of neural populations described by rate models . . . . .	45
3.6	Dynamics of a spiking neural network model . . . . .	46
3.7	Associative memory in the Hopfield model . . . . .	48
3.8	Pattern formation in a neural medium . . . . .	52
4.1	Scheme of the system used to study CD . . . . .	56
4.2	Response of a postsynaptic neuron under poissonian input . . . . .	59
4.3	Example of a CD map . . . . .	60
4.4	Effect of STF in several CD maps . . . . .	64
4.5	Fraction of area for good signal detection for different conditions . . . . .	65
4.6	Behavior of the error function for different firing threshold values . . . . .	66
4.7	Optimal frequency for CD . . . . .	67
4.8	Range of good CD for different conditions . . . . .	68
4.9	Effect of jitter in the EPSC . . . . .	71
4.10	Effect of jittered signals in CD maps . . . . .	73
4.11	Detection of firing rate changes . . . . .	75
5.1	Scheme of the system used to study SR in neural media . . . . .	80

---

5.2	Mean EPSC and its fluctuations, for dynamic synapses . . . . .	83
5.3	SR profile for static synapses . . . . .	85
5.4	SR curves for STD, STF, and adaptive threshold . . . . .	87
5.5	Effect of adaptive thresholds in SR properties of neurons . . . . .	89
5.6	Phase diagram of the SR behavior of the system . . . . .	91
5.7	SR profiles with FHN neuron model and stochastic dynamic synapses	93
5.8	Comparison between numerical SR curves and experimental data . .	96
6.1	Criterion chosen to calculate the maximum storage capacity . . . . .	108
6.2	Effect of STF on critical storage capacity of the network (I) . . . . .	109
6.3	Effect of STF on critical storage capacity of the network (II) . . . . .	110
6.4	Surface plot of the critical storage capacity for different conditions . .	112
6.5	Memory retrieval under external repetitive stimuli . . . . .	113
6.6	Effect of STF on the basins of attraction . . . . .	115
7.1	Experimental observation of up and down cortical transitions . . . . .	121
7.2	Time series of the mean firing rate of a neural population with stochastic depressing synapses . . . . .	123
7.3	Strategies employed in the mean-field calculations for up-down neural dynamics . . . . .	127
7.4	Effect of $D$ in the duration of up states . . . . .	129
7.5	Statistics of the model of up-down dynamics used . . . . .	130
7.6	Effect of different parameters on the duration of up states . . . . .	131
7.7	Time series of the mean-firing rate with stochastic depressing synapses, for a monostable potential function . . . . .	133
7.8	Permanence times in the up state for stochastic depressing synapses and a monostable potential function . . . . .	134
7.9	Phase plot of the dynamics of the system . . . . .	135
C.1	Effect of STF on the critical temperature . . . . .	153
C.2	Effect of STF in the critical line $T$ , $\alpha$ . . . . .	154

# Chapter 1

## General introduction

The nervous system is considered, up to date, the most efficient natural device for information-processing. Even the simplest neural architectures of small invertebrates seem to surpass the capacity of the latest state-of-the-art human technology to handle and process information. Thanks to the nervous system, living organisms are able to deal with dynamically changing external stimuli and to respond accordingly, enhancing the probability of success in many vital tasks such as feeding, escaping from a predator, or reproduction. As the organisms have evolved to more complicated living forms, their nervous systems have also become more sophisticated and has acquired a robust hierarchical architecture, anatomically and functionally speaking. The development of the brain, as the central unit of the nervous system, has implied an enormous improvement in the abilities of higher animals to solve high-level problems, and even a notable capacity for learning in the case of mammals. The particular case of humans is the clearest example of what the ultimate implications of such machinery of information processing are: language and social interactions of high level, logical thinking, Science, Poetry or Music are only a few examples that come to mind.

Some of the most prominent useful characteristics of the nervous system for the processing of information have captured the attention of many researchers from different fields in the past century. For instance, the first attempts to design artificial devices which presented some of the advantages of actual neural systems yielded a great development of new emerging fields, such as robotics and computer science. An important number of computational strategies and highly optimized algorithms were developed, some of them concerning categorization of images, optimization problems in science and engineering, or the design of human-centric computer interfaces (see, for instance, (Cabestany et al., 2009)). In spite of these advances, our knowledge about the strategies that constitute the key to the efficiency of actual neural systems is still shallow.

In the last few decades, however, there has been a notable effort to investigate in deep what the computational strategies that the nervous system employs to perform adequately are. The discipline emerging from such an effort, commonly known as *Computational Neuroscience*, studies the nervous system from the point of view of its functionality in order to uncover some of these basic computational strategies. To achieve this purpose, it relies both on mathematical models of individual neurons and networks, and on experimental data which help to develop these models. Typically, experimental studies on their own are not enough to completely address how information processing occurs, because neural systems are only partially observable with the current electrophysiology and imaging techniques. In addition, a significant part of the complex phenomenology associated with brain functions may be the result of the collective effect of many interacting elements (of about  $\sim 10^{10}$ , when such elements are considered to be neurons), a possibility that can not be experimentally controlled.

In situations in which the relevant magnitudes are not accessible via experimental techniques, mathematical models may constitute a useful mechanism to analyze the role of different variables in the system under study, and could serve as a complementary method to obtain information about how the brain works. Moreover, from a more pragmatical point of view, Computational Neuroscience methods can be of great utility to predict the outcome of experiments. The process of designing an experiment to test a hypothesis involves making predictions about what the possible results of such an experiment might be, and to work out the implications of each one of these possible results. This is commonly a difficult task in most biological systems, especially in those which, as the brain, involve many interacting parts. Therefore, as a consequence of being a tool for prediction, Computational Neuroscience methods may be highly useful to design new experiments. Finally, in many cases mathematical models are able to provide new insights and hypotheses that are suitable to be tested experimentally. Indeed, a model may reveal assumptions about the system that were not fully appreciated in experiments.

Due to this feedback between model and experiment, Computational Neuroscience has become a highly interdisciplinary field, in which experimentalists coming from biological sciences and more theoretically-oriented researchers have contributed to the recent increasing advance in the field. This methodology is reflected, for instance, in the mathematical neuron model by Hodgkin and Huxley in 1952, designed to quantitatively describe the membrane properties recorded in electrophysiological experiments in the giant squid's axon (Hodgkin and Huxley, 1952b). This model is one of the most successful and representative mathematical descriptions in neuroscience, and constituted a prominent advance in the field. In the last decades, indeed, a wide variety of neuron models have been built in order to improve, or sim-

plify, the mathematical paradigm of Hodgkin and Huxley (Izhikevich, 2004), and to extend its applicability to other neural media.

The development of attractor neural network models constitutes another interesting example, from a more theoretical point of view, of the recent advance of Computational Neuroscience. Since most neural systems are constituted by a large number of minimal working units – neurons –, it is sometimes useful to adopt theoretical tools from Statistical Mechanics to achieve a successful description of the system under study. Typically, Statistical Mechanics deals with large systems of stochastically interacting microscopic elements (such as gasses, magnets, swarms, spin glasses, or vehicles in traffic models, to name a few). This discipline abandons any ambition to solve exactly all the involved equations of motion at the *microscopic* level, and it uses the individual microscopic laws to describe the emergent collective behavior of the system via a set of *macroscopic* observables (Marro and Dickman, 1999; Cortes, 2005). Under some assumptions, neural systems may be studied within this theoretical level of description. A notable example are the so called attractor neural networks (ANN), and in particular the Hopfield model of *associative memory* (Hopfield, 1982) which illustrates one of the simplest manners in which collective neural computation may work.

Within this theoretical framework, neurons are considered to be the fundamental computational engines for information processing and coding, with the synapses treated as mere connections between neurons across which the information is transmitted. Such a traditional view, however, may turn out to be excessively simplistic, since many recent works indicate that synapses participate actively in the processing of information in the brain. In the last few years, for instance, it has been reported that the strength of synaptic connections may vary on short time scales depending on presynaptic activity (Abbott et al., 1997; Tsodyks and Markram, 1997; Abbott and Regehr, 2004). It has also been found that such variations can be used to process information in a nontrivial way (Abbott et al., 1997). This finding indicates that, in addition to neurons, synapses may have an active role in neural computations.

The possibility to have activity-dependent synaptic modifications on short time scales is usually known as *short-term plasticity* (Zucker and Regehr, 2002; Hempel et al., 2000), and the synapses which display such behavior are called *dynamic synapses*. According to underlying biophysical process involved, there are two major mechanisms responsible for short-term plasticity: the so called short-term depression (STD) and short-term facilitation (STF). The former is responsible of the decrease of the postsynaptic response under repetitive presynaptic stimulation, whereas the latter induces an increment of the postsynaptic response for the same type of stimulus.

The complete computational and functional implications of STD and STF are

not clear yet, although these processes could be of vital importance in the processing of information in neural systems. Very recent studies have shown, for instance, that the presence of STD has a strong influence on the dynamics of neural systems, and is implicated in membrane gain control (Abbott et al., 1997), maintenance of high activity states in the cortex (Romani et al., 2006), storage of information in attractor neural networks (Bibitchkov et al., 2002; Torres et al., 2002), detection of coincident signals (Pantic et al., 2003), or the appearance of switching between different activity patterns in recurrent neural networks, which could be related with spontaneous voltage transitions in cortical areas (Pantic et al., 2002; Holcman and Tsodyks, 2006). Most of these studies, however, do not take into account the effects produced by STF, which is also present in most of the brain structures analyzed in these works. This constitutes a highly relevant issue, because STD and STF have *a priori* opposite effects on the postsynaptic response, and taking into account STF could notably affect the behavior of a neural system with depressing synapses. Moreover, the consideration of both mechanisms together could reveal novel emergent phenomena caused by the *interplay* between STD and STF. Indeed, such interplay could help to explain several features of actual neural systems which remain far from being totally understood. Some of these features include the detection of weak signals over a broad range of network activity levels (Abbott et al., 1997), the ability of neural circuitry to optimally store and retrieve information while maintaining an efficient processing of signals (Pantic et al., 2003), or the level of irregularity observed even in highly synchronized neural dynamics, such as the heterogeneity of the duration of high activity states during series of up-down cortical transitions (Anderson et al., 2000). In spite of its possible implications on all these phenomena, the study of the interplay between STD and STF in different neural systems has not been addressed in detail up to date.

**Within the framework given above, the aim of this thesis is to investigate the role and implications of the interplay between short-term synaptic depression and facilitation on the computational properties of several neural systems of interest.**

### *Main objectives of the thesis*

The work presented in this thesis pursues, as has been already stated, to study the effects of short-term plasticity mechanisms on the behavior of neural systems. In most of the cases, the analysis developed along the following has been achieved both theoretically and numerically, and employing different levels of mathematical description for both neurons and synapses. More concretely, the main research objectives that we have attempted to achieve within this thesis are the following:

- To gain a deeper understanding of the influence of several biophysical synaptic mechanisms (such as STD and STF) on the abilities of typical neural systems to detect and process relevant information embedded in neural noisy environments. This constitutes a highly relevant issue since, although it is well known that short-term synaptic plasticity has a strong effect on the amplitude of the postsynaptic response to an incoming stimulus, its implications on actual cortical computations (in which a certain level of background noisy activity is commonly present) remain far from being explained. Moreover, STD and STF have been reported to occur widespread through the cortex (Thomson and Deuchars, 1994). Therefore, without a complete characterization of such influence of STD and STF, future theoretical predictions and estimations concerning actual neural computations in cortical media could be wrong.
- To investigate the effect of the possible competition and *interplay* between STD and STF (and other mechanisms which could be also present in actual neural structures) on the emergent behavior of neural systems. Such study constitutes an essential part in the characterization of the effects of short-term synaptic plasticity in realistic conditions, and may also be useful to identify new emergent phenomena which would have not been found if each synaptic mechanism were studied individually (and, therefore, which would be a consequence of such interplay).
- To address the role of short-term synaptic mechanisms in several collective behaviors of relevance, such as in associative memory tasks or in the coherent dynamics constituting the up and down voltage transitions observed in the cortex. In particular, since it is considered that these two phenomena strongly depend on synaptic properties, a detailed analysis of the influence of STD and STF on these behaviors could highlight the origin of several concrete features not explained yet.

### *Structure of the thesis*

The study presented in this thesis is structured as follows: chapter 2 constitutes a basic general introduction to the biology of neural systems. Once the biological background has been provided, chapter 3 aims to introduce the reader into the framework of Computational Neuroscience and to expose the basic features of short-term synaptic plasticity at the mathematical level. After that, in the following chapters the original contributions of this thesis are presented. For instance, chapter 4 is concerned with the analysis of the role of STD and STF in the detection of coincident signals of neurons embedded in an environment of noisy activity. This

study is extended in chapter 5, where we investigate the interplay between STD, STF, and other adaptive mechanisms in the detection of weak signals. Chapter 6 presents the consequences of introducing short-term plasticity in the synapses of a large population of interconnected neurons which presents associative memory properties. In chapter 7, the dynamics of a neural population presenting complex switching of neural activity is analyzed, highlighting the influence of short-term plasticity mechanisms. Finally, in chapter 8 the main conclusions of the work are presented, and the implications for future research are outlined.

The thesis is also structured from low to high complexity of the neural system under study. Chapters 4 and 5, for instance, concern small perceptron-like neural circuits, in which the aim is to analyze the input-output relation (i.e., the transmission of information from a presynaptic neural population to a postsynaptic neuron). On the other hand, chapters 6 and 7 are focused on large recurrent neural populations of interconnected neurons, in which the cooperativity between neuronal and synaptic effects produce nontrivial and novel collective phenomena that are analyzed in detail.

From the point of view of the biological realism of the mathematical models employed, however, the thesis is top-down structured: chapters 4 and 5, for instance, consider realistic (although still very simplified) mathematical models of neurons and synapses, while in chapter 6 an Ising-like model of binary neurons, which is useful to describe associative memory properties, is employed. Finally, a coarse-grained description (namely, a rate model) of a homogeneous neural population is assumed in chapter 7 to study the role of short-term plasticity on the complex switching series of cortical activity. Therefore, from a methodological point of view, the more complex the neural system addressed, the simpler the mathematical model considered for its study.

In the following, some brief details concerning each chapter are presented, including the original contributions of this thesis (mainly, chapters 4-7):

In **chapter 2** we present a brief physiological review of the nervous system. This review covers the biological aspects employed in the subsequent chapters, and provides some useful references for the interested reader. The chapter starts with an exposition of the main parts of the central nervous system, focusing on the particular case of the cerebral cortex. After that, some basic features of neurons are explained, and finally the main aspects of the synapses are reviewed, paying special attention to the biophysical mechanisms which induce the different short-term plasticity mechanisms. Such review is highly convenient to understand the effect of short-term synaptic mechanisms on the computational properties of different neural systems which, as we have already explained, is the goal of this thesis.

In **chapter 3** a review of some mathematical paradigms commonly used to model

neural systems is presented, to complement the biological introduction of chapter 2. We briefly cover several neuron models of interest, starting from highly detailed neural paradigms (such as the Hodgkin-Huxley neuron model) and finishing with very simplified ones (such as the binary neuron). After that, some mathematical descriptions of the synapses are presented, including some of the models of short-term plasticity which will be employed in the following chapters. Finally, different approaches to model large neural populations are sketched out as well.

Once the biological background and the methods have been introduced in chapters 2 and 3, we start to study the role of STD and STF in very simple neural systems. In particular, **chapter 4** is concerned with detection of correlated inputs by simple neural circuits with short-term plasticity in noisy environments. More precisely, using a realistic model of depressing and facilitating synapses, we studied the conditions in which a postsynaptic neuron efficiently detects temporal coincidences of spikes which arrive from  $N$  different presynaptic neurons at a certain frequency  $f$ . A numerical and analytical treatment of this system showed that: i) STF enhances the detection of correlated signals arriving from a subset of presynaptic excitatory neurons, and ii) the presence of STF yields a better detection of firing rate changes in the presynaptic activity. We also observed that facilitation determines the existence of an optimal input frequency which allows the best performance for a wide (maximum) range of the neuron firing threshold. This optimal frequency can be controlled by means of facilitation parameters. Finally, we showed that these results are robust even for very noisy signals and in the presence of synaptic fluctuations produced by the stochastic release of some molecules involved in synaptic transmission (the so called *neurotransmitters*).

In **chapter 5**, we extended the analysis of chapter 4 by studying the detection of weak stimuli by spiking (integrate-and-fire) neurons in the presence of a certain level of noisy background neural activity affecting the postsynaptic response via dynamic synapses. Employing mean-field techniques as well as numerical simulations, we found that there are *two* possible noise levels which optimize signal transmission (such phenomena is referred here as *bimodal resonance*). This new finding is in contrast with the classical theory of stochastic resonance, which is able to predict only one optimal level of noise for the detection of weak signals. We found that the complex interplay between adaptive neuron threshold and activity-dependent synaptic mechanisms is responsible for this new phenomenology. Our results were confirmed by employing a realistic FitzHugh-Nagumo neuron model, which displays threshold variability within its own dynamics, as well as by considering more realistic synaptic models. We also supported our findings with recent experimental data of stochastic resonance in the human tactile blink reflex.

Our next step was to extend the study to models of large neural populations.

Concretely, in **chapter 6** we studied, analytically and employing Monte Carlo simulations, the influence of the competition between several activity-dependent synaptic processes, such as STF and STD, on the maximum memory storage capacity in an attractor neural network. In contrast with the case of synaptic depression, which drastically reduces the capacity of the network to store and retrieve “static” activity patterns, synaptic facilitation enhances the storage capacity in different contexts. In particular, we found *optimal* values of the relevant synaptic parameters (such as the neurotransmitter release probability or the characteristic facilitation time constant) for which the storage capacity can be maximal and similar to the one obtained with *static* synapses, that is, without activity-dependent processes. We concluded that depressing synapses with a certain level of facilitation allow to recover the good retrieval properties of networks with static synapses while maintaining the nonlinear characteristics of dynamic synapses, convenient for information processing and coding.

After the analysis of retrieval abilities of neural networks with dynamic synapses, which may be seen as steady state properties, we focused in the effect of STD on the dynamics of the activity of neural populations. In particular, in **chapter 7** we addressed the study of the voltage transitions between up and down states observed in cortical areas in the brain, which constitute a paradigmatic example of complex coherent neural dynamics. We study this phenomenon via a biologically motivated stochastic model of up and down transitions. The model employed was a simple bistable rate model, where the synaptic current is modulated by short-term synaptic processes (such as STD) which introduce stochasticity and temporal correlations. A complete analysis of our model, both with theoretical approaches and numerical simulations, showed the appearance of complex transitions between high (up) and low (down) neural activity states, driven by the synaptic noise, with permanence times in the up state distributed according to a power-law. These results are in agreement with recent experimental observations in up and down transitions in cortical activity which indicate the onset emergence of criticality in the hopping dynamics between collective neural states.

Finally, in **chapter 8** the main conclusions of this thesis are presented, focusing on the role of the interplay between short-term depression and facilitation in the computational and functional properties of different neural systems at different levels of description. The possible implications of this interplay on several brain tasks and behavior, and also the future research lines that this thesis may suggest, are summarized as well.

# Chapter 2

## Basic biological principles

In this chapter, we will introduce several biological concepts of interest concerning actual neural systems. More precisely, we will review some well known features of the central nervous system and its constituting elements, namely neurons and synapses. The aim of such review is to introduce the reader to a basic biological framework which may be convenient for a complete understanding of the results presented in this thesis.

### 2.1 Introduction

The nervous system is a hierarchical structure which spreads over the whole body. It is basically constituted by specialized nerve cells called neurons, which process the information coming from the senses in a complex manner, and glial cells, which support neurons in their task by, for instance, supplying nutrients to them. In the case of humans as well as other mammals, the nervous system can be divided broadly into two categories: the central nervous system (CNS) and the peripheral nervous system (PNS). The CNS is the main and more complex structure and constitutes the largest part of the nervous system, whereas the PNS is constituted by all the structures that do not lie directly in the CNS, such as the nerves. The CNS is roughly constituted by several parts, and ultimately, by large populations of neurons interconnected between them. In this section, some basic concepts about the nervous system, including a classification of the CNS regions in mammals and a basic description of neurons and synapses, will be briefly laid out. The anatomical and physiological requirements to understand the work presented in this thesis will be covered by these brief descriptions. However, the reader is invited to deepen into more specific textbooks (see the bibliography at the end of the chapter, and in particular (Kandel et al., 2000; Bear et al., 2006; <http://neuroscience.uth.tmc.edu>)) in order to gain a broader understanding of neural structures and functions.

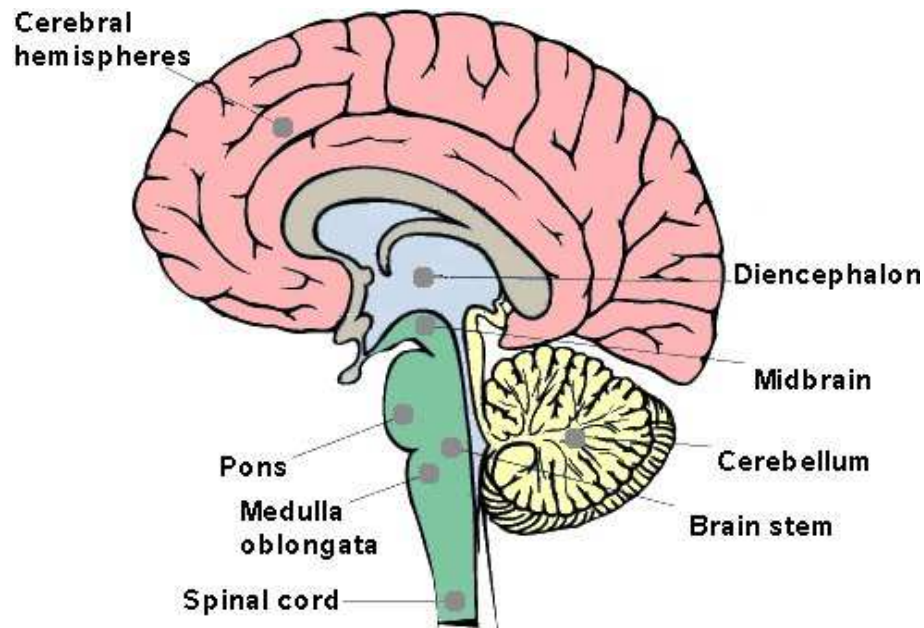


Figure 2.1: The seven main structures of the CNS of humans. The medulla oblongata, the pons and the midbrain constitutes a region called brain stem, which is also indicated in the figure.

## 2.2 The central nervous system

Basically, the CNS is a bilateral and essentially symmetrical structure with seven main parts: the spinal cord, medulla oblongata, pons, midbrain, cerebellum, diencephalon, and the cerebral hemispheres. According to the current beliefs in modern Neuroscience, each one of these regions is specialized for different specific functions (Kandel et al., 2000). The seven main structures of the CNS are illustrated in figure 2.1, while some details concerning their functionality are given below:

- The *spinal cord* is a long, thin, tubular bundle of nervous tissue and support cells, enclosed within and protected by the vertebral column. It is the most caudal part of the CNS, and receives and processes sensory information from the skin, joints and muscles of the limbs and trunk, thus acting as a transmissor between the CNS and the rest of the body. It also controls the movements of the limbs and the trunk. As we ascend through the spinal cord, we arrive at a region called the brain stem, composed by the medulla oblongata, the pons and the midbrain.
- The *medulla oblongata* is located immediately above the spinal cord, and is one of the structures constituting the brain stem. It contains several neuronal centers which are responsible for vital autonomic functions, such as breathing, digestion, and the control of heartbeats.

- The *pons* is a structure of the brain stem, and lies above the medulla oblongata. It coordinates information between the cerebral hemispheres and the cerebellum, and plays a role also in the regulation of respiration. More precisely, the anterior portion of the pons contains a large number of neuronal clusters, known as the pontine nuclei, that relay information about movement and sensation from the cerebral cortex to the cerebellum, while the posterior portion contains structures involved in breathing, taste, and sleep.
- The *midbrain* is the smallest part of the brain stem, and is located above the pons. Neurons of this part control many sensory and motor function, and link other parts involved in motor tasks, such as the cerebellum, the basal ganglia, and the cerebral hemispheres. The midbrain also contains components of the auditory and visual system. It is involved, for instance, in controlling eye movements and auditory reflexes.
- The *cerebellum* lies behind the pons, and is connected to the brain stem by several major fiber tracts called peduncles. The cerebellum contains a far greater number of neurons than any other single subdivision in the brain, including the cerebral hemispheres. Nevertheless, it is constituted by a relatively small number of neuron types, and as a consequence of that its circuitry is well understood. This structure plays an important role in the integration of sensory perception, receiving somatosensory information from the spinal cord. It is also important in many coordination and motor control tasks, such as the maintenance of the posture and the coordination of head and eye movements. Finally, the cerebellum is also involved in fine tuning the movements of muscle and in the learning of motor skills.
- The *diencephalon* is located above the midbrain and contains two structures: the thalamus and the hypothalamus. The thalamus processes most of the sensory information (except the olfactory) reaching the cerebral cortex from the rest of the CNS. It also takes part in the gating and modulation of this sensory information, rather than being a simple transmissor of sensory stimuli. The hypothalamus regulates several functions that are essential for homeostasis and reproduction. Examples of these functions include growth, eating, drinking or maternal behavior, to name a few. It constitutes, in general, a basic control structure of different autonomic, endocrine, and visceral functions.
- The *cerebral hemispheres* are constituted by a heavily wrinkled outer layer, the cerebral cortex, and three deep-lying structures: the basal ganglia, the hippocampus, and the amygdaloid nuclei. These four structures have quite

different functions: the basal ganglia is involved in the regulation of the motor performance, the hippocampus participates in certain aspects of memory storage, the amygdaloid nuclei coordinate autonomic and endocrine responses of emotional states, and the cerebral cortex is responsible for high cognitive abilities in humans and other mammals.

Other classifications are possible, although the vast majority of them distinguish three major parts of the CNS: the spinal cord, the brain stem - cerebellum, and the cerebral hemispheres. Most of the neural systems and situations analyzed in this thesis are assumed to correspond to cortical regions, and for this reason some basic concepts about the cerebral cortex will be reviewed in the following.

## 2.3 The cerebral cortex

The cerebral cortex, also called *neocortex* within the classification adopted here, is basically concerned with cognitive functioning. Thus, while most of the vital functions are mediated and controlled by different regions of the spinal cord, brain stem, and diencephalon, the majority of executions and actions of our everyday life are mediated by the cerebral cortex. It is constituted by a highly convoluted thin layer structure of  $2 \sim 4$  mm of thickness (Kandel et al., 2000). The concrete function for this convoluted form is still unknown, although it has been suggested that it could be the maximization of the cortical area. From an anatomical point of view, the cortex can be divided into four regions or *lobes*: frontal, parietal, temporal, and occipital (see the scheme of figure 2.2). These four regions have different functional specializations. The frontal lobe, for instance, is concerned with planning future actions and with the control of movement. In fact, a subdivision of the frontal lobe called the prefrontal cortex is known to play an important role in planning immediate actions, via the maintenance of information coded in the form of a relatively high level of persistent activity, phenomenon which is known as *working memory* (Fuster, 1995; Goldman-Rakic, 1995; Sanchez-Vives and McCormick, 2000). The parietal lobe is related with somatic sensation, with forming a body image, and with relating the image of the own body with extrapersonal space. The occipital lobe plays a main role in vision, by processing the information arriving from the retina. Finally, the temporal lobe processes the auditory information, and it is also involved in certain aspects of language comprehension, learning and memory. The four lobes also interact with other structures of the cerebral hemispheres, such as the hippocampus and the amygdaloid nuclei, in order to perform computations concerning learning, memory, and emotion.

Although the four lobes are quite different regarding their function, the internal

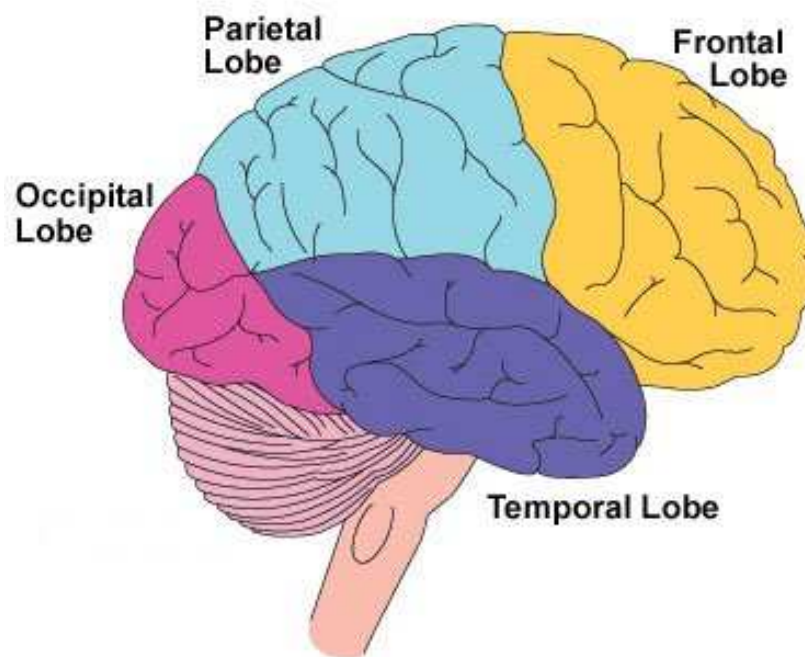


Figure 2.2: The four lobes of the human cortex.

anatomical details of the cortex are fairly homogeneous along the lobes, and even among different species. For instance, the thickness of the cortex is roughly constant for all the cortical regions<sup>1</sup>. Globally, the most striking feature of the cortex is that it is anatomically and functionally organized in cell layers. Although the number of layers and their functional details may vary depending on the cortical region considered, a typical picture consists in a cortical surface composed by six layers. In addition to this structure, interconnected neurons within the layers are grouped in cell assemblies called *columns*, across which the information is thought to be processed.

To understand how sensory information is processed and coded (and how it is employed to make predictions about the real world) in these structures, it is necessary to identify the minimal units of information processing of the brain, and to understand how they work. In the next section, we briefly describe the basic features of neurons, which are usually thought to be such minimal units.

---

<sup>1</sup>Several differences can be found, though. For instance, the cortical thickness of humans is slightly greater in the occipital lobe than in other regions (Bear et al., 2006; Kandel et al., 2000). However, these differences should not impede neuroscientists to describe, as a first approach, the cerebral cortex as a largely homogeneous structure.

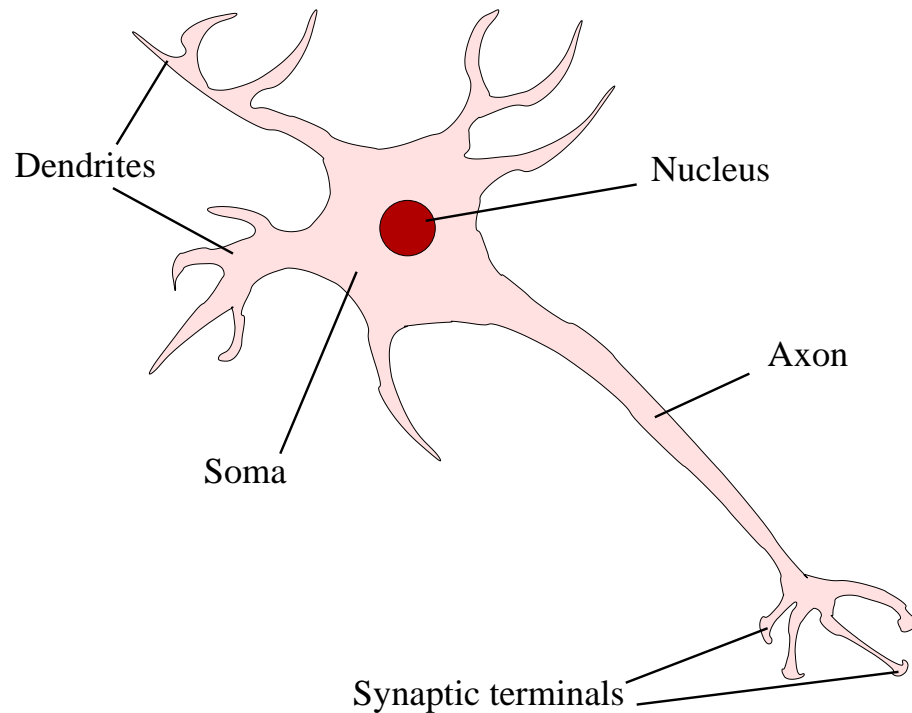


Figure 2.3: A typical scheme of a neuron, showing its main parts: a number of tree-like processes called dendrites, the soma or cell body (which contains the cellular nucleus as well as other organelles), and a long process called the axon, which ends with button-like structures (the synaptic buttons or synaptic terminals).

## 2.4 Neurons

Neurons are the specialized nerve cells constituting the nervous system. They are responsible for the processing and transmission of information by means of electrical and/or chemical signaling. Although there are multiple types of neurons, as we will see below, one can establish certain features common to all neurons. A typical neuron, for instance, has three well defined structures: soma, axon and dendrites (see figure 2.3). The *soma*, or cell body, is the metabolic center of the cell. It contains the cellular nucleus as well as other important organelles, such as the endoplasmatic reticulum or the mytocondria. The cell body usually gives rise to two kind of *processes* (that is, projections of tissue from the cell body): the *dendrites* and the *axon*. Dendrites are short tree-like processes which are responsible of receiving signals from other neurons. The axon, on the other hand, is a single long process that extends away from the cell body, and serves to conduct signals to other neurons. The length of the axon ranges from 0.1 *mm* to 3 *m* (Kandel et al., 2000), allowing neurons to communicate between them through long distances. The axon ends in button-like structures called presynaptic terminals, which are typically close to some specific receptors located in the soma or dendrites of other neurons. The

space between the presynaptic terminals of one neuron and the receptors of the other neuron establishes a connection between them, and such connection is called (chemical) *synapse*.

The picture presented above constitutes the traditional description of a neuron, which includes the basic features of nerve cells. It is worth noting, however, that neurons can display a high variability in their morphology, structure and function, as we will see in the following section.

### 2.4.1 Classification of neurons

Neurons constitute the basic units of information processing in many areas of the nervous system. Since such areas are commonly involved in quite differentiated functions, it is plausible to think that neurons of each region have specialized features which serve to optimize their computations. Indeed, the huge quantity of well differentiated neurons allows to establish a large number of neuronal classes, and also multiple criteria for these classifications. A complete description of all possible classifications is out of the scope of this chapter, and therefore we will just briefly mention some classifications of interest.

Attending to their functionality, for instance, neurons can be classified in the following categories:

- *Sensory neurons*, which convey information from tissues and organs into the CNS.
- *Motor neurons*, which transmit signals from the CNS to different kinds of effector cells, such as muscle and gland cells.
- *Interneurons*, which connect neurons within specific regions in the CNS, and perform computations to elaborate the response to a stimulus.

In general, one of the features that most distinguishes one neuron from another is their morphology. This was already appreciated by Ramón y Cajal in his pioneering works (see, for instance, (Ramon y Cajal, 1977)) a century ago. In a concise manner, and on the basis of morphology, neurons can be classified into three large groups: unipolar, bipolar, and multipolar (see figure 2.4).

- *Unipolar neurons* are the simplest nerve cells since they have a single primary process. This process usually gives rise to many branches, including the axon and the dendrites. Unipolar cells are common in the nervous system of invertebrates.

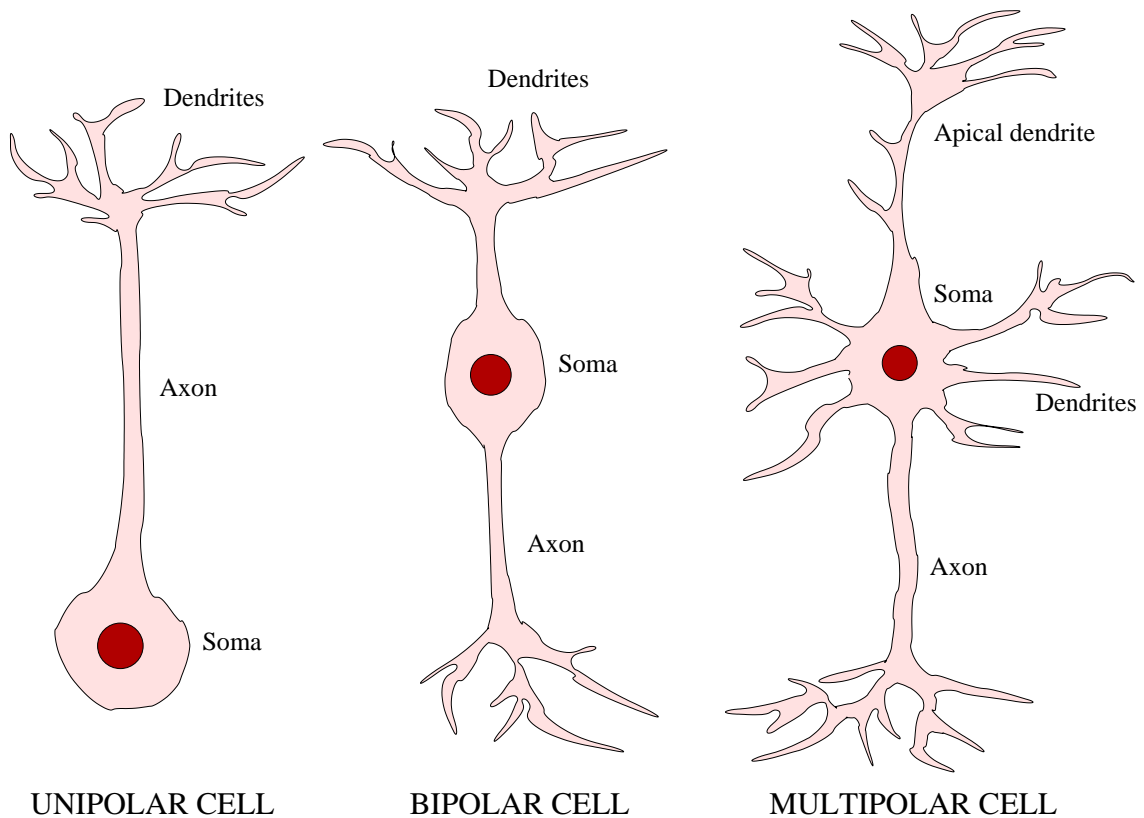


Figure 2.4: Different types of neurons attending to their morphology. From left to right: unipolar neuron, bipolar neuron, and multipolar neuron (concretely, a pyramidal neuron). Some details concerning the different parts of the cells are also denoted in the figure for each neuron type.

- *Bipolar neurons* are characterized by a soma from which two processes arise. One of the processes gives rise to dendritic terminals, and the other constitutes the axon. Most of the sensory neurons fall into this category.
- *Multipolar neurons* are constituted by a soma and multiple processes that arise from it. Typically, one of these processes corresponds to the axon, and the other ones are dendrites. Multipolar cells vary greatly in shape, and are the predominant neuron type in the CNS of vertebrates. It is worth noting that the existence of multiple processes in these neurons may have strong implications for the topological properties of networks constituted by multipolar neurons.

Additional classification criteria for neurons include those focusing on the particular location of neurons in the nervous system, on the specific discharge patterns, or in the chemical transmitters that neurons produce, to name a few. In the following, unless it is explicitly specified, we will consider interneuron multipolar cells as our basic neuron paradigm.

### 2.4.2 Generation of neural signals: the action potential

Neurons generate and transmit signals in the form of *action potentials*. The action potential (AP) is a self-regenerating electrical signal, originated in the soma, whose amplitude does not attenuate as it moves down the axon (due to some reinforcement mechanisms). This signal takes the form of a well located peak of electrical activity which moves towards the end of the axon, where the information will be transmitted to other neurons. The AP, also called *spike*, is the primary electrical signal generated by neurons, although it also occurs in other types of excitable cells, such as cardiac muscle cells (Keener and Sneyd, 2008) or fibroblasts (Roos et al., 1997; Harks et al., 2003).

The biophysical mechanism responsible for the generation and propagation of a neural AP strongly relies on the flow of ions through voltage-gated channels located in the neuron membrane. At rest, there is an excess of positive charges (cations) on the outside of the neuron membrane, and an excess of negative charges (anions) on the inside. The most abundant ions found outside the membrane, in the extracellular medium, are  $Na^+$  and  $Cl^-$ , whereas typical ions which are found inside the cell include  $K^+$  and several organic anions. All these ions are distributed in such a way that the distribution of charges mentioned above is maintained, with the help of active ion pumps spread out along the membrane.

This separation of charges gives rise to a difference of electrical potential across the membrane, called the *membrane potential*. In absence of stimuli from other neurons, and for most types of neurons, the membrane potential is at rest, and takes a typical value of  $-65\text{ mV}$ , as can be easily measured in experiments and/or calculated via the Nernst and Goldman equations (Koch, 1999). In the presence of external signals from other neurons, however, this equilibrium is disturbed. An external signal arriving to a neuron is reflected in the opening of ion channels and the subsequent influx of ions (positive or negative) through these channels into the cell. A net influx of positive charges into the neuron makes the membrane potential tend to be less negative, a tendency which is known as *depolarization*. On the other hand, a net influx of negative charges into the neuron increases the separation of charges across the membrane, and therefore the membrane potential moves to more negative values. This phenomenon is called *hyperpolarization* of the neuron membrane potential.

For small perturbations, the neuron is able to recover its equilibrium situation passively once the stimulus has finished. However, if the depolarization is sufficiently strong, the response of the neuron to the stimulus becomes active. More specifically, when the depolarization reaches a certain *threshold* value of the membrane potential (also called the firing threshold), a number of voltage-gated  $Na^+$  channels open



Figure 2.5: First published intracellular recording of an AP, obtained in 1939 by Hodgkin and Huxley from the squid giant axon. The vertical scale indicates, in millivolts, the potential of the internal electrode used to perform the recording. Adapted from (Hodgkin and Huxley, 1939).

rapidly. This causes a net influx of positive charge into the neuron that produces a further depolarization. This strong depolarization causes more voltage-gated  $Na^+$  channels to open, increasing even more the depolarization, and this leads to a fast feedback loop which drives the membrane potential towards values close to the  $Na^+$  equilibrium potential. When the membrane potential is approaching this limit, two processes start to actively repolarize the membrane potential towards its resting value. The first one is the closing of a high number of voltage-gated  $Na^+$  channels via several inactivation processes. The second one is the opening of voltage-gated  $K^+$  channels that produce an increasing efflux of  $K^+$ . These two effects together lead to a net current of positive charge from the neuron to the extracellular medium, resulting in a fast hyperpolarization of the membrane potential which is kept until the resting potential is reached.

This whole process describes the generation of an AP, and as we stated before, it takes place at the soma of a neuron. Once an AP is generated, it propagates along the axon due to the existence of many voltage-gated channels distributed along the membrane. The AP constitutes the main electrical signal that neurons use to communicate between them, and the understanding of how basic biophysical mechanisms allow its generation constitutes one of the highest achievements of modern Neuroscience.

Although of vital importance, the generation of an AP does not ensure the transmission of information from one neuron to another. When an AP reaches the

presynaptic terminals at the end of the axon, a number of biophysical processes take place in the synapses in order to transmit the information encoded in the AP to other neurons; this constitutes the synaptic transmission.

## 2.5 Synapses

The communication between neurons is mediated by specific structures called *synapses*. A synapse establish a connection between two neurons: a neuron that sends signals in the form of APs, which is called the presynaptic neuron, and a neuron which receives these signals, called the postsynaptic neuron. A typical neuron establishes about 1000 synaptic connections. Since the human brain contains about  $10^{11}$  neurons approximately, this makes a total of  $10^{14}$  synaptic connections in the whole brain. Therefore, neural systems are often described and modelled as large networks of densely interconnected elements. In this section some of the main features of synapses will be reviewed.

### 2.5.1 Classification of synapses

Although the function of all synapses is to transmit information between neurons, the manner in which this transmission is performed is not the same for all synaptic connections. We will briefly describe here some basic classifications of synapses according to: 1) the biophysical mechanism involved in the transmission, 2) the location of the connection along the cell body, and 3) the effect produced on the postsynaptic neuron.

1. According to the general biophysical mechanism involved in the transmission of information, the synapses can be either *electrical* or *chemical*. In an electrical synapse, the presynaptic and postsynaptic membranes, separated by approximately  $3.5 \text{ nm}$  (Kandel et al., 2000), are joined by specific protein structures called *gap junctions*. These protein structures are specialized ionic channels that connect the cytoplasm of both cells. When an AP arrives at the gap junction, the fast variation of the membrane potential induces the opening of these ionic channels, and the diffusion of ions through them from one neuron to the other. The influx of ions into the postsynaptic neuron causes a depolarization (or hyperpolarization) which, depending on the concrete situation, can yield the generation (or inhibition) of an AP. A remarkable characteristic of electrical synapses is that, due to the fact that the information is transmitted directly by the flow of current from one cell to the other, electrical synapses are bidirectional.

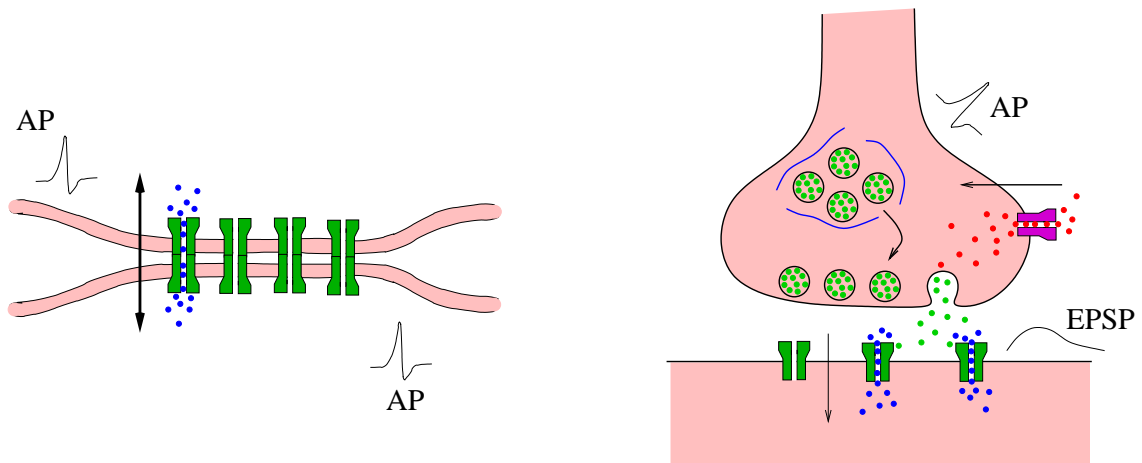


Figure 2.6: Classification of synapses according to the biophysical mechanism implicated in the transmission. Left: Electrical synapse, which allows for a bidirectional transmission of information between two nearby neurons. Such transmission involves the flux of intracellular ions (blue dots) through protein structures called gap junctions (in green). Right: Chemical synapse, in which the transmission occurs via the influx of calcium ions (red dots) into the presynaptic terminal, induced by the arrival of an AP to this terminal. The  $Ca^{2+}$  induces the release of neurotransmitters (green dots), contained in synaptic vesicles located at the ready releasable pool, to the synaptic cleft. After that, neurotransmitters bind to specific postsynaptic receptors (in green), and these receptors allow the entrance of extracellular ions such as  $Na^+$  and  $K^+$  (blue dots). The used vesicles are replaced by other vesicles coming from the reserve pool (depicted as a close region delimited by blue lines on the figure), or recycled to be used again. See the main text for details.

In chemical synapses, on the other hand, the separation between the presynaptic and postsynaptic cells is larger than in electrical synapses, of about  $20 \sim 40 \text{ nm}$  approximately. Due to this space, called the *synaptic cleft*, the cells are not in physical contact with each other. The transmission of information occurs then as follows (see right panel of figure 2.6): when an AP arrives at the end of the presynaptic axon, it induces the influx of  $Ca^{2+}$  into the presynaptic terminals. These  $Ca^{2+}$  ions induce the fusion of some vesicles (located in a ready releasable pool near the membrane) with the presynaptic membrane. These vesicles contain specific chemical messengers called *neurotransmitters* and, as a consequence of the fusion, a large amount of these neurotransmitters is released to the synaptic cleft. After that, the released neurotransmitters diffuse towards the postsynaptic membrane and can bind to specific receptors located there. This induces the opening of ion channels on the postsynaptic membrane and the consequent influx of ions from the extracellular medium, which causes a modification of the postsynaptic membrane potential. A net influx of positive ions induces an excitatory postsynaptic cur-

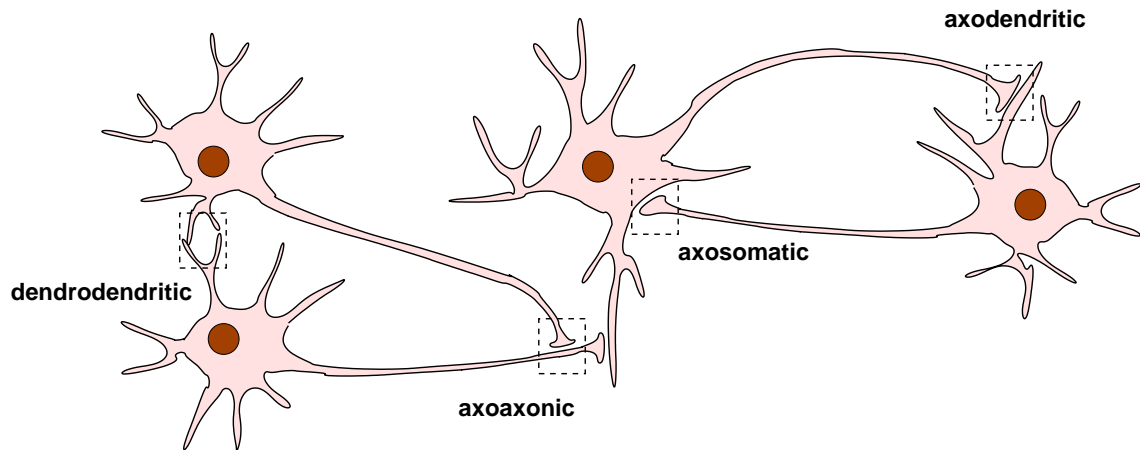


Figure 2.7: Different types of synapses, according to the concrete structures in which the presynaptic terminals and the postsynaptic receptors are located. In the figure, one can observe dendrodendritic, axoaxonic, axosomatic and axodendritic connections.

rent (EPSC) which causes depolarization, while a net influx of negative ions induces an inhibitory postsynaptic current (IPSC) which tends to hyperpolarize the postsynaptic membrane. Finally, the released vesicles are replaced by other vesicles stored in the so called reserve pool, which is located at a certain distance from the ready releasable pool, or recycled via other mechanisms. The transmission for chemical synapses is, therefore, unidirectional.

Chemical synapses are commonly found, for instance, in the long distance connections between neurons, which are responsible for the high connectivity observed in nervous systems. In the following, and unless the contrary is specified, we will employ the term synapse to refer to chemical synapses.

2. According to the type of presynaptic and postsynaptic structure, synapses can be classified into several categories as well. Typically, the cellular structures which can house presynaptic terminals are the axon and the dendrites, while postsynaptic receptors can be located in the axon, the dendrites, or the soma of the postsynaptic cell. When presynaptic terminals are located in the axon, synapses can be axo-dendritic, axo-axonic, or axo-somatic, depending on the structure that houses the receptors. Similarly, dendro-dendritic, dendro-axonic, or dendro-somatic synapses have also been found (Pinault et al., 1997). Figure 2.7 illustrates examples of several synaptic connections attending to this classification.
3. Finally, and attending to the effect produced on the postsynaptic neuron, synapses can be either excitatory or inhibitory. In excitatory synapses, the release of neurotransmitters and their binding to postsynaptic receptors pro-

duces a depolarization of the postsynaptic membrane potential. This depolarization is typically due to the influx of  $Na^+$  or  $Ca^{2+}$  ions through postsynaptic ion channels, which open due to the binding of the neurotransmitter to the receptors. In inhibitory synapses, on the contrary, the binding of the neurotransmitters to postsynaptic receptors induces a hyperpolarization in the postsynaptic membrane potential, typically via an efflux of  $K^+$  ions from the cell to the extracellular medium or the influx of  $Cl^-$  ions into the cell.

The effects of excitatory and inhibitory synapses does not depend only on the type of neurotransmitter, but on the specific postsynaptic receptors. For instance, while the mayor neurotransmitter involved in excitatory synapses is glutamate, the effect produced on the postsynaptic neuron strongly depends on the type of receptor. There exist mainly two kinds of receptors associated with glutamate: AMPA receptors, which have a fast ( $\sim 3\text{ ms}$ ) kinetics, and NMDA receptors, with a much slower kinetics of about  $\sim 100\text{ ms}$  (Koch and Segev, 1998). Therefore, the excitatory postsynaptic current can constitute a short event (for AMPA receptors) or be consistent in time (for NMDA receptors). Similarly, the most common neurotransmitter found in inhibitory synapses, gamma-aminobutyric acid (GABA), can bind to fast receptors (namely GABA<sub>A</sub> receptors) or slow ones (namely GABA<sub>B</sub> receptors), producing instantaneous or prolonged hyperpolarizations in the postsynaptic cell.

It is worth noting that, in the vast majority of neural circuits (such as those of the hippocampus or several cortical regions), each neuron displays only one type of synapse: their connections are either excitatory or inhibitory (see, for instance, (Sossin et al., 1990)). This phenomenological principle is known as Dale's law, in honor of the neuroscientist Henry Dale. As a consequence of this principle, neurons themselves can be classified as either excitatory or inhibitory neurons, a classification which turns out to be quite useful to study, for instance, cortical layers.

### 2.5.2 Synaptic plasticity

One of the most relevant properties of synapses, due to its possible relationship with high-level brain functions, is the so called *synaptic plasticity*. This property reflects the ability of synapses to change their strength and adapt themselves as a function of external signals coming from other neural areas or even from the senses. It has been reported that synaptic plastic modifications occur in many kinds of synapses, and via multiple biophysical mechanisms (Bear and Malenka, 1994; Song et al., 2000; Abbott and Nelson, 2000; Tsodyks and Markram, 1997). Attending to

the time scale on which the modification of the synaptic strength occurs, one can distinguish between long-term plasticity and short-term plasticity. In the following we will describe some of the main features of both types of synaptic plasticity.

### A. Long-term plasticity

Long-term plasticity is concerned with modifications in the strength of the synapses which occur on a time scale of minutes or more. These long-term synaptic modifications depends on pre- and postsynaptic activity, and they may lead to an increase or a decrease of the synaptic weight. The corresponding processes for these two situations are known as *long-term potentiation* (LTP) and *long-term depression* (LTD), respectively. According to experimental evidences, long-term modifications could occur via two general mechanisms: the alteration of existing synaptic proteins, or the regulation of gene transcription mediated by second messengers (Kandel et al., 2000). This second mechanism can be triggered by protein phosphorylation, which takes longer and lasts longer, providing the mechanism for long-lasting memory storage. From a general point of view, the biophysical mechanisms that provide long-term modifications at synapses are still debated, although the common assumptions include changes in the release probability of neurotransmitters, insertion or removal of postsynaptic receptors, or changes in the conductance of these receptors, to name a few.

Probably, the most relevant implications of long-term synaptic modifications are *learning* and *memory*. It is commonly established that, as a consequence of synaptic plasticity, the brain is able to acquire new information and to store it for retrieval in subsequent situations, which yield the appearance of memories. This hypothesis has been addressed by multiple psychophysical and *in vitro* experimental studies (Bliss and Collingridge, 1993; Malenka and Nicoll, 1999; Lynch, 2004), and recent *in vivo* experiments have confirmed it (Gruart et al., 2006).

The relation between changes in synaptic strength and memory can be understood by means of the hebbian prescription. In 1943, Donald Hebb established a physiological principle which states that, when two interconnected neurons generate APs strongly correlated in time, the synaptic connection between these two neurons is strengthened (Hebb, 1949). In other words, when two neurons communicate via APs very frequently, the synapses that link them become more reliable and stronger. This principle, known currently as Hebb's rule, states the physiological basis of learning, since it explains how neural activity is able to induce biophysical changes on the synapses that may influence the performance of the brain in later situations. In this context, attractor neural network (ANN) models were of much help to understand the deepest implications of Hebb's rule in the performance of associative memory tasks, as we will see in the chapter concerning methods and models.

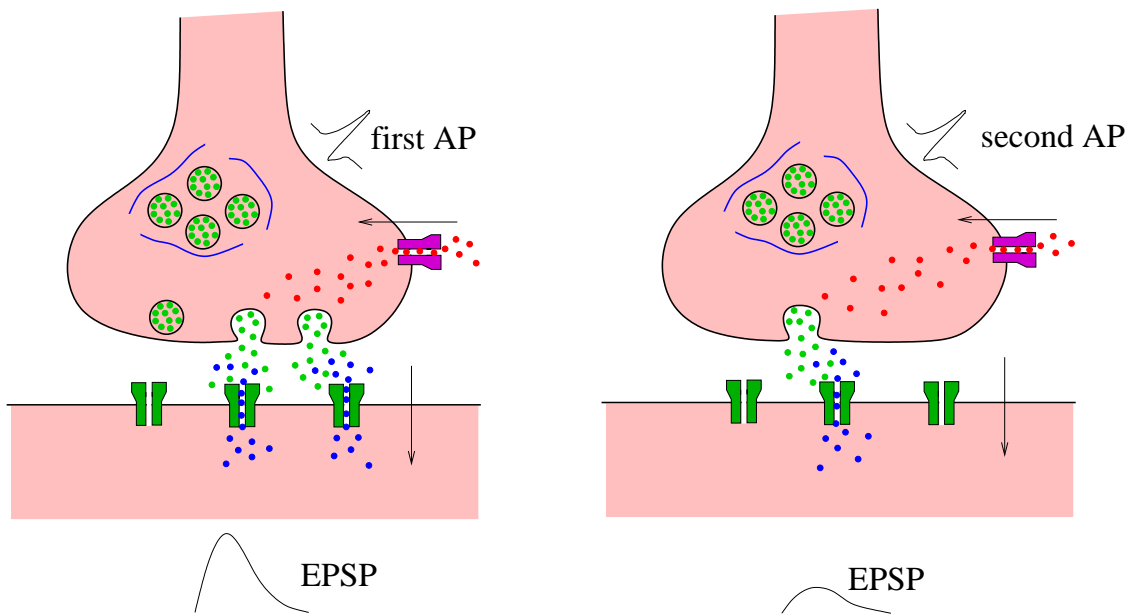


Figure 2.8: Scheme of the basic mechanism of STD. Left: A first AP induces, via an influx of  $Ca^{2+}$  into the cell, the fusion of a certain number of vesicles with the membrane, and the release of their neurotransmitters into the synaptic cleft. The binding of the neurotransmitters to the postsynaptic receptors causes a flux of extracellular ions into the postsynaptic cell, and this induces an EPSP. Right: After a relatively short period of time, a second AP arrives at the presynaptic terminal. Since the neuron needs some time to replenish the resources of the ready releasable pool, the amount of neurotransmitter released will be lower than in the case of the first AP. As a consequence, a smaller number of postsynaptic receptors open, and therefore the EPSP will be smaller than the first one.

### B. Short-term plasticity

Synapses have been traditionally treated as *static* identities, with the only possible modification of synaptic strength due to a slow learning process. In the last decades, however, it has been reported that the amplitude of postsynaptic potentials at short time scales depends on presynaptic activity (Zador and Dobrunz, 1997; Abbott and Regehr, 2004; Bertram et al., 1996). This finding indicates that synaptic strengths can vary at such time scales (of the order of milliseconds). Synapses which present this property are called short-term activity-dependent synapses, or simply *dynamic synapses*. The two mayor mechanisms responsible for activity-dependent plasticity are known as *short-term synaptic depression* and *short-term synaptic facilitation*.

Short-term depression (STD) is a synapse-level biophysical mechanism that induces a decrease in the postsynaptic response for repetitive presynaptic stimuli (Zador and Dobrunz, 1997; Abbott et al., 1997). From a biophysical point of view, STD is a consequence of the limited number of neurotransmitter vesicles which are

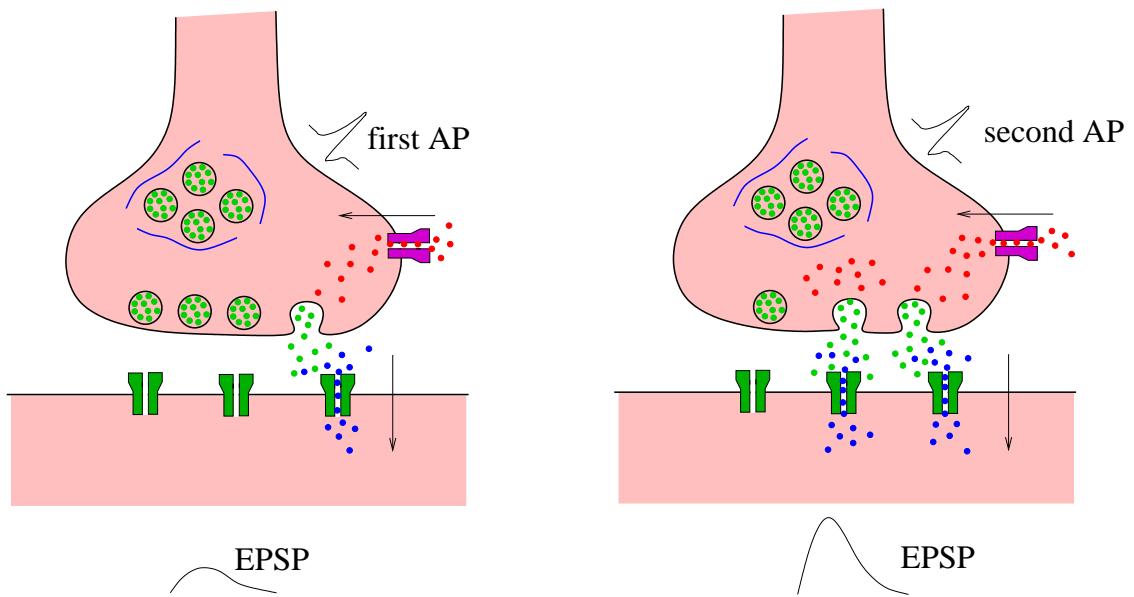


Figure 2.9: Scheme of the mechanism of STF. Left: A first AP induces, via the influx of  $Ca^{2+}$  into the cell, the fusion of a certain number of vesicles and the release of their neurotransmitters into the synaptic cleft. The binding of the neurotransmitters to the postsynaptic receptors causes a flux of extracellular ions into the postsynaptic cell, and this induces an EPSP. Right: After a relatively short period of time, a second AP arrives at the presynaptic terminal. This induces a new influx of extracellular  $Ca^{2+}$  into the presynaptic terminal, which still houses a *residual* amount of  $Ca^{2+}$  from the first AP. Since the concentration of presynaptic  $Ca^{2+}$  is larger than before, a higher amount of neurotransmitter will be released, and as a consequence the EPSP will be larger than the first one.

located in the ready releasable pool of the presynaptic terminals. A number of these vesicles can fuse with the membrane each time an AP arrives at the presynaptic terminal (as explained above), releasing neurotransmitters to the synaptic cleft. The fused vesicles are then substituted by new ones coming from the reserve pool (or generated by other mechanisms) after a certain interval of time. If the presynaptic stimulation has a high frequency, however, the neuron may not be able to restore the vesicles of the ready releasable pool before a new AP arrives at the terminal. In that case, the neuron is not able to efficiently transmit the incoming APs (the synapse is *fatigued*) and the postsynaptic response becomes weaker. This process, which characterizes the STD, occurs in the cortex at time scales of several hundreds of milliseconds (Tsodyks and Markram, 1997), which is the approximate mean time employed by the neuron to restore the ready releasable pool of its presynaptic terminals.

The mechanism of short-term facilitation (STF), on the other hand, induces an increment in the postsynaptic response of repetitive presynaptic stimuli (Bertram

et al., 1996). It is also a synapse-level mechanism, and it can occur simultaneously with STD (as usually occurs indeed). Attending at the involved biophysical mechanism, STF takes into account that, after the arrival of an AP to the synapse and the corresponding influx of  $Ca^{2+}$  into the cell, a certain quantity of these ions remains in the presynaptic terminals near the ready releasable pool. This *residual calcium* may remain until the arrival of a second AP, if the frequency of the stimulus is sufficiently high. The residual  $Ca^{2+}$  ions are added to those that entered into the cell due to the arrival of the second AP to the synapse. As a consequence of this increment in the concentration of cytosolic  $Ca^{2+}$  near the ready releasable pool, the number of neurotransmitter vesicles that can fuse with the membrane is larger than for the first AP, and therefore the postsynaptic response is strengthened. This increment of the postsynaptic current occurs on a time scale of several hundreds of milliseconds (Tsodyks et al., 1998).

The mechanism of STD has been found to be involved in several complex behaviors observed in actual neural systems, such as selective attention (Buia and Tiesinga, 2005), up and down cortical transitions (Pantic et al., 2002; Holcman and Tsodyks, 2006), or cortical gain control (Abbott et al., 1997), to name a few. On the other hand, STF has been the focus of little attention until now, although very recent studies reveal that it could have a role in working memory tasks (Romani et al., 2006) or in slow oscillations (Melamed et al., 2008). However, a complete analysis of the effects that STF could have, either treated in isolation or considered together with STD, on the dynamics of neural systems is still lacking, and it constitutes one of the objectives of this thesis. The main functional characteristics and consequences of STD and STF, as well as several mathematical models of both mechanisms, will be covered in the next chapter.

# Chapter 3

## Methods in computational neuroscience

In this chapter we briefly review some of the most common mathematical descriptions of neurons, synapses and networks used in the literature. This includes the mathematical models and nonlinear systems used in chapters 4-7 for the study of some particular neural systems of interest, and which constitutes the original contributions of this thesis to the field.

### 3.1 Introduction

For many decades, different theoretical and computational tools have been used to construct mathematical models of neural systems, in order to analyze and interpret experimental data and perform a deeper study of the phenomena occurring in the brain. There exists an increasing wide variety of simulation platforms which allow to model neural systems up to some level of detail. Several of these platforms, such as NEURON and GENESIS, can be employed to build biological structures ranging from subcellular components and chemical reactions to complex models of single neurons, simulations of large neural networks, and system-level models (Hines and Carnevale, 1997; Bower and Beeman, 1994). Some of these platforms also support parallelization, which results in a great advantage when working on computers with multiple processors or with supercomputers.

However, these available simulation platforms present several inconveniences, concerning for instance the versatility in the modeling of some particular neural systems and the lack of optimization of the algorithms used in each particular situation. In the case of simulations of large neural systems, such as those performed in the Blue Brain Project, these points are of vital importance to permit simulations of thousands of interconnected neurons modelled in a quite realistic manner

(Markram, 2004). For these reasons, it is sometimes convenient to build specific programs for the particular neural system under study, and this requires a certain level of knowledge about the state-of-the-art of neural modeling.

In this chapter, we briefly introduce some mathematical models commonly employed in the literature for the study of neural systems. The chapter is structured as follows: first, we present some neural modeling paradigms of interest, starting with the more realistic neuron models and finishing with the simpler ones, and discussing briefly their biophysical relevance. After that, we present some basic mathematical approaches for synaptic transmission. Here, we will focus in some descriptions regarding activity-dependent synapses. Finally, we shortly review some of the basic models of large populations of interconnected neurons, and we discuss their range of application to model different actual large scale structures in the brain.

## 3.2 Neuron models

It is well established that the nervous system can process the information at subcellular, cellular, network and system levels. The time scale for any of these processes ranges from milliseconds to many hours or more. To identify a minimal unit of information processing in such a framework is, therefore, not trivial. A widespread view, which we will follow here, considers neurons as the basic units of information processing in neural systems.

In the last few decades, a significant number of mathematical descriptions of neurons have been developed to understand and simulate the behavior of these excitable cells. Nowadays, there exist models for a great number of particular neurons, such as pyramidal neurons, interneurons, Purkinje cells, granule cells, or different types of motoneurons, to name a few (see, for instance, (<http://senselab.med.yale.edu/modeldb>)). In addition, each neuron can be described in different levels of detail, which can include nonlinear membrane properties, dendritic integration and morphology, or multicompartmental modeling (Koch, 1999). However, a complete description of the neuron models available in the literature, or even a detailed description of the main ones for each class of neuron is beyond the scope of this chapter. Here we will describe a small number of generic (that is, not neuron-specific) neuron modeling paradigms, which are commonly used in the literature to describe, in a simplified way, a wide variety of neural systems. In particular, we will focus on single-compartmental models, that is, the membrane potential of the neuron is described by a single variable  $V(t)$ . Multi-compartmental descriptions, on the contrary, divide the neuron into several isopotential compartments and consider a variable  $V_i(t)$  to describe the dynamics of the membrane potential of each compartment, thus allowing to take into account the precise morphology of the neuron. The extension from

single to multi-compartmental descriptions is, in most of the cases, a straightforward procedure and will not be considered here.

### 3.2.1 The Hodgkin-Huxley model

The main signals that neurons employ to communicate among each other are the APs. Because of that, there was a huge effort in the past century to understand the principles for the generation of these rapid changes in the voltage of the cell membrane. At present, it is well known that the biophysical processes underlying the generation of APs are the result of the competition of different ionic currents flowing across the cell membrane. Neuron membranes contain several types of voltage-dependent ionic channels (such as sodium, potassium and calcium channels), and the dynamics of these channels can also depend on the concentration of specific ions. Under a mathematical point of view, these ionic currents may be easily modelled using the Ohm's law, with parameters obtained by fitting with voltage current clamp experiments. In addition, a voltage-independent leakage current, which takes into account other ionic currents (that are difficult to describe experimentally), is often considered to fit the model to concrete experimental realizations. As a consequence of the flow of all these ionic currents, voltage changes are generated and propagated across the membrane.

The process roughly described above was modelled for the first time in 1952 by Hodgkin and Huxley (Hodgkin and Huxley, 1952b). It constitutes a paradigmatical model for the generation of APs, and it assumes that the membrane potential of the cell is described by the set of nonlinear differential equations

$$\begin{aligned}
 C_m \frac{dV(t)}{dt} &= \bar{G}_L[V_L - V(t)] + \bar{G}_{Na}m(t)^3h(t)[V_{Na} - V(t)] + \bar{G}_Kn(t)^4[V_K - V(t)] + I(t) \\
 \frac{dm(t)}{dt} &= \frac{m_\infty(V) - m(t)}{\tau_m(V)} \\
 \frac{dh(t)}{dt} &= \frac{h_\infty(V) - h(t)}{\tau_h(V)} \\
 \frac{dn(t)}{dt} &= \frac{n_\infty(V) - n(t)}{\tau_n(V)},
 \end{aligned}
 \tag{3.1}$$

where  $V(t)$  is the membrane potential and  $m(t)$ ,  $h(t)$ ,  $n(t)$  are phenomenological variables which describe the activation and inactivation of the ionic conductances. The so called Hodgkin-Huxley (HH) model, as presented above, considers two ac-

tive channels (a  $Na^+$  channel and a  $K^+$  channel), and a passive leakage channel  $L$ . The parameter  $C_m$  is the capacitance of the membrane,  $I(t)$  is the external current arriving to the neuron, and  $\bar{G}_i, V_i$  are, respectively, the maximum conductance and reversal potential of the corresponding ionic channel  $i$ . Finally, the steady state values of the active conductance variables  $m_\infty, h_\infty, n_\infty$  and the time constants  $\tau_m, \tau_h, \tau_n$  for channel activation and inactivation have a nonlinear voltage dependence, typically through sigmoidal or exponential functions, whose parameters can be fitted from experimental data.

In general, HH-type neuron models are one of the most successful phenomenological descriptions of neural activity. As it is presented here, it describes a wide range of phenomenology observed in actual neurons, such as tonic and phasic regimes for the generation of APs, subthreshold oscillations, bursting behavior, or chaotic dynamics, to name a few (Izhikevich, 2004). It can also be easily improved by considering additional ionic currents, which increase the success of the model at emulating the activity patterns of actual neurons. However, the high number of variables involved in equations (3.1), as well as the nonlinearities which they present, implies that obtaining a theoretical solution of the model, even approximate, is not possible. In addition to that, until recently the Hodgkin-Huxley model was considered prohibitive from a computational point of view when simulating large populations of neurons, due to the high number of operations needed to numerically compute a single step of the neural dynamics. For these reasons, a great number of simplified models have been developed in the literature. Such models lose certain realistic features of neural activity present in the HH model, but are simple enough to be implemented in simulations of large systems, and some of them are even analytically tractable by employing certain approximations.

### 3.2.2 The FitzHugh-Nagumo model

The FitzHugh-Nagumo (FHN) neuron model describes the excitation properties of the neurons without taking into account a detailed representation of intracellular ionic currents or other biophysically realistic considerations (FitzHugh, 1969; Koch, 1999). Instead of this, the dynamics is described by a set of two coupled differential equations (whose nonlinearities are polynomial) for the membrane potential ( $V$ ) and a slower auxiliary variable ( $W$ ). The model is commonly presented as

$$\begin{aligned} \epsilon \frac{dV(t)}{dt} &= V(t)[V(t) - a][1 - V(t)] - W(t) + I(t) \\ \frac{dW(t)}{dt} &= bV(t) - W(t), \end{aligned} \tag{3.2}$$

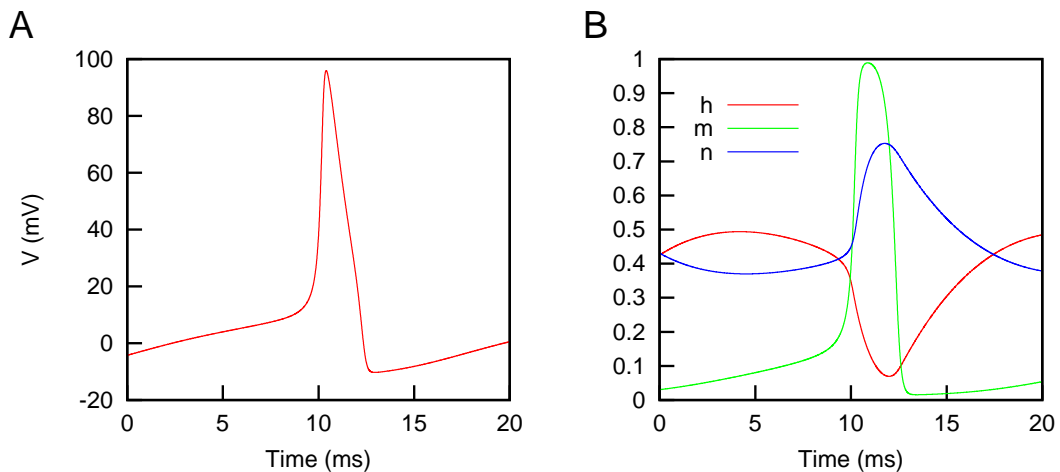


Figure 3.1: Left: a typical AP generated by the Hodgkin-Huxley model when a constant current  $I(t)$  is injected. The resting potential was set to  $V = 0$ . Right: temporal evolution of the variables  $m$ ,  $n$ ,  $h$  during the generation of the AP depicted in the left panel of the figure.

where  $I(t)$  is the input current, and  $a$ ,  $b$ ,  $\epsilon$  are parameters which can be tuned to set the model in different dynamical regimes, such as excitable, bistable and oscillatory. This versatility of regimes and dynamical properties make the FHN model a good choice not only to simulate neurons, but a significative quantity of excitable and bistable systems. Some versions of the FHN description may be analytically derived from the HH neuron model (Abbott and Kepler, 1990), after making several assumptions about the kinetics of activation and inactivation time constants (for instance, considering that the dynamics of  $m(t)$  is very fast compared to those of  $n(t)$  and  $h(t)$ ).

As a consequence of its low dimensionality, the FHN model is commonly studied from the point of view of dynamical systems theory. This fact, together with its capacity to generate APs, allows to consider the FHN model as a useful paradigm to describe an excitable medium. Moreover, due to its capacity to exhibit rebound spiking, threshold variability, and other nonlinear excitable properties, the FHN neuron model is one of the most employed simplified descriptions of neural activity. It also allows for (partial) analytical treatment in some cases, as for instance the calculation of its nonequilibrium potential, which explores several of its excitable properties (Izuz et al., 1998).

### 3.2.3 The Izhikevich model

The use of a simplified neuron model implies neglecting some physiologically realistic neural features (present, for instance, in the HH model) in order to gain analyti-

cal tractability or computational efficiency. It is, therefore, an important issue in computational neuroscience to find computationally-fast models which also show as many realistic neural features as possible. One of the models that best fits this compromise is the Izhikevich neuron model (Izhikevich, 2004). It is described by the following set of equations

$$\begin{aligned}\frac{dV(t)}{dt} &= \alpha V(t)^2 + \beta V(t) + \gamma - W(t) + I(t) \\ \frac{dW(t)}{dt} &= a[bV(t) - W(t)],\end{aligned}\tag{3.3}$$

where  $I(t)$  represents an external input current and  $\alpha$ ,  $\beta$ ,  $\gamma$ ,  $a$ ,  $b$  are parameters of the model. In addition to these equations, there is an auxiliary condition for the generation of the AP: if the membrane voltage exceeds a certain threshold  $V_{th}$ , a spike is generated and the variables  $V(t)$  and  $W(t)$  are reset to  $c$  and  $W(t)+d$ , respectively, where  $c$ ,  $d$  are model parameters. Summarizing, the model is constituted by two differential equations, seven parameters and one resetting condition. A parameter space of seven dimensions makes this model difficult to analyze in detail. On the other hand, this huge parameter space allows the model to exhibit a rich repertoire of phenomena (also observed in actual neurons in different brain areas), such as spike frequency adaptation, spike latency, or inhibition-induced spiking and bursting (Izhikevich, 2004). Therefore, if we know the value of the parameters which allow for a desired set of neural features to be present, this model becomes one of the most convenient in order to simulate large neural populations with a realistic single-cell behavior.

The auxiliary condition for the generation of APs sets the Izhikevich model into the category of the *threshold-firing* neuron models, in opposition with the previous models in which the mechanisms for the generation of APs are included in the proper dynamics of the system. Threshold-firing neuron models precise an external auxiliary condition for the generation of APs, but on the other hand this condition simplifies the nonlinearities of the model equations, allowing to have computationally faster and simpler models of neurons.

### 3.2.4 The integrate and fire model

The integrate and fire (IF) model constitutes the paradigm of the threshold-firing neuron models. It was introduced by Lapicque in 1907 (Lapicque, 1907; Brunel and van Rossum, 2007) as a highly simplified model which presented the most basic features of actual neurons. Employing a threshold-firing condition, it reduces the complexity of the HH model to a single differential equation, which has the form

$$\tau_m \frac{dV(t)}{dt} = -V(t) + R_m I(t), \quad (3.4)$$

where  $I(t)$  is the input current and  $\tau_m$  is the membrane time constant, which is related with the membrane resistance  $R_m$  and the membrane capacitance  $C_m$  by the expression  $\tau_m = R_m C_m$ . The auxiliary condition states that, when the membrane potential exceeds the threshold  $V_{th}$ , an AP is generated, and the membrane potential is reset to a resting value  $V_r$  and remains in it for a short period of time  $\tau_{ref}$ , the absolute refractory period.

The simplicity of this model implies that only a few realistic neural features are preserved, such as tonic spiking and integrating capacities. Therefore, one must take into account that most of the phenomenology observed in actual neural systems could not be reflected by circuits built with IF neuron models (Feng, 2001; Izhikevich, 2004). However, this model presents some advantages from a theoretical point of view, since in many cases one can analytically solve the dynamics of IF neurons, or at least to find approximate solutions by employing mean-field techniques. For instance, if the input current is sufficiently simple, it is possible to find adequate solutions which yields magnitudes of interest, such as the mean firing rate or the coefficient of variation of the neural activity (Tuckwell, 1989).

On the other hand, the IF model can be easily extended to include more biophysically realistic features, such as neural adaptation, bursting activity, resonance properties, or spike latency, to name a few (Izhikevich, 2004, 2001; Ermentrout, 1996). In addition, the parameters employed in the basic IF model are physiologically meaningful (such as the membrane resistance  $R_m$ , the refractory time  $\tau_{ref}$ , or the membrane threshold  $V_{th}$ ), and therefore they can be measured directly in experiments and give a good fitting values of the parameters. For all these reasons, the IF neuron model is one of the most studied and used in the literature. The question about its usefulness to reflect realistic neural behavior in particular circumstances should be always taken into account, through (Feng, 2001; Shinomoto et al., 1999).

### 3.2.5 The McCulloch-Pitts model

The McCulloch-Pitts (MP) paradigm was the first computational model of the so called *artificial neurons*. According to this mathematical description, the neurons are modelled as two-state functions, and the time is commonly considered in discrete steps. The model is then described by the dynamics

$$S(t+1) = \Theta[R I(t) - \theta] \quad (3.5)$$

where  $\Theta(x) = 1$  if  $x > 0$ , and  $\Theta(x) = 0$  otherwise, represents the Heaviside step function. The input current is given by  $I(t)$ ,  $R$  is the input resistance, and  $\theta$  is

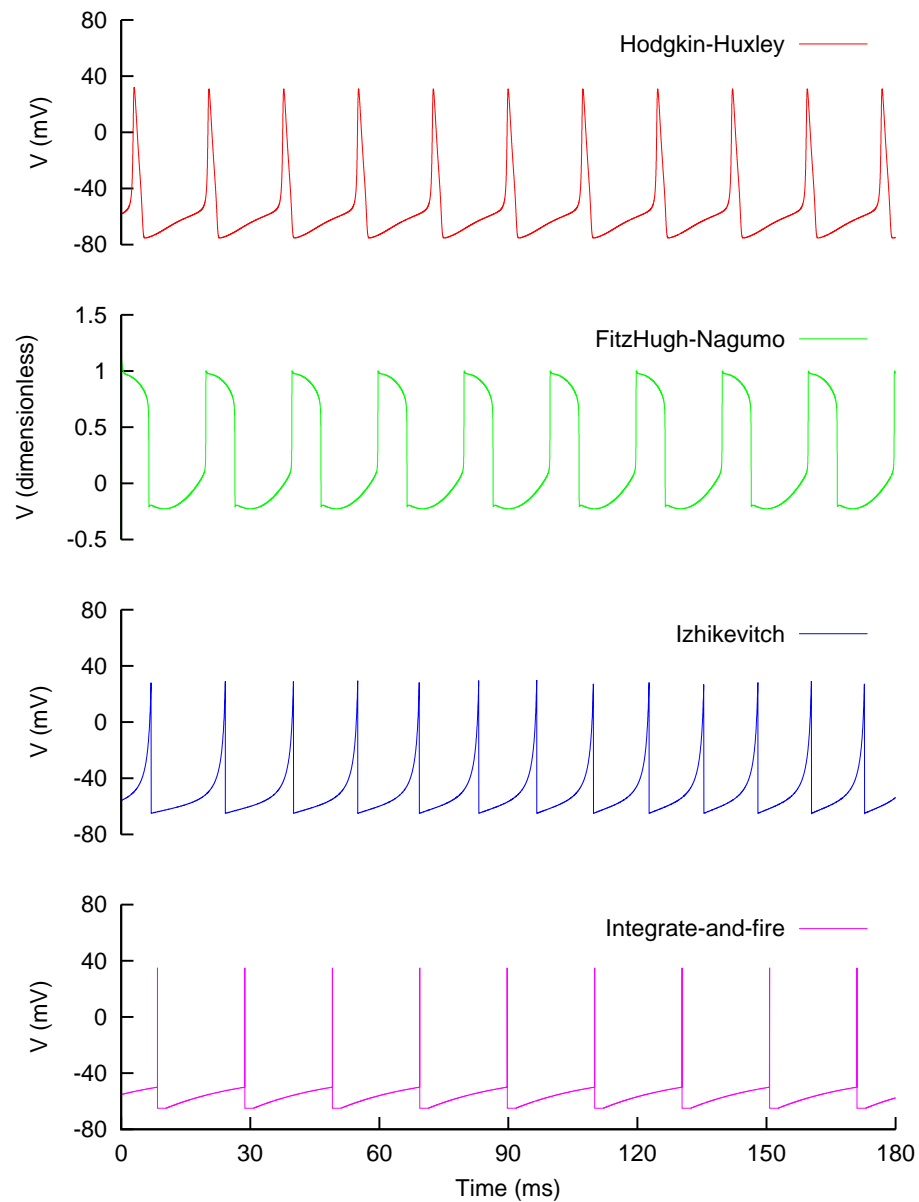


Figure 3.2: Tonic spiking neural activity for different neural models, as a result of the injection of a constant current. From top to bottom: Hodgkin-Huxley, FitzHugh-Nagumo, Izhikevich and integrate-and-fire models. For all models (except the FHN, which is not displayed in  $mV$ ) the resting potential was set to  $V = -65 mV$ .

a threshold parameter. This model defines the so called *binary neurons*, that is, neurons that can be firing ( $S(t) = 1$ ) or silent ( $S(t) = 0$ ) at a certain time  $t$ . Several variants are popular in the literature, such as considering the code  $S = \{+1, -1\}$  instead of  $S = \{+1, 0\}$  for the binary variables, or employing a probabilistic version where the step function is substituted by a smooth sigmoidal function and the deterministic dynamics (3.5) is substituted by a probabilistic one. Despite its simplicity, or perhaps because of it, this model and its variations have been extensively studied

in the literature. It is, for instance, commonly employed to construct *perceptrons* and other artificial intelligence structures, since it is computationally the fastest neuron model available.

Some variants of this neuron model are also used to describe neural systems employing the tools of Statistical Mechanics, because their simplicity usually allows for a theoretical treatment of large networks of simple binary elements – neurons (see section 3.4, which is focused on large network models). For instance, the Hopfield model, which considers a variant of the MP neuron model and constitutes one of the simplest descriptions of neural networks, can be analytically studied employing mean-field approaches from Statistical Mechanics due to its similarity with Ising-like models (Peretto, 1992; Amit, 1989). This constitutes a great advantage, and it is of special interest for studying large neural networks, where it is not uncommon to observe emergent cooperative behavior (such as the property of associative memory). Since this, however, is not always the case, one should consider more realistic models in order to test the results obtained with systems constituted by MP-like neurons.

### 3.3 Synapse models

In actual neural systems, neurons are interconnected by means of synapses, as we have explained in section 2.5. Synaptic connections display multiple forms and functions, and surpass the number of neurons by a factor of  $10^3 \sim 10^4$  in the neocortex, for instance (Kandel et al., 2000). Because of this, neural systems are usually described as highly connected networks of excitable elements. This high connectivity is responsible for most of the emergent collective phenomena observed in the brain, and constitutes one of the most well-known features of neural tissue. Appropriate mathematical descriptions of synapses are, therefore, of vital importance to study such emergent collective properties. It is useless to model a neural system employing only realistic mathematical descriptions for neurons if realistic considerations about the synapses are not taken into account.

In this section we briefly review some of the basic mathematical models of synapses which are commonly used in the literature. As we have already seen, synapses can be classified depending on the presynaptic and postsynaptic cellular structures involved in signal transmission. Here, for simplicity purposes, we will assume that neurons are modelled as point excitable elements, and therefore the classification of synapses as a function of morphological aspects is not considered. We start by presenting some mathematical models for electrical and chemical synapses. After that, we will focus on mathematical models concerning several dynamical properties of synapses.

### 3.3.1 Electrical synapses

In an electrical synapse, the presynaptic and postsynaptic membranes are joined by specific protein structures, the gap junctions. These protein structures connect the cytoplasm of both cells, allowing the direct flux of ions between them. As a consequence, signals in the form of APs or even in the form of electrotonic (that is, subthreshold) signals can be transmitted from one cell to the other.

Electrical synapses can be modelled in a simple and direct manner employing Ohm's law. Concretely, the synaptic current received by neuron  $i$  from neuron  $j$  is given by

$$I_{ij}(t) = \overline{G}_{ij} [V_i(t) - V_j(t)], \quad (3.6)$$

where  $V_k$  is the membrane potential of neuron  $k$ , and  $\overline{G}_{ij}$  is the maximal synaptic conductance. This conductance is considered constant for electrical synapses, and thus the synaptic current is directly proportional to the difference between the presynaptic and postsynaptic membrane potential. The above expression also takes into account the bidirectional nature of electric synapses. Equation (3.6), therefore, describes electrical synapses adequately by taking into account the passive diffusion of ions through the gap junctions.

Electrical synapses are commonly used in the modeling of neural networks with nearest-neighbors connections, where neurons are precisely located in space and close enough to each other (Rabinovich et al., 1999). The existence of such nearest-neighbors interactions can explain different kinds of complex collective behavior observed in the brain, such as synchrony or pattern formation (Rabinovich et al., 1999; Varona et al., 2001). However, the high degree of connectivity of most neurons, which is responsible of a wide variety of collective phenomena observed in the brain, is not only due to electrical synapses, but to the existence of a high number of long-range connections which are typically constituted by chemical synapses.

### 3.3.2 Chemical synapses

In most neural systems, neurons are densely connected among each other, yielding a complex network structure in which information is processed. In the vast majority of the cases, the connections of this network correspond to chemical synapses<sup>1</sup>. The basic features of synapses and their biophysical mechanisms have been already introduced in chapter 2. Here we will review some models of synapses which are commonly used in the literature (see, for instance, (Chapeau-Blondeau and Cham-

---

<sup>1</sup>In the following, unless specified otherwise, we will refer chemical synapses simply as synapses.

bet, 1995)). Concretely, we will focus on three levels of description: 1) ion channel kinetics, 2) synaptic conductance dynamics, and 3) synaptic weights.

1. *Ion channel kinetics:* A realistic description of synaptic transmission should include details about postsynaptic receptors and the opening-closing kinetics of the ionic channels involved. For instance, according to the model proposed in (Destexhe et al.), the binding of neurotransmitter molecules  $T$  with a postsynaptic receptor  $R$  to give the bounded form of postsynaptic receptors  $RT^*$  follows a first order kinetic scheme



where  $k_1$  and  $k_2$  are the binding and unbinding rates, respectively. The binding of transmitter to a postsynaptic receptor directly gates the opening of a particular ion channel of electric conductance  $g_c$ . Then, the total synaptic conductance through all channels of a synapse is  $G(t) = g_c n_c(t)$ , where  $n_c(t)$  is the number of bound receptors (or, similarly, open channels) at time  $t$ . In addition, it is generally assumed that, after the arrival of an AP to the presynaptic terminal at time  $t_0$ , the density of neurotransmitters in the synaptic cleft varies in time as an *alpha function*  $\alpha(t - t_0)$ . Common choices for the alpha function used in the literature includes  $\alpha(t) = \frac{t}{\tau^2} \exp(-t/\tau)$ , with  $\tau$  being a characteristic time scale for the neurotransmitter inactivation, or  $\alpha(t) = \frac{1}{\tau_d - \tau_r} [\exp(-t/\tau_d) - \exp(-t/\tau_r)]$ , with  $\tau_d$ ,  $\tau_r$  being the decay and rise time scales of neurotransmitter concentration, respectively. By considering an extra factor  $Q$  conveniently dimensioned, one can write the transmitter pulse probability due to the arrival of an AP to the presynaptic terminal at time  $t_0$  as  $q(t) = Q\alpha(t - t_0)$ .

According to this scheme, at time  $t$  a bound receptor has a probability per unit time  $k_2$  of becoming unbound, and an unbound receptor has a probability per unit time  $k_1 q(t)$  of becoming bound (assuming that an AP arrives at presynaptic terminals at  $t_0$ ). Now, considering a number of postsynaptic receptors  $N$  sufficiently large, the number of bound receptors follows the dynamics

$$\frac{dn_c(t)}{dt} = k_1 q(t) [N - n_c(t)] - k_2 n_c(t) \quad (3.8)$$

and the total synaptic conductance varies in time as

$$\frac{dG(t)}{dt} = -k_2 G(t) + [\bar{G} - G(t)] k_1 q(t) \quad (3.9)$$

with  $\bar{G} \equiv g_c N$  being the maximum (or saturating) value of the conductance. Equation (3.9) constitutes the continuum limit of the discrete stochastic kinetics discussed above, and its validity can be considered acceptable only for sufficiently large  $N$ . In general, for a pulse-like function  $q(t)$  that starts at  $t = t_0$ , the conductance  $G(t)$  also has a pulse-like shape which starts at  $t = t_0$ . If  $q(t)$  has a typical duration of  $\sim \tau_q$ , then the rise time of  $G(t)$  is approximately  $\tau_q$ . For  $t$  sufficiently larger than  $\tau_q$ , i.e. when  $q(t)$  has vanished, the decay of  $G(t)$  is exponential with a time constant  $1/k_2$ . Equation (3.9), therefore, relates the level of ion channel kinetics with the synaptic conductance level, as we will see below.

2. *Synaptic conductance dynamics:* In most cases, when one is interested in modeling the behavior of neural systems at a cellular level, the consideration of the detailed kinetics of postsynaptic receptors may be avoided for simplicity. One can simply consider the temporal evolution of the conductance  $G(t)$  as the evolution of a coarse-grained quantity, provided that the resulting dynamics coincides qualitatively with those described by equation (3.9). The simplest way to do this is considering a linear dynamics for the conductance, such as the one proposed in (Wilson and Bower, 1989). According to this model, the synaptic conductance evolves as

$$\tau_G \frac{dG(t)}{dt} = -G(t) + \bar{G}W \sum_k \delta(t - t_k) \quad (3.10)$$

where  $\tau_G$  is the conductance time scale, and  $W$  is a parameter that takes into account the strength of the synapse. The sum  $\sum_k \delta(t - t_k)$  runs over the instants in which the  $k$ -th AP arrives at the synapse (which occurs at time  $t_k$ ). We have assumed here that the neurotransmitter transmitter pulse is no longer modeled as an alpha function, but as a simpler delta function centered at the time at which the AP arrives at the presynaptic terminal. It is worth noting that equation 3.10 is assumed here as our basic description of a synapse, while for the ion channel kinetics level a similar equation is found only when the number of postsynaptic receptors is large enough.

The conductance time scale  $\tau_G$  can vary significantly, depending on the type of postsynaptic receptors under consideration. For instance, AMPA receptors of excitatory synapses usually have a fast kinetics, with the corresponding time scale around  $\tau_A \sim 3$  ms. On the other hand, NMDA receptors, that have a much slower kinetics, are usually modeled with a time scale of  $\tau_N \sim 100$  ms. The same can be applied to GABAa and GABAb receptors of inhibitory synapses, which have fast and slow kinetics respectively.

3. *Synaptic weights:* Finally, in order to obtain a minimal model of synaptic transmission, one can assume that the kinetics of the postsynaptic receptors, as well as the diffusion of neurotransmitters in the synaptic cleft, is instantaneous. This can be done by considering the limit  $\tau_G \rightarrow 0$  in equation (3.10), leading to

$$G(t) = \overline{G}W \sum_k \delta(t - t_k). \quad (3.11)$$

In this equation,  $\overline{G}$  is usually incorporated into  $W$  to reduce the parameters of the model. Therefore, the synapse is mostly characterized by the synaptic weight  $W$ , which modulates the strength of the contribution of the  $k$ -th AP to the dynamics of the postsynaptic neuron.

Although this delta-type synaptic transmission may be an oversimplification in a significant number of situations, it can be a good approximation in systems whose synapses present only postsynaptic receptors with fast kinetics (such as AMPA or GABA<sub>A</sub> synapses). In addition, this simplified model allows one to obtain analytical descriptions of the dynamics of large neural networks, as for instance the mean-field solution of certain models of associative memory (Hopfield, 1982; Amit et al., 1987). We will briefly review some of these models later in this chapter.

Independently of the level of detail considered in the modeling of synapses, the general picture presented in these models treats synapses as static elements, in the sense that the contribution of a synapse to the postsynaptic potential is given by a fixed synaptic weight. However, we have already seen in the previous chapter that synaptic weights are not time-independent, and can vary both on long time scales and short time scales. The variation in short time scales (also known as short-term plasticity) is particularly interesting for information processing purposes, as we will see below.

### 3.3.3 Dynamic synapses

It has been found in the last decade that synaptic strength can vary on short time scales depending on the presynaptic activity (Abbott et al., 1997; Tsodyks and Markram, 1997). Synapses presenting such activity-dependent dynamics are also known as dynamic synapses, and are mostly characterized by two mechanisms that we have already introduced in section 2.5.2: short-term depression (STD) and short-term facilitation (STF). In this section, some mathematical descriptions of these mechanisms will be briefly reviewed.

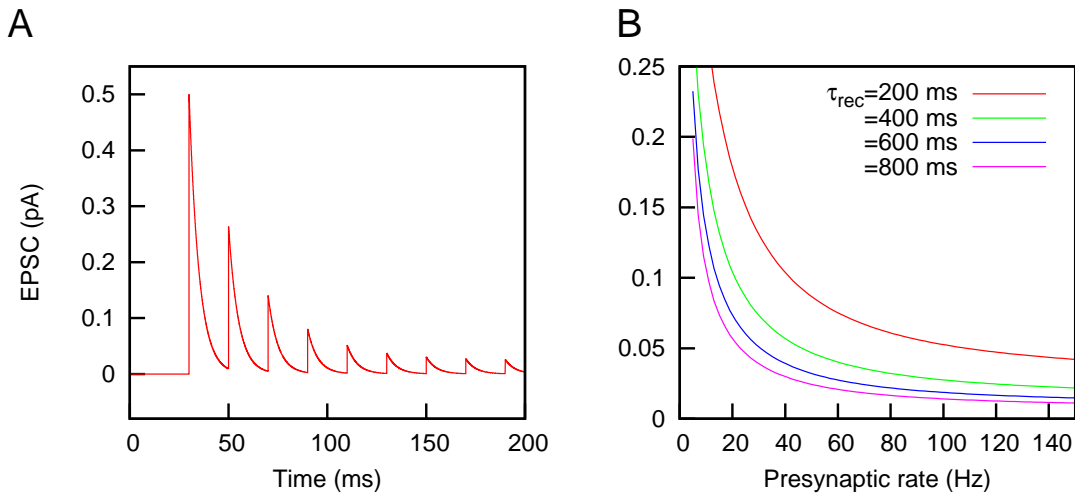


Figure 3.3: Effect of STD on the postsynaptic response according to the model (Tsodyks and Markram, 1997). (A) EPSC vs time for a depressing synapse ( $\tau_{rec} = 800$  ms,  $U_{SE} = 0.5$ ,  $\tau_{in} = 5$  ms) receiving a presynaptic spike train of firing rate 50 Hz. The decrement of the peak amplitude with time is due to synaptic fatigue, as explained in the main text. (B) Steady-state amplitude of the EPSC, as a function of the presynaptic firing rate, for different values of  $\tau_{rec}$ . Other parameters are  $U_{SE} = 0.5$  and  $\tau_{in} = 5$  ms. For simplicity, we have considered that the EPSC is given by  $EPSC = C y(t)$ , with  $C$  being a constant.

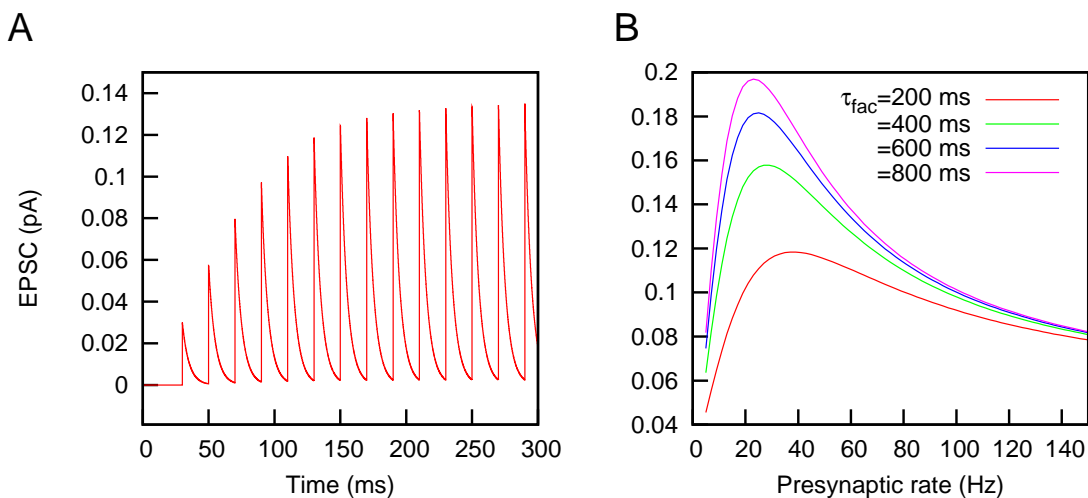


Figure 3.4: Effect of STF on the postsynaptic response according to the model (Tsodyks and Markram, 1997). (A) EPSC vs time for a typical facilitating synapse ( $\tau_{rec} = 100$  ms,  $\tau_{fac} = 500$  ms,  $U_{SE} = 0.03$ ,  $\tau_{in} = 5$  ms) receiving a presynaptic spike train of firing rate 50 Hz. (B) Steady-state amplitude of the EPSC, as a function of the presynaptic firing rate, for different values of  $\tau_{fac}$ . Other parameters are  $\tau_{rec} = 100$  ms,  $U_{SE} = 0.03$  and  $\tau_{in} = 5$  ms. For simplicity, we have considered that the EPSC is given by  $EPSC = C y(t)$ , with  $C$  being a constant.

*A. Deterministic description:*

One of the most successful models of dynamic synapses is the one proposed in (Tsodyks and Markram, 1997; Tsodyks et al., 1998). This model presents a phenomenological coarse-grained description of synaptic resources (neurotransmitters), via a set of coupled differential equations. According to this model, the dynamical state of a synapse  $i$  is described by

$$\begin{aligned}\frac{dx_i(t)}{dt} &= \frac{z_i(t)}{\tau_{rec}} - u_i(t)x_i(t) \sum_k \delta(t - t_k) \\ \frac{dy_i(t)}{dt} &= -\frac{y_i(t)}{\tau_{in}} + u_i(t)x_i(t) \sum_k \delta(t - t_k) \\ \frac{dz_i(t)}{dt} &= \frac{y_i(t)}{\tau_{in}} - \frac{z_i(t)}{\tau_{rec}},\end{aligned}\tag{3.12}$$

where the variables  $x_i(t)$ ,  $y_i(t)$ ,  $z_i(t)$  denote the fraction of neurotransmitters in a *recovered*, *active* and *inactive* state, respectively. To be more precise,  $x_i(t)$  represents the fraction of neurotransmitters that are located in the vesicles of the ready releasable pool at time  $t$ , whereas  $y_i(t)$  denotes the fraction of neurotransmitters that are bound to receptors of the postsynaptic cell at time  $t$ , and therefore are contributing to the transmission of an AP. The variable  $z_i(t)$  is an auxiliary quantity to ensure a proper normalization (note from the above equation that  $x_i(t) + y_i(t) + z_i(t) = 1$  for any value of  $t$ ). The time constant  $\tau_{rec}$  determines the working time scale of STD, and  $\tau_{in}$  is the inactivation time constant of the postsynaptic receptors. In this model, depressing synapses are obtained for  $u_i(t) = U_{SE}$  constant (which represents the maximum fraction of neurotransmitters which can be released after the arrival of a single presynaptic spike). The sum over delta functions in equation (3.12) takes into account the arrival of each AP of the presynaptic spike train to the presynaptic terminal. For low values of  $\tau_{rec}$  (compared with the typical inter-spike time interval) the variable  $x_i(t)$  quickly approaches its resting value  $x_i = 1$ . In the limit  $\tau_{rec} \rightarrow 0$  one has  $x_i(t) = 1 \forall t$ , which correspond to the case of the classical description of a synapse with fixed strength, also called *static synapse* (see discussion above).

The mechanism of STF can be introduced in this general model by considering that  $u_i(t)$  has its own dynamics related with the influx of  $Ca^{2+}$  into the cytosol of the presynaptic terminals from the extracellular medium and the intracellular endoplasmatic reticulum every time an AP arrives. According to (Tsodyks et al., 1998), this dynamics is given by

$$\frac{du_i(t)}{dt} = \frac{U_{SE} - u_i(t)}{\tau_{fac}} + U_{SE}[1 - u_i(t)] \sum_k \delta(t - t_k).\tag{3.13}$$

In absence of stimuli, the variable  $u_i(t)$  tends to its lower limit value  $U_{SE}$  with a

typical decay time of  $\tau_{fac}$ , whereas the arrival of presynaptic APs, denoted by the second term in the right-hand side of equation (3.13), increase temporally its value. In the limit of  $\tau_{fac} \rightarrow 0$  the resting value  $u_i(t) = U_{SE} \forall t$  is obtained, suppressing all the STF effects, and therefore one recovers a pure depressing synapse (if  $\tau_{rec} > 0$ ) or a static synapse (if  $\tau_{rec} = 0$ ).

Equations (3.12-3.13) constitute a close phenomenological description of activity dependent short-term synaptic mechanisms. Some of the main functional properties of STD and STF can be understood via these equations. One may assume, for instance, a presynaptic excitatory neuron connected to a postsynaptic one via a depressing synapse (that is, equations (3.12-3.13) with  $\tau_{rec} > 0$  and  $\tau_{fac} = 0$ ). We also assume that the presynaptic neuron fires APs periodically, being  $T$  the time interval between two successive presynaptic spikes and  $f \equiv 1/T$  the corresponding presynaptic firing rate. In this simple situation, analytical solutions of the model can be obtained easily (Tsodyks et al., 1998). Figure 3.3 shows that the effect of repetitive presynaptic stimulation in the presence of STD is a decrease of the EPSC, until a stationary EPSC value is reached. This effect is observed in experimental *in vitro* recordings, and numerical simulations of the model presented above nicely fits such behavior (Tsodyks and Markram, 1997). The decrease in the EPSC occurs because a high-frequency input can lead to synaptic fatigue. Such fatigue weakens the strength of the synapse<sup>2</sup> and, as a result, the postsynaptic response becomes weaker. A straightforward consequence is that this *filtering* effect depends on the presynaptic firing rate, in such a way that higher firing rates induce stronger decreases of the EPSC. A similar effect can be obtained also by increasing the value of  $\tau_{rec}$  (which is a measure of the mean time employed by the synapses in refilling the ready releasable pool) instead of the presynaptic firing rate. As a consequence of such effects, STD provides a synapse-level mechanism to control the gain of postsynaptic responses in an activity dependent manner (Abbott et al., 1997).

On the other hand, the inclusion of STF induces an increment in the postsynaptic response under repetitive presynaptic stimuli. This can be seen by setting  $\tau_{rec} > 0$  and  $\tau_{fac} > 0$  in the model and analyzing the effect of a presynaptic periodic stimulation in the EPSC in the presence of STD and STF (see figure 3.4). The particular stationary value of the postsynaptic response depends on the presynaptic firing rate and/or the facilitation time constant  $\tau_{fac}$ . When both STD and STF mechanisms are considered together, a competition between the two *a priori* opposite tendencies can occur. In this particular situation, a maximum value of the postsynaptic response is obtained for certain value of the presynaptic firing rate, as the figure 3.4 shows. The implications of the coexistence of STD and STF for more

---

<sup>2</sup>In the sense that the amount of available neurotransmitters decreases.

elaborated (and biophysically relevant) systems is one of the main objectives of this thesis, and will be studied in detail in the following chapters.

*B. Stochastic description:*

Dynamic synapses can be modelled using more realistic considerations. For instance, it is known that real synapses have a stochastic nature (Dobrunz and Stevens, 1997) and their fluctuations can play an important role in neural computation (Dobrunz and Stevens, 1997; Zador, 1998). Therefore, they should be taken into account in order to design more realistic models of dynamic synapses. A simple description that extends the synaptic STD model exposed above to include the effects due to synaptic stochasticity is presented in (de la Rocha and Parga, 2005). This intrinsically stochastic model considers that each connection between neurons has a number of functional contacts, or synaptic buttons, and this number is randomly chosen (for each particular connection) following a Gaussian distribution of mean  $M$  and standard deviation  $\Delta_M$ . In addition, the strength of each individual synaptic button is also randomly determined following a Gaussian distribution of mean  $J$  and standard deviation  $\Delta_J$ . The release of a neurotransmitter vesicle from a synaptic button to the synaptic cleft (when an AP arrives at the button) is modeled as a random event. After that release, the recovering of the synaptic button is considered as a probabilistic event following a Poisson distribution with a typical time  $\tau_{rec}$ . This probabilistic model gives the same mean values for the EPSC as the model given by equations (3.12-3.13), but the fluctuations differ from the deterministic model, providing a higher level of description for the fluctuations of dynamic synapses. Details on the performance of this stochastic model of dynamic synapses can be seen in (de la Rocha and Parga, 2005).

## 3.4 Network models

In the two previous sections, we have reviewed some of the basic mathematical descriptions of neurons and synapses commonly used in the literature. In addition to appropriately select some of these models, there exists several important issues in the modeling and study of neural systems: the concrete topology of the underlying network (all to all connected, random sparsely connected, or small-world topology, for instance (Torres et al., 2004; Johnson et al., 2008)), considering or not spatially located neurons (with implications on the delay time and synchronization properties (Rabinovich et al., 1999)), or including several types of neural populations (inhibitory, excitatory) which compete with each other (Brunel, 2000), to name a few.

Since, in some cases, numerical simulations of large networks of interconnected neurons could be computationally expensive, it is also highly relevant to identify models of neural networks which could, in some sense, be analytically tractable. Mean-field network approaches as well as approximate expressions for the macroscopical magnitudes of interest, or even a qualitative description of the different regimes of behavior of the system, are of great importance when working with models of a high number of interconnected neurons. In this section we will review some representative examples of mathematical models of neural networks, describing its main features and possible analytical approaches.

### 3.4.1 The rate model

The most simple manner to model the activity of a large population of interconnected neurons is to employ a simple dynamical system describing the global activity of the network. This approach, which defines the so called rate models, describes the temporal evolution of the network mean firing rate (that is, the average over neurons of the number of AP per unit of time). Within this description, the dynamics of the system is given by a single differential equation:

$$\tau_r \frac{dr(t)}{dt} = -r(t) + S(I(t) - \theta) \quad (3.14)$$

where  $r(t)$  resembles the network mean firing rate,  $\tau_r$  is a time constant,  $\theta$  is a threshold, and  $S(x)$  is a transduction function, which gives the effect that the global synaptic currents  $I(t)$  causes in the mean firing rate. Usually,  $S(x)$  takes the form of a threshold-linear function or a sigmoidal function. The global synaptic current includes both external stimuli coming from sensory receptors (or from other neural populations) and recurrent currents generated internally in the population considered. Therefore, the global current is given by

$$I(t) = I_{ext}(t) + J r(t - d) \quad (3.15)$$

where  $I_{ext}(t)$  is the external input and the second term takes into account the recurrent current, with  $J$  being the total synaptic coupling factor. The parameter  $d$  is positive and denotes a possible time delay due to spatial extension of the network, for instance, although it is commonly set to zero for simplicity.

Rate models of neural activity constitutes the simplest option to model a neural population, although such simplicity neglects most of the complex features of the system under study. They are useful, however, to model the interaction between different neural populations with different characteristics (employing several variables:  $r_1(t)$ ,  $r_2(t)$ ,  $r_3(t)$  ...), and to obtain analytical results for the stationary states by solving the corresponding set of coupled equations. It is worthy to note

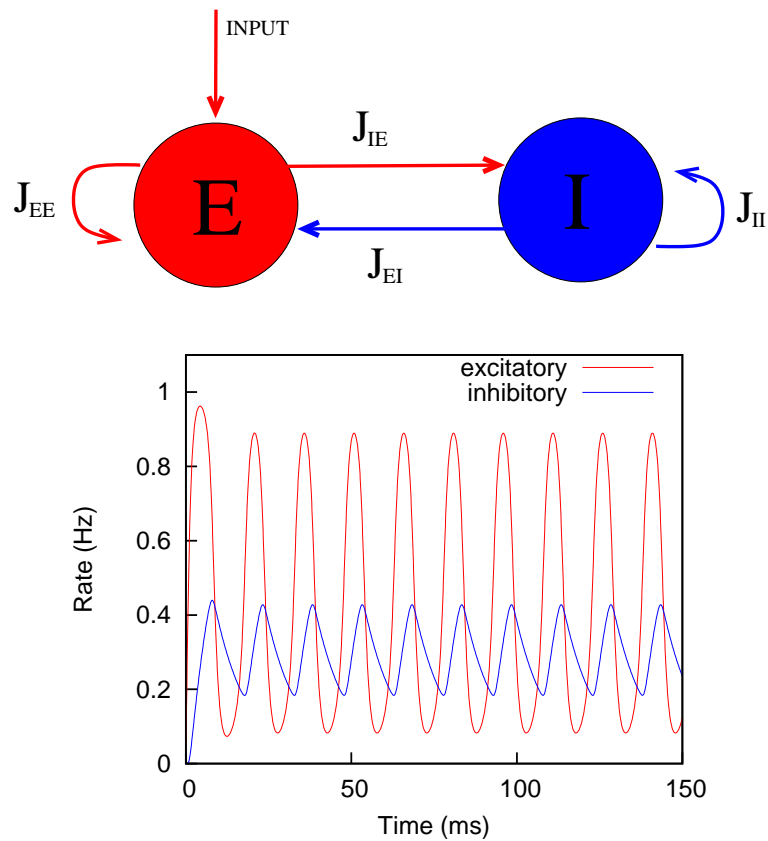


Figure 3.5: Dynamics of two coupled neural populations (one constituted by excitatory neurons and the other by inhibitory neurons) described with rate models. (Top) Basic scheme of the system considered. The global current for the excitatory population is given by  $I_e(t) = I_{input} + J_{EE} r_e + J_{EI} r_i$ , and for the inhibitory population one has  $I_i(t) = J_{IE} r_e + J_{II} r_i$ . The variables  $r_e$ ,  $r_i$  denotes the firing rate of the excitatory and inhibitory population, respectively, and  $J_{ab}$  is the (fixed) synaptic strength of the connection between the presynaptic population  $b$  and the postsynaptic population  $a$ . (B) For some values of the model parameters, the system displays periodic oscillations of activity, induced by the competition between excitation and inhibition (see (Wilson and Cowan, 1972) for a detailed analysis).

that, although the model is able to show oscillatory synchronized behavior (that is, a periodic dynamics of  $r(t)$ ), the internal structure of such dynamics is not reflected (since the dynamics of individual neurons is not considered). Therefore, the model works with the implicit assumption of spontaneous activity, and its predictions will fail when correlations between neurons are important for the dynamics (for instance, when certain types of neural synchronization emerge in the dynamics of the system (Brunel, 2000; Brunel and Hansel, 2006)).

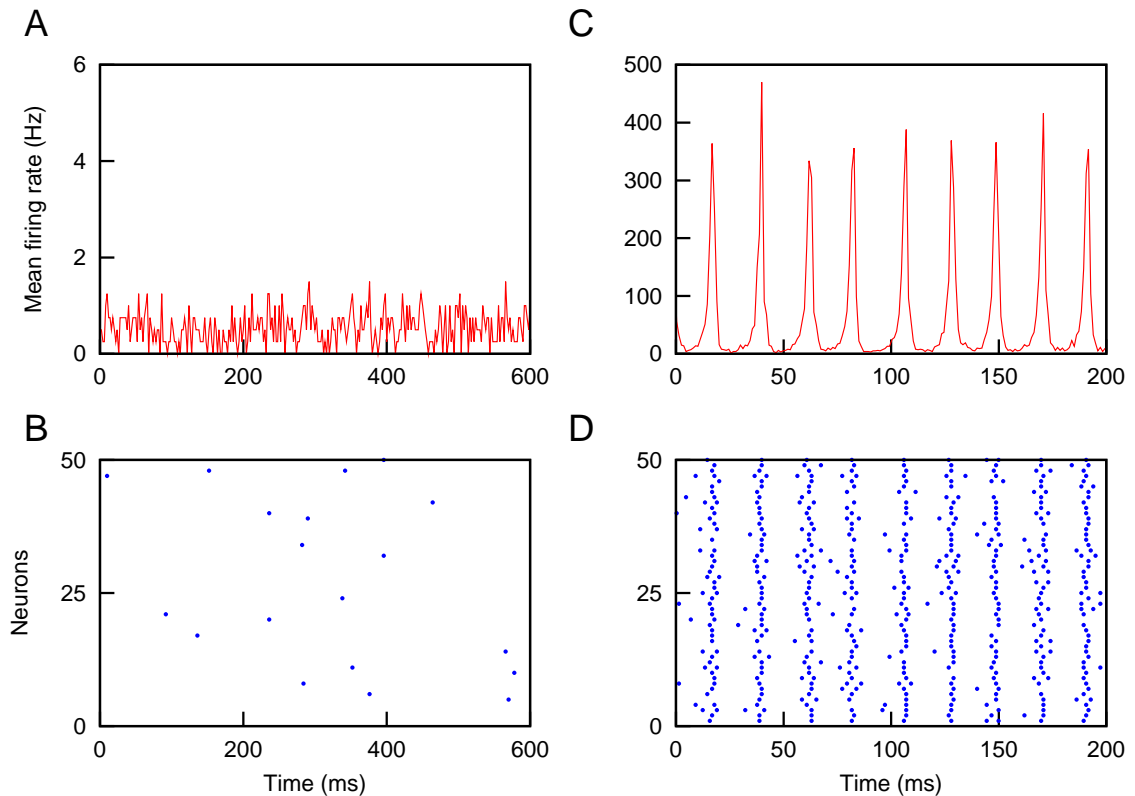


Figure 3.6: Dynamics of a spiking neural network constituted by excitatory IF neurons, connected in an all-to-all manner. (A) Temporal evolution of the network mean firing rate when a weak external input is injected into every neuron. The resulting activity is asynchronous, as can be also seen in panel (B), which shows a raster plot of the activity of a small group of neurons of the system. Panels (C) and (D) present the same study, but considering a strong external input injected into every neuron. In these conditions, the dynamics of the network activity becomes highly synchronized, and displays the so called *population bursts*.

### 3.4.2 The spiking network model

The simulation of large neural networks is usually carried out by simply considering a large number of interconnected neurons, described with computationally efficient neuron and synapse models. This strategy is commonly denoted as spiking network model, since it is constituted by a network of interconnected spiking neurons<sup>3</sup>. Here we will focus on networks of IF neurons, which are convenient to numerically simulate large neural populations due to the computational efficiency of this neuron model. In addition, the mathematical simplicity of the IF neuron allows to obtain analytical

<sup>3</sup>The term spiking neuron reflects the capacity of a neuron model to generate well defined APs or spikes, in opposition with the McCulloch-Pitts neuron model in which a spike is represented roughly with a binary value  $s = +1$ .

expressions of the network activity for several situations of interest, and assuming certain approximations. Therefore, IF spiking networks constitutes a useful tool to investigate network dynamics as a first step, in order to translate their predictions into networks built with more complicated and detailed neuronal paradigms.

The system is constituted by  $N$  interconnected neurons, modelled with  $N$  differential equations of the form

$$\tau_m \frac{dV_i(t)}{dt} = -V_i(t) + I_i(t), \quad i = 1, \dots, N \quad (3.16)$$

where  $V_i(t)$  represents the membrane potential of the  $i$ -th neuron of the network,  $I_i(t)$  is the input current on the same neuron, and  $\tau_m$  is the membrane time constant. As it is explained in the section 3.2.4, a spike is generated by the  $i$ -th neuron when the membrane potential reaches certain threshold value, that is, when  $V_i(t) \geq V_{th}$ , and after that the voltage is set to  $V_i(t) = V_r$  during a refractory time  $\tau_{ref}$ . The input current  $I_i(t)$  is usually composed of a term corresponding to a external stimuli and a term associated with the signals arriving from the other neurons in the network, namely  $I_i(t) = I_i^{ext}(t) + I_i^{rec}(t)$ . While the expression of the external stimuli strongly depends on the particular modeling interest, the recurrent part is in general given by

$$I_i^{rec}(t) = \sum_{j \neq i}^N \sum_{k=1}^{N_t} \tau_m J \delta(t - t_j^k - d), \quad (3.17)$$

where the first sum is extended to all neurons in the network, and the second sum takes into account the signals (spikes) arriving to the  $i$ -th neuron from the other neurons in the network. The parameter  $J$  denotes the synaptic strength, which is assumed here to be the same for all synapses and also fixed in time. Also, equation (3.17) considers that synaptic transmission occurs instantly and, therefore, is described by delta functions, that is, rise and decay synaptic times are zero (see section 3.3.2 for details). Finally, it is worthy to note that the resulting network is fully-connected (that is, each neuron is connected to all the other neurons of the network), although other network topologies can be included easily.

In addition to be computationally convenient, the system described above allows a mean-field treatment that proportionates a theoretical description of the network dynamics and statistics up to some level. For instance, the network mean firing rate, coefficient of variation (CV), or even the probability distribution of inter-spike-intervals (also called ISI distributions) can be obtained for this type of networks (Tuckwell, 1989; Brunel, 2000). The stability properties of the solutions can be theoretically studied as well by employing different techniques (Brunel, 2000; Brunel and Hansel, 2006).



Figure 3.7: The Hopfield model, although of vital importance for the understanding of several brain processes such as associative memory, is also employed in the framework of artificial intelligence. In particular, it can be used to reconstruct previously stored images starting from impaired or incomplete versions of such images (Peretto, 1992). More elaborated versions, which take into account several synaptic considerations, allow for the classification and categorization of images, as well (Cortes et al., 2005).

This model, although allows to employ biophysically meaningful descriptions of neurons and synapses, is not convenient to assess the effect of certain collective properties of the neural systems. In particular, considering a single synaptic strength value  $J$  for all synapses constitutes a strong simplification in order to study certain neural features. The phenomenon of associative memory, for instance, strongly relies on synaptic modifications at large time scales, thus leading to certain level of synaptic heterogeneity. One of the strategies employed to study this issue is to consider several spiking network populations, and introducing inhomogeneity among the synapses of the different populations. This strategy, however, increases significantly the complexity and number of parameters of the system, and the extraction of useful information from the mean-field treatment becomes significantly more difficult. A simpler manner to address this issue in a theoretical manner is to employ tools from Statistical Mechanics on simplified neural network models, as we will see in the next section.

### 3.4.3 The Hopfield model

As we have briefly mentioned above, there are several interesting features of actual neural systems that cannot be achieved by considering networks with a single synaptic strength value  $J$  for all synapses of the network. One of the most astonishing is the phenomenon known as associative memory, which has been extensively studied in the literature (Hertz et al., 1991; Peretto, 1992; Hopfield, 1982). By virtue of this phenomenon, neural networks are able to retrieve information previously stored by simply presenting an input information sufficiently similar to the one previously stored.

Before analyzing in deep this property, we have to briefly review the physiological implications of *learning*. As we have mentioned in section 2.5.2, the Hebb's rule establishes the relation between the reinforcement of a synapse and the level of correlation in the activity of the two neurons linked by such synapse (Hebb, 1949). That is, reiterative activity is able to induce long-term plastic modifications which lead to specific changes in the synaptic weights. Synaptic reinforcements induced by neural activity have been measured in a wide variety of experimental situations, both *in vivo* and *in vitro*, as well as in psychophysical experiments (see, for instance, (Bliss and Collingridge, 1993; Malenka and Nicoll, 1999; Gruart et al., 2006)). However, the way these changes in synaptic weights lead to memory is not well understood yet. In the following, we will present a hypothesis which is well established in the computational neuroscience community.

It is generally assumed that when we contemplate a picture, meet a friendly face or experience a sensation, certain groups of neurons in the cortex start to fire. If this firing is prolonged enough, it will produce a strengthen in synapses connecting active neurons, as the hebbian rule states. As an example, let  $S_1$  and  $S_2$  be two of these active neurons, then the synaptic connection  $J_{12}$  which links them will be increased in strength in a certain quantity  $J_{12} \rightarrow J_{12} + \delta$ , with  $\delta > 0$  (for simplicity, we assume here a symmetric connection, that is,  $J_{12} = J_{21}$ ). Later, if we experience a similar sensation, some (but not all) of the neurons which were previously active will start firing again. This partial reactivation will drive the network, due to the prior selective reinforcement of synapses, towards the original pattern of activity associated with the first experience (which therefore has become an attractor of the dynamics of the system). In our previous example, if  $S_1$  is firing in the new situation but  $S_2$  is not, the previous reinforcement of the connection  $J_{12}$  will increase the signal strength that  $S_2$  receives from  $S_1$ , and as a consequence  $S_2$  will start firing. The phenomenon described above is known in the literature as associative memory, and constitutes a paradigmatical example of emergent large-scale phenomena induced by cooperativity between microscopic elements —neurons and synapses.

The first mathematical model which quantitatively demonstrated the plausibility of associative memory was developed independently by Amari (Amari, 1972) and Hopfield (Hopfield, 1982), although nowadays it is commonly referred as the Hopfield model. The model is constituted by  $N$  binary (McCulloch-Pitts like) neurons, which evolve in discrete time steps according to some probabilistic rule

$$\text{Prob}[s_i(t+1) = 1] = \mathcal{S}[\beta h_i(t)], \quad (3.18)$$

where  $s_i(t)$  represent the activity state of the  $i$ -th neuron of the network, being  $s_i(t) = -1$  a silent neuron and  $s_i(t) = +1$  a firing neuron. The function  $\mathcal{S}(x)$  represents a sigmoidal function which ranges from  $-1$  to  $+1$ , as for instance  $\mathcal{S}(x) = \tanh(x)$ . The parameter  $\beta \equiv 1/T$  is related with the level of stochasticity in the network, with  $T$  being the temperature of the system—in the sense of the Statistical Mechanics theory. The local field  $h_i(t)$  of the  $i$ -th neuron, which can be identified as the input current to that neuron, is expressed as

$$h_i(t) = \sum_{j \neq i}^N J_{ij} s_j. \quad (3.19)$$

In order to *store* a given number  $P$  of memories or activity patterns, the synaptic intensities  $J_{ij}$  have to take convenient values. They are usually chosen to follow a simple hebbian rule, expressed in the following form

$$J_{ij} = \frac{1}{N} \sum_{\mu=1}^P \xi_i^\mu \xi_j^\mu, \quad (3.20)$$

where  $\xi_i^\mu = \pm 1$  is the activity of the  $i$ -th neuron for the  $\mu$ -th stored pattern. Via equation (3.20), a number  $P$  of activity patterns can be stored in the synaptic weights  $J_{ij}$ ,  $\forall i, j \in [1, 2, \dots, N]$ . It is worthy to note that the hebbian rule here exposed is symmetric, that is,  $J_{ij} = J_{ji}$ ,  $\forall i, j$ . Although this hypothesis is far from being biophysically realistic, it is quite useful from a theoretical point of view, since it allows to employ here some of the mathematical tools of Statistical Mechanics of disordered systems. In particular, the stationary state of the system is characterized by a Gibbs-like probability distribution  $P(\mathbf{s}) \sim \exp(-\beta H(\mathbf{s}))$ , with  $H(\mathbf{s}) = -\frac{1}{2} \sum_i h_i(t)$  being the equilibrium hamiltonian of the system (see, for instance, (Peretto, 1992)).

The storage of a given pattern of activity in the synaptic weights  $J_{ij}$  yields the appearance of two attractor in the dynamics of the system. Concretely, when a pattern  $\mu$  is stored, an attractor associated with such pattern appears, and also an attractor associated with the corresponding *antipattern* ( $\xi_i^\mu \rightarrow -\xi_i^\mu$ ,  $\forall i$ ). However, since antipatterns do not provide new information to be retrieved, they are usually ignored in the computations of storage capacity of Hopfield networks. Due to this

association between stored activity patterns and dynamical attractors, Hopfield-like models are commonly denoted as attractor neural networks (ANN) in the literature.

How can an ANN exhibit associative memory properties? When one sets an initial condition similar enough to one stored pattern  $\mu$ , we are setting an initial condition for the dynamics of the system which is located, in the phase space of the system, within the basin of attraction of the stored pattern  $\mu$ . As a consequence of that, the activity of the system will rapidly tend to the attractor  $\mu$  and the stored information will be retrieved. This retrieval property mimics the associative capacities of the brain to recover previously learned information and complete memories from partial or incomplete information about them. The degree of similarity of a certain state of the network with a given pattern  $\mu$  is usually measured by defining the overlap function with such pattern, that is

$$m^\mu(t) \equiv \frac{1}{N} \sum_{i=1}^N s_i(t) \xi_i^\mu. \quad (3.21)$$

The Hopfield model can be analytically solved within the Statistical Mechanics theory for spin-glasses, by using a mean-field replica trick (Amit et al., 1987). This mean-field treatment allows to characterize the phases of the system, the stability of such phases, or the maximum storage capacity of the model, for instance. Although the steady state of the general model defined above represents an equilibrium system in the sense of the Statistical Mechanics, some nonequilibrium versions of such model can be studied by using for instance effective hamiltonians or different approaches, giving theoretical predictions which fits quite well with numerical simulations. Some interesting situations, such as the presence of fast synaptic mechanisms which strongly alters the dynamics of the system, fall into this class of nonequilibrium frameworks. Therefore, the Hopfield model constitutes not only a highly useful neural network model (from the conceptual point of view), but also a relevant model for the Statistical Physics community, with a significative number of interesting collective properties and emergent behaviors.

#### 3.4.4 The neural field model

The neuron models introduced previously consider explicitly the dynamics of individual neurons, or small populations of them. Since they constitute a good description for small homogeneous structures, the lack of spatial metric on these models may be an inconvenient when modeling large-scale structures such as a macroscopic volume of the cortex. Since the number of neurons and synapses in even a small piece of cortex is immense, the use of large-scale models of the cortex is sometimes more convenient. A popular choice is to take a continuum limit and interpret the neural

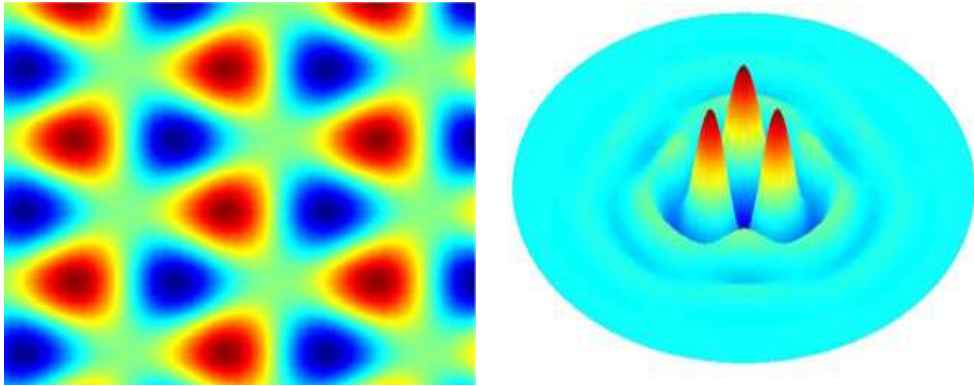


Figure 3.8: Left: An activity profile of a hexagonal pattern emerging beyond a Turing instability in a two-dimensional neural field model with short-range excitation and long-range inhibition. Right: A spatially localized 3-bump solution in a two-dimensional neural field model. Figure and caption have been taken from (Coombes, 2006).

activity as a magnitude which varies smoothly in space and time. Such approach is of big help to model situations in which spatial structuring of the neural activity becomes relevant, such as the pattern formation of electrical activity in large scale cortical regions. The models that work at this level are called neural field models, and relies on tissue level equations that describe the spatiotemporal evolution of coarse grained variables, such as the mean firing rate of neural populations.

One of the basic neural field models was presented in (Wilson and Cowan, 1973). Following this model, the neural field  $\phi(x, t)$ , which represents the local activity at time  $t$  of a population of neurons located at position  $x$ , evolves according to

$$\tau \frac{\partial \phi(x, t)}{\partial t} = -\phi(x, t) + \int_{-\infty}^{\infty} dy W(y) \mathcal{S}[\phi(x - y, t - |y|/v)] \quad (3.22)$$

where  $\tau$  is a constant related with the temporal decay of the neural field and  $\mathcal{S}(x)$  is the transduction function, which relates the input entering to a neuron with the activity caused by this input. The function  $W(y)$ , also referred as the synaptic footprint, gives the strength of the connections between two neurons separated by a distance  $y$ , where it is generally assumed that the system is spatially homogeneous and isotropic. One of the most common assumptions is to consider that  $W(y)$  follows a Mexican hat dependence, which implies local excitation and distal inhibition (Amari, 1975, 1977). It is worthy to note that the neural field variable inside the integral is delayed in time, due to the finite speed  $v$  of signal traveling over a distance  $y$ .

Neural field models have been used to investigate EEG rhythms, visual hallucinations, mechanisms for short term memory and motion perception, to name a few (Coombes, 2006; Ermentrout and Cowan, 1979; Bressloff, 2001). Despite its util-

ity, this kind of models present certain inconveniences, though. For instance, the nonlocal characteristics of neural field models make it difficult to obtain analytical results, even approximate. Therefore, this description strongly relies on numerical simulations to work, and this must be taken into account when considering the level of detail presented by the model, in order to keep the computation time within reasonable limits.

# Chapter 4

## Spike coincidence detection

In this chapter, we start presenting our original results concerning the study of the influence of short-term synaptic plasticity mechanisms in the computational properties of different neural systems of interest. Our first contribution has been the analysis of the effect of STD and STF in a basic information processing task: the detection of correlated signals in an environment of noisy activity. Since cortical activity is usually quite irregular, to understand the effect of short-term synaptic plasticity in the detection of correlated signals under such noisy conditions constitutes a highly relevant issue.

### 4.1 Introduction

It is widely known that *in vivo* cortical neurons usually present a high temporal irregularity in their firing patterns (Softky and Koch, 1993; Compte et al., 2003; Renart et al., 2007; Barbieri and Brunel, 2007). Such irregular behavior is observed at spontaneous activity levels, as well as in high persistent cortical states (Softky and Koch, 1993; Compte et al., 2003). The origin of this irregularity remains far to be understood, although several explanations concerning balanced states of network activity have been proposed (van Vreeswijk and Sompolinsky, 1996). It is commonly assumed that the irregularity of cortical states may constitute an advantage to several neural tasks, such as detecting weak signals (Ho and Destexhe, 2000; Fellous et al., 2003) (see also chapter 5) or switching between patterns of neural activity (Pantic et al., 2002; Torres et al., 2007) (see also chapter 7). Because of this, the study of the biophysical mechanisms involved in the transmission of signals in neural noisy environments constitute a relevant issue.

This transmission of meaningful information embedded in noisy inputs, however, may be strongly dependent of several synaptic processes, such as short-term depression and facilitation, which could modulate the postsynaptic response in different

manners. As we already introduced in chapter 2, the first of these mechanisms considers that the amount of available neurotransmitters in the synaptic buttons is limited and, therefore, the neuron needs some time to recover these synaptic resources in order to transmit the next incoming spike. As a consequence, the dynamics of the synapse is affected by an activity-dependent mechanism which produces non-linear effects in the postsynaptic response. This picture differs from the classical synaptic description which considers the synaptic strengths as static identities, with the only possible time modification due to a slow learning process (Hopfield, 1982). Moreover, it is well known that short-term depression plays an important role in several emerging phenomena in the brain, such as selective attention (Buia and Tiesinga, 2005; McAdams and Maunsell, 1999) and cortical gain control (Abbott et al., 1997), and it is responsible for the complex switching behavior between activity patterns observed in neural network models with depressing synapses (Pantic et al., 2002; Cortes et al., 2006). However, a complete theoretical study of other synaptic mechanisms, as synaptic facilitation – which compete with depression during synaptic transmission in networks of pyramidal neurons – is still lacking. Synaptic facilitation is produced by the influx of calcium ions into the cell through voltage-sensitive channels which favors the neurotransmitter vesicle depletion. This has been reported to be relevant for synchrony and selective attention (Buia and Tiesinga, 2005), and in the detection of bursts of action potentials (AP) (Matveev and Wang, 2000; Destexhe and Marder, 2004). One would expect, therefore, that synaptic facilitation had a positive effect, for instance, in the efficient transmission of temporal correlations between spike trains arriving from different synapses. This feature, known as synaptic coincidence detection (CD), has been measured *in vivo* in cortical neurons and related with some dynamical processes which affect to neuron firing thresholds (Azouz and Gray, 2000), so that it seems to be an important mechanism for efficient transmission of information in actual neural media.

In this chapter, we used the phenomenological model of dynamic synapses originally introduced in (Tsodyks et al., 1998) (see also chapter 3), which includes depressing and facilitating mechanisms, to explore the consequences of the cooperative effect of both in spike CD tasks. That is, we computed the regions, in the space of the relevant parameters, in which a postsynaptic neuron can efficiently detect temporal coincidences of spikes arriving from  $N$  different afferents. The aim of such study is to determine the range of the parameters which defines the dynamic of the synapses and the neuron for which the performance of the neural system in such experiments is improved. Our study shows that facilitation enhances the detection of correlated spikes and firing rate changes in situations for which the mechanism of depression alone does not perform well. These main results are robust and persist even when one decreases the degree of correlation between the afferents or consider

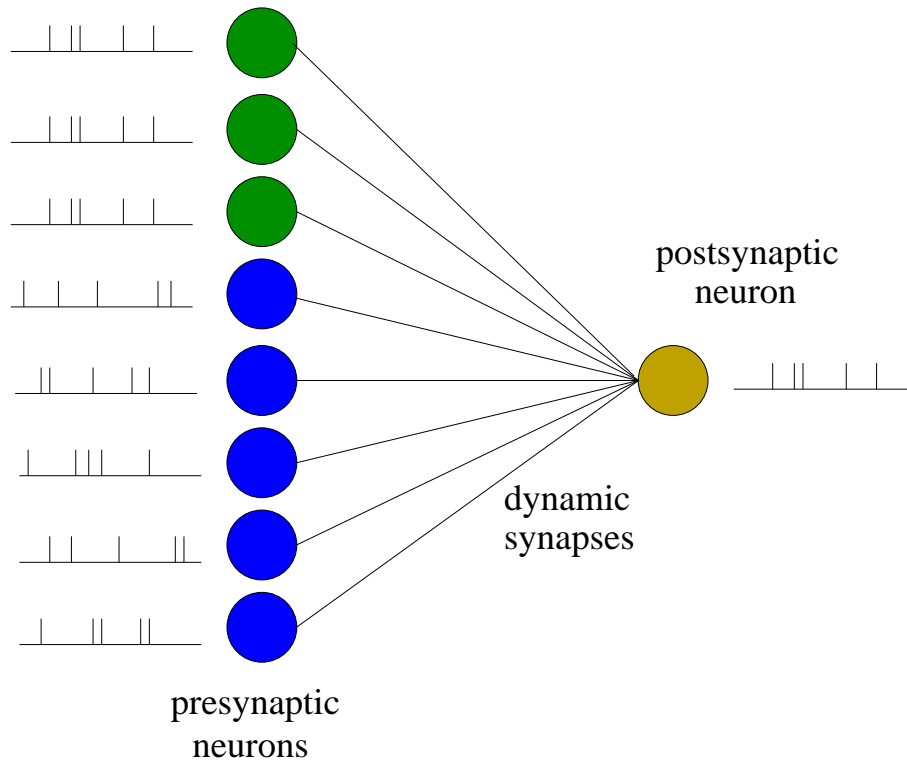


Figure 4.1: Scheme of the system under study. The postsynaptic neuron (in yellow) receives signals from  $N$  presynaptic neurons. A certain subset of  $M$  ( $< N$ ) neurons (in green) fire APs strongly correlated in time, while the rest of neurons fire independently of each other (in blue). This may be appreciated in the time series of APs next to each neuron in the plot. The aim is to analyze the conditions in which the postsynaptic signal is able to detect the coincident inputs (that is, the signal term) within a uncorrelated background activity (which acts as a noise term).

more realistic situations, as for instance, stochastic individual synapses (Dobrunz and Stevens, 1997; de la Rocha and Parga, 2005). Synaptic facilitation also determines the existence of an optimal frequency which allows the best performance for a wide range of values of the neuron firing threshold. The location of this optimal frequency can also be controlled by means of facilitation control parameters. This property could be important for actual neural media, constituted by neurons which presents heterogeneity in their firing thresholds (Azouz and Gray, 2000), to efficiently process information codified, for instance, at this frequency.

## 4.2 The model

The system under study is schematized in figure 4.1. We consider a postsynaptic neuron which receives signals from  $N$  presynaptic neurons through excitatory synapses. As a first approximation to model experimental data, we assume that

the stimulus received by a particular neuron, as a consequence of the overall neural activity, is modeled by a spike train following a Poisson distribution with mean frequency  $f$  (see (Tsodyks et al., 1998) for details). According to the phenomenological model presented in (Tsodyks and Markram, 1997) (and already introduced in chapter 3), we consider that the state of the synapse  $i$  is governed by the system of equations

$$\begin{aligned}\frac{dx_i}{dt} &= \frac{z_i}{\tau_{rec}} - U_i(t)x_i\delta(t - t_{sp}) \\ \frac{dy_i}{dt} &= -\frac{y_i}{\tau_{in}} + U_i(t)x_i\delta(t - t_{sp}) \\ \frac{dz_i}{dt} &= \frac{y_i}{\tau_{in}} - \frac{z_i}{\tau_{rec}},\end{aligned}\tag{4.1}$$

where  $x_i, y_i, z_i$  are the fraction of neurotransmitters in a recovered, active and inactive state, respectively. Here,  $\tau_{in}$  and  $\tau_{rec}$  are the inactivation and recovery time constants, respectively. Depressing synapses are obtained for  $U_i(t) = U_{SE}$  constant, which represents the maximum amount of neurotransmitters which can be released (activated) after the arrival of each presynaptic spike. The delta functions appearing in (4.1) consider that an AP arrives at the synapse in a fixed time  $t = t_{sp}$ . Typical values of these parameters in cortical depressing synapses are  $\tau_{in} = 3 \text{ ms}$ ,  $\tau_{rec} = 800 \text{ ms}$ , and  $U_{SE} = 0.5$  (Tsodyks and Markram, 1997).

The synaptic facilitation mechanism can be introduced assuming that  $U_i(t)$  has its own dynamics related with the release of calcium from intracellular stores and the influx of calcium from the extracellular medium each time an AP arrives. Here, we consider the dynamics proposed in (Tsodyks and Markram, 1997), that is,

$$U_i(t) \equiv u_i(t)(1 - U_{SE}) + U_{SE}\tag{4.2}$$

with

$$\frac{du_i(t)}{dt} = -\frac{u_i(t)}{\tau_{fac}} + U_{SE}[1 - u_i(t)]\delta(t - t_{sp}).\tag{4.3}$$

Here,  $u_i(t)$  is a dynamical variable which takes into account the amount of calcium ions entering into the presynaptic neuron near the synapse due to the opening of voltage-sensitive ion channels when the AP reaches this region (Bertram et al., 1996). These ions can usually bind to some acceptor which gates and facilitates the release of neurotransmitters. A typical value for the facilitation time constant is  $\tau_{fac} = 530 \text{ ms}$  (Markram et al., 1998). The variable  $U_i(t)$  in (4.2) represents then the maximum fraction of neurotransmitters that can be activated, either by the arriving of a presynaptic spike ( $U_{SE}$ ) and by means of facilitating mechanisms (i.e.,  $u_i(t)(1 - U_{SE})$ ).

One can think that the postsynaptic current generated in a particular synapse is proportional to the fraction of neurotransmitters which are in the active state, that

is,  $I_i = A_{SE} \cdot y_i$ , where  $A_{SE}$  is the maximum postsynaptic current that can be generated<sup>1</sup>. Hereafter, we will choose  $A_{SE} \approx 42.5 \text{ pA}$  which is within the physiological range and gives an optimal system performance for  $V_{th} = 13 \text{ mV}$ . In fact, we used this value of  $V_{th}$  because is very near to the mean value threshold measured in some cortical areas (Azouz and Gray, 2000). The total postsynaptic current, generated by signals arriving from the  $N$  excitatory synapses, can be written, therefore, as  $I_{total} = \sum_{i=1}^N I_i$ . This current generates a postsynaptic membrane potential which we modeled using an integration-and-fire (IF) neuron model, i.e.,

$$\tau_m \frac{dV}{dt} = -V + R_{in} I_{total}, \quad (4.4)$$

where  $R_{in} = 0.1 \text{ G}\Omega$  and  $\tau_m = 15 \text{ ms}$  are, respectively, the input resistance and the membrane time constant. These typical values have been taken also from pyramidal cells (Tsodyks and Markram, 1997). The IF neuron model assumes that, once the membrane potential reaches a certain threshold  $V_{th}$ , above the resting potential  $V_{rest} = 0$ , an AP is generated and  $V(t)$  is reset to zero. We assume, in addition, the existence of a refractory period of  $\tau_{ref} = 5 \text{ ms}$  during which  $V(t)$  remains in zero after the generation of each postsynaptic AP.

### 4.3 Results

We have studied first the postsynaptic response of a neuron receiving input signals from  $N = 1000$  excitatory synapses, with a subset of  $M = 200$  synapses stimulated by identical spike trains with mean frequency  $f$ . These strongly correlated afferents fire spikes which are synchronized in time and we consider them as a *signal* term. The remaining  $N - M$  synapses receive uncorrelated spike trains (also with mean frequency  $f$ ) which constitute, therefore, a *noisy* background of activity which is added to the signal. We have investigated, both analytically and numerically, spike coincidence detection (CD) experiments. Our interest is to determine the values of the synapse and neuron parameters for which the postsynaptic neuron can detect the embedded signal, i.e., its response is strongly correlated with the input signal.

A typical CD experiment is illustrated in Fig. 4.2. This shows the effect of including facilitation compared with the situation in which only depression is considered. For relatively high values of the parameter  $U_{SE}$ , the system presents good performance in the CD of the incoming signals for both cases, and the simulations

---

<sup>1</sup>Note that it is the synaptic conductance, rather than the synaptic current, which depends on  $A_{SE} \cdot y(t)$ . Our assumption for the current, however, is a good approximation when the membrane potential  $V(t)$  is below the firing threshold  $V_{th}$  and  $\tau_m \gg \tau_{in}$ , so that  $V(t)$  remains constant during the temporal variation of the synaptic conductance.

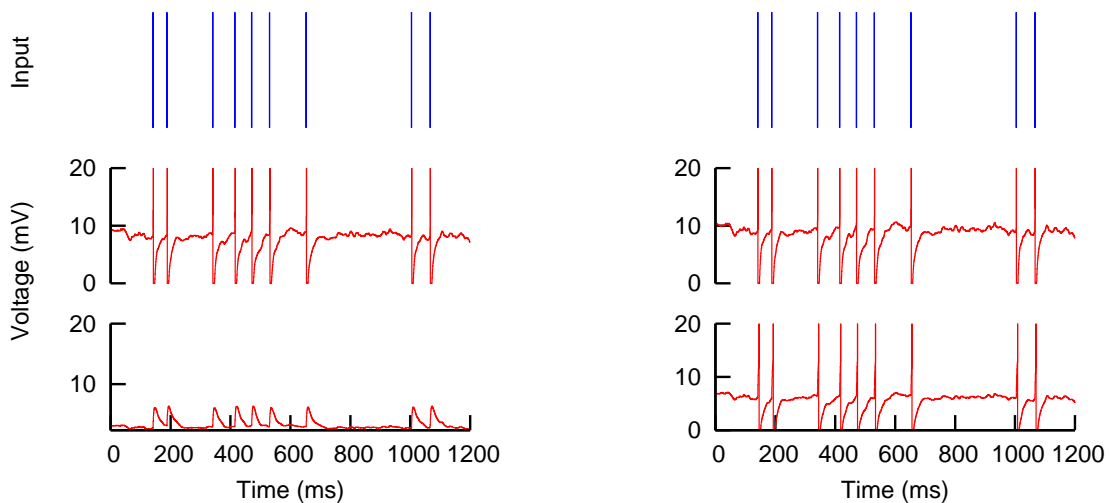


Figure 4.2: Response of a postsynaptic neuron receiving a Poisson spike train (Top panel) at frequency of  $10 \text{ Hz}$  from  $N = 1000$  presynaptic neurons through dynamic synapses. Left and right panels correspond, respectively, to the case of depressing and facilitating synapses. In the simulations,  $U_{SE}$  takes the values  $0.5$  (middle panel) and  $0.01$  (bottom panel), respectively, and the threshold is fixed to  $13 \text{ mV}$ . The figure shows that facilitation enhances CD tasks for relatively low values of  $U_{SE}$ .

do not show any remarkable differences when one includes facilitation. The reason is that the facilitation term becomes irrelevant in equation 4.2 for high values of  $U_{SE}$ , and depression is the only mechanism contributing to the dynamics. For small  $U_{SE}$ , however, the detection of the signal is improved in the presence of the facilitating mechanism. In fact, when  $U_{SE}$  takes low values, the contribution of depression to  $U_i(t)$  – which gives the strength of the synapse – becomes irrelevant. In this situation, facilitation still contributes to maintain  $U_i(t)$  highly enough to allow a good performance on the CD task.

For a more general evaluation and quantification of the role of the facilitating mechanism, one may compute the fraction of errors that occur in the detection of the presynaptic signal by the postsynaptic neuron, as a function of the incoming frequency  $f$  and the neuron threshold  $V_{th}$ . These 2-dimensional CD error *maps* give a better perspective of the regions, in the space of the relevant parameters, where the system has good performance. Thus, for each pair  $(f, V_{th})$ , one can compute, in the stationary regime and during a large temporal interval  $T$ , 1) the number of coincidence-input-events produced by strongly correlated signals through  $M$  presynaptic neurons, namely  $N_{inputs} \equiv f \cdot T$ , 2) the number of output spikes in the postsynaptic neuron which occur immediately within a time-window of  $\Delta = 5 \text{ ms}$  after

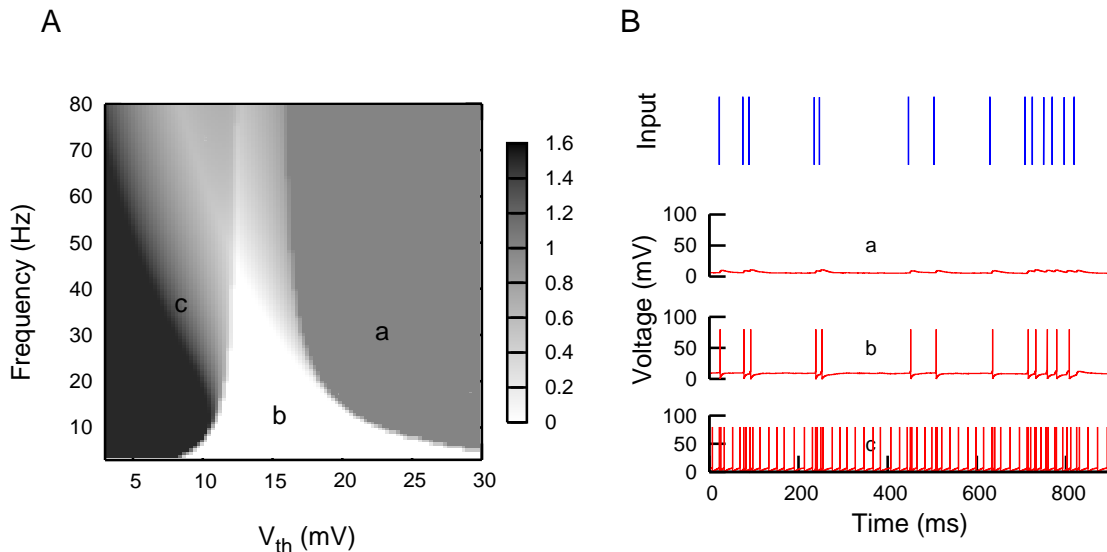


Figure 4.3: Panel A shows a typical coincidence detection map, as defined in the text, with depressing synapses ( $U_{SE} = 0.5$ ,  $\tau_{rec} = 800$  and  $\tau_{fac} = 0$ ). Panel B depicts the corresponding temporal behavior of the postsynaptic membrane potential for several situations marked in the map with labels. It shows examples of failures in the detection (a), successful detections or hits (b) and false spikes (c). Situations (a) and (c) correspond in the map to high error zones.

each coincidence-input-event, that is  $N_{hits}$ ,<sup>2</sup> 3) the number of output spikes which are not hits,  $N_{falses}$ , and finally 4) the number of coincidence-input-events which did not result in output spikes within the time window  $\Delta$ , namely  $N_{failures}$  (Pantic et al., 2003). The fraction of errors is then defined as

$$E(f, V_{th}) \equiv \frac{N_{failures} + N_{falses}}{N_{inputs}}. \quad (4.5)$$

Analytical expressions for the quantities appearing in (4.5) have been obtained by integration of the model equations (4.1-4.4) and their derivation is explained in the following section.

### 4.3.1 Mean-field calculations

Motivated by the preliminary numerical simulations presented in the previous section, we derive here analytical expressions for the functions appearing in the definition of the error function (4.5). This error function will be used to theoretically obtain the regions for good spike coincidence detection in the  $(f, V_{th})$  parameter space.

<sup>2</sup>The specific value of  $\Delta$  is not too critical for the results found if moderated values are used. In particular, it is convenient to have  $\Delta \sim \tau_{ref}$  since this is a natural window for spike detection.

First, we assume that the total presynaptic current can be divided in two terms: a signal term containing the correlated embedded signal and a noise term formed by the background of uncorrelated spikes.

#### A. Noise contribution

To take into account the noise generated by  $N - M$  uncorrelated spikes trains, we assume that the current at time  $t = t^* + \tau$  generated by a single spike arriving to the synapse  $i$  at time  $t^*$  is given by a simplified alpha function (when we have considered that the rise time constant is small enough), that is,

$$I_i(\tau, t^*) = I_{peak} \exp(-\tau/\tau_{in}) \quad (4.6)$$

where  $I_{peak}$  represents the averaged stationary EPSC amplitude obtained after stimulation with a periodic spike train, assumption that we also suppose valid for Poisson distributed spike train. After this consideration, one easily obtains from equations (4.1-4.3) that

$$I_{peak} = A_{SE} \frac{U_\infty (1 - \exp(-1/f\tau_{rec}))}{1 - (1 - U_\infty) \exp(-1/f\tau_{rec})} \quad (4.7)$$

with  $U_\infty = u_\infty(1 - U_{SE}) + U_{SE}$ , where  $u_\infty$  is the value of  $u(t)$  in the stationary state ( $t \rightarrow \infty$ ). For a periodic spike train,  $u_\infty$  is given by

$$u_\infty = U_{SE} \frac{\exp(-1/f\tau_{fac})}{1 - (1 - U_{SE}) \exp(-1/f\tau_{fac})}. \quad (4.8)$$

We can compute the mean noise contribution of the current and fluctuations using the standard expressions

$$\begin{aligned} I_{noise} &\equiv \langle I \rangle, \\ \sigma_{I_{noise}}^2 &\equiv \langle I^2 \rangle - \langle I \rangle^2. \end{aligned} \quad (4.9)$$

From these definitions and using the central limit theorem we obtain

$$I_{noise} = (N - M) A_{SE} f \tau_{in} U_\infty \frac{1 - \exp(-1/f\tau_{rec})}{1 - (1 - U_\infty) \exp(-1/f\tau_{rec})} \quad (4.10)$$

where we assumed that  $\tau_{in} \ll \tau_{rec}$  (for details on this calculation for periodic and poissonian spike trains see appendix A). If we neglect fluctuations ( $\sigma_{I_{noise}} = 0$ ), we can write  $V_{noise} = R_{in} I_{noise}$ . Using this expression one can compute  $N_{falses}$  taken into account that false firing occurs when  $V_{noise} > V_{th}$  so by a direct integration of equation (4.4) in a period of time  $T$  gives  $N_{falses} \approx T / \{\tau_{ref} - \tau_m \ln(1 - V_{th}/V_{noise})\}$  (Koch, 1999). Now using that  $f = N_{inputs}/T$ , we finally obtain as in (Pantic et al., 2003)

$$N_{falses} = \frac{\Theta(V_{noise} - V_{th}) N_{inputs}}{f(\tau_{ref} - \tau_m \ln(1 - V_{th}/V_{noise}))} \quad (4.11)$$

where  $\Theta(x)$  is the Heaviside step function, which takes into account that for  $V_{noise} < V_{th}$ , one obtains  $N_{falses} = 0$ .

To take into account fluctuations of  $I_{noise}$  one can use the so called hazard function approximation (Plesser and Gerstner, 2000) but it has been reported that it gives the same results than those obtained using the formula (4.11) for high frequencies and, on the contrary to the expression (4.11), it does not work properly for small frequencies (see details in (Pantic et al., 2003)). Therefore, hereafter we will neglect fluctuations in  $I_{noise}$  and use (4.11) as an approximatively valid expression to analytically compute  $N_{falses}$ .

### B. Signal contribution

To analyse the signal contribution (arising from  $M$  coincident spikes) we used the same method developed in (Pantic et al., 2003) for the case of only-depressing synapses. That is, assuming that  $V(0; t^*)$  is the membrane potential at  $t = t^*$  when  $M$  coincident spikes arrive, by direct integration of the equation (4.4) the membrane potential at time  $t = t^* + \tau$  is

$$V(\tau; t^*) = e^{\tau/\tau_m} \left\{ V(0; t^*) + \frac{R_{in} M I_{peak}}{\tau_m \alpha} [e^{\alpha \tau} - 1] \right\} \quad (4.12)$$

where  $\alpha = \frac{\tau_{in} - \tau_m}{\tau_{in} \tau_m}$  and  $I_{peak}$  is given by (4.7) and it includes all the effects due to synaptic depression and facilitation. If the next signal event (that is, the next  $M$  coincident spikes) occurs at  $t = t'$  one can obtain the following recurrence relation:

$$V(0; t') = e^{\Delta t / \tau_m} \left\{ V(0; t^*) + \frac{R_{in} M I_{peak}}{\tau_m \alpha} [e^{\alpha \Delta t} - 1] \right\} \quad (4.13)$$

with  $\Delta t = t' - t^*$ , which allows for computing the stationary value for the membrane potential at the exact time of the signal-event arrival (see also (Kistler and van Hemmen, 1999)), that is:

$$V_{st} = e^{-\Delta t / \tau_m} \frac{R_{in} M I_{peak}}{\tau_m \alpha} \frac{e^{\alpha \Delta t} - 1}{(1 - e^{-\Delta t / \tau_m})}. \quad (4.14)$$

We define  $V_{signal}$  as the maximum of the membrane potential reached between the arrival of two consecutive signal events separated by a time  $\Delta t$ . This can be easily computed from equation (4.12) with  $V(0, t^*)$  being replaced by  $V_{st}$ :

$$V_{signal} = \left[ \frac{\tau_m (1 - \exp(-1/f \tau_m))}{\tau_{in} (1 - \exp(-1/f \tau_{in}))} \right]^{\frac{\tau_m}{\tau_{in} - \tau_m}} R_{in} M I_{peak}, \quad (4.15)$$

where we consider  $\tau = \Delta t \simeq 1/f$ .

The expression of  $V_{signal}$  allows for an evaluation of the number of failures assuming that  $N_{failures} = N_{inputs} - N_{hits}$ . Then, one obtains by direct integration of equation (4.4) an using the same reasoning that for  $N_{false}$  case that

$$N_{failures} = N_{inputs} \left[ 1 - \frac{\Theta(V_{noise} + V_{signal} - V_{th})}{f[\tau_{ref} - \tau_m \ln(1 - (V_{th} - V_{signal})/V_{noise})]} \right], \quad (4.16)$$

where we have considered a hit event every time  $V_{noise} + V_{signal}$  reach  $V_{th}$ . Note that from (4.16) if  $V_{noise} + V_{signal} < V_{th}$  we will have  $N_{failures} = N_{inputs}$ . Expression for  $N_{false}$ ,  $N_{failures}$  allows for theoretically compute the fraction of errors, as defined in equation (4.5), in the CD maps for different situations of interest.

### 4.3.2 Detection of strongly correlated signals

In order to characterize the CD abilities of the system, we have computed both theoretical and numerical CD maps using the error function (4.5) for different values of the neuron and synapse relevant parameters. An illustrative example of these maps is shown in Fig. 4.3A. The light area corresponds to regions where the postsynaptic neuron is able to efficiently detect the coincidence-input-events, and to generate a postsynaptic response strongly correlated with the embedded signal (see time series "b" on Fig. 4.3B). Simulations show that this low error situation mainly occurs for  $E \lesssim 0.6$ . Dark areas, however, are regions with a high percentage of errors ( $E \geq 1$ ). These errors can be produced, for instance, when  $N_{failures}$  is large (see time series "a" on Fig. 4.3B), which occurs for  $V_{th}$  very large (grey areas), or when  $N_{false}$  increases (see time series "c" on Fig. 4.3B), normally for small  $V_{th}$ , such that any current can produce a false event (black areas).

On the other hand, figure 4.4 depicts the role of the inclusion of synaptic facilitation on signal detection compared with the situation of only-depressing synapses. For a fixed value of the facilitation time constant  $\tau_{fac}$ , there is a clear dependence on  $U_{SE}$  in the signal detection properties of the system. When its value increases (from top to bottom) the width of the light area enlarges and spreads to the right, allowing a better CD for regions with high thresholds. The left panels correspond to numerical simulations whereas the central panels are the same error function evaluated using the analytical formulas derived in section 4.3.1. The figure also shows the good agreement between theory and simulations. In the right panels, we computed the same CD maps but considering only the mechanism of synaptic depression. One observes that for only depression and a limited amount of neurotransmitters ( $U_{SE} < 0.5$ ), the low-error region is narrower, and one has a large region of good detection only for  $U_{SE}$  near to one. Similar results are found when one fixes  $U_{SE}$  and varies  $\tau_{fac}$ .

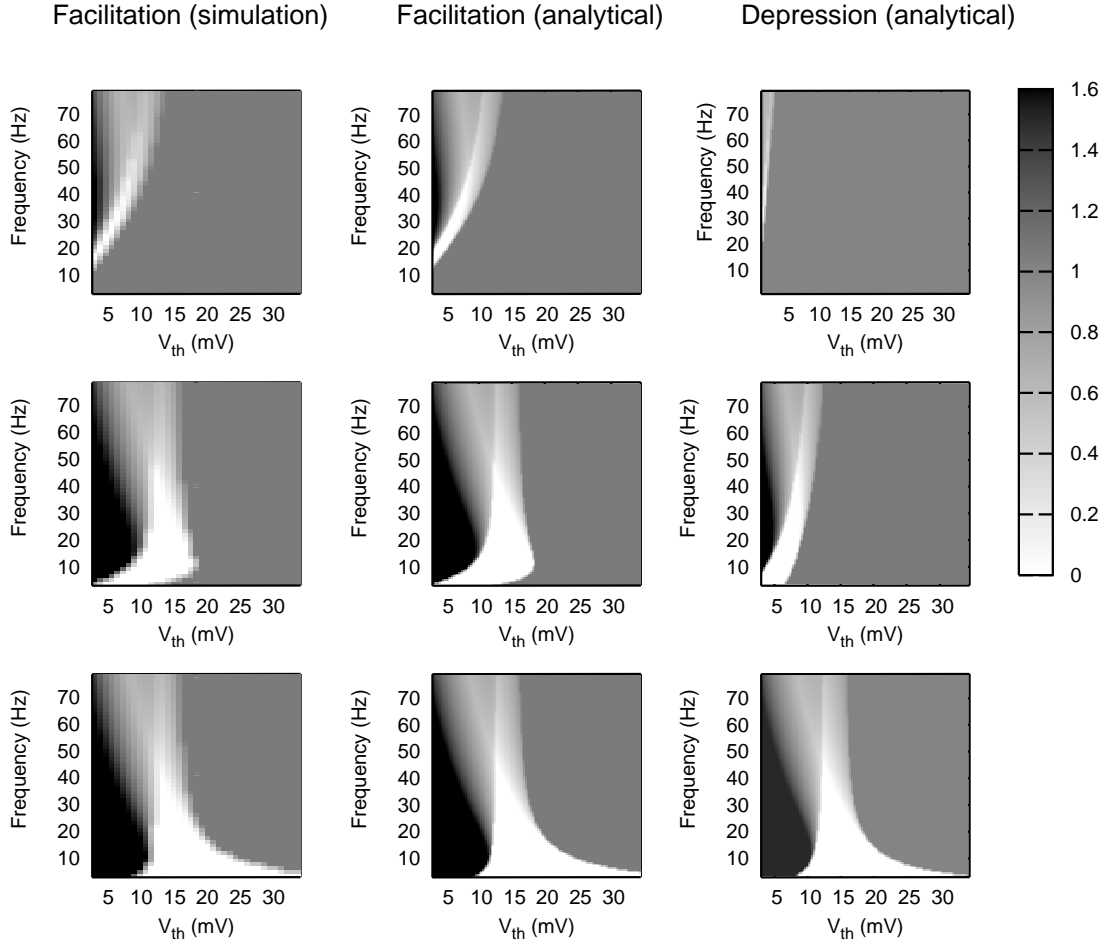


Figure 4.4: Coincidence detection maps for a system with facilitating synapses with  $\tau_{fac} = 530 \text{ ms}$  (left and center panels). The values of  $U_{SE}$  were, from top to bottom, 0.002, 0.05 and 0.5, respectively. The effect of increasing  $U_{SE}$  was the spreading of the region of good CD (light zone) to the right. Simulations (left) confirm the analytical results (center). In the right panels are presented the same CD maps for  $\tau_{fac} = 0$ , that is, the case of only-depressing synapses.

A better quantification of the role of synaptic facilitation can be visualized by computing the area of the light zones in the CD maps (low error zones, that is,  $E(f, V_{th}) < E_0 = 0.5$ ), and study the influence of  $\tau_{fac}$  and  $U_{SE}$  on the size of this area. Large light areas will indicate good performance of the system for a large variety of working frequencies and neuron firing thresholds. For this purpose we defined the quantity

$$F = 1 - \frac{1}{A} \int_{V_{th}} \int_f \Theta[E(f, V_{th}) - E_0] dV_{th} df, \quad (4.17)$$

which gives the fraction of area with small errors over the whole map. Here,  $A =$

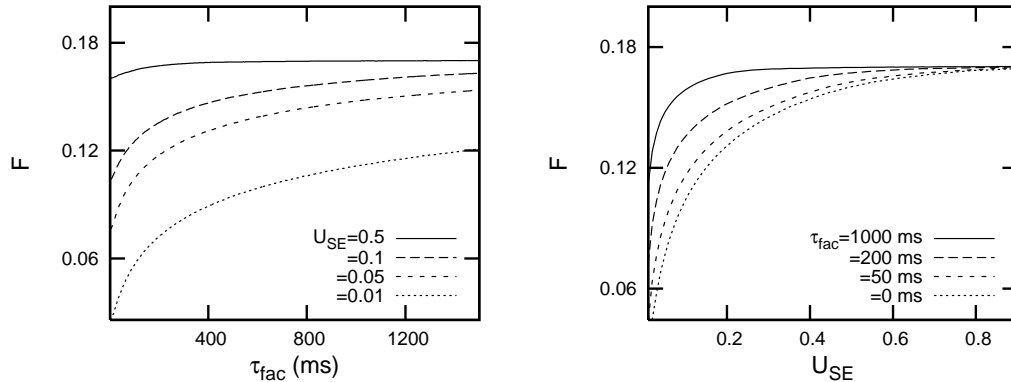


Figure 4.5: Fraction of area for good signal detection (that is, the region in which the error is below a certain value  $E_0$ ) as a function of  $\tau_{fac}$  (left plot) or  $U_{SE}$  (right plot), with  $E_0 = 0.5$ . Both maps show quantitatively that the inclusion of facilitation enlarges the area in which the signal is efficiently transmitted (note that the case of only-depressing synapses corresponds to  $\tau_{fac} = 0$ ). The window considered to calculate the area was  $f \in [1, 80]$ ,  $V_{th} \in [1, 35]$ .

$\int_{V_{th}} \int_f dV_{th} df$  is the total area of the map and  $\Theta(x)$  is the step function. Figure 4.5 shows the dependence of  $F$  with  $\tau_{fac}$  (left panel) and  $U_{SE}$  (right panel). Since  $F$  is an increasing function of  $\tau_{fac}$  (left panel) and the only-depression case corresponds to  $\tau_{fac} = 0$ , one concludes that the inclusion of facilitation leads to a higher area of good CD in the maps, for different values of  $U_{SE}$ . Similar results are found when one studies  $F$  as a function of  $U_{SE}$  (right panel). In this graph, the lowest curve corresponds to the case of only-depressing synapses ( $\tau_{fac} = 0$ ), and one observes that the addition of facilitation always leads to a higher  $F$  for any value of  $U_{SE}$ . These results are also robust for different values of  $E_0$  and different sizes of the  $(f, V_{th})$ -window which we use to calculate the total area. All these results show that, for the same value of the amount of activated neurotransmitters, the overall performance of the system is better with facilitation than if one only considers depressing mechanisms. This conclusion can be also observed when one fixes  $U_{SE}$  and varies the facilitation time constant  $\tau_{fac}$ . A large value for  $\tau_{fac}$  means an increase in the duration of the facilitating effect. As a consequence, the region for good detection enlarges compared with the situation of only depression, in special when the fraction of available resources is not too high.

A detailed observation of Fig. 4.4 also reveals the existence of a certain frequency, namely  $f_{opt}$  which allows a good performance for a wide (maximum) range of values of  $V_{th}$ . The center map in Fig. 4.4, for instance, shows a good perfor-

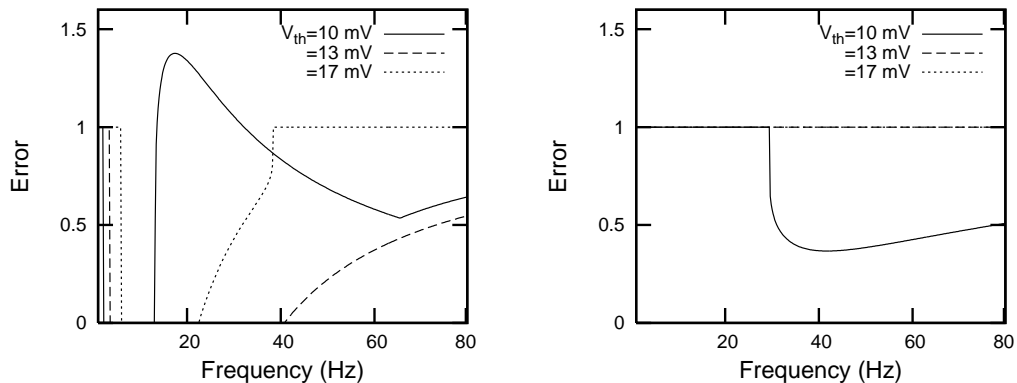


Figure 4.6: Behavior of the error function  $E(f, V_{th})$ , as defined in the text, for  $U_{SE} = 0.05$  and three different values of  $V_{th}$ , namely, 10 mV (solid line), 13 mV (dashed line) and 17 mV (dotted line). Left (Right) panel corresponds to depression-facilitation (only-depression) case. In the left panel, one can see a small region of frequencies (around  $\sim 10$  Hz) that allow to have zero error for the three threshold values considered. Indeed, there is a maximum interval of threshold values from 9 to 18 mV such that, this small region of frequencies tends to a single “optimal” frequency around 7 Hz.

mance in detecting signal frequencies around 7 Hz for a threshold ranging from 8 to 18 mV. The existence of this *optimal* frequency can be seen more clearly if we take several sections of the CD maps, with  $V_{th}$  fixed at certain value, as it is shown in Fig. 4.6. For depressing-facilitating synapses (left panel in the figure) there is a certain frequency value ( $\sim 7$  Hz) for which the error is zero for very different voltage threshold values within the range (10–17 mV). This feature is not found in the case of only-depressing synapses (right panel in the figure). Theoretically,  $f_{opt}$  can be computed from the analytical expression for  $V_{signal}$  and  $V_{noise}$  (see section 4.3.1) taking into account that, in general, it appears at relatively low frequencies. At these frequencies, the low error zone is obtained for  $V_{th} \in [V_{noise}, V_{noise} + V_{signal}]$ . Maximizing this range gives  $f_{opt}$ , as the solution of the equation

$$\left| \frac{\partial V_{signal}(f)}{\partial f} \right|_{f=f_{opt}} = 0. \quad (4.18)$$

A more detailed study using (4.18) reveals that  $f_{opt}$  decreases for increasing values of  $U_{SE}$ , or  $\tau_{fac}$ , as it is shown in Fig. 4.7 (Left panel). One also observes that the range of thresholds which allow for a good CD at  $f_{opt}$ , which corresponds to  $\Delta V_{th} \approx V_{signal}(f_{opt})$ , increases with  $U_{SE}$ , or  $\tau_{fac}$  (cf. Fig. 4.7 right panel). In the limit  $\tau_{fac} \gg 1$ , one expects, therefore, the larger  $\Delta V_{th}$  at  $f_{opt}$  near zero. For low

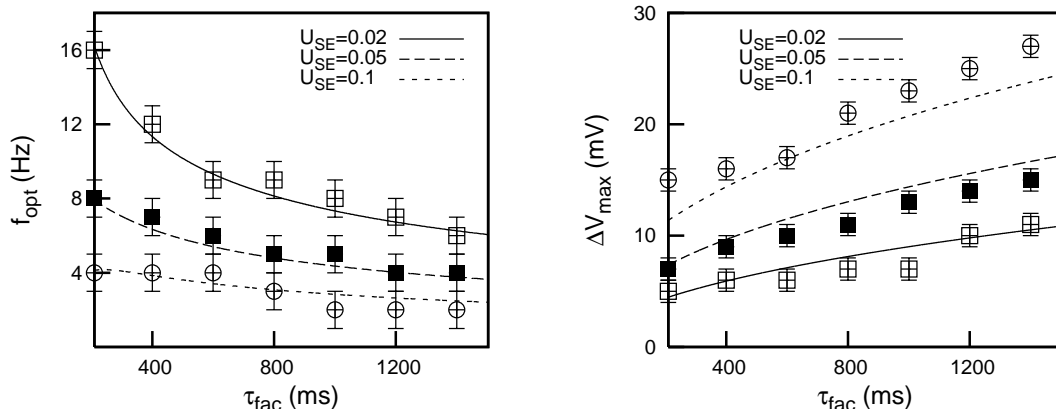


Figure 4.7: Dependence of  $f_{opt}$  and  $\Delta V_{th}$  (that is, the corresponding threshold-window of good CD) with the facilitation parameters  $\tau_{fac}$  and  $U_{SE}$ . The graph show that  $f_{opt}$  can be tuned by means of the facilitation parameters. The figure also shows the agreement between theory (lines) and simulations (symbols).

levels of facilitation, however, there is a critical value of  $\tau_{fac}$ , such that  $\Delta V_{th}$  at  $f_{opt}$  starts to become lower than  $\Delta V_{th}$  at zero frequency, and we have, then,  $f_{opt} = 0$  (data not shown). For only-depressing synapses, i.e.,  $\tau_{fac} = 0$ , one has always  $f_{opt} = 0$ . The conclusion is that a moderate level of facilitation is needed in order to have a non-zero  $f_{opt}$ . The possibility to tune this optimal frequency by means of the facilitation parameters could be important, for instance, to understand how actual neural systems – where different types of neurons may have non-identical firing thresholds – can self-organize to efficiently detect and process correlated signals at this optimal frequency.

By direct observation of the CD maps (for instance, the ones in figure 4.4), one also observes that, at certain threshold, there is a range of working frequencies, namely  $\Delta f$ , within which the neuron is able to efficiently detect and process incoming signals (with errors, for instance, less than 0.5). The study of the variation of  $\Delta f$  in the presence of facilitation and/or depression tell us, for instance, the ability of the neuron to detect or not complex signals that include many frequencies. In Fig. 4.8 we have performed this analysis for a fixed threshold around  $V_{th} = 13 mV$  – which is within the physiological range in cortical neurons – and study the system behavior for fixed  $U_{SE}$  and varying  $\tau_{fac}$  and vice versa. The figure shows (left panel) that  $\Delta f$  decreases with  $U_{SE}$  for the case of only-depressing synapses, and even vanishes for  $U_{SE} < 0.05$ . However, if the facilitating mechanism is also present, the system is able to recover the good performance by increasing the facilitation time constant.

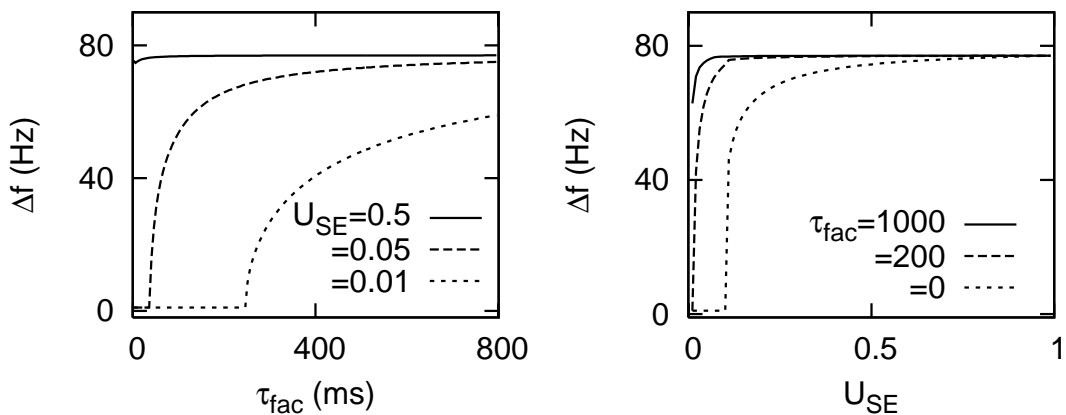


Figure 4.8: Variation of  $\Delta f$ , as defined in the text, for different values of  $U_{SE}$  and  $\tau_{fac}$ . Left panel:  $\Delta f$  as a function of  $\tau_{fac}$  for three fixed values of  $U_{SE}$ . Right panel:  $\Delta f$  as a function of  $U_{SE}$  for three fixed values of  $\tau_{fac}$ . In all cases  $V_{th}$  was set to  $13\text{ mV}$ . In both panels the only-depression case corresponds to  $\tau_{fac} = 0$ .

The figure also reveals (right panel) that facilitation always enlarges the maximum range of frequencies for any fixed value of  $U_{SE}$ . We conclude, therefore, that for any values of the synapse parameters the inclusion of facilitation improves the detection towards wider ranges of frequencies. Note that there is an abrupt change, from zero to nonzero values of  $\Delta f$ , in both panels of the figure 4.8 when one varies the synapse parameters  $U_{SE}$  or  $\tau_{fac}$ . The reason is that the analysis has been performed for  $V_{th}$  fixed around  $V^* = 13\text{ mV}$ . Then, one has  $\Delta f = 0$  for values of  $U_{SE}$  and  $\tau_{fac}$  such that the region of good detection occurs at thresholds smaller than  $V^*$  and, therefore, none frequency range is detected at  $V^*$ . Otherwise, non-zero  $\Delta f$  start to appear when, by increasing  $U_{SE}$  or  $\tau_{fac}$ , the light area of the map spreads to higher threshold values and reaches  $V^*$ .

### 4.3.3 The effect of jitter and synaptic fluctuations

The study of the detection of coincident signals which arrive from different presynaptic neurons has been treated in the previous section in an approximate way, i.e., the embedding signal was constituted by fully correlated temporal events that produce synchronized responses. In real situations, however, the incoming signals from different synapses do not produce strong correlated postsynaptic responses, mainly due to stochasticity during transmission through individual synapses (Dobrunz and Stevens, 1997). The model we used for synaptic transmission does not allow to consider these fluctuations because is deterministic. In this section, however, we explored how the main conclusions reported before are not affected by the inclusion

of some desynchronization (jitter) in the signal term which induces fluctuations in the postsynaptic response. We also studied in detail CD tasks with a more realistic stochastic synapse model which naturally induces such fluctuations in its dynamics.

*A. The effect of jitter:*

A first step to artificially introduce synaptic fluctuations, or other sources of noise in our system, is to assume a signal term, in the synaptic current, constituted by the effect of  $M$  presynaptic events that arrive at random times  $t_i$ , distributed around certain time  $t_0$ . We used here, for instance, a Gaussian distribution  $p(t_i)$  with a certain standard deviation or *jitter*  $\sigma$ . In the following, we consider the implications of this assumption to test the validity of the results previously obtained, and to investigate the effect of the jitter in the detection of signals that are not fully correlated in time.

We start by computing the excitatory postsynaptic current generated in a synapse  $i$  due to a single presynaptic AP occurring at time  $t_i$ , i.e.,

$$I_i(t) = I_{peak} \exp[-(t - t_i)/\tau_{in}], \quad t > t_i, \quad (4.19)$$

where  $I_{peak}$  is the steady-state maximum current through a synapse obtained after stimulation with a periodic spike train (see section 4.3.1 for details). Since  $t_i$  is a Gaussian distributed stochastic variable with  $\langle t_i \rangle = t_0$  and standard deviation  $\sigma$ ,  $q_i(t) \equiv \exp[-(t - t_i)/\tau_{in}]$  (with  $t$  fixed) is also a random variable with range  $[0, 1]$  and probability distribution given by

$$\mathcal{P}[q_i(t)] = \frac{2\tau_{in}}{q_i(t) \operatorname{erfc}\left(-\frac{t-t_0}{\sqrt{2}\sigma}\right)} \frac{1}{\sqrt{2\pi}\sigma} \exp\left[-\frac{(t-t_0 + \tau_{in} \ln[q_i(t)])^2}{2\sigma^2}\right], \quad (4.20)$$

where  $\operatorname{erfc}(x) = 1 - \operatorname{erf}(x)$  and  $\operatorname{erf}(x)$  is the error function. One can easily compute the two first moments for  $\mathcal{P}[q_i(t)]$ , i.e.:

$$\langle q_i(t) \rangle_q = \exp\left[\frac{1}{2}(\sigma/\tau_{in})^2 - (t-t_0)/\tau_{in}\right] \frac{\operatorname{erfc}\left[\frac{\sigma^2 - (t-t_0)\tau_{in}}{\sqrt{2}\sigma\tau_{in}}\right]}{\operatorname{erfc}\left[-\frac{t-t_0}{\sqrt{2}\sigma}\right]}, \quad (4.21)$$

$$\langle [q_i(t)]^2 \rangle_q = \exp\left[2(\sigma/\tau_{in})^2 - 2(t-t_0)/\tau_{in}\right] \frac{1 + \operatorname{erf}\left[\frac{-2\sigma^2 + (t-t_0)\tau_{in}}{\sqrt{2}\sigma\tau_{in}}\right]}{\operatorname{erfc}\left(-\frac{t-t_0}{\sqrt{2}\sigma}\right)}, \quad (4.22)$$

with  $\langle f(q) \rangle_q \equiv \int dq f(q) \mathcal{P}(q)$ . In the case of many afferents, the total postsynaptic current is  $I(t) = I_{peak} \sum_{i=1}^{\nu(t)} q_i(t)$ . Here,  $1 \leq \nu(t) \leq M$  is the fraction of the  $M$  afferents in which the AP has already generated a postsynaptic response at time  $t$ , and it is given by  $\nu(t) \approx M \int_{-\infty}^t p(t_i) dt_i$ . This number depends on time due to the

existence of the jitter that desynchronizes the postsynaptic effect of the AP in all afferents. For  $t \ll t_0$ ,  $\nu(t)$  is, therefore, small but for  $t$  near to and large than  $t_0$ ,  $\nu(t)$  is high and we can use the central limit theorem to obtain:

$$I(t) = I_{peak}\xi(t, t_0), \quad (4.23)$$

where  $\xi(t, t_0)$  is a Gaussian variable with mean and variance given by

$$\langle \xi(t, t_0) \rangle_\xi = \nu(t) \langle q(t) \rangle_q \quad (4.24)$$

and

$$\sigma_\xi^2 = \nu(t) [\langle q^2(t) \rangle_q - \langle q(t) \rangle_q^2], \quad (4.25)$$

with  $\nu(t) = \frac{M}{2} [\text{erf}(\frac{t-t_0}{\sigma}) + 1]$ . We will use, hereafter, this analytical approach to compute CD maps of a jittered signal.

Since  $\nu(t)$  needs to be high to use the central limit theorem, one expects that the theoretical current defined by equations (4.23-4.25) will fit better the numerical results for  $t > t_0$ . In fact, this is depicted in Fig. 4.9, where the analytically computed current after the arrival of  $M$  jittered APs (grey dots) is compared with the simulated current (red curve), for different values of the jitter  $\sigma$  and different values of the inactivation time constant  $\tau_{in}$ . The figure shows the good agreement between the theoretically and numerically computed currents. One observes, moreover, that the effect of increasing the jitter is the temporal spreading of the current so that the signal influence occurs during a large period of time but with a smaller amplitude. This will cause a small decreasing in the capacity of the system to detect spikes. On the other hand, if we fix the jitter the effect of increasing  $\tau_{in}$  is the appearance of longer tails for  $t > t_0$ , which would be a desirable effect since the response to the next incoming AP will be higher. However, no changes are detected in the amplitude of the current when  $\tau_{in}$  is modified. Note that the effect of jitter does not depend on other parameters driving the dynamics of synapses, as  $U_{SE}$ ,  $\tau_{rec}$  or  $\tau_{fac}$ , which only affect to the amplitude  $I_{peak}$  (see section 4.3.1). One should not expect, therefore, a strong effect of jitter on the emergent properties due to facilitation and/or depression.

In order to compute CD maps, we have to calculate the voltage generated by the jittered signal, so that we have to integrate the Langevin equation

$$\tau_m \frac{dV}{dt} = -V + R_{in} I_{peak} \sum_{t_0} \xi(t, t_0). \quad (4.26)$$

Here the sum extends to a train of *events*, each one consisting of  $M$  jittered AP centered around a particular instant of time  $t_0$  in the event train. In order to give a first approximation to the solution of this equation, the EPSC fluctuations are

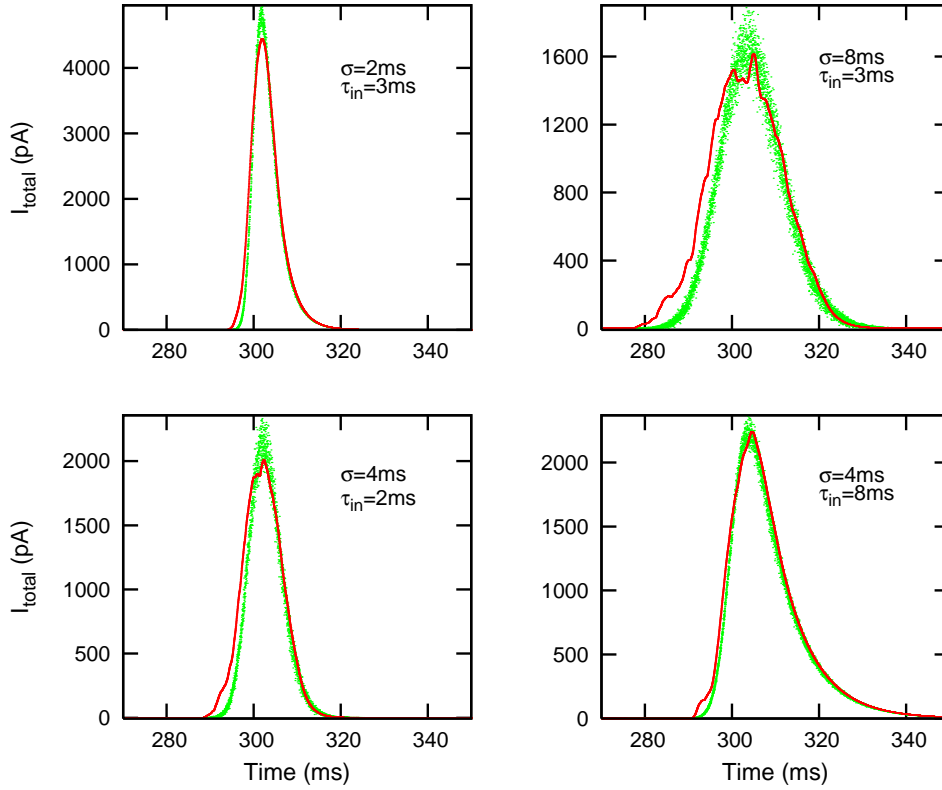


Figure 4.9: Excitatory postsynaptic current generated in a neuron which receives an single AP through  $M = 200$  synapses. In each presynaptic neuron, the AP occurs at different times  $t_i$  which are Gaussian distributed around  $t_0 = 300$  ms. The figure shows that the effect of jitter is the spreading of the current curve, whereas an increment in the inactivation time constant causes longer right tails. Numerical results (lines) are in concordance with the analytical derivation of the current (dots) (see main text for an explanation).

neglected. Therefore, the factor  $\xi(t, t_0)$  is now a Gaussian function of time, centered at  $t_0$  for each event in the train. Using standard methods and assuming a periodic train of events that occur at times  $t_0 = 0, 1/f, 2/f, \dots$ , one can easily integrate the equation (4.26) to obtain

$$V(t) = \exp(-t/\tau_m) \left[ \exp(-1/f\tau_m) \frac{W(1/f)}{1 - \exp(-1/f\tau_m)} + W(t) \right] \quad (4.27)$$

where

$$W(t) = \frac{R_{in}}{\tau_m} \int_0^t \exp(t'/\tau_m) I(t') dt' \quad (4.28)$$

and

$$I(t) = I_{peak} \langle \xi(t, 0) \rangle, \quad (4.29)$$

which determines the temporal evolution of the postsynaptic membrane potential. Simulations show that this expression is also valid for Poisson distributed event trains (data not shown). One can use (4.27) then to evaluate the CD maps similarly to the case of  $\sigma = 0$  (non-jittered events). Indeed, as it is shown in section 4.3.1, to do that is necessary the evaluation of the maximum value of  $V(t)$  generated by the signal term, i.e.  $V_m$ , during the signal event duration. In the practice, this can be analytically done only in the case of  $\sigma = 0$ . For  $\sigma \neq 0$ ,  $V_m$  must be numerically computed from (4.27).

The maps for the detection of strongly jittered events ( $\sigma = 3 \text{ ms}$ ) are presented in Fig. 4.10 (top panels), for the case of only-depressing (left) and depressing-facilitating synapses (right). An important conclusion is that the CD maps here are qualitatively the same than those obtained previously in the zero-jitter case (cf. Fig. 4.4). Increasing the value of the jitter yields to a decreasing of the area of good performance, as one could expect. This effect in the light zone is not too dramatic for  $\sigma \lesssim 4$ , however. The jitter also causes a small delay to reach the membrane threshold, as it is shown in Fig. 4.9 where one has the event at  $t_0 = 300 \text{ ms}$  and the maximum of the generated current occurs at  $t = t_0 + \delta t$ . This fact turns into an increment in the number of failures and false hits. This effect should be considered in the numerical counting of hits, failures and falses, specially for high values of the jitter.

#### *B. Intrinsic stochastic synapses:*

Other possible source of noise to consider in our signal-detection analysis is the existence of fluctuations during synaptic transmission due, mainly, to the intrinsic dynamics of the synapses. To take into account this source of intrinsic synaptic noise, we used the model of stochastic transmission in individual synapses reported in (de la Rocha and Parga, 2005), which accounts the release of neurotransmitters in a single synapse as a stochastic event<sup>3</sup>. The CD maps obtained using this model are shown in Fig. 4.10 (bottom panels), for only-depressing (left) and depressing-facilitating (right) synapses. For a comparison with top panels, in this model we chose parameters  $A_{SE} = 32 \text{ pA}$ ,  $U_{SE} = 0.02$  and  $\tau_{rec} = 200 \text{ ms}$ , which are within the physiological range (Markram et al., 1998). We make this choice to obtain the same qualitatively behavior than the previous model with jittered signals, for the case of depressing synapses. Although this stochastic model introduces additional source of noise which makes the input-output correlation weaker and, therefore, the error in detection is slightly higher, one can see that the effect of including facilitation

---

<sup>3</sup>See also some details concerning this model in section 3.3.3.

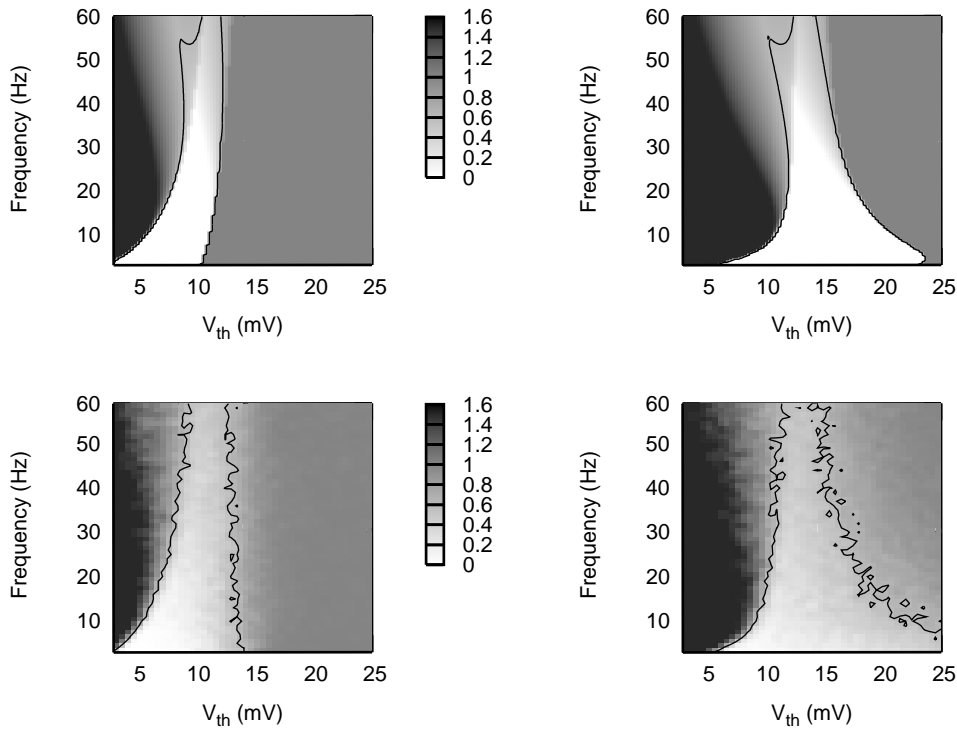


Figure 4.10: The effect of jitter and synaptic fluctuations on coincidence detection maps. Top panels shows CD maps corresponding to highly jittered signals ( $\sigma = 3$  ms) for only-depressing (left panel,  $\tau_{fac} = 0$ ) and depressing-facilitating synapses (right panel,  $\tau_{fac} = 1000$  ms). The maps have been obtained with the postsynaptic membrane potential computed with the expression (4.27). The effect of the jitter is a small and non-relevant decreasing of the good CD regions. Other synapse parameters were  $A_{SE} = 42$  pA,  $\tau_{rec} = 800$  ms and  $U_{SE} = 0.1$ . The bottom panels show the same CD maps obtained with a stochastic synapse model assuming six functional contacts per synapse and one released vesicle per functional contact (see also section 3.3.3). Similarly to top panels, differences between only-depressing (left,  $\tau_{fac} = 0$  ms) and depressing-facilitating synapses (right panel,  $\tau_{fac} = 1300$  ms) are shown. Other synapse parameters in this case were  $A_{SE} = 32$  pA,  $\tau_{rec} = 200$  ms and  $U_{SE} = 0.02$ . In all panels, the solid line delimits regions where  $E(f, V_{th}) < 0.6$  (light areas).

is also the same. That is, it induces the spreading of the region of good detection (light area) towards high threshold values.

We conclude, therefore, that the general results obtained in section 4.3.2 are robust for a more realistic treatment of the input presynaptic trains, including the case of jittered signals, and more realistic model of synapses with realistic stochastic release of neurotransmitters.

### 4.3.4 Detection of presynaptic firing rate changes

In the analysis we have performed until now in this chapter, we have considered the overall presynaptic firing rate as a fixed parameter. This assumption is not realistic enough when one studies actual neural systems, and an interesting possibility is to consider the firing rate as a dynamic variable, as it happens in real neuronal tissue. The rate changes in the presynaptic neuron, during normal functioning, leads to a transient behavior in the excitatory postsynaptic potential (EPSP) which could cause a burst or an AP in the postsynaptic neuron (Tsodyks and Markram, 1997; Pantic et al., 2003; Abbott et al., 1997). The question that arises then is if the postsynaptic neuron is able to detect synchronous changes (increases) in the afferent firing rates. This property have been found, in previous works, only for depressing synapses and not for static synapses (Pantic et al., 2003). Another question is if synaptic facilitation could have some positive effect in the detection of these rates changes by the postsynaptic neuron. In this section we address these questions by studying the effect of increasing facilitation in spite of depression in the optimal detection, by the postsynaptic neuron, of rate changes in the presynaptic neurons.

To start, we assume a population of  $N = 1000$  afferents firing uncorrelated Poisson spike trains with a certain frequency  $f$  into a postsynaptic neuron. In addition, we consider that this population changes its mean firing rate every  $1000\text{ ms}$ . Figure 4.11 shows a comparison in the subsequent output of the postsynaptic neuron for the case of facilitating and depressing synapses. The threshold for firing was fixed in  $V_{th} = 17\text{ mV}$  and  $U_{SE} = 0.1$  (which are within the physiological range). Simulations show that facilitating synapses ( $\tau_{fac} = 500\text{ ms}$ ) allow for a better detection of rate changes, and over a larger range of frequencies, than depressing synapses. In general, the regions in which depressing and facilitating synapses perform well can vary and this strongly depends on the given values of  $U_{se}$ ,  $\tau_{rec}$  and  $\tau_{fac}$ . Thus, there are special situations where facilitation is needed to detect presynaptic rate changes and vice versa.

A simple theoretical approach, which has been used previously in the case of depressing synapses (Pantic et al., 2003) and agrees qualitatively with simulations (data not shown), can help us to find the regions in which firing rate changes are detected. To obtain such transient behavior, which allows rate-change detection, the threshold of the postsynaptic neuron must satisfy  $C f_2 \omega(f_1) > V_{th} > C f_2 \omega(f_2)$ , where  $f_1$  is the initial rate,  $f_2$  is the firing rate after the change,  $C = R_{in} N \tau_{in}$  and  $\omega(f)$  is the stationary postsynaptic current strength for a given frequency. From the system of equations (4.1) and following a reasoning similar to the strategy used in section 4.3.1, one can easily obtain

$$\omega(f) = \frac{A_{SE} U_{\infty}}{1 + f \tau_{rec} U_{\infty}} \quad (4.30)$$

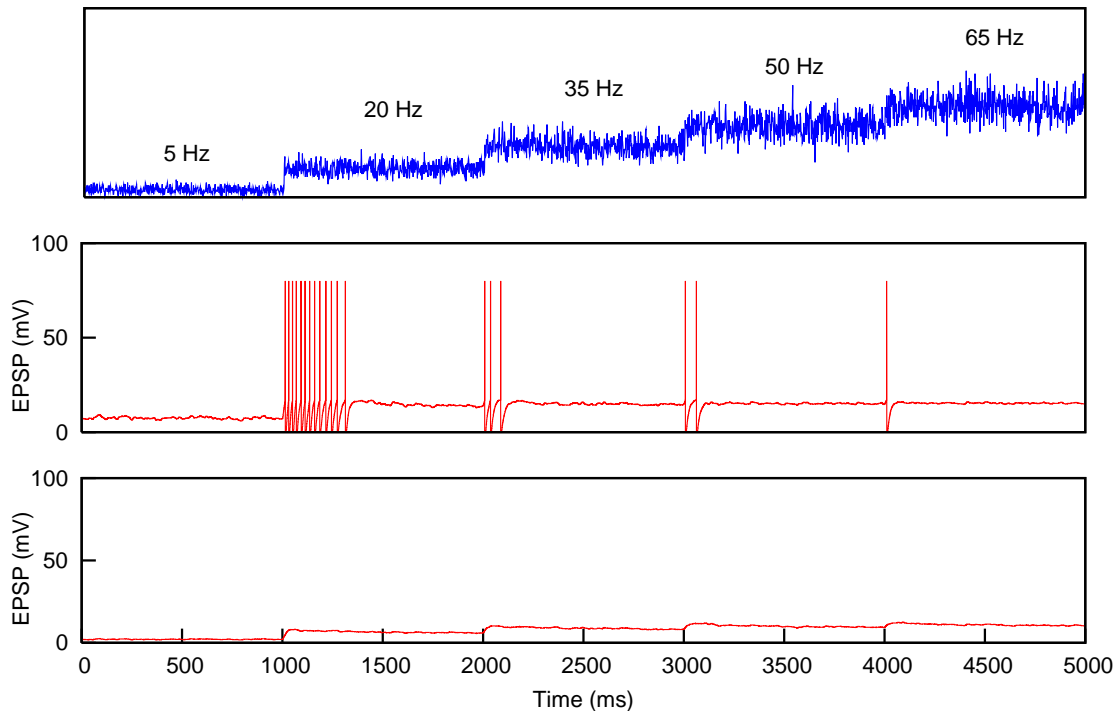


Figure 4.11: Detection of firing rate changes with depressing and facilitating synapses. The top panel shows the mean firing rate of the  $N = 1000$  presynaptic neurons as a function of time. Middle and bottom panels show the response of the postsynaptic membrane potential for facilitating and depressing cases, respectively. In these simulations parameters were  $U_{SE} = 0.1$  and  $\tau_{fac} = 500$  ms ( $0$  ms) for the facilitating (depressing) case, respectively. According to our results, detection of variations onto lower frequencies are not possible only with these synaptic mechanisms.

where  $U_{\infty}$  is the steady state valued of  $U(t)$ . If now we fix the frequency step  $\delta f = f_2 - f_1$ , the resulting expressions will only depend on  $f_1$ . Since for large enough frequencies  $Cf_2\omega(f_1)$  is a decreasing function of  $f_1$  and  $Cf_2\omega(f_2)$  is an increasing function of  $f_2$  (and therefore of  $f_1$ ), these two tendencies will converge for some  $f_1$ . This leads to a close area of good rate change detection between the two curves. These two theoretical functions depends on the synapse relevant parameters and, therefore, allows for a theoretical treatment of the regions in which firing rate changes can be detected, depending on the balance between depression and facilitation.

## 4.4 Discussion

In this chapter, we have presented a detailed theoretical and numerical study of how the competition between synaptic facilitation and depression affects the neural

detection of temporal correlations between different presynaptic neurons in a background of uncorrelated noise. Our study shows that the inclusion of the facilitation mechanisms enhances the performance of cortical neural systems to perform this task, for a wide range of frequencies and neuron thresholds and for any possible values of the parameters which define the dynamics of the synapses, namely,  $U_{SE}$ ,  $\tau_{fac}$  and  $\tau_{rec}$ . In particular, we have shown that the transmission of information, codified in spike trains through the synapses, is enhanced and the detection of firing rate changes is also improved compared with the case of only-depressing synapses. Thus, contrary to what happens with only depression, the presence of facilitation makes not necessary to have a high value for the maximum amount of active neurotransmitters to efficiently detect correlated signals. This would lead us to think that facilitation has a crucial role in the processing of information through synapses even when the neuron does not have enough synaptic resources.

Facilitation also determines the existence of an optimal frequency which allows good performance for a wide range of neuron firing thresholds. In particular, these results could be important to understand how actual neural systems – where different types of neurons with non-identical firing thresholds are connected in a complex way – can self-organize to efficiently detect and process relevant information (Azouz and Gray, 2000). Thus, the existence of this optimal frequency could be related with recent experimental findings which reveals the existence of similar optimal frequencies in the presence of facilitation in the heterogeneous pyramidal network of the prefrontal cortex (Wang et al., 2006).

We have also seen that, although important, it is not crucial to have a strong correlation between the different presynaptic afferents to have a good detection of signals, and our results also fulfill for noisy signals. This is of special relevance since it is well known that the intrinsic stochasticity of actual synapses causes fluctuations that disrupt the synchrony between the afferents and produce a highly fluctuating postsynaptic response (Dobrunz and Stevens, 1997). To account for that more precisely, we have study the role of the balance between synaptic facilitation and depression with a more realistic stochastic model of synaptic transmission (de la Rocha and Parga, 2005). The results of this analysis have shown that our main conclusions also fulfill for this case.

We have considered in this chapter that the signal term and the noise term are described by the same EPSC maximal amplitude  $A_{SE}$  and the same mean firing rate  $f$ . However, this is not always the case when one considers actual neural systems. In some circumstances, for instance, the signal term is sensibly different than the noise term. To take into account this possibility, the particularly interesting case of detection of weak slow signals in highly noisy environments will be treated in the next chapter.

# Chapter 5

## Bimodal resonances

The study presented in chapter 4 concerning CD tasks in the presence of noisy activity may be extended to several situations of interest, such as the detection of weak (subthreshold) signals in noisy environments. Following the general lines established in this thesis, in this chapter we analyze the effect of the interplay between short-term synaptic processes and adaptive properties of neurons in the detection of weak signals embedded in a background of noisy neural activity, by employing a stochastic resonance formalism.

### 5.1 Introduction

It is known that a certain level of noise can enhance the detection of weak input signals for some nonlinear systems. This phenomenon, known as stochastic resonance (SR), is characterized by the presence of a peak, or a bell-shaped dependence, in some information transfer measurement as a function of the noise intensity (Gammaitoni et al., 1998; Wiesenfeld and Moss, 1995; Lindner et al., 2004). More precisely, for low noise levels the system is not able to detect the signal due to its small amplitude. For moderate noise levels, however, the noise is able to enhance the signal up to a certain detection threshold, and this makes the system respond in a highly correlated fashion with the signal (and a peak of information transfer appears). Finally, for too high noise levels the output is dominated by the noise and the signal is not detected.

Stochastic resonance has been measured in a wide variety of physical and biological systems, including bidirectional ring lasers (McNamara et al., 1988), electronic circuits (Fauve and Heslot, 1983), crayfish mechanoreceptor (Wiesenfeld et al., 1994), or voltage-dependent ion channels (Bezrukov and Vodyanoy, 1995). In the brain, it has been found in different types of sensory neurons (Longtin et al., 1991; Greenwood et al., 2000), in the hippocampus (Stancey and Durand, 2000), in the

brain stem (Yasuda et al., 2008), and in some cortical areas (Chialvo and Apkarian, 1993; Ho and Destexhe, 2000; Manjarrez et al., 2002; Fellous et al., 2003). Although SR behavior has been extensively studied in many works, most of them assume a controlled source of noise that affects the dynamics of the system additively and, in some cases, without temporal correlations. Such assumption is no longer valid in *in vivo* experiments in actual neural systems, where noise is the result of the inherent activity of the medium (which could be, for instance, the highly irregular spontaneous activity of other cortical regions projecting to the structure of interest) and, therefore, not easily controlled by the experimentalist. The effect of such stochasticity on the dynamics of a particular neuron could, indeed, involve details concerning concrete biological mechanisms not considered yet. In particular, since neurons receive signals from its neighbors through synapses, the concrete characteristics of synapses may strongly influence the SR properties of *in vivo* neural circuits. It is known, for instance, that actual synapses present activity dependent mechanisms, such as short-term depression (STD) and short-term facilitation (STF), that may strongly modify the postsynaptic neural response in a nontrivial way. The former of these mechanisms considers that the amount of neurotransmitter ready to be released – due to the arrival of an action potential (AP) – is limited, and the synapse needs some time to recover these resources in order to transmit the next incoming AP. Synaptic facilitation, on the other hand, has an opposite effect and increases the postsynaptic response under repetitive presynaptic stimulation. Such increment is mediated by the influx of calcium ions into the presynaptic terminal (Bertram et al., 1996). The competition between STD and STF may be highly relevant in signal detection in noisy environments, as for instance in cortical gain control (Abbott et al., 1997) or in spike coincidence detection (Mejias and Torres, 2008), and therefore they could have a main role in SR tasks.

In addition to these synaptic mechanisms, the dynamics of the neuron firing threshold due to slow membrane depolarizations – namely, adaptive thresholds – constitutes another important issue to be considered in SR phenomena in neural media. Indeed, high cortical activity levels could provoke such slow depolarizations and affect the excitability properties of the neuron, and therefore its information transmission properties. In cat striate cortex, for instance, the existence of adaptive neural thresholds seems to play an important role in stimulus orientation by reducing cellular sensitivity to slow depolarizations (Azouz and Gray, 2000, 2003). Adaptive thresholds mechanisms have been captured by a number of neuron models (Hodgkin and Huxley, 1952a,b; Noble, 1966; Fricker et al., 1999; Kobayashi et al., 2009). However, the complex interplay between dynamic synapses and adaptive thresholds has caught little attention from researchers, despite the computational implications that it may have in SR properties of actual neural systems.

In this chapter, we use a phenomenological model of dynamic synapses and a standard integrate-and-fire (IF) neuron model with an input-dependent threshold to study the interaction between adaptive threshold, STD and STF in the detection of weak (subthreshold) signals under a noisy environment. More precisely, we consider a system of  $N$  presynaptic neurons which transmit APs, within a Poisson distribution with mean frequency  $f_n$ , to a postsynaptic neuron through dynamic synapses. In these conditions, a weak and low-frequency sinusoidal signal is also transmitted to the postsynaptic neuron to study its response and the conditions in which SR occurs. Our results show that new phenomena can emerge as a consequence of the interplay between the adaptive threshold and short-term synaptic processes. Concretely, this interplay induces the appearance of a second resonance peak at relatively high frequencies, which coexists with the standard SR peak located at low frequencies. The coexistence of these two resonance peaks allows the system to efficiently detect incoming weak signals for two well defined network noise levels. The precise frequency at which each one of these two resonance peaks appear is determined by the particular values of the relevant parameters involved in the dynamics of the synapses. Our main results are confirmed by employing a more realistic FitzHugh-Nagumo (FHN) neural model (which possesses an intrinsic adaptive threshold mechanism), as well as by considering more realistic stochastic synaptic models and poissonian-like weak input signals. Finally, we have compared the results of our study with recent experimental data which seems to show two stochastic resonance peaks in the human tactile blink reflex (Yasuda et al., 2008).

## 5.2 Model and methods

The system under study is schematized in figure 5.1. It consists of a postsynaptic neuron which receives both a slow, weak external signal -for simplicity, considered periodical- and the uncorrelated activity of a network of  $N$  excitatory neurons. The membrane potential  $V(t)$  of the postsynaptic neuron is assumed as in the IF neuron model, namely

$$\tau_m \frac{dV(t)}{dt} = -V(t) + R_{in}I(t) \quad (5.1)$$

where  $\tau_m$  is the membrane time constant, and the neural input or excitatory postsynaptic current (EPSC) is given by  $I(t)$ , which is multiplied here by the input resistance  $R_{in}$ . Due to the input current  $I(t)$ , the membrane potential  $V(t)$  depolarizes, and when it reaches a certain threshold  $\theta$  an AP is generated. The membrane potential is then reset to its resting value  $V_r$  for a short period of time, called the absolute refractory period, namely  $\tau_{ref}$ .

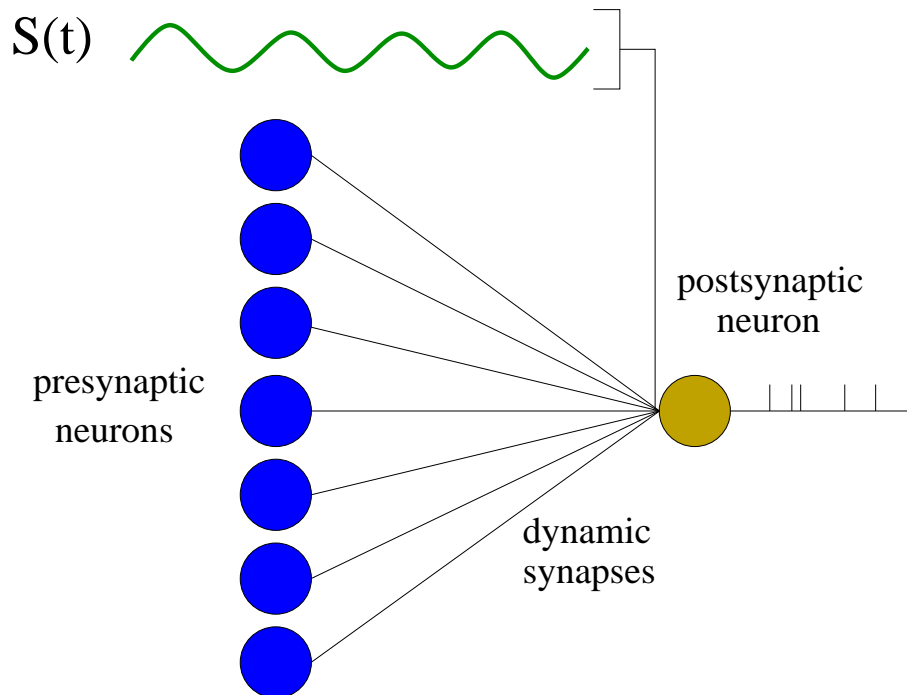


Figure 5.1: Schematic plot of the system considered in our study. The postsynaptic neuron (in yellow) receives a weak input periodic signal, and is exposed to the noisy background activity of other neurons (in blue). These neurons transmit Poissonian spike trains of frequency  $f_n$  through dynamic synapses. The aim is to determine how the properties of these synapses can influence the detection of the weak signal by a postsynaptic neuron having nonlinear membrane excitability properties.

We also assume that the neural input consists of two terms, namely  $I(t) = S(t) + I_n(t)$ . The first term,  $S(t) \equiv d_s \sin(2\pi f_s t)$ , is the input weak signal, with frequency  $f_s$  and amplitude  $d_s$ . The second term is the total synaptic current generated by  $N$  uncorrelated presynaptic neurons, namely  $I_n(t) \equiv \sum_{i=1}^N I_i(t)$ . This accounts for the noisy current induced by the other neurons in the network, and its level is controlled by the mean firing rate of the network  $f_n$ . This noisy current involves an activity-dependence of the synaptic strength as proposed in a phenomenological model presented in (Tsodyks and Markram, 1997). According to this model, as we have already seen in section 3.3.3, the state of the synapse  $i$  is governed by the system of equations

$$\begin{aligned}
\frac{dx_i(t)}{dt} &= \frac{z_i(t)}{\tau_{rec}} - u_i(t) x_i(t) \delta(t - t_{sp}) \\
\frac{dy_i(t)}{dt} &= -\frac{y_i(t)}{\tau_{in}} + u_i(t) x_i(t) \delta(t - t_{sp}) \\
\frac{dz_i(t)}{dt} &= \frac{y_i(t)}{\tau_{in}} - \frac{z_i(t)}{\tau_{rec}},
\end{aligned} \tag{5.2}$$

where  $x_i(t), y_i(t), z_i(t)$  are the fraction of neurotransmitter in a recovered, active and inactive state, respectively (see (Tsodyks and Markram, 1997) for details). Here,  $\tau_{in}$  and  $\tau_{rec}$  are the synapse inactivation and active neurotransmitter recovery time constants, respectively. The delta functions in equation (5.2) take into account that an AP arrives to the synapse at some fixed time  $t = t_{sp}$ . On the other hand,  $u_i(t)$  is an auxiliary variable such that  $u_i(t)x_i(t)$  stands for the fraction of available neurotransmitter that is released after the arrival of a presynaptic AP at time  $t$  or, from a probabilistic point of view, the neurotransmitter release probability at that time. Synaptic facilitation is introduced by considering the following dynamics for  $u_i(t)$ :

$$\frac{du_i(t)}{dt} = \frac{U_{SE} - u_i(t)}{\tau_{fac}} + U_{SE} [1 - u_i(t)] \delta(t - t_{sp}). \tag{5.3}$$

This equation considers the influx of calcium ions into the neuron near the synapse through voltage-sensitive ion channels. These ions usually can bind to some molecular receptor which gates and facilitates the release of neurotransmitters (Bertram et al., 1996). Pure depressing synapses correspond to  $u_i(t) = U_{SE}$  constant (which is also obtained in the limit  $\tau_{fac} \rightarrow 0$ ), where  $U_{SE}$  is the neurotransmitter release probability without the facilitation mechanism. Within this model, the excitatory postsynaptic current generated in the synapse  $i$  is considered to be proportional to the amount of active neurotransmitter (i.e., that which has been released into the synaptic cleft after the arrival of an AP), namely  $I_i(t) = A_{SE} y_i(t)$ .

As can be easily checked in equations (5.2-5.3), in activity dependent or dynamic synapses, the degree of synaptic depression and facilitation increases with  $\tau_{rec}$  and  $\tau_{fac}$ , respectively, and these levels are also controlled by  $U_{SE}$ . On the other hand, *static* synapses (i.e., when synapses are not activity dependent) are obtained for  $\tau_{rec}, \tau_{fac} \rightarrow 0$ .

To complete the description of the system, we assume that the firing threshold  $\theta$  of the postsynaptic neuron follows the dynamics

$$\tau_\theta \frac{d\theta(t)}{dt} = -\theta(t) + \delta + R_{in} I(t). \tag{5.4}$$

where  $\tau_\theta$  is the threshold variation time scale and  $\delta$  is a small positive constant. This dynamics implies that, in steady state conditions, the firing threshold displays approximately a linear dependence with the steady state postsynaptic membrane potential  $\bar{V} \equiv R_{in}\bar{I}$ , with  $\bar{I}$  being the steady state EPSC. This property has been observed in many neural media<sup>1</sup>, and it is known as *adaptive threshold* (Azouz and Gray, 2003; Hodgkin and Huxley, 1952a; Fricker et al., 1999). To obtain a slow threshold dynamics as is reported in (Azouz and Gray, 2003), we set  $\tau_\theta = 800$  ms (although other values are also possible and yield the same results for our study). The parameter  $\delta$  ensures that the firing threshold lies above the mean membrane potential  $\bar{V}$ , and it guarantees that the output spiking activity is driven by the current fluctuations which lead to fast depolarizations (Azouz and Gray, 2003). Moreover, we assume that the signal  $S(t)$  is too weak to have an appreciable effect on the value of the threshold, and therefore we set  $\bar{V} = R_{in}\bar{I} \simeq R_{in}\bar{I}_n$  in equation (5.4). To ensure physiological values of the neuron threshold, we also impose a minimum value for the firing threshold of  $\theta_m = 7$  mV. In the following, unless specified otherwise, we choose  $N = 200$ ,  $\tau_m = 10$  ms,  $R_{in} = 0.1$  G $\Omega$ ,  $V_r = 0$ ,  $\tau_{ref} = 5$  ms,  $f_s = 5$  Hz,  $d_s = 10$  pA, and  $\tau_{in} = 3$  ms, values which are within the physiological range for cortical neurons.

Using our IF neuron model with adaptive threshold, we have studied the level of background noisy activity received by a postsynaptic neuron which improves its ability to detect an incoming weak signal. This signal is considered weak in the sense that, if the level of noise is zero or sufficiently low, the neuron does not generate APs strongly correlated with the signal (Stemmler, 1996). In order to quantify the level of coherence between the input signal  $S(t)$  and the response of the postsynaptic neuron, we employed a cross-correlation function defined as in (Collins et al., 1995), that is,

$$C_0 \equiv \langle S(t)R(t) \rangle = \frac{1}{T} \int_0^T S(t)R(t)dt, \quad (5.5)$$

where  $T$  is the total recording time of each trial, typically much greater than the signal period  $f_s^{-1}$ , and  $R(t)$  is the instantaneous firing rate of the postsynaptic neuron. This type of cross-correlation functions have been extensively used in the literature to measure the input-output dependence in neuron models and experiments (see, for instance, (Palm et al., 1988; Collins et al., 1995; Yasuda et al., 2008)).

---

<sup>1</sup>The linear dependence which equation (5.4) implies also holds for more realistic neuron models, as we will show later on.

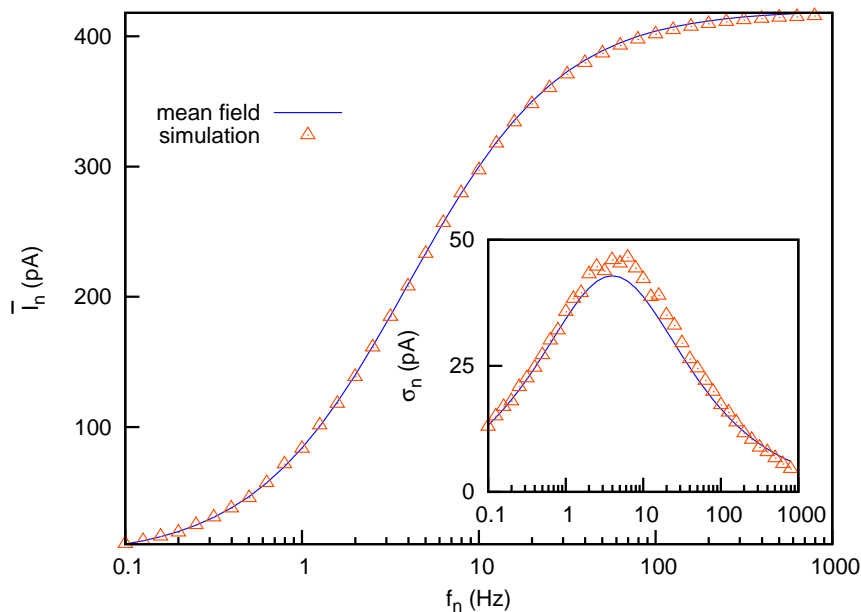


Figure 5.2: Mean EPSC as a function of the mean firing rate  $f_n$ , with  $U_{SE} = 0.5$ ,  $A_{SE} = 70$  pA and  $\tau_{rec} = 500$  ms. Numerical simulations (symbols) are supported by mean field results (lines). In the inset, we can see the good agreement between mean field and simulations for the EPSC fluctuations.

## 5.3 Results

### 5.3.1 Mean-field calculations

One can easily derive an analytical expression for the cross-correlation measure  $C_0$  between the response of the postsynaptic neuron and the weak input signal, in the presence of noisy activity. In order to achieve that, first we will obtain the expressions for the noisy EPSC with dynamic synapses, for both the deterministic model and the stochastic model. After that, we will obtain the expression for the mean firing rate of the IF postsynaptic neuron in the presence of such noisy EPSC, and we will use this expression to obtain a mean-field formula for  $C_0$ .

Following the same procedure that the one employed in chapter 4, we consider a population of  $N$  presynaptic neurons firing uncorrelated Poisson spike trains at a certain frequency  $f_n$ . We also assume that the synaptic current  $I_i(t)$  generated by an AP arriving at time  $t^*$  in a particular synapse  $i$  is proportional to the fraction of active neurotransmitters in that synapse, namely,  $y_i(t)$  (cf equation (5.2)). In this situation (see also section 4.3.1 and appendix A) the postsynaptic current at time  $t = t^* + \tau$  is given by

$$I_i(\tau, t^*) = I_p \exp(-\tau/\tau_{in}), \quad (5.6)$$

where  $I_p$  is the peak value of the EPSC, reached at time  $t = t^*$ . Considering

a stimulation with a stationary Poissonian AP train, the peak value  $I_p$  can be substituted by an averaged stationary EPSC amplitude. One easily obtains from equations (5.2-5.3) that

$$I_p = A_{SE} u_\infty x_\infty \quad (5.7)$$

where  $u_\infty$  and  $x_\infty$  are, respectively, the facilitation and depression variables in the stationary state, and their expressions are given by

$$u_\infty = \frac{U_{SE} + U_{SE} \tau_{fac} f_n}{1 + U_{SE} \tau_{fac} f_n}, \quad (5.8)$$

$$x_\infty = \frac{1}{1 + u_\infty \tau_{rec} f_n}. \quad (5.9)$$

Using the fact that  $N$  is large enough, the mean current of the presynaptic population and its fluctuations are given by

$$\bar{I}_n = N f_n \tau_{in} I_p \quad (5.10)$$

$$\sigma_n^2 = \frac{1}{2} N f_n \tau_{in} (I_p)^2 \quad (5.11)$$

where we assumed that  $\tau_{in} \ll \tau_{rec}$ . Equations (5.10) and (5.11) allow to characterize the noisy input from the presynaptic neurons. The dependence of these quantities with  $f_n$  is shown in figure 5.2. It is worthy to note that, although we have assumed a poissonian distribution for the spike trains, the mean-field approach considered here holds for other distributions of the spike trains (Mejias and Torres, 2008), as long as presynaptic neurons remain uncorrelated in time and their number is large enough.

With these expressions, one can obtain the mean firing rate of the postsynaptic neuron by solving the Fokker-Planck equation associated with the dynamics of the membrane potential (see appendix B, and also (Tuckwell, 1989; Brunel, 2000)). We define the quantities

$$y_\theta(t) = \frac{\theta - R_{in} \bar{I}_n + S(t)}{R_{in} \sigma_n} \quad (5.12)$$

$$y_r(t) = \frac{V_r - R_{in} \bar{I}_n + S(t)}{R_{in} \sigma_n}, \quad (5.13)$$

and assume that the weak signal  $S(t)$  evolves slowly compared with the neuron dynamics. The firing rate of the postsynaptic neuron is then given by (see also appendix B)

$$R(t) = \left[ \tau_{ref} + \tau_m \int_{y_r(t)}^{y_\theta(t)} dz \sqrt{\pi} \exp(z^2) (1 + \operatorname{erf}(z)) \right]^{-1}. \quad (5.14)$$

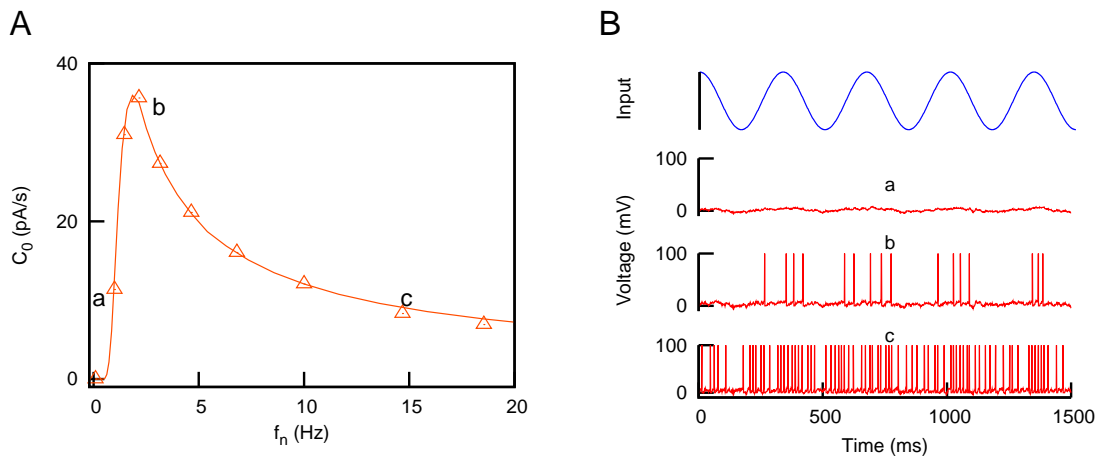


Figure 5.3: (A) Characteristic curve of SR as a function of the mean network rate  $f_n$ . Numerical simulations of the model (symbols) agree with our mean-field theory (solid line). (B) The input signal and several time series (marked as a, b, c) of the postsynaptic membrane potential  $V(t)$  for different input noise frequencies. This is for static synapses ( $\tau_{rec} = \tau_{fac} = 0$ ),  $U_{SE} = 0.4$ ,  $A_{SE} = 120$  pA,  $f_s = 3$  Hz and a fixed threshold  $\theta = 10$  mV.

For the case in which we have an adaptive threshold, we set  $\frac{d\theta(t)}{dt} = 0$  on equation (5.4) to obtain the steady state value  $\theta = \delta + R_{in}\bar{I}_n$ , with  $\bar{I}_n$  given by equation (5.10). On the other hand, for the fixed threshold approach we simply set  $\theta = V_{th}$ . Equation (5.14), together with the expressions of the EPSC and the threshold conditions obtained above, allows to evaluate (5.5) and to obtain

$$C_0(\nu) = \int_0^{1/f_s} f_s d_s \sin(2\pi f_s) \left[ \tau_{ref} + \tau_m \int_{y_r(t)}^{y_\theta(t)} dk \sqrt{\pi} \exp(k^2) (1 + \operatorname{erf}(k)) \right]^{-1} dt, \quad (5.15)$$

where we have set  $T = 1/f_s$ . By evaluating numerically this expression, one obtains analytical curves for the input-output correlation which can be compared with the results from numerical simulations of the system sketched in figure 5.1.

### 5.3.2 Emergence of bimodal resonances with STD

As we have mentioned before, the phenomenon of stochastic resonance has been measured in neurons under different conditions and, in particular, in the cortex (Rudolph and Destexhe, 2001; Fellous et al., 2003; Ho and Destexhe, 2000; Manjarrez et al., 2002). An example of stochastic resonance in the case of a presynaptic population with static synapses is shown in figure 5.3. For low noise frequencies, the neuron is not able to fire, and therefore, to detect the weak signal. This is reflected in the fact that  $C_0$  takes low values. However, when the noise frequency is increased, both

noise and signal terms contribute to make the system follow the signal, that is, the neuron response becomes highly correlated with the stimulus. As a consequence of this, a maximum value of  $C_0$  is reached. Beyond that point, the activity of the presynaptic neurons produces a high and noisy postsynaptic response, which impedes the postsynaptic neuron to detect the weak signal, and therefore the cross-correlation function  $C_0$  decays with its characteristic shape.

This typical resonance behavior appears when synapses do not show any fast variability in their strength, or when the variation is only due to a slow learning processes, which we do not consider here. However, we must take into account that actual synapses show activity-dependent variability at short time scales, and this feature could modify the response of the postsynaptic neuron to the signal. In particular, since STD is a mechanism that usually modulates the high frequency inputs, one can wonder about its effect in the SR curve. In fact, our results show that this effect is quite notorious as can be viewed in figure 5.4A. The figure shows the emergence of *bimodal* resonances in the presence of STD. More precisely, in addition to the standard SR peak, a second resonance peak appears at high frequencies and moves towards lower frequency values as the degree of depression increases. This second peak allows the system to efficiently detect the weak input signal among a wide range of high frequencies (note the logarithmic scale on  $f_n$ ). Therefore, this new resonance peak reflects that the neuron is able to properly detect the incoming signal for both low and high values of the mean network rates. This phenomenology is quite robust and can also be obtained by using other SR measurements, such as the signal-to-noise ratio (as defined, for instance, in (McNamara and Wiesenfeld, 1989)) (data not shown).

We also observe that the location of the second resonance peak has a nonlinear dependence with  $\tau_{rec}$ . To better visualize this effect we plot in figure 5.4B the behavior of  $f^*$ , defined as the noise frequency value at which the second resonance peak is located, as a function of  $\tau_{rec}$ . We can observe in this figure that data from numerical simulation agrees with our mean-field prediction. In the following and unless specifically specified, we have considered a time window of  $\sim 10$  seconds for the simulations of the SR curves, and we have averaged each data point over 30 trials.

### 5.3.3 Bimodal resonances with STF

As well as STD, the facilitation mechanism is able to modulate the intensity of the postsynaptic response in a nonlinear manner for given presynaptic conditions. Following a similar reasoning to the one considered above, we expect synaptic facilitation to have an important effect in the signal detection properties of the post-

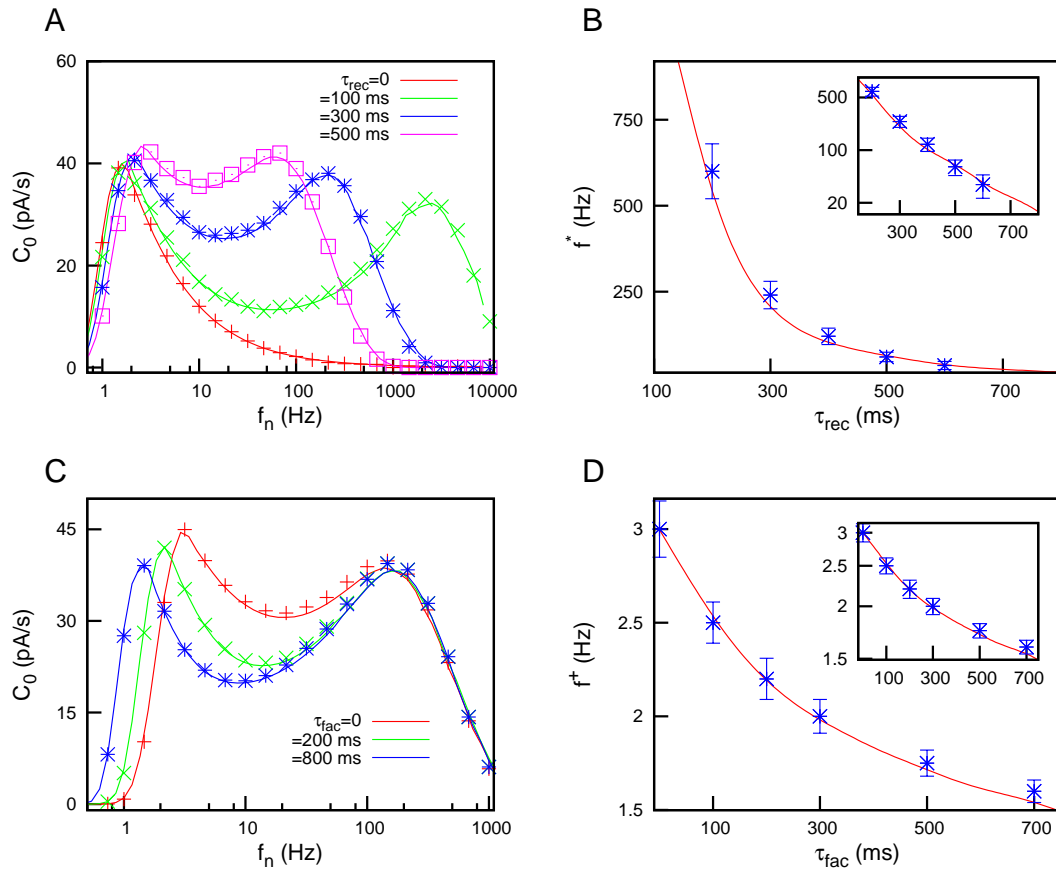


Figure 5.4: (A) Bimodal SR curves for several values of  $\tau_{rec}$ , considering  $U_{SE} = 0.4$  and  $A_{SE} = 120$  pA. This shows that the effect of STD in stochastic resonance is the production of a second resonance peak at certain frequency  $f^*$  which decreases when  $\tau_{rec}$  is increased. This is illustrated in panel (B), where the inset is a semi-logarithmic plot of the same data. (C) Bimodal SR curves for different values of  $\tau_{fac}$ , with  $U_{SE} = 0.1$  and  $A_{SE} = 350$  pA. The panel (D) illustrates a decrease of the frequency  $f^+$  at which the first resonance peak appears as  $\tau_{fac}$  is increased. The inset in (D) is a semi-logarithmic plot of the same data. In all panels, data from numerical simulations (denoted with symbols) show a good agreement with mean-field predictions (denoted with lines).

synaptic neuron under noisy conditions. This effect is shown in figure 5.4C where, depending on the value of  $\tau_{fac}$ , the resonance peak located at low frequencies can be tuned among different values of  $f_n$ . It is worthy to note that the appearance of the low frequency peak is not induced by the presence of depression or facilitation mechanisms in the synapse, since it also appears for static synapses (see figure 5.3A). Therefore, it corresponds to the standard SR phenomena observed in many excitable nonlinear systems. However, its precise location in the frequency range

is influenced by STF. Concretely, since the effect of facilitation is to potentiate the postsynaptic response, one should expect that levels of noise which are too low to cause high  $C_0$  values with static synapses would, in the presence of STF, contribute to the resonance. On the other hand, the noise frequency values which were optimal to cause SR in absence of STF, becomes too high in the presence of STF and provoke a decrease in  $C_0$ . Considering these two effects together, one should expect a displacement of the first resonance peak towards lower values of  $f_n$  as  $\tau_{fac}$  increases, which is what we observe in simulations. Since the position of the first peak is highly sensitive to the value of  $\tau_{fac}$ , STF could have an important role for a precise discrimination of the network noisy activity level needed for the optimal detection of weak signals. The second peak, which is mainly caused by the depression mechanism, does not change its position when  $\tau_{fac}$  is varied, due to the prevalence of the STD effect over the STF at high frequencies. The dependence of the position of the low frequency peak, namely  $f^+$ , with the facilitation characteristic time is shown in the figure 5.4D.

### 5.3.4 The role of adaptive neuron threshold

The appearance of these bimodal resonances is not exclusively due to the dynamical characteristics of synapses. Considering adaptive thresholds is of vital importance for the emergence of bimodal resonances. To illustrate this, we have computed SR curves for different values of  $\tau_{rec}$  and an IF neuron with fixed firing threshold (that is, an input-independent threshold), namely  $V_{th}$ . The result is shown in figure 5.5A, where one can see that STD is not able to induce a second resonance peak when neuron threshold is considered independent of the mean membrane potential. Instead of this, we found that  $C_0$  does not decay from its peak value to zero for high  $f_n$  values, but it stabilizes at a steady value  $C_0^*(\tau_{rec})$ . Such high steady value means that some level of coherence between the weak signal and the postsynaptic response is maintained for arbitrarily high mean rates. It is worthy to note that, for a particular value of  $\tau_{rec}$  (500 ms in the figure), the value of  $C_0^*$  obtained is similar to its peak value, thus allowing a good detection over a wide range of background firing rate values.

This saturation of  $C_0$  for strong enough STD, which is due to the oversimplification assumed by the IF model with fixed threshold, can be easily explained as follows. Firstly, our simulations show that, in order to have large values of  $C_0$ , a necessary condition is that  $\bar{I}_n \approx V_{th}/R_{in}$ , with  $\bar{I}_n$  being the mean noisy input current<sup>2</sup>.

---

<sup>2</sup>If  $\bar{I}_n \ll V_{th}/R_{in}$  the postsynaptic neuron is not firing at all, and if  $\bar{I}_n \gg V_{th}/R_{in}$  the postsynaptic neuron is firing all the time.

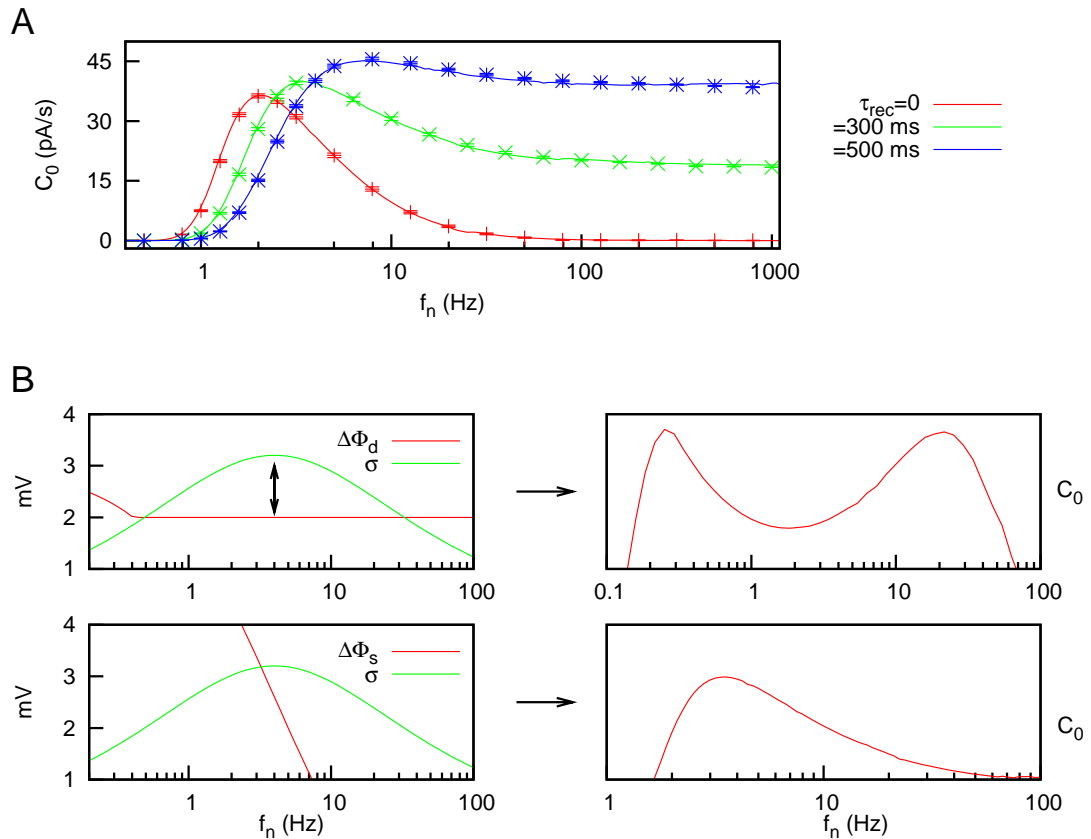


Figure 5.5: (A) SR curves for an IF neuron model with fixed threshold  $\theta = 8$  mV receiving a weak signal and a noisy input modulated by depressing synapses, for  $U_{SE} = 0.5$ ,  $A_{SE} = 90$  pA and different values of  $\tau_{rec}$ . This shows that ignoring the adaptive threshold can lead to drastic modifications in the performance of the system (cf. figure 5.4A, see also the main text for details). Numerical simulations (symbols) are consistent with a mean field approach (lines). (B) Schematic plot to illustrate how a resonance peak appears when the amplitude of the voltage variations induced by synaptic current fluctuations (that is,  $\sigma \equiv R_{in}\sigma_n$ ) is comparable with the barrier height  $\Delta\Phi$  (see main text). In the case of an IF neuron model with adaptive threshold and in the presence of dynamic synapses, this occurs at two frequency values separated by a frequency range where  $\sigma \gg \Delta\Phi \equiv \Delta\Phi_d$  (which induces sustained spiking activity and therefore decreases the coherence  $C_0$  between the two maxima). For an IF neuron model with fixed threshold, however,  $\sigma$  is comparable with  $\Delta\Phi_s$  only for a single frequency value which explains the emergence of a single resonance peak.

Secondly, in the presence of STD and for high background noise rate, the mean noisy input current  $\bar{I}_n$  saturates at certain value  $I_\infty \equiv \lim_{f_n \rightarrow \infty} \bar{I}_n$  – see expressions for the mean and peak value of the postsynaptic current in section 5.3.1 – which is infinity for  $\tau_{rec} = 0$  and decreases as  $\tau_{rec}$  increases. Moreover, for  $\tau_{rec}$  sufficiently high

(strong depression), the mean noisy current is near to its asymptotic value  $I_\infty$ , for a finite and relatively low noise frequency  $f_n$ . As a consequence, there is a sufficiently high value of  $\tau_{rec}$  for which  $\bar{I}_n \approx I_\infty \approx V_{th}/R_{in}$ , for high enough presynaptic firing rate. In this situation an optimal  $C_0$  value will be maintained over a wide range of network firing rates, as the figure 5.5A shows.

Since short-term synaptic mechanisms alone are not able to induce bimodal resonances in simple IF neurons with fixed threshold, as we have already seen, a plausible hypothesis is that this two-peak resonant behavior emerges from the interplay between these synaptic mechanisms and adaptive thresholds. To illustrate this hypothesis, we can sketch a simple explanation of such cooperative effect by considering that, for an excitable system displaying SR, a resonance peak is obtained when the strength of the fluctuations is approximately equal to some potential barrier height (McNamara and Wiesenfeld, 1989). That is, if we define in our system the barrier height as  $\Delta\Phi \equiv \theta - R_{in}\bar{I}_n$  (that is, the distance in voltage between the mean membrane potential and the firing threshold), a resonance peak will appear each time the condition  $R_{in}\sigma_n \simeq \Delta\Phi$  is satisfied (i.e., when the current fluctuations are of order of the barrier height). Considering a threshold dependence such as the one defined in equation (5.4) in the steady state, the barrier height takes the value of a small constant ( $\Delta\Phi \equiv \Delta\Phi_d \simeq \delta$ ) for large enough  $f_n$ . Since the dependence of  $R_{in}\sigma_n$  with  $f_n$  is non-monotonic for dynamic synapses (see section 5.3.1 and figure 5.2 for details), plotting together the expressions of  $R_{in}\sigma_n$  and  $\Delta\Phi_d$  as a function of  $f_n$  shows two well located crossing points, as the top panels of figure 5.5B illustrate. Each one of these crossing points is associated then with a maximum in  $C_0$  (as we have argued above), and therefore a bimodal resonance is obtained. The local minimum in  $C_0$  is due to a high number of erratic firings of the postsynaptic neuron, which is caused by high values of the current fluctuations (compared with the barrier height) around the point where the local minimum appears. This feature is depicted in the top-left panel of figure 5.5B with a double-head arrow. Without such large current fluctuations, the local minimum of  $C_0$  would vanish and the bimodal resonance would be lost. On the other hand, for the case of an IF neuron with fixed threshold, the barrier height  $\Delta\Phi \equiv \Delta\Phi_s$  is a monotonically decreasing function of  $f_n$ . In these conditions, a single crossing point between  $R_{in}\sigma_n$  and  $\Delta\Phi_s$  is obtained<sup>3</sup>, and therefore the SR curve presents a single peak, as the bottom panels of figure 5.5B show.

---

<sup>3</sup>For certain sets of values of the model parameters, two crossing points between the level of EPSC fluctuations and the barrier height can be also found for a fixed neuron threshold. However, in such situations  $\Delta\Phi_s$  is large and comparable with  $\sigma$ . As a consequence, the local minimum of  $C_0$  cannot be obtained, and the SR curve remains with the characteristic single-peak shape.

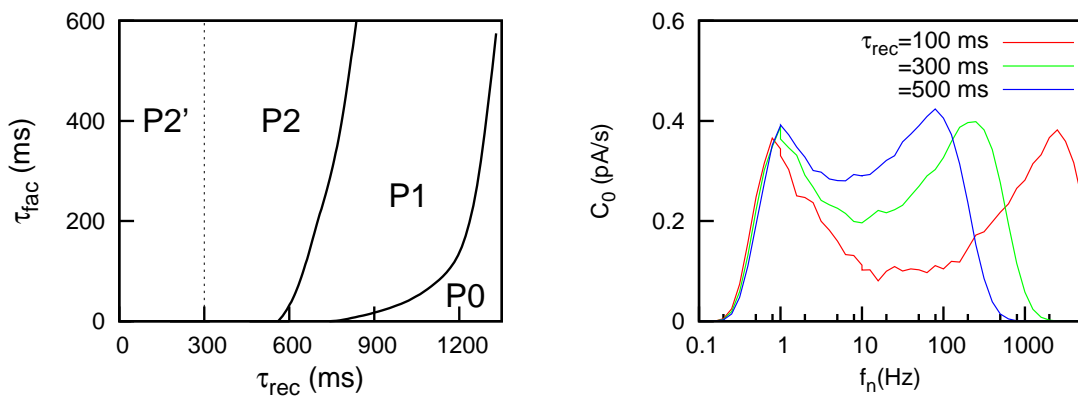


Figure 5.6: (A) Phase diagram, obtained from our mean-field approach, which shows different regimes of the behavior of the system, for  $U_{SE} = 0.1$  and  $A_{SE} = 120$  pA. Labels P0, P1, P2 denote, respectively, regions in which zero, one, or two resonance peaks occur. The region P2' denotes values of the synaptic parameters for which a second resonance appears, but at a frequency too high to be considered realistic (that is,  $f^* > 1/\tau_{ref} = 200$  Hz). For  $\tau_{rec} \rightarrow 0$  the typical single resonance peak is recovered. (B) Bimodal resonances obtained for a realistic signal (a poissonian spike train influenced by STD mechanisms), with  $U_{SE} = 0.5$  and  $\tau_{fac} = 0$ .

The appearance of bimodal resonances gives a high versatility to neurons as weak signals detectors. In actual neural media, populations of neurons could take advantage of such versatility, and they could use the high heterogeneity of synaptic properties (Wang et al., 2006) to organize groups of neurons with non-resonance, single-resonance or two-resonance peak behavior. A phase diagram, which locates the repertoire of different behaviors in the space of synaptic relevant parameters, is shown in figure 5.6A. For realistic synaptic conditions, the three types of behavior are accessible. The region P2' corresponds initially to two resonances, but the second resonance is usually located in an extremely high network rate ( $f^* > 200$  Hz), which means that the second resonance does not occur in realistic conditions. If we increase  $\tau_{rec}$  (for a given value of  $\tau_{fac}$ ), the system pass from a single-peak resonance behavior (region P2') for low  $\tau_{rec}$ , to the bimodal resonance phase P2 (because increasing  $\tau_{rec}$  implies lowering  $f^*$ ). After that, the system reaches a single-peak behavior again (due to the fusion of the two peaks of the bimodal resonance into just one peak, namely region P1). Finally, increasing  $\tau_{rec}$  even more would lead to a decrement of the detection ability of the neuron, leading to the zero-resonance phase (labeled as P0 in the figure).

### 5.3.5 Further analysis with more realistic considerations

#### A. Poissonian signal term

The fact that we considered a simplified neuron model allowed us to make an analytical treatment, which confirmed the numerical results both for STD and STF, as we have already seen. However, we should consider whether bimodal resonances appear in more realistic conditions. For instance, so far we assumed (as a first approximation) that the signal term was a sinusoidal function of weak amplitude and slow frequency. It is well known, however, that *in vivo* neural signals are usually encoded in spike trains. Moreover, since these presynaptic spike trains affect the postsynaptic neuron via the synapses, STD mechanisms should, *a priori*, affect the signal term as well. To account for this and to test our results in more realistic conditions, we consider a signal term given by  $S(t) = d_s y(t)$ , where  $d_s = 7 \text{ pA}$  is the amplitude of the signal, and  $y(t)$  introduces STD on the signal (see equation (5.2)). We also assume a poissonian train of pulses of frequency  $f_s = 5 \text{ Hz}$  for the signal. The consideration of this more realistic signal term does not have a dramatic effect on the resonant behavior of the neuron, as can be seen in figure 5.6B. Indeed, STD induces, as before, the appearance of a second resonance peak. This second resonance peak also appears for the same range of values of  $\tau_{rec}$  and  $f_n$  than before, which implies that our results are robust with this more realistic assumption for the signal term.

#### B. More realistic neuron models

The emergence of bimodal resonances is also maintained when one considers a more realistic neuron model to simulate the response of the postsynaptic neuron. Although we have employed an adaptive threshold to include some of the nonlinear features of actual neurons into the IF neuron model, it should be convenient to test our findings by considering an intrinsic nonlinear neuron model which could present this type of threshold variability without additional ingredients. A common simple model employed in the literature to describe the nonlinear excitability properties of actual neurons is the FitzHugh-Nagumo neuron model (Koch, 1999), which can be defined as

$$\begin{aligned} \tau_m \frac{dv(t)}{dt} &= \tau_m \epsilon [v(t)(v(t) - a)(1 - v(t)) - w(t)] + S(t) + R I_n(t) \\ \frac{dw(t)}{dt} &= b v(t) - c w(t), \end{aligned} \tag{5.16}$$

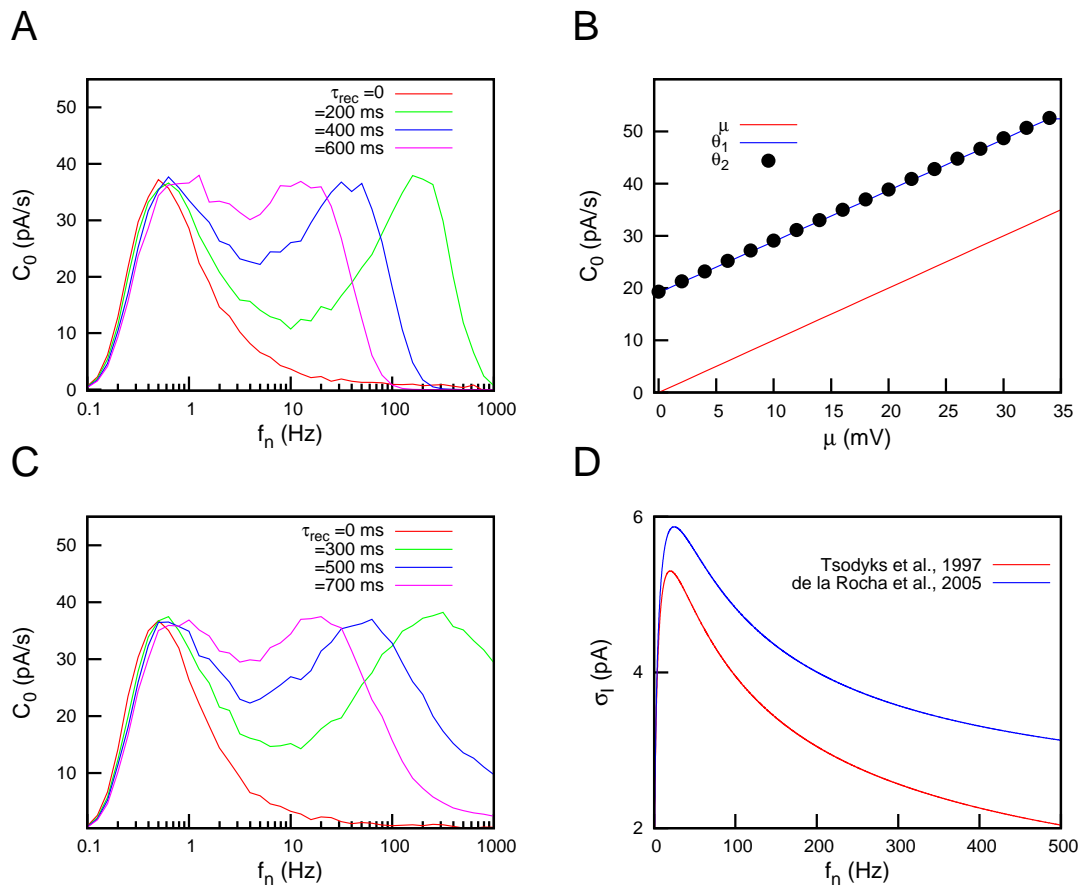


Figure 5.7: (A) Numerical SR curves for a postsynaptic FHN neuron model receiving a weak signal and uncorrelated background noisy activity of frequency  $f_n$ , for  $\tau_{fac} = 0$ ,  $U_{SE} = 0.5$ ,  $A_{SE} = 15$  pA and different values of  $\tau_{rec}$ . In order to estimate the firing times of the FHN model, the dynamics of the variable  $v(t)$  was thresholded at  $v = 0.8$ . (B) Estimation of the neuron firing threshold for different values of the constant input current  $\mu$ , and employing two different measures (see the main text for details). (C) Numerical SR curves for several  $\tau_{rec}$  values and  $U_{SE} = 0.5$ , when a more realistic stochastic model for the synapses is employed (see main text). We set the parameters of the stochastic model in  $M = 50$ ,  $J = 3$  pA,  $\Delta_M = 0.1$  and  $\Delta_J = 1$  pA. (D) Comparison of the standard deviation of the synaptic current for the two synaptic models employed in our study. The conditions are the same than those in panel C and  $\tau_{rec} = 100$  ms. Although the difference between the predictions of these two models is about 60 % for high frequencies, similar bimodal resonances are obtained in both cases.

where  $v(t)$  represents the postsynaptic membrane potential,  $w(t)$  is a slow recovery variable related with the refractory time, and  $a = 0.001$ ,  $b = 3.5$  ms<sup>-1</sup>,  $c = 1$  ms<sup>-1</sup>,  $\epsilon = 1000$  ms<sup>-1</sup> are parameters of the model. With this choice of values for the parameters, the model is set in the excitable regime, the (dimensionless)

voltage  $v(t) = 1$  corresponds to  $100mV$  and time is given in  $ms$ . We also consider  $R = 0.1 G\Omega/mV$  and  $\tau_m = 10 ms$ , which lie within the physiological range of actual cortical neurons. The terms  $S(t)$  and  $I_n(t)$  are described as before, with  $d_s = 5$ . We have performed numerical simulations of the system schematized in figure 5.1, but considering now this FHN model for the membrane potential of the postsynaptic neuron. The results are shown in figure 5.7A, which illustrates that for large enough values of  $\tau_{rec}$  a bimodal resonance also appears. The location of the second peak moves towards lower values of  $f_n$  as  $\tau_{rec}$  increases, as it was found with the IF model with adaptive threshold. The range of values of the noisy frequency  $f_n$  at which the second peak is located is also the same than in the previous model.

It is necessary to demonstrate here that the FHN model presents several threshold variability properties which are similar to those we assumed for the IF neuron model with adaptive threshold. In order to check this, we define two types of temporal stimuli that the postsynaptic neuron can receive (in addition to the weak signal):  $h_1(t)$  and  $h_2(t)$ . The first stimulus,  $h_1(t)$ , consists in a train of narrow ( $\sim 2 ms$ ) square pulses of frequency  $f_s$  (that is, the same frequency as the signal). We impose that each one of these pulses arrives to the postsynaptic neuron every time the weak signal  $S(t)$  reaches its maximum value, namely  $d_s$ . Similarly, the other type of stimulus,  $h_2(t)$ , consists in a train of narrow ( $\sim 2 ms$ ) square pulses also of frequency  $f_s$ , but in this case each pulse arrives at the postsynaptic neuron when  $S(t) = -d_s$  (that is, every time the signal takes its lowest value). We also set a constant input  $\mu$ , in such a way that the total input to the postsynaptic neuron is given by  $S(t) + \mu + h_1(t) + h_2(t)$ . For a given fixed value of  $\mu$ , we can determine the value of the neural firing threshold by increasing the strength of the stimulus  $h_1(t)$  (that is, the height of the narrow pulses) until an AP is generated as a consequence of such stimulus. This measure of the firing threshold will be denoted as  $\theta_1$ . Similarly, we can perform a second estimation of the neuron threshold, namely  $\theta_2$ , by varying the strength of  $h_2(t)$  until an AP is generated in response to this second stimulus. Both estimations of the firing threshold, as a function of the constant input  $\mu$ , are shown in figure 5.7B. The figure illustrates two major features of the excitability properties of the FHN neuron model. The first one is that, independently of the value of  $\mu$ , both estimations give almost identical results for the value of the neural firing threshold of the FHN neuron model. Since the only distinction between the stimuli  $h_1(t)$  and  $h_2(t)$  is a difference in amplitude of  $2 d_s$ , which is due to the signal term, this result indicates that the weak signal does not influence the value of the firing threshold (independently of the value of the constant input  $\mu$ ). This confirms the assumption we made for the IF model in equation (5.4). The second major feature illustrated by the figure 5.7B is that the value of the firing threshold varies with  $\mu$  as  $\theta \simeq C + \mu$ , with  $C$  being a constant. This dependence coincides with

the expression for the steady state of the firing threshold obtained from equation (5.4), which we assumed for the IF model with adaptive threshold. Therefore, the hypothesis we made on the modeling of the threshold variability for the IF model is appropriate as is confirmed by using more realistic neuron models, such as the FHN model (which incorporates nonlinear excitability properties).

### *C. More realistic synapse models*

The robustness and generality of our previous results can be also tested by considering a more realistic model for the activity-dependent synaptic mechanisms. For instance, until now we have treated the synapses employing a deterministic model of dynamic synapses for the sake of simplicity. However, it is known that actual synapses have a stochastic nature (Dobrunz and Stevens, 1997) and their fluctuations can play an important role in neural computation (Dobrunz and Stevens, 1997; Zador, 1998), and therefore they should be taken into account. In particular, since the SR curves depend strongly on the noise properties, it is important to consider the additional source of noise due to synaptic fluctuations, since this could lead to a very different emergent behavior in the system. To see the influence of such fluctuations in our analysis, we have simulated our system using an intrinsically stochastic model of dynamic synapses presented in (de la Rocha and Parga, 2005). This model considers that each connection between neurons has a finite number of functional contacts, or synaptic buttons, and this number is randomly chosen (for each particular connection) from a Gaussian distribution of mean  $M$  and standard deviation  $\Delta_M$ . In addition, the strength of each individual synaptic button is also randomly determined from a Gaussian distribution of mean  $J$  and standard deviation  $\Delta_J$ . The release of a neurotransmitter vesicle from a synaptic button to the synaptic cleft, when an AP arrives at the button, is modeled as a random event. After that release, the recovering of the synaptic button is considered as a probabilistic event following a Poisson distribution with a typical time  $\tau_{rec}$ . This probabilistic model gives the same mean values for the EPSC, but the fluctuations differ from the deterministic model of dynamic synapses (de la Rocha et al., 2004). Concretely, the EPSC fluctuations for an uncorrelated noisy input are now given by (see also figure 5.7D)

$$\sigma_n^2 = NMJ^2 u_\infty x_\infty f_n \left[ 1 + \Delta_J^2 + \frac{u_\infty [M(1 + \Delta_M^2) - 1]}{1 + u_\infty \tau_{rec} f_n (1 - u_\infty/2)} \right]. \quad (5.17)$$

As it is shown in figure 5.7C, this stochastic model induces the same phenomenology during SR experiments as those for the deterministic model described by (5.2-5.3). That is, for the case of static synapses, a single resonance peak at low frequencies is obtained as usual, and when  $\tau_{rec}$  is increased, a second peak appears at high

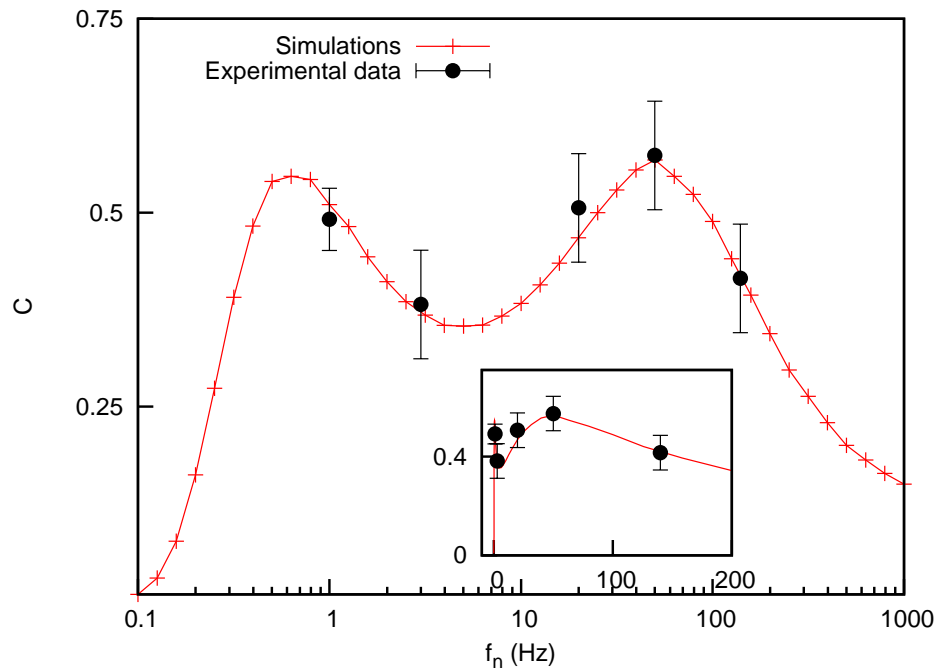


Figure 5.8: Comparison between experimental data from (Yasuda et al., 2008) and numerical simulations of the FHN neuron model and an stochastic dynamic synapse model with  $J = 3 \text{ pA}$ ,  $\Delta_J = 1 \text{ pA}$ ,  $M = 50$ ,  $\Delta_M = 0.1$ ,  $U_{SE} = 0.5$  and  $\tau_{rec} = 500 \text{ ms}$ . We assumed a linear relationship between auditory noise intensity and the mean firing rate ( $f_n = a_1 A_n + a_2$ , with  $(a_1, a_2) = (6, -370)$  for  $A_n \geq 60 \text{ dB}$  and  $(a_1, a_2) = (0.1, -2.5)$  for  $A_n < 60 \text{ dB}$ ), although other dependences are possible and also show good agreement between experiments and simulations with realistic parameter values. Each simulation point has been averaged over 100 trials. The inset shows the same data in a linear scale.

frequencies, with the resonance peak location moving towards low noise rates. We also tested our results by considering a conductance based description of the synaptic current, leading to the appearance of bimodal resonances as well (data not shown).

### 5.3.6 Experimental evidences of bimodal resonances

While this bimodal resonance behavior could be difficult to measure directly in *in vivo* cellular recordings, several experimental methodologies are available to study the occurrence of this phenomenology in actual systems. For instance, recent experimental studies (Yasuda et al., 2008; Simons-Weidenmaier et al., 2006) have shown that STD has a strong impact in the detection of weak tactile signals by caudal pontine reticular nucleus (PnC) neurons. This region of the brain stem is responsible for auditory startle reflex (Lingenhohl and Friauf, 1994), and thus an auditory noisy input may act as a noise term, enhancing the tactile blink reflex response to stimuli (Yasuda et al., 2008). In addition, as well as STD, some adaptation processes

of the neuron membrane potential seem to play a role in this brain area (Lingenhohl and Friauf, 1994; Pilz and Schnitzler, 1996). As a consequence of these factors, PnC would be an excellent brain structure to search for the existence of bimodal resonances similar to those we have theoretically obtained. With this in mind, we have compared the predictions of our study with experimental data<sup>4</sup> taken from (Yasuda et al., 2008). In this work it is reported that the ability of air-puff stimulations to an eyelid (input) to induce blinks (output) is improved by the addition of auditory white noise. To measure this improvement, a cross-correlation parameter equivalent to the one we used is employed. As one can see in figure 5.8, experimental data show clear evidences of two resonance peaks. These resonances are well explained with our FHN model receiving a weak signal and a noisy current modulated by STD, as indicates the good fitting between experiments and our simulation results. In order to relate the auditory noise intensity  $A_n$  (measured in  $dB$ ) with the mean firing rate  $f_n$ , we assumed two separate regions in the noise domain ( $A_n \geq 60dB$  and  $A_n < 60dB$ ), and we also considered a linear relationship  $A_n = a_1 f_n + a_2$  for each region. This distinction was done in order to separate the effect of giant PnC neurons with medium ( $A_n < 60dB$ ) and high ( $A_n > 60dB$ ) detection threshold (Lingenhohl and Friauf, 1994). However, other types of dependence (such as a linear dependence for all the range of  $A_n$ ) are also plausible and does not affect the appearance of bimodal resonances from the experimental data. These results suggest that PnC neurons actually employ the two-resonance phenomena to increase their ability to detect weak tactile inputs over different auditory noise levels.

## 5.4 Discussion

It is widely known that noise can have relevant and positive effects in many nonlinear systems in nature. These effects include noise-induced phase transitions (van den Broeck et al., 1994, 1997), stochastic dynamics of domain growth (Ibanes et al., 2000), or multiple types of stochastic resonance (McNamara and Wiesenfeld, 1989; Wiesenfeld et al., 1994; Collins et al., 1995), to name a few. The particular case of stochastic resonance has been widely studied in the context of biological systems (Wiesenfeld et al., 1994; Bezrukov and Vodyanoy, 1995), and in particular in the brain. More precisely, stochastic resonance phenomena could occur in many brain areas, such as the cortex (Ho and Destexhe, 2000; Manjarrez et al., 2002; Fellous et al., 2003), the hippocampus (Stancey and Durand, 2000), or the brain

---

<sup>4</sup>We have employed the experimental data from Table 1 of Ref. (Yasuda et al., 2008), and we obtained the values of the cross-correlation function following the same protocol that the authors used in this work.

stem (Yasuda et al., 2008). Therefore, it is highly relevant to understand the influence that some features of actual neural systems could have in the emergence of stochastic resonance phenomena.

Short-term synaptic mechanisms are, in this framework, a good candidate to consider. It is known, for instance, that both STD and STF play an important role in the transmission of relevant correlations between neurons in noisy environments (Mejias and Torres, 2008), in the temporal maintenance of information in persistent states of working memory tasks (Mongillo et al., 2008), in the recall of stored memories on attractor neural networks (Mejias and Torres, 2009b), or in the switching behavior between neural activity patterns (Torres et al., 2007). However, the interplay between these two mechanisms, or between them and other adaptation processes of neurons, has not been fully addressed yet.

In this chapter we have considered the role of dynamic synapses in the detection of weak signals by neurons embedded in neural networks, via a stochastic resonance formalism. To the best of our knowledge, this is the first study that shows the dramatic effect of the interplay between the dynamical nature of synapses and adaptive threshold mechanisms on the stochastic resonance properties of neurons. More precisely, we have demonstrated that this interplay originates the appearance of bimodal resonances, where the location of the resonances in the frequency domain is related with the relevant synaptic parameters. In addition, to test our findings we have used several neuron and synapse models, as well as a number of realistic considerations such as poissonian input spike trains (both for signal and noise terms), for instance. While such bimodal resonances have been found in several systems (Tessone et al., 2006; Volkov et al., 2003), their occurrence in neural media has not been reported up to date.

Recent studies (Zalanyi et al., 2001; Yasuda et al., 2008) have also suggested a relevant role of STD in neural stochastic resonance, but the emergence of bimodal resonances, which is the crucial point of our study, is missed in these works. Our findings are also supported by experimental data taken from (Yasuda et al., 2008), and by other experimental works (Lugo et al., 2008). Several questions should be experimentally tested, though. An interesting prediction to test is, for instance, whether STF has the effect on the first resonance peak predicted by our results. This gives an idea of the relevance of the dynamics of intracellular calcium in processing weak signals at spontaneous activity states, which are common in cortical areas. The observed dependences of the position of the peaks with the synaptic characteristic time scales could be confirmed experimentally as well. Finally, the question of how these bimodal resonances can be measured in actual cortical structures, and its effect in the collective dynamics of large cortical neural networks, constitutes an interesting issue that still remains open.

# Chapter 6

## Storage capacity of attractor neural networks

In this chapter we extend the study of the two previous chapters, concerning the effects of STD and STF in the processing of information in small neural circuits, to the case of large recurrent networks of neurons. Concretely, we focus on the role of short-term synaptic plasticity in the storage capacity and retrieval abilities of attractor neural networks, which constitute a prominent example of emergent collective behavior of neural systems.

### 6.1 Introduction

One interesting topic which arises in the study of biologically motivated neural systems is how dynamical processes affecting the synapses in different time scales can influence the collective behavior of large neural assemblies. A well known example is the slow change in the synaptic strength due to a learning process of activity patterns, that can be modelled as a neural network which includes a hebbian prescription for the synaptic intensities (Hebb, 1949) (see also section 3.4.3). As a consequence of this process, the network is able to retrieve previously *learned* patterns, mimicking the associative memory tasks which occur in the brain (Amari, 1972; Hopfield, 1982; Amit et al., 1987). The maximum number of such patterns ( $M_{\max}$ ), per neuron, that the network is able to store without having significant errors in the recovery task is called the critical (or maximum) storage capacity of the system. This capacity is commonly denoted by the ratio  $\alpha_c \equiv M_{\max}/N$ , with  $N$  being the number of neurons in the network. It is well known that the critical storage capacity is affected by certain considerations about real neural systems, such as constraints in the range of values of the synaptic strength (Fusi and Abbott, 2007), the mean activity level of the stored patterns (Tsodyks and Feigelman, 1988;

Amit and Tsodyks, 1991), or the topology of the network (McGraw and Menzinger, 2003; Torres et al., 2004). None of these works take into account, however, that the synaptic strength also varies in short-time scales producing a fluctuating response which can be depressed (synaptic depression) or enhanced (synaptic facilitation) depending on the presynaptic activity (Abbott et al., 1997; Markram et al., 1998; Tsodyks et al., 1998), which defines the so called *dynamic synapses* (as we have explained in the previous chapters).

Short-term depression and facilitation have been proposed as dynamical processes responsible for many kinds of complex behavior found in neural systems. For instance, recent theoretical works have reported the importance of these mechanisms in the appearance of periodic and chaotic switching between stored activity patterns (Pantic et al., 2002; Torres et al., 2007), which could be related to the oscillations between up and down cortical states (Holcman and Tsodyks, 2006). They are also responsible for the generation of persistent activity in working memories (Romani et al., 2006; Barak and Tsodyks, 2007; Mongillo et al., 2008), and enhance the detection of correlated inputs in a background of noisy activity under different conditions (Mejias and Torres, 2008) (see also chapter 4). As discussed in section 2.5.2, synaptic depression occurs due to the existence of a *limited* amount of neurotransmitter vesicles in the synaptic button, ready to be released into the synaptic cleft if a presynaptic action potential (AP) arrives. This produces, for a high frequency stimulus, a decrease of the postsynaptic response – which is a measure of the synaptic strength – as is shown in (Abbott et al., 1997) and in chapter 3. On the other hand, synaptic facilitation takes into account the effect of the influx of extracellular calcium ions into the neuron near the synapse after the arrival of each presynaptic AP (Bertram et al., 1996). As discussed previously, these ions bind to some receptors which favors the neurotransmitter vesicle depletion, in such a way that the postsynaptic response increases for successive APs (Kamiya and Zucker, 1994). Facilitation, therefore, increases the synaptic strength for high frequency presynaptic stimuli. The effect of the competition between these two a priori opposite mechanisms has been shown to be highly relevant in the emergent behavior of attractor neural networks (ANN) with activity-dependent dynamic synapses with a finite number of stored patterns (Torres et al., 2007). However, until now the effect of such competition in the critical storage capacity has not been reported. Only very recently, a few studies have analyzed this particularly interesting issue for depressing synapses, and showed that the critical storage capacity of stable memory patterns is severely reduced in this case (Bibitchkov et al., 2002; Torres et al., 2002; Matsumoto et al., 2007). Our aim in this chapter is to compute the critical storage capacity of an ANN, with both depressing and facilitating mechanisms competing in the synapses, to quantitatively analyse the effect of including facilitation in the sys-

tem. We demonstrate that synaptic facilitation improves the storage capacity with respect to the case of depressing synapses, for a certain range of the synaptic parameters. Moreover, if the level of depression is not too large, facilitation can increase the critical storage capacity, reaching in some cases the value obtained with static synapses – which is the maximum that one can obtain considering a hebbian learning rule with unbiased random patterns in a fully connected network. Our results suggest that a certain level of facilitation in the synapses might be positive for an efficient memory retrieval, while the function of strongly depressed synapses could be more oriented to other tasks concerning, for instance, the dynamical processing of data.

## 6.2 The model

Our starting point is a fully connected network of  $N$  binary neurons whose state  $\mathbf{s} \equiv \{s_i = 0, 1; \forall i = 1, \dots, N\}$  follows a probabilistic *Little* (parallel and synchronous) dynamics (Peretto, 1992):

$$\text{Prob}[s_i(t+1) = 1] = \frac{1}{2} \{1 + \tanh[2\beta(h_i(\mathbf{s}, t) - \theta_i)]\} \quad \forall i = 1 \dots N, \quad (6.1)$$

where  $h_i(\mathbf{s}, t)$  is the local field or the total input synaptic current to neuron  $i$ , namely

$$h_i(\mathbf{s}, t) = \sum_{j \neq i} \omega_{ij} x_j(t) F_j(t) s_j(t). \quad (6.2)$$

Here,  $\beta = T^{-1}$  is a temperature or noise parameter (i.e., for  $\beta \rightarrow \infty$  we have a deterministic dynamics in equation (6.1)), and  $\theta_i$  represents the neuron firing threshold. The coefficients  $\omega_{ij}$  are fixed maximal synaptic conductances, consequence of the slow learning process of  $M$  memory patterns of activity. In the following we will choose a hebbian prescription for such learning via the standard covariance rule (Tsodyks and Feigelman, 1988)

$$\omega_{ij} = \frac{1}{Nf(1-f)} \sum_{\mu=1}^M (\xi_i^\mu - f)(\xi_j^\mu - f), \quad (6.3)$$

where  $\{\xi_i^\mu = 0, 1; i = 1 \dots N\}$  represents the  $M$  stored random patterns with mean activity  $\langle \xi_i^\mu \rangle = f = 1/2$ . On the other hand, the variables  $x_j$ ,  $F_j$  appearing in  $h_i$  describe the short-term depression and facilitation synaptic mechanisms, respectively. For simplicity, we assume that these variables evolve according to the discrete

dynamics<sup>1</sup> (Tsodyks et al., 1998; Torres et al., 2002)

$$x_j(t+1) = x_j(t) + \frac{1 - x_j(t)}{\tau_{rec}} - U_{SE}F_j(t)x_j(t)s_j(t) \quad (6.4)$$

$$u_j(t+1) = u_j(t) + \frac{U_{SE} - u_j(t)}{\tau_{fac}} + U_{SE}(1 - u_j(t))s_j(t), \quad (6.5)$$

where  $u_j(t) \equiv U_{SE}F_j(t)$ . Here,  $U_{SE}$  represents the maximum fraction of neurotransmitters which can be released in absence of facilitation each time a presynaptic AP arrives to the synapse, and  $\tau_{rec}, \tau_{fac}$  are, respectively, the time constants for depressing and facilitating processes. The dynamics (6.4-6.5) allows to recover the critical storage capacity of the standard Hopfield model ( $\alpha_c \simeq 0.138$ ) (Amit et al., 1987) for static synapses, that is, when  $x_i = F_i = 1, \forall i, t$ . By a simple inspection of equations (6.4-6.5), this limit corresponds to the case of  $\tau_{rec}, \tau_{fac} \ll 1$  which makes  $x_j$  and  $u_j \forall j$  to quickly reach their maximum values, namely 1 and  $U_{SE}$ , and implies  $x_j = F_j = 1 \forall j, t^2$ . In this limit one has the relation  $2[h_i(\mathbf{s}, t) - \theta_i] = h_i^H(\mathbf{s}, t)$  where  $h_i^H(\mathbf{s}, t)$  stands for the local field of the classic Hopfield model with zero threshold, which assumes a  $\{-1, +1\}$  code for the neuron states and implies for  $\theta_i$  the form

$$\theta_i = \frac{1}{2} \sum_{j \neq i} \omega_{ij}. \quad (6.6)$$

Instead, we used in this chapter the  $\{1, 0\}$  code because it is more related with biology and allows for a clear separation of the synaptic current  $h_i(\mathbf{s}, t)$  from the neuron threshold  $\theta_i$  and, therefore, it enables one to study the effect of synaptic depression and facilitation alone, without including other adaptive effects related, for instance, with threshold dynamics.

## 6.3 Results

### 6.3.1 Mean-field analysis

From the definition of  $h_i(\mathbf{s}, t)$  and equations (6.3) and (6.6), we obtain

$$2[h_i(\mathbf{s}, t) - \theta_i] = \sum_{\mu} \epsilon_i^{\mu} \overline{m}^{\mu}(\mathbf{s}, t) - 2\alpha x_i(t)F_i(t)s_i(t) + \alpha \quad (6.7)$$

---

<sup>1</sup>A continuous version of this dynamics for the synapses, together with a sequential updating of neuron states, also gives a similar behavior of the system.

<sup>2</sup>Note that, more precisely, the static synapse limit is obtained for  $\tau_{rec}, \tau_{fac} \rightarrow 0$ , but due to the discrete dynamics represented by equations (6.4-6.5) one can have some dynamical instabilities during the simulation of the map for very small time constants. However, a continuous version of the dynamics (6.4-6.5) or considering only steady-state conditions (as we assume in this chapter) allows to consider without any problem that limit.

where  $\alpha \equiv \frac{M}{N}$ ,  $\epsilon_i^\mu \equiv 2\xi_i^\mu - 1$ , and  $\overline{m}^\mu(\mathbf{s}, t) \equiv \frac{1}{N} \sum_j \epsilon_j^\mu [2x_j(t)F_j(t)s_j(t) - 1]$ .

We assume now that the system reaches some stationary state ( $t \rightarrow \infty$ ) which corresponds to a fixed point of the dynamics. In order to work with the term  $x_i(t)F_i(t)s_i(t)$  and to obtain an approximately valid mean field theory, we also assume that the working temperature ( $T$ ) in the system is very small (to avoid as much as possible thermal fluctuations). This hypothesis is reasonable because our goal is to compute maximum storage capacity, so at the end we have to perform the limit  $T \rightarrow 0$ . One has then two possible scenarios:

- (a)  $T = 0$ . The state of the system is *quenched* and it does not present any temporal fluctuations in  $s_i$ . Therefore, one can assume that in each site  $s_i$  takes a fixed value (namely  $s_i^\infty = 1, 0$ ) for all times. We can then evaluate the fixed point in equations (6.4) and (6.5) as a function of  $s_i^\infty$  and obtain (Matsumoto et al., 2007)

$$F_i = \frac{1 + \tau_{fac} s_i^\infty}{1 + U_{SE} \tau_{fac} s_i^\infty}; \quad x_i = \frac{1}{1 + U_{SE} F_i \tau_{rec} s_i^\infty}. \quad (6.8)$$

Taking into account that  $s_i^\infty$  takes the values  $\{0, 1\}$ , we can simplify the expression for the product  $x_i F_i s_i$ , leading to

$$x_i F_i s_i = \frac{\gamma'}{1 + \gamma \gamma'} s_i^\infty \quad (6.9)$$

where  $\gamma \equiv U_{SE} \tau_{rec}$  and  $\gamma' \equiv \frac{1 + \tau_{fac}}{1 + U_{SE} \tau_{fac}}$ . One can easily check that the static limit (Hopfield model) is obtained again for  $\tau_{rec}, \tau_{fac} \rightarrow 0$  which implies  $\gamma \rightarrow 0$ ,  $\gamma' \rightarrow 1$ , respectively.

- (b)  $T \simeq 0$  ( $1 \ll \beta < \infty$ ). For very low temperatures and in the steady state, the typical time interval between thermal fluctuations is very large compared with  $\tau_{rec}$  and  $\tau_{fac}$ , due to the exponential dependency on  $\beta$  for the probability to have such fluctuations, so between two consecutive fluctuations the condition (6.9) still holds<sup>3</sup>. Therefore, averaging (6.9) over all temporal fluctuations of  $s_i$  during a large time window  $\Delta t \rightarrow \infty$  in the steady state, one has

$$x_i F_i s_i \simeq \frac{\gamma'}{1 + \gamma \gamma'} \langle s_i \rangle_t, \quad (6.10)$$

with  $\langle s_i \rangle_t \equiv \lim_{\Delta t \rightarrow \infty} \frac{1}{\Delta t} \sum_{t=t_0}^{t_0 + \Delta t} s_i(t)$ . Note that  $\langle s_i \rangle_t = s_i^\infty$  for  $T = 0$  and we recover (6.9), so it is reasonable to assume that the approach (6.10) holds for low (non-zero) temperatures.

---

<sup>3</sup>Note, for instance, that if neuron  $i$  is in the state  $s_i^\infty = 1$  (one has  $h_i > \theta_i$ ) the probability to fluctuate to the state  $1 - s_i^\infty = 0$  is  $1 - p$  with  $p$  given by (6.1), which gives  $(1 - p) \sim e^{-2\beta(h_i - \theta_i)} \ll 1$ . Similarly, if  $s_i^\infty = 0$  ( $h_i < \theta_i$ ) the probability to fluctuate to the state  $s_i^\infty = 1$  is  $p \sim e^{2\beta(h_i - \theta_i)}$  which is also exponentially small.

In order to compute the critical storage capacity let us consider this second scenario, namely the case of  $\beta$  very large and finite. In the limit of  $N, M \rightarrow \infty$  with  $\alpha = M/N$  finite, one can assume the standard mean-field approach  $s_i \approx \langle s_i \rangle$ , which is a good approximation for systems involving long-range interactions as in the case we are considering here, that is, a fully connected network. Under this assumption one has  $\langle s_i \rangle_t = \langle s_i \rangle$  and the steady-state condition (6.10) allows to write  $\overline{m}^\mu(\mathbf{s}) \approx \overline{m}^\mu \equiv \frac{1}{N} \sum_j \epsilon_j^\mu [2 \frac{\gamma'}{1+\gamma\gamma'} \langle s_j \rangle - 1]$ . This quantity is related with the usual mean-field overlap function  $m^\mu \equiv \frac{1}{N} \sum_j \epsilon_j^\mu \langle \sigma_j \rangle$  (where  $\sigma_j = 2s_j - 1$ ) by the expression

$$\overline{m}^\mu = \frac{\gamma'}{1+\gamma\gamma'} m^\mu - \left(1 - \frac{\gamma'}{1+\gamma\gamma'}\right) B^\mu, \quad (6.11)$$

where  $B^\mu \equiv \frac{1}{N} \sum_j \epsilon_j^\mu$  is typically of order  $\mathcal{O}\left(\frac{1}{\sqrt{N}}\right)$  for random unbiased patterns.

Expression (6.11) can be used to calculate the steady state mean-field equations for the system if one assumes that the system reaches a steady state in which the network has a macroscopic overlap with a particular pattern, the so called *condensed pattern*, with the remaining  $M - 1$  being of order  $\mathcal{O}(1/\sqrt{N})$ . In the following and without loss of generality, we choose  $\mu = 1$  as the condensed pattern.

Using the probability (6.1) in the steady state, it is easy to compute  $\langle s_i \rangle$  to obtain, for the mean-field overlap function,

$$m^\mu = \frac{1}{N} \sum_i \epsilon_i^\mu \tanh [2\beta(h_i - \theta_i)]. \quad (6.12)$$

If we neglect the self-energy terms in (6.7) then  $2(h_i - \theta_i) \simeq \sum_\nu \epsilon_i^\nu \overline{m}^\nu$ . Inserting this into equation (6.12) for  $\mu = 1$  and using (6.11), the steady state mean-field equation for  $m^1 \equiv m$  reads

$$m = \left\langle \left\langle \tanh \left[ \beta \left( \frac{\gamma'}{1+\gamma\gamma'} m + \zeta \right) \right] \right\rangle \right\rangle \quad (6.13)$$

where  $\langle \langle \cdot \cdot \rangle \rangle$  indicates an average over a distribution  $\mathcal{P}(\zeta)$ . Here,  $\zeta$  is a gaussian white noise due to the effect of  $M - 1$  non-condensed patterns, and it is obtained, as we will explain later, taking the limit  $N \rightarrow \infty$  in the term  $\sum_{\mu \neq 1} \epsilon_i^\mu \overline{m}^\mu$ . To derive equation 6.13, we employed the expression  $\overline{m}^1 \simeq \frac{\gamma'}{1+\gamma\gamma'} m^1$  for the condensed pattern, after neglecting the  $\mathcal{O}(1/\sqrt{N})$  contribution in (6.11). Similarly and following standard techniques, one can compute the *spin-glass* order parameter in our probabilistic approach, that is,  $q \equiv \frac{1}{N} \sum_i \tanh^2 [2\beta(h_i - \theta_i)]$  (see for instance, (Hertz et al., 1991)) which gives

$$q = \left\langle \left\langle \tanh^2 \left[ \beta \left( \frac{\gamma'}{1+\gamma\gamma'} m + \zeta \right) \right] \right\rangle \right\rangle, \quad (6.14)$$

and the pattern interference parameter  $r \equiv \frac{1}{\alpha} \sum_{\mu \neq 1}^M (m^\mu)^2$ , which in this limit becomes

$$r = \frac{q}{\left(1 - \beta \frac{\gamma'}{1+\gamma\gamma'} (1 - q)\right)^2}. \quad (6.15)$$

Equations (6.13-6.15) for  $m$ ,  $q$  and  $r$  constitute the mean-field solution of the model. However, we must characterize the distribution  $\mathcal{P}(\zeta)$  to have a complete solution. In the derivation of equations (6.13-6.15), we can obtain an explicit expression for  $\zeta$  from the variable

$$\zeta_i \equiv \sum_{\mu \neq 1} \epsilon_i^1 \epsilon_i^\mu \bar{m}^\mu, \quad (6.16)$$

after taking the limit  $N \rightarrow \infty$  and self-averaging over the distribution of random unbiased patterns. Considering equation (6.11),  $\zeta_i$  can be written as a combination of the variables  $z_1 \equiv \frac{1}{\sqrt{\alpha r}} \sum_{\mu \neq 1} \epsilon_i^1 \epsilon_i^\mu m^\mu$  and  $z_2 \equiv \frac{1}{\sqrt{\alpha}} \sum_{\mu \neq 1} \epsilon_i^1 \epsilon_i^\mu B^\mu$ , and in the limit of interest explained above, both can be considered as uncorrelated gaussian random variables  $N[0, 1]$ . In fact, we have

$$\zeta = \sqrt{\alpha r} \frac{\gamma'}{1 + \gamma\gamma'} z_1 - \sqrt{\alpha} \left( 1 - \frac{\gamma'}{1 + \gamma\gamma'} \right) z_2 \equiv C_1 z_1 - C_2 z_2. \quad (6.17)$$

For simplicity in the calculations, it is convenient to rewrite  $\zeta$  as  $\bar{\zeta} \equiv \frac{\zeta}{C_1}$ . Since  $z_1$ ,  $z_2$  are normal-distributed, we can compute the probability distribution  $\mathcal{P}(\bar{\zeta})$  employing standard techniques, that is,  $\mathcal{P}(\bar{\zeta}) = \int \int \delta \left[ \bar{\zeta} - z_1 + \frac{C_2}{C_1} z_2 \right] p(z_1) p(z_2) dz_1 dz_2$  where  $p(z)$  is the normal distribution  $N[0, 1]$ . Computing this integral yields  $\mathcal{P}(\bar{\zeta}) = N[0, \sigma^2]$ , that is, a gaussian distribution with zero mean and variance  $\sigma^2 = 1 + C_2^2/C_1^2$ . This allows to consider

$$\zeta \approx \frac{\gamma'}{1 + \gamma\gamma'} \left( \alpha r + \alpha \left( \frac{1 + \gamma\gamma' - \gamma'}{\gamma'} \right)^2 \right)^{1/2} z \quad (6.18)$$

where  $z$  is a normal-distributed variable  $N[0, 1]$ .

Finally, the mean-field equations (after introducing the rescaled inverse of the temperature  $\hat{\beta} \equiv \frac{\gamma'}{1 + \gamma\gamma'} \beta$ ) take the form

$$m = \left\langle \left\langle \tanh \left[ \hat{\beta} \left( m + z \sqrt{\alpha r + \alpha \left( \frac{1 + \gamma\gamma' - \gamma'}{\gamma'} \right)^2} \right) \right] \right\rangle \right\rangle \quad (6.19)$$

$$q = \left\langle \left\langle \tanh^2 \left[ \hat{\beta} \left( m + z \sqrt{\alpha r + \alpha \left( \frac{1 + \gamma\gamma' - \gamma'}{\gamma'} \right)^2} \right) \right] \right\rangle \right\rangle \quad (6.20)$$

$$r = \frac{q}{\left( 1 - \hat{\beta}(1 - q) \right)^2}. \quad (6.21)$$

The equations (6.19-6.21) constitute the complete mean-field solution of the system for a working temperature near to zero  $1 \ll \beta < \infty$ . It is noticeable that the effect of including synaptic depression competing with facilitation is not a simple rescaling of temperature (marked by the presence of  $\hat{\beta}$ ) compared with the case of

the classical static Hopfield model. On the contrary, the dynamics of the synapses affects in a different manner the signal and noise terms produced by the interference of the remaining  $(M - 1)$  patterns. This becomes evident in the explicit expression of the noise term (6.18). As we will see below, our results show that this term has a strong influence on the critical storage capacity when depression and facilitation are present, producing a non-trivial behavior.

Although equations (6.19-6.21) have been derived assuming  $1 \ll \beta < \infty$ , one can give some arguments to extend their validity for any  $T$  if the system reaches a steady state (for instance, a recall, non-recall or a *spin-glass* state). In fact, for relatively high temperatures (and sufficiently low values of  $\tau_{rec}$  and  $\tau_{fac}$ ) the dynamics (6.4-6.5) for both  $x_i(t)$  and  $u_i(t)$  is mainly driven for the fluctuating term which contains  $s_i(t)$ , instead of the deterministic exponential behavior with time constants  $\tau_{rec}$  and  $\tau_{fac}$ . Under this condition a plausible hypothesis is to consider both  $x_i(t)$  and  $u_j(t)$  as binary variables which follow the probabilistic dynamics of  $s_i(t)$  and fluctuate in time between only two possible values, namely  $x^{(1)}$  ( $u^{(1)}$ ) when  $s_i(t) = 1$ , and  $x^{(0)}$  ( $u^{(0)}$ ) when  $s_i(t) = 0$ . A possible choice (but not the only one) for  $x^{(1,0)}$  ( $u^{(1,0)}$ ) is the two steady state values of  $x_i(t)$  ( $u_i(t)$ ) at  $T = 0$  – see expressions in equation (6.8). This choice implies avoiding any temporal correlations or *memory* introduced by  $\tau_{rec}$  or  $\tau_{fac}$  in the values of  $x_i(t)$  and  $u_i(t)$ . Considering these assumptions one has<sup>4</sup>

$$\begin{aligned} x_i(t) &\approx 1 + \left( \frac{1}{1+\gamma\gamma'} - 1 \right) s_i(t) \\ F_i(t) &= \frac{u_i}{U_{SE}} \approx 1 + (\gamma' - 1)s_i(t), \end{aligned} \quad (6.22)$$

which gives again

$$x_i(t)F_i(t)s_i(t) = \frac{\gamma'}{1 + \gamma\gamma'} s_i(t) \quad \forall t. \quad (6.23)$$

Note that in (6.23) there is now a dependency on  $t$  compared with the case of (6.9). Now computing  $\langle s_i(t) \rangle$  in the steady state using (6.1), as in the standard Hopfield model, one obtains again equations (6.19-6.21) which are, therefore, approximately valid for all the range of temperatures of interest<sup>5</sup>. However, this strongly relies on the assumption that a fixed point solution will be reached, and in general this may not be true for relatively large values of  $\tau_{rec}$  and  $\tau_{fac}$ . In this situation, some stationary oscillatory states can emerge as a result of the presence of depression and/or facilitation (see, for instance, (Pantic et al., 2002; Torres et al., 2007)). Concretely,

---

<sup>4</sup>Note that the effect of facilitation and/or depression in this approach is to change the size of the fluctuation between these two values for  $x_i(t)$  and  $u_i(t)$ . For instance, for  $\tau_{rec}, \tau_{fac} \rightarrow 0$  one has  $x^{(1)} = x^{(0)} = 1$  and  $u^{(1)} = u^{(0)} = U_{SE}$ , so  $x_i(t)$  and  $u_i(t)$  do not fluctuate.

<sup>5</sup>Some preliminary results in the limit of  $\alpha \rightarrow 0$  have confirmed the validity of (6.19-6.21) for any value of  $T < T_c$ , if the system reaches a stable fixed point (see appendix C).

the appearance of these oscillatory states is a consequence of the temporal correlations driven by the deterministic part of the dynamics (6.4-6.5). This deterministic part, which is coupled with the stochastic fluctuations driven by  $s_j$ , can destabilize the fixed point steady states. As a consequence, the system starts to continuously jump between these metastable states. In this study, since we are interested in computing the maximum storage capacity, and this quantity is evaluated at  $T = 0$ , we will not find these oscillatory solutions and the mean-field theory remains valid.

In general, equations. (6.19-6.21) cannot be solved analytically. However, one can still get some information about the critical storage capacity because this is computed for  $\beta \rightarrow \infty$  (the zero temperature limit). In this situation one can perform the substitutions

$$\int \frac{dz}{\sqrt{2\pi}} \exp(-z^2/2) \tanh[\widehat{\beta}(az + b)] \simeq \operatorname{erf}\left(\frac{b}{a\sqrt{2}}\right)$$

$$\int \frac{dz}{\sqrt{2\pi}} \exp(-z^2/2) \left(1 - \tanh^2[\widehat{\beta}(az + b)]\right) \simeq \frac{1}{a\widehat{\beta}} \sqrt{\frac{2}{\pi}} \exp\left(-\frac{b^2}{2a^2}\right).$$
(6.24)

This allows to write down the following expressions

$$m \simeq \operatorname{erf}(y)$$
(6.25)

$$q \simeq 1 - \frac{1}{a\widehat{\beta}} \sqrt{\frac{2}{\pi}} \exp(-y^2),$$
(6.26)

where the variable  $y$  is given by

$$y \equiv \frac{b}{a\sqrt{2}} \equiv \frac{m}{\left(2\alpha r + 2\alpha \left(\frac{1+\gamma\gamma' - \gamma'}{\gamma'}\right)^2\right)^{1/2}}$$
(6.27)

Employing these approaches together with equation. (6.21) ones obtains a simplified expression for the complete solution, namely

$$y \left[ \sqrt{2\alpha \left(1 + \left(\frac{1 + \gamma\gamma' - \gamma'}{\gamma'}\right)^2\right)} + \frac{2}{\sqrt{\pi}} \exp(-y^2) \right] = \operatorname{erf}(y),$$
(6.28)

where we assumed  $r \simeq 1$  in order to get a closed expression. This assumption works well as an approximation since  $r \simeq 1$  in the memory phase. equation. (6.28) allows to compute the maximal storage capacity for different synaptic conditions, as we will see below, including the competition between synaptic depression and facilitation.

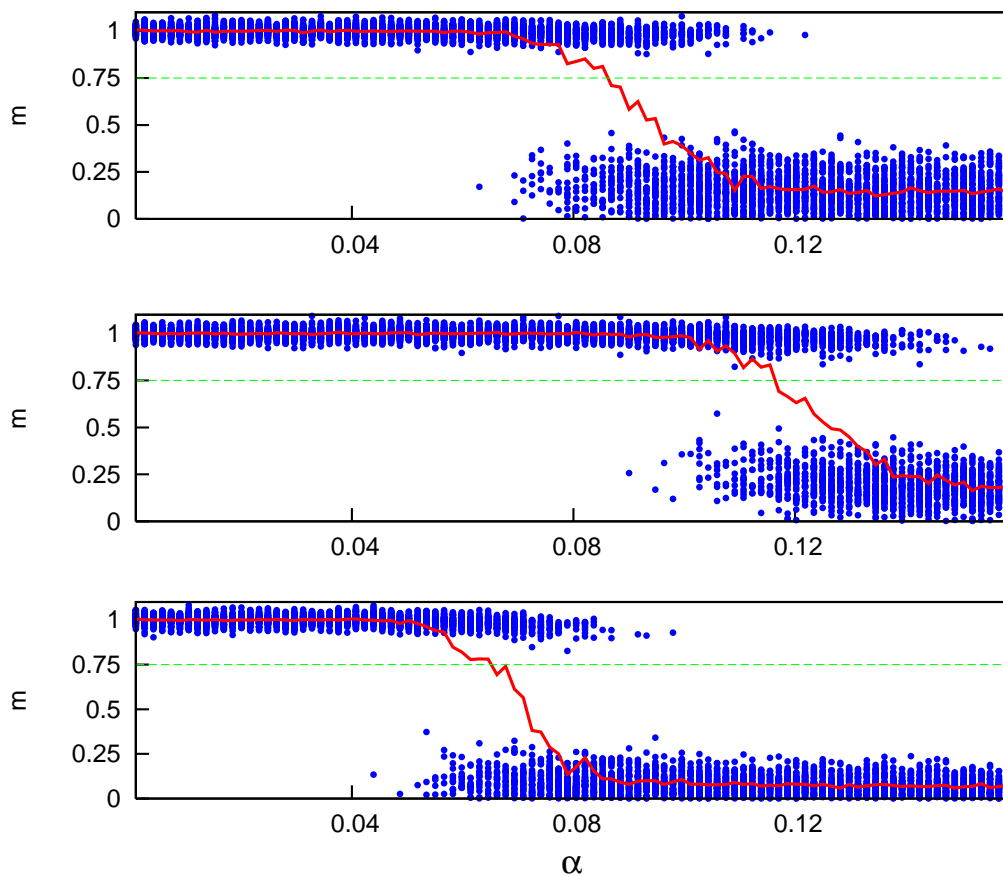


Figure 6.1: Criterion chosen for the calculation of  $\alpha_c$  in Monte Carlo simulations. Each panel shows, for  $U_{SE} = 0.05, 0.5, 0.7$  (from top to bottom), a numerical estimate of the critical storage capacity, obtained by averaging the stationary value of the macroscopic overlap (solid line) over many realizations of the stored patterns (dots). The value of  $\alpha_c$  corresponds to the crossing point between the averaged overlap and the dashed line  $m = 0.75$  that we used as a criterion for good retrieval of the condensed pattern. Other synaptic parameters were  $\tau_{rec} = 2$  and  $\tau_{fac} = 200$ .

### 6.3.2 Maximum storage capacity

In order to obtain the critical storage capacity  $\alpha_c$  for a given set of values of the synaptic parameters, we have to find the maximal value of  $\alpha$  for which nontrivial solutions ( $y \neq 0$ ) appear. More specifically, we look for the maximal value of  $\alpha$  for which the stationary value of the macroscopic overlap is  $m \geq 0.75$ . This criterion, which is usually taken for the numerical evaluation of the critical storage capacity in simulations, is illustrated for three different numerical examples in Fig. 6.1. The figure shows that the value of the critical storage capacity depends on the synaptic parameters, as it was found in (Torres et al., 2002; Bibitchkov et al., 2002; Matsumoto et al., 2007). In these works, the inclusion of synaptic dynamics (in particular, synaptic depression) led to a monotonic decrease of the critical storage

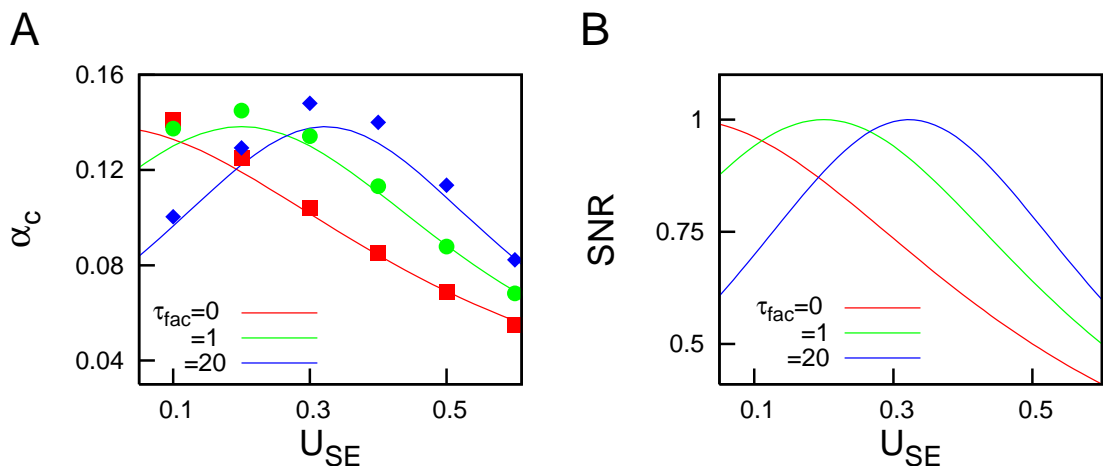


Figure 6.2: (A) Critical storage capacity  $\alpha_c$  as a function of  $U_{SE}$  for fixed  $\tau_{rec} = 2$  and different values of  $\tau_{fac}$ . The inclusion of facilitation causes the appearance of a non-monotonic behavior of the critical capacity of the network as a function of  $U_{SE}$  and  $\tau_{fac}$ , with a maximum which reaches the limit of static synapses ( $\alpha_c \simeq 0.138$ ). Different symbols correspond to numerical simulations of a network with  $N = 3000$  neurons and different synaptic parameters. (B) Behavior of  $SNR$ , as defined in the text, for the same value of parameters as in panel A. This shows the origin of the non-monotonic behavior of the critical storage capacity found for different values of the synapse parameters.

capacity of the network as one increases the synaptic parameters  $\tau_{rec}$  and  $U_{SE}$ . This decrease was found to be caused by the loss of stability of the memory fixed points of the system, in the presence of depression. In Fig. 6.1, however, we see that intermediate values of  $U_{SE}$  give higher values of  $\alpha_c$ , suggesting the possibility of a non-monotonic dependence of  $\alpha_c$  on  $U_{SE}$ , which is mainly due to the presence of facilitation.

A more detailed analysis of this phenomenon is shown in Fig. 6.2A. The figure shows that the inclusion of synaptic facilitation in a network with depressing synapses ( $\tau_{rec} = 2$ , fixed) induces the appearance of a non-monotonic behavior of  $\alpha_c$  with a maximum value for a given  $U_{SE}^*$  which depends on  $\tau_{fac}$ . The figure also shows the good agreement of our mean-field theory with simulation of a network of  $N = 3000$  neurons (symbols). In the particular case of  $\tau_{fac} = 0$ , we recover the results reported in (Torres et al., 2002), that is, the fact that the static limit  $\alpha_c \simeq 0.138$  is only obtained for  $\tau_{rec}U_{SE} = 0$ . However, if we include the possibility of synaptic facilitation in the synapses, one can obtain  $\alpha_c \simeq 0.138$  for  $\tau_{rec}U_{SE} > 0$ , (that is, for synapses with a certain level of depression). This implies that dynamic synapses are not only convenient for dynamical processing of information in real neurons (Abbott et al., 1997; Abbott and Regehr, 2004), or to explain the appear-

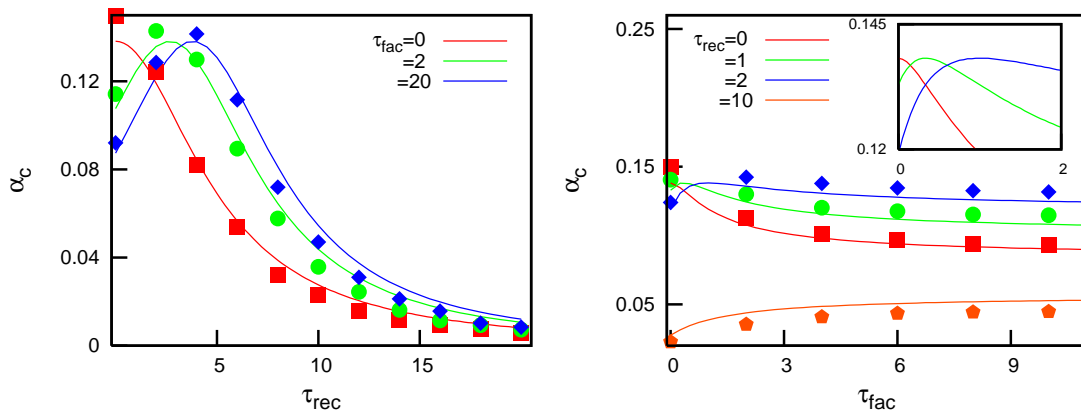


Figure 6.3: Left:  $\alpha_c$  as a function of  $\tau_{rec}$ , for different values of  $\tau_{fac}$ . Facilitation induces the appearance of non-monotonic dependences in the critical storage capacity with a maximum which reaches the limit of static synapses. Right:  $\alpha_c$  as a function of  $\tau_{fac}$ , for different  $\tau_{rec}$ . For  $\tau_{rec}$  relatively small,  $\alpha_c$  takes high values for the whole range of values of  $\tau_{fac}$ . The inset shows a detail near the maximum of the mean field curves. Other parameters used in simulations were  $U_{SE} = 0.2$  and  $N = 3000$ .

ance of global oscillations and other emergent phenomena in neural systems (Torres et al., 2007; Pantic et al., 2002; Holcman and Tsodyks, 2006). In fact, an optimal balance between depression and facilitation is necessary to recover the high retrieval properties of networks with static synapses.

We can also obtain a non-monotonic behavior of  $\alpha_c$  if we fix  $U_{SE}$  and vary the other synaptic parameters, as it is shown in Fig. 6.3. As a function of  $\tau_{rec}$ , the critical storage capacity reaches the classical static limit for a certain nontrivial  $\tau_{rec}$  value if facilitation is present. As a function of  $\tau_{fac}$ , the classical limit is also obtained providing that depression is not too strong (see, for instance, the curve for  $\tau_{rec} = 10$  in right panel of Fig. 6.3, where a large depression time constant induces lower  $\alpha_c$  values). The figure also shows the good agreement of mean-field curves and simulations (symbols). The appearance of these maxima in Figs. 6.2A and 6.3 can be explained due to the competition between depression and facilitation mechanisms. That is, once the system has arrived to a fixed point of the dynamics, the effect of depression and facilitation is mainly a modification of the (fixed) strength of the synapses. Depression produces a decrease of the synaptic strength when the presynaptic neuron is active all the time. As a consequence, and compared with the static case, the pattern destabilizes for lower values of the noise produced by the interference with other patterns. This leads to a lower critical storage capacity value (Bibitchkov et al., 2002; Torres et al., 2002). Facilitation, however, has the

opposite effect as it increases the synaptic strength. Therefore, facilitation can enlarge the critical storage capacity for a given level of noise with respect to the depressing case. The increase in the synaptic strength due to facilitation can only be induced until it reaches the static synapse strength limit – because the product  $x_i F_i$  in (6.2) cannot be larger than one. Thus, one can think that since these two mechanisms are regulated by different parameters, their competition would lead to the appearance of a maximum in  $\alpha_c$ . This argument is not sufficient to explain the appearance of such a maximum since one has to consider that such competition affects both the signal term and the noise produced by the interference with other patterns. Only the consideration of the cooperative effect of all these mechanisms can explain the appearance of a maximum in  $\alpha_c$ , as it is observed.

To measure how the relative strength of the signal compared with the noise is affected by the competition between these two synaptic mechanisms one can compute, for instance, the ratio between the signal and noise contributions to the overlap (see equation. (6.19)), that is

$$SNR \equiv \frac{1}{1 + \left( \frac{1 + \gamma\gamma' - \gamma'}{\gamma'} \right)^2}, \quad (6.29)$$

where we used  $r \approx 1$  and  $m \approx 1$  which is a good approximation at  $T = 0$ . For static synapses one has  $SNR = 1$ . One can now understand the maximum appearing in figure 6.2A, for certain values of  $\tau_{fac}$  and  $\tau_{rec}$ , as a function of  $U_{SE}$ , by inspection of figure 6.2B. If one plots  $SNR$  as a function of  $U_{SE}$  one observes that it also has a maximum at a certain value  $U_{SE}^*$ , where  $SNR = 1$ , which is the value corresponding to the static synapse limit (in the figure, this maximum appears at  $U_{SE}^* \approx 0.33$  for  $\tau_{rec} = 2$ ,  $\tau_{fac} = 20$ ). Therefore, it matches with the maximum observed in the behavior of  $\alpha_c$  for the same value of the synaptic parameters (see figure 6.2A). For other values of  $\tau_{rec}$ ,  $\tau_{fac}$  and  $U_{SE}$ , the shape of the  $SNR$  should be different but, similarly to the previous example, it can easily explain the non-monotonic behavior of  $\alpha_c$  as a function of all these parameters.

In general, we can see that large values of  $\alpha_c$  appear when  $U_{SE}$  and  $\tau_{rec}$  have moderate values, and large enough  $\tau_{fac}$ . These values coincide qualitatively well with those described in facilitating synapses of some cortical areas, where  $U_{SE}$  is low compared with the corresponding values found in depressing synapses, and  $\tau_{rec}$  is several times lower than  $\tau_{fac}$  (Markram et al., 1998). To have such a relatively low value for  $U_{SE}$  is important because it allows for a stronger recovery of the synaptic strength due to facilitation. In addition, it is worthy to note that obtaining high  $\alpha_c$  values is possible for a wide range of synaptic conditions, as it is shown in right panel of Fig. 6.3 and more explicitly in Fig 6.4. For instance, high capacities ( $\alpha_c \geq 0.1$ ) can be obtained for very different values of  $\tau_{fac}$ . Since actual synapses usually present

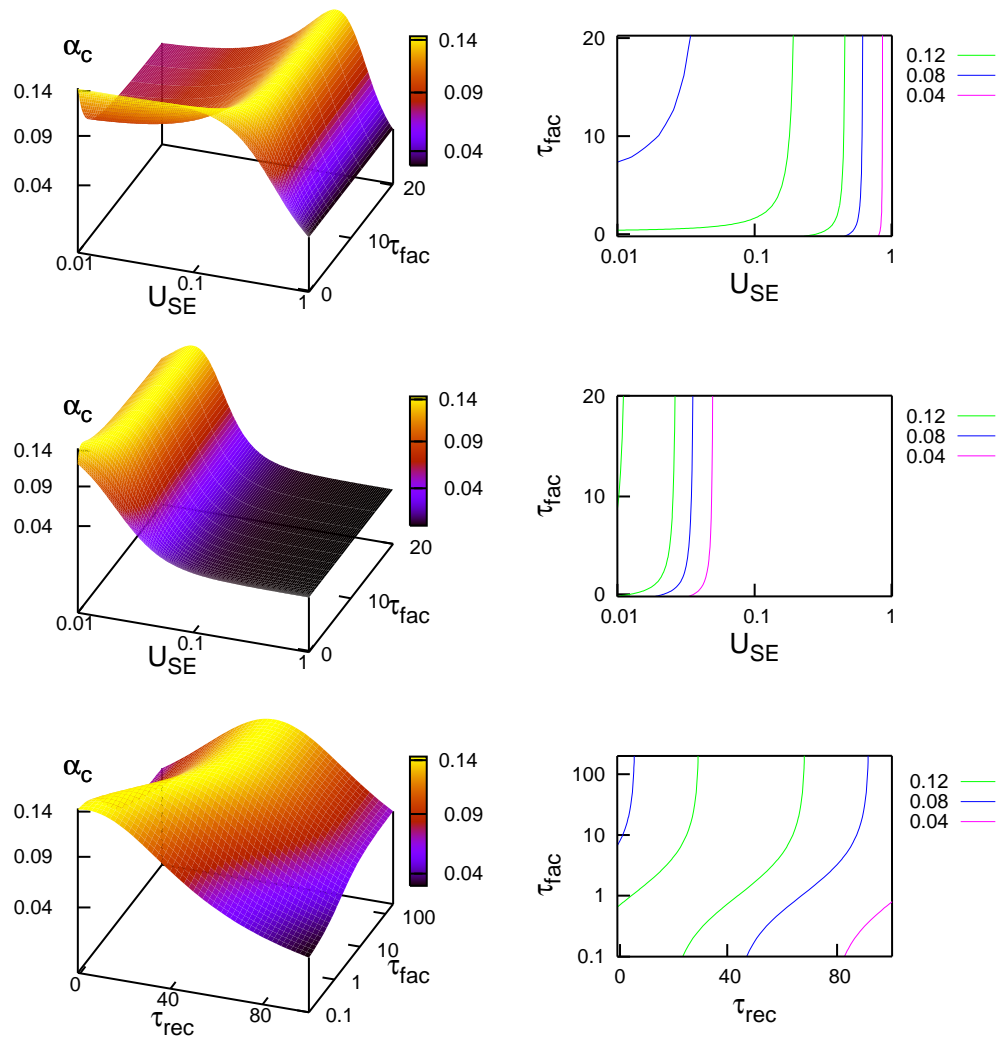


Figure 6.4: Left: Surface plots of the critical storage capacity  $\alpha_c$  as a function of different synaptic parameters, for fixed  $\tau_{rec} = 2$  (top),  $\tau_{rec} = 50$  (middle) and  $U_{SE} = 0.02$  (bottom). Right: Contour plots which correspond to the surfaces on the left. Regions inside the lines corresponds to a set of parameters for which the critical storage capacity is high. Middle and bottom panels correspond to a more realistic set of parameters (if one assumes that the Monte Carlo step is of order of a typical refractory period of 2 *ms*), and they illustrate that high capacities are obtained for a realistic values of the synaptic parameters. As one can see, the inclusion of facilitation is able to double the critical storage capacity for certain situations (see main text).

a high heterogeneity in the degree of depression  $\tau_{rec}$ , and even more in the degree of facilitation  $\tau_{fac}$  (see, for instance, (Markram et al., 1998; Wang et al., 2006)), our results predict high values of  $\alpha_c$  for realistic conditions. This is shown in middle

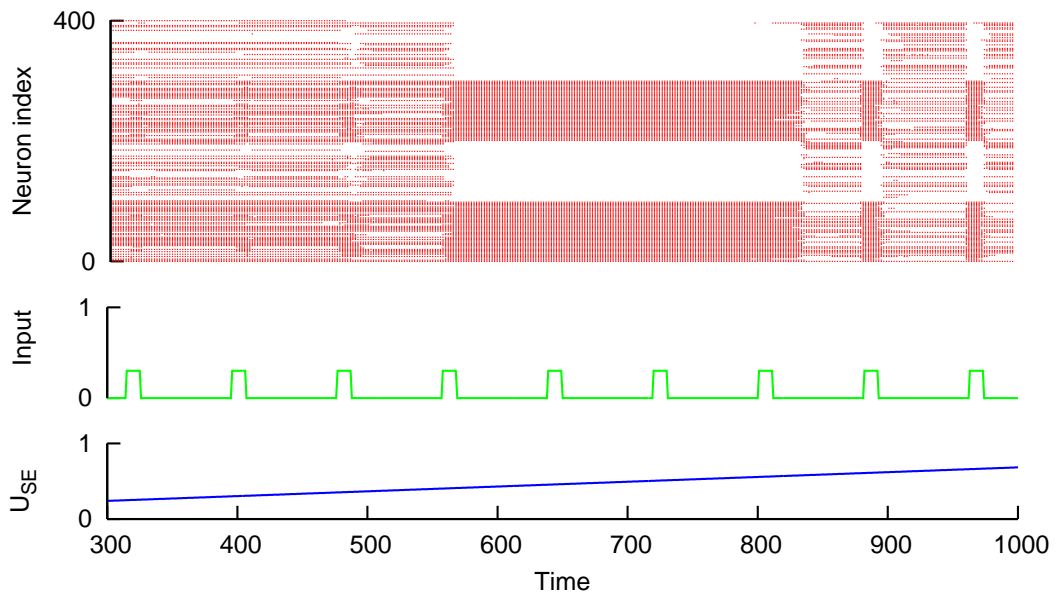


Figure 6.5: Memory retrieval under external stimulus for a network of  $N = 400$  neurons with dynamic synapses. The network is stimulated with a periodic weak input train (middle panel) which, in the memory phase, is able to induce the retrieval of a certain activity pattern (constructed in a band-like fashion to allow a clearer visualization). The value of  $U_{SE}$  is slowly incremented in time (bottom panel) while the synaptic parameters  $\tau_{rec} = 2$  and  $\tau_{fac} = 20$  remain fixed. Good retrieval occurs only for a certain window of values of  $U_{SE}$ , which shows a non-monotonic dependency of  $\alpha_c(U_{SE})$ .

and bottom panels of Fig. 6.4 where the high critical storage capacity is mainly obtained for a wide range of  $\tau_{fac}$  (concretely, for  $\tau_{fac} > 10$ ) around  $U_{SE} = 0.02$ , and  $\tau_{rec} = 50$ . Assuming that our Monte Carlo time step is comparable with a typical refractory period of  $2 \text{ ms}$ , these values would correspond to  $U_{SE} = 0.02$ ,  $\tau_{rec} = 100 \text{ ms}$  and  $\tau_{fac} > 20 \text{ ms}$ , which are within the range of realistic values in several cortical areas (Markram et al., 1998). Actual neural systems could, indeed, take advantage of this peculiarity to preserve a possible fine tuning of the degree of facilitation for other purposes, such as a fast dynamical processing of data, while an optimal recall of the memories is conserved.

The improvement in the critical storage capacity for these realistic values ( $U_{SE} = 0.02$ ,  $\tau_{rec} = 100 \text{ ms}$  and  $\tau_{fac} > 20 \text{ ms}$ ) in comparison with the case of only depressing synapses is highly significant. Looking at bottom panels of Fig. 6.4, for instance, one can see that the critical storage capacity reaches  $\alpha_c \simeq 0.138$  for the parameter values mentioned above. However, if we consider only the effect due to depressing synapses (that is, we set  $\tau_{fac} = 0$ ), we obtain  $\alpha_c \simeq 0.07$ . That is, the capacity decreases around 50% of its value with facilitation. This indicates that facilitation could have a highly important role in the storage and recall of memories.

As an illustrative example of the implications of the results reported above, let us consider a system constituted by a network of  $N$  fully connected neurons which receive an additional weak external input during a very short period of time. The total synaptic current to each neuron  $i$  then becomes  $h_i(\mathbf{s}, t) + h_i^{ext}(t)$ . If the system is in the memory phase, we expect the external input to drive the system towards a stationary attractor state  $\{\xi_i^{\mu_0}\}$ . We will also consider that the input stimulus occurs periodically in time as follows

$$h_i^{ext}(t) = \begin{cases} h\xi_i^{\mu_0} & t_n \leq t < (t_n + \delta t) \quad \forall n = 0, \dots, N_{inputs} \\ 0 & \text{otherwise} \end{cases} \quad (6.30)$$

where  $h \ll 1$  is the amplitude of the weak input,  $t_n$  is the time at which the  $n$ -th input event occurs,  $\delta t$  is the duration of a single input event and  $\mathcal{T} = t_{n+1} - t_n$  is the period of the stimulus. If the system is in the memory phase, the stimulus will lead the system into the  $\mu_0 - th$  attractor and the memory retrieval will be successful. Otherwise, for large number of stored patterns, namely  $M > \alpha_c N$  the system will fall in a *spin-glass* state characterized by a mixture of a high number of patterns, and the retrieval will have failed. We explored how certain synapse parameters affects the retrieval process under this type of stimulus. This is shown in Fig. 6.5 for a network of  $N = 400$  neurons and  $M = 48$  patterns ( $\alpha = 0.12$ ), with the pattern  $\mu_0$  constituted by consecutive groups —100 neurons each— of alternate firing and silent neurons, and the remaining  $M - 1$  being random unbiased patterns. As an example, we consider dynamic synapses with fixed characteristic time constants  $\tau_{rec} = 2$  and  $\tau_{fac} = 20$ , and  $U_{SE}$  varying in time for the whole duration of the stimulus. The figure shows that facilitation, which induces the appearance of a non-monotonic relation  $\alpha_c(U_{SE})$ , allows for a good response to the external weak stimulus for a certain window of values of  $U_{SE}$ . In particular, for values of  $U_{SE} \simeq 0.4$  the stimulus is able to drive the system towards the attractor and recover the corresponding memory pattern  $\mu_0$ . The range of values of  $U_{SE}$  at which the system retrieves the pattern coincides with those between the points at which the line  $\alpha = 0.12$  crosses the critical mean-field line  $\alpha_c(U_{SE})$  showed in Fig. 6.2 for  $\tau_{rec} = 2$  and  $\tau_{fac} = 20$ . A similar type of behavior also occurs fixing  $U_{SE}$  and  $\tau_{rec}$  and varying now  $\tau_{fac}$  (data not shown), which also shows the main role of facilitation in memory recall.

### 6.3.3 Basins of attraction

The effect caused by dynamic synapses does not only affect the stability of fixed points of the system, which gives us the critical storage capacity, but also the dynamics of the network. This has been recently investigated for the case of a single stored pattern ( $\alpha \rightarrow 0$ ) at finite temperature (Torres et al., 2007). For many patterns, however, the interference among them can influence the behavior of the system

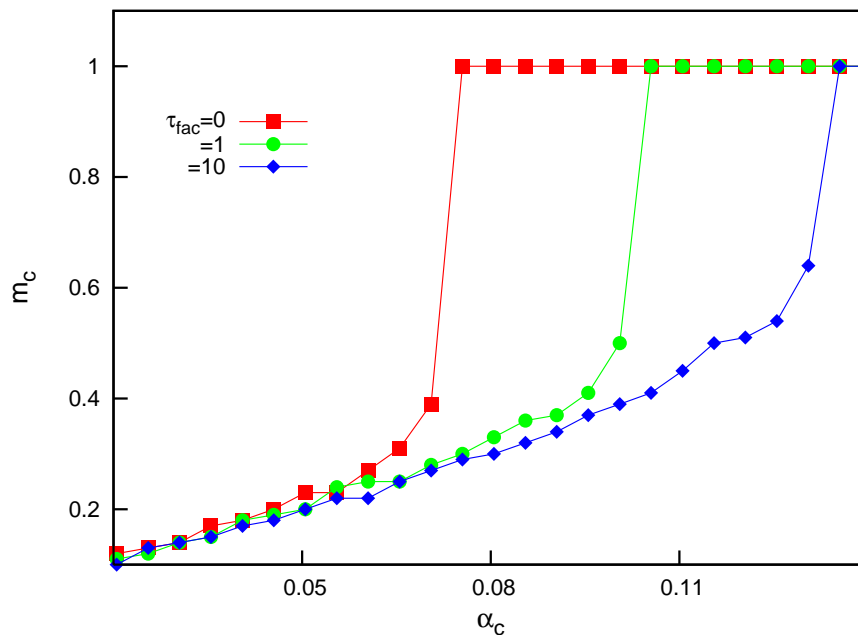


Figure 6.6: Basins of attraction of a neural network in the presence of dynamic synapses. We can see that facilitation enlarges the basins of attraction with respect to synapses with only depressing mechanisms. This allows to retrieve the previously stored patterns even if the initial condition for the network is only weakly correlated with the corresponding pattern. Parameter values are  $U_{SE} = 0.2$  and  $\tau_{rec} = 5$ .

near the attractors due to the appearance of many local minima associated to *spin-glass* states (Amit et al., 1987). To analyse this effect, we can define the basin of attraction of an activity pattern  $\mu$  as the minimal value for the initial condition, namely  $m_c^\mu$ , that allows the system to tend to this attractor (Bibitchkov et al., 2002; Matsumoto et al., 2007). The measure of the basins of attraction is highly relevant because the system will not easily tend to the stored attractors if their basins are too shallow. Since we know that dynamic synapses have indeed a notable effect in the dynamics of the network at finite  $\beta$ , we expect them to influence the dynamics also at  $\beta \rightarrow \infty$ , and therefore modify the basins of attraction in some way. We have explored this issue, and the results are shown in Fig. 6.6. We can see that the inclusion of facilitation in a network of depressing synapses leads to an increment of the basins of attraction. Since basins of attraction are associated with the error-correcting ability of the system<sup>6</sup>, our results show that networks with facilitating synapses are adequate for recovering patterns, even from initial conditions only

<sup>6</sup>The error-correcting ability resembles the capacity of an attractor neural network to properly recognize an activity pattern when the given initial condition is not strongly correlated with the corresponding pattern.

weakly correlated with the patterns. One can conclude, therefore, that facilitation increases the stability of the fixed points by increasing the basins, and this leads to a higher critical storage capacity, as we have reported previously.

## 6.4 Discussion

In this chapter we have focused on the role of the competition between several synaptic activity-dependent mechanisms, such as short-term depression and facilitation, in the capacity of attractor neural networks to store and retrieve information codified as activity patterns. Previous studies have found that depressing synapses drastically reduce the capacity of the network to properly retrieve patterns (Bibitchkov et al., 2002; Torres et al., 2002; Matsumoto et al., 2007). These results highlight the role of depression on the processing of spatio-temporal information at short time scales (which allows for the appearance of dynamical memories), in detriment of its function in stable recall necessary for memory-oriented tasks. The consideration of additional potentiating mechanisms, such as synaptic facilitation, turns out to be convenient then for memory recall in these dynamical conditions, reaching in some cases the static limit  $\alpha_c \simeq 0.138$ . This leads to think that synaptic facilitation could have a crucial role in the performance of memory retrieval tasks, while maintaining the well known nonlinear properties of dynamic synapses, convenient for information processing and coding (Abbott and Regehr, 2004).

Our results also indicate that the range of parameters for which facilitation allows to have a good memory performance is notably wide, and therefore, these benefits can be achieved without a precise fine tuning of the synaptic parameters of the model. For instance, it is well known that dynamic synapses, and in particular facilitating synapses, usually present a high heterogeneity in their concrete characteristics (Markram et al., 1998; Wang et al., 2006). Since the conditions for which we found high critical storage capacities for random unbiased patterns (i.e.,  $\alpha_c > 0.1$ ) are very general, in the framework of our model, this can support the idea that actual neural systems could indeed take advantage of this fact to perform additional tasks –which are considerably different from a dynamical point of view – while the optimal access to memories is maintained.

Although we have derived a mean-field theory for unbiased random patterns  $f = 0.5$ , there exist other mean-field approaches in the literature which can corroborate our main conclusions about storage capacity and can be useful to extend our study for other types of stored patterns. One can employ, for instance, the mean-field theory developed in (Shiino and Fukai, 1993) valid also for other values of  $f$ , or the one presented in (Tsodyks and Feigelman, 1988). Our approximate theory presents, however, several differences which we consider of convenience here.

Concretely, the fact that it allows to work with a network with temperature, even in an approximate way, represents a significant practical advantage. It could, in principle, be a good approximation for high temperatures, and preliminary results confirm this hypothesis ((Mejias et al., 2009), see also appendix C). In addition, the assumption of having the same threshold level for all neurons, as is done in (Tsodyks and Feigelman, 1988), seems to be too restrictive for the modeling of biologically motivated neural networks due to the well known variability observed in the voltage threshold of actual neurons (Azouz and Gray, 2000). In this chapter, however, this experimental fact is taken into account by considering a threshold  $\theta_i$  given by (6.6) for each neuron, an assumption which considers such variability and also induces the existence of the noise term  $B^\mu$  (which, as we have seen, has a strong effect in the behavior of  $\alpha_c$ .)

In order to treat the effect of dynamic synapses, and concretely of short-term depression and facilitation, we have employed a simple model for synapse dynamics (Tsodyks et al., 1998). The predictions of this model agree with the experimental data from cortical slices, as one can see in (Markram et al., 1998) (see explanation in the results section). However, there are more realistic models which could be used to test our results. It is known, for example, that the stochastic nature of the transmitter release could play an important role in synaptic fluctuations (Dobrunz and Stevens, 1997). Models which take into account this stochasticity (such as (de la Rocha and Parga, 2005)) could be used to test our results with fluctuating synapses, although the complexity of such stochastic models would not allow to develop a simple mean-field theory, even approximate.

It is also known that dynamic thresholds are responsible for several complex phenomena in ANN (Horn and Usher, 1989), that could be similar to the ones observed in ANN with dynamic synapses (Pantic et al., 2002; Torres et al., 2007). This could lead us to think about the influence of dynamical thresholds in the network critical storage capacity, and its relation with the results presented here. While this is an interesting issue not reported yet, it is worth noting that although dynamical thresholds also induce the appearance of oscillatory states similar to the case of dynamical synapses, a direct mathematical relation between the dynamics of thresholds, as the model reported in (Horn and Usher, 1989) and the phenomenological model of dynamical synapses by (Tsodyks et al., 1998) cannot be derived (see discussion about this important issue in (Pantic et al., 2002)).

Finally, and attending to the dynamics and error-correcting abilities, the effect of synaptic depression on the basins of attraction has been previously studied (Bibitchkov et al., 2002; Matsumoto et al., 2007). In these works, neural networks with a general inhibitory contribution are considered, and several assumptions such as a fixed threshold value for all neurons are made. On the other hand, our study

---

considers general networks in which excitation and inhibition are treated in the same way (in particular, our neurons are not purely excitatory or inhibitory), and each neuron possesses its own particular threshold value which is also in agreement with several experimental evidences (Azouz and Gray, 2000). Our study shows that facilitation enlarges the basins of attraction compared with the case of only depressing synapses. As a consequence, we find that a convenient balance between synaptic depression and facilitation is necessary for neural networks to work optimally at different dynamical tasks. This is in agreement with recent experimental results which show a heterogeneous level of depression and facilitation in real synapses (Markram et al., 1998; Wang et al., 2006).

# Chapter 7

## Up and down critical dynamics

To finish with the original contributions presented in this thesis, we extend the study of the implications of short-term plasticity in the behavior of large populations of neurons. More precisely, in this chapter we investigate the role of STD and synaptic stochasticity in the voltage transitions observed in actual cortical structures, which seems to present some characteristics typically found in systems at criticality.

### 7.1 Introduction

Neural systems, even in the absence of external stimuli, can exhibit a wide variety of coherent collective behaviors, as *in vivo* and *in vitro* experiments show (Steriade et al., 1993a; Arieli et al., 1996; Sanchez-Vives and McCormick, 2000). One of the most prominent examples is the spontaneous transition between two different voltage states, namely up and down states, observed in simultaneous individual single neuron recordings as well as in local field measures (see figure 7.1). Such behavior, which is generated within the cortex, may provide a framework for neural computations (McCormick, 2005), and could also coordinate some sleep rhythms into a coherent rhythmic sequence of recurring cortical and thalamocortical activities (Sanchez-Vives and McCormick, 2000; Steriade et al., 1993c,b). The phenomenon of *up and down transitions* has been measured in a number of situations, such as in the primary visual cortex of anesthetized animals (Lampl et al., 1999; Anderson et al., 2000), during slow-wave sleep (Steriade et al., 1993c,b,a), in the somatosensory cortex of awake animals (Petersen et al., 2003), or in slice preparation under different experimental protocols (Sanchez-Vives and McCormick, 2000; Cossart et al., 2003; Shu et al., 2003), to name a few. The origin of such structured neuronal activity is still unclear, although several studies have shown that both intrinsic cell properties (Mayor and Tank, 2004; Loewenstein et al., 2005; Parga and Abbott, 2007) and the high level of recurrency present in actual neural circuits (Sanchez-

Vives and McCormick, 2000; Steriade et al., 2001; Holcman and Tsodyks, 2006) may contribute to the generation of up and down transitions. In particular, the contribution that reverberations in recurrent neural networks may have in the appearance of these transitions could depend strongly on synaptic properties. It is known, for instance, that excitatory synapses with a slow dynamics (such as synapses mediated by NMDA receptors) may play a relevant role in the generation of persistent activity or up cortical states (Wang, 1999). On the other hand, several modeling studies indicate that activity-dependent synaptic mechanisms, such as short-term synaptic depression and facilitation, can induce voltage transitions between up and down neural states as well (Pantic et al., 2002; Holcman and Tsodyks, 2006; Torres et al., 2007; Melamed et al., 2008).

Many crucial points about the understanding of up and down transitions are, however, still lacking. For instance, *in vivo* experiments in the cat visual cortex show that the permanence times in the depolarized or up state present a high variability, and can range from a scale of milliseconds to seconds (Lampl et al., 1999). Such complexity in the time series of the neuron membrane potentials remains far to be explained, and could reflect scale invariance in permanence times, which could be indicative of criticality. In fact, there are many recent studies that have shown criticality in different contexts in the brain (Eguiluz et al., 2005; Beggs and Plenz, 2003), as well as in neural network models which present self-organization and criticality properties (Lazar et al., 2007; Gomez et al., 2009; Lazar et al., 2009).

To study in detail this relevant issue, we propose in this chapter a minimal model for up and down transitions in neural media. We consider a simple bistable rate model whose stable solutions represent two possible voltage states of the mean membrane potential of the network. More precisely, such states correspond, respectively, to high and low levels of activity in the network (that is, the up and down cortical states). In addition, we consider that the synaptic connections between neurons of the network present short-term synaptic depression (STD) mechanisms, which introduce temporal correlations, as well as synaptic stochasticity, in the dynamics of the system (Abbott et al., 1997; Zador and Dobrunz, 1997; Dobrunz and Stevens, 1997; Zador, 1998). A complete analysis of this simple mathematical model depicts (both numerically and within a theoretical probabilistic approach) the appearance of power-law dependences in the distribution of permanence times in the up state. Our results show that the appearance of such scale free distributions is due to the complex interplay between several factors including synaptic stochasticity and the temporal correlations introduced by STD. The emergence of power-law dependences could explain the high variability in permanence times in the up state suggested by experiments (Lampl et al., 1999), and is in agreement with preliminary results found in *in vivo* recordings (de Franciscis et al., 2009).

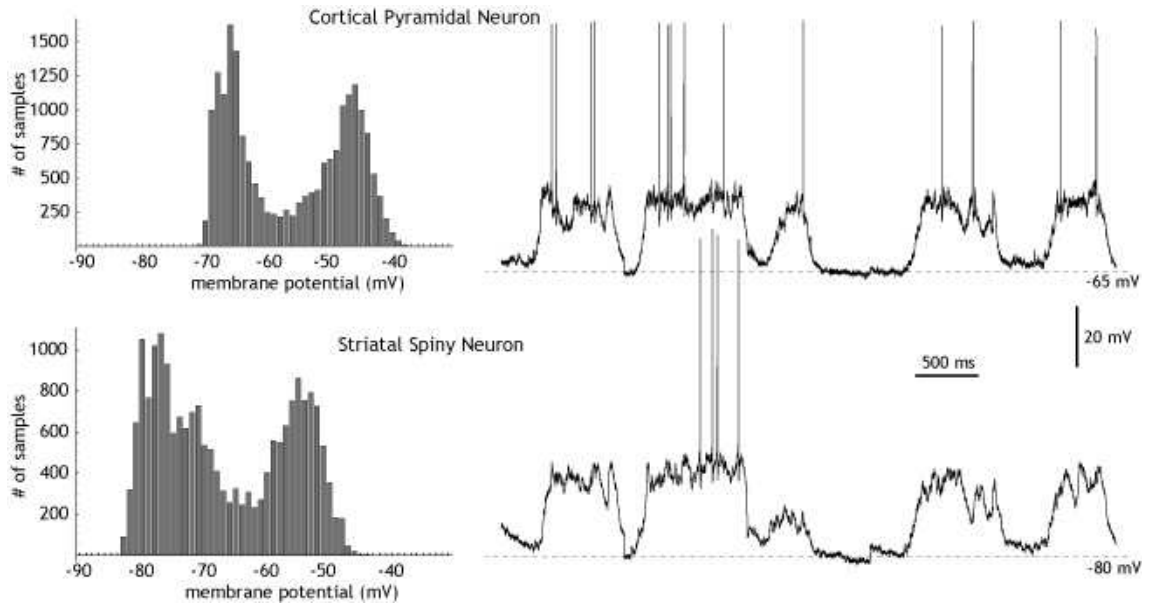


Figure 7.1: Typical simultaneous recordings of up and down transitions in two different types of neurons *in vivo*. The histogram to the left of each one shows the amount of time the cell spends at each value of membrane potential. Both cells switch between two preferred membrane potentials, one very hyperpolarized (down state), and one more depolarized (up state). In both cells, the up state is only a few millivolts from the action potential threshold. Usually, membrane potential fluctuations around the up state are of higher amplitude, whereas the down state is relatively free of noise. Both figure and caption have been taken and adapted from (Wilson, 2008).

## 7.2 Model

Our starting point is a bistable rate model, which mimics the dynamics of the electrical activity of a population of interconnected excitatory neurons (although it can be easily extended to other situations) with two stable levels of activity. The model has the form (Wilson and Cowan, 1972)

$$\tau_\nu \frac{d\nu(t)}{dt} = -\nu(t) + \nu_m \mathcal{S}[Jx(t)\nu(t) - \theta] + \zeta(t), \quad (7.1)$$

where  $\nu(t)$  is the mean firing rate of the (homogeneous) neural population,  $\nu_m$  is the maximum level of activity which can be reached by the population (in absence of noise),  $J(> 0)$  is the synaptic coupling strength in absence of STD, and  $\theta$  is the firing threshold of the neurons in the population. The variable  $\zeta(t)$  is a Gaussian white noise of zero mean and variance  $\delta^2$ , which takes into account the inner stochasticity of the neural population (caused by other sources of uncontrolled noise in the system). The parameter  $\tau_\nu$  is the population time constant, which may be assumed to be around the duration of the synaptic current pulse (Gerstner, 2000; Gerstner and Kistler, 2002). For simplicity, we set  $\tau_\nu \sim 1$  ms. The term  $\mathcal{S}(z) \equiv \frac{1}{2}(1 + \tanh(z))$

represents the transduction function, which gives the nonlinear effect that the mean postsynaptic current (coming from recurrent connections of the neural population) induces in the network mean firing rate. Employing this form for  $\mathcal{S}(z)$ , the up and down stable levels of activity correspond to  $\nu \simeq \nu_m$  and  $\nu \simeq 0$ , respectively.

On the other hand, the variable  $x(t)$  in equation (7.1) takes into account the dynamical modification of the strength of the synaptic connections during short time scales due to high network activity, and it is usually named short-term synaptic plasticity. Based on the model proposed in (Abbott et al., 1997; Tsodyks and Markram, 1997) for short-term depression, we assume that  $x(t)$  evolves according to

$$\frac{dx(t)}{dt} = \frac{1 - x(t)}{\tau_r} - ux(t)\nu(t) + \frac{D}{\tau_r}\xi(t), \quad (7.2)$$

where  $\tau_r$  is the characteristic time scale of the STD mechanism, and  $u$  is a parameter related with the reliability of the synaptic transmission. According to experimental measurements for these parameters in the somatosensory cortex of the rat (Tsodyks and Markram, 1997), we set  $\tau_r = 1000 \text{ ms}$  and  $u = 0.6$ . The last term on the right hand side of equation (7.2) is added to the original model in (Tsodyks and Markram, 1997) to include some level of stochasticity in this, otherwise, deterministic description of synaptic transmission. The parameter  $D$  controls the strength of this fluctuating term, and  $\xi(t)$  is a Gaussian white noise with zero mean and variance one.

Equations (7.1) and (7.2) constitute our minimal model of an excitatory neural network with stochastic depressing synapses. A typical time series of the dynamics of the model, for the case of deterministic synapses (that is,  $D = 0$ ), is depicted in figure 7.2A. In this case, the mean firing rate of the population is characterized by a periodic switching between up and down states. This type of periodic behavior was already found and analyzed in previous studies (Pantic et al., 2002; Holcman and Tsodyks, 2006; Parga and Abbott, 2007) and yields bimodal histograms for the mean firing rate of the neural population (see figure 7.2B), as the experiments indicate (Sanchez-Vives and McCormick, 2000). However, these approaches ignore the stochastic nature of synaptic transmission, which seems to be crucial for information processing in neural systems (Dobrunz and Stevens, 1997; Zador, 1998; de la Rocha and Parga, 2005). Considering a certain level of synaptic stochasticity in addition to STD in our model, one obtains a qualitatively different emergent behavior, as is shown in figure 7.2C for  $D = 20 \text{ ms}^{1/2}$ . The mean firing rate presents then a complex switching between up and down states, and in particular involves a high variability in the permanence times in the up state, as indicated by the power-law dependences in the probability distribution of permanence times depicted in figure 7.4. Experimental evidences of irregularity in the duration of the up states in the cat

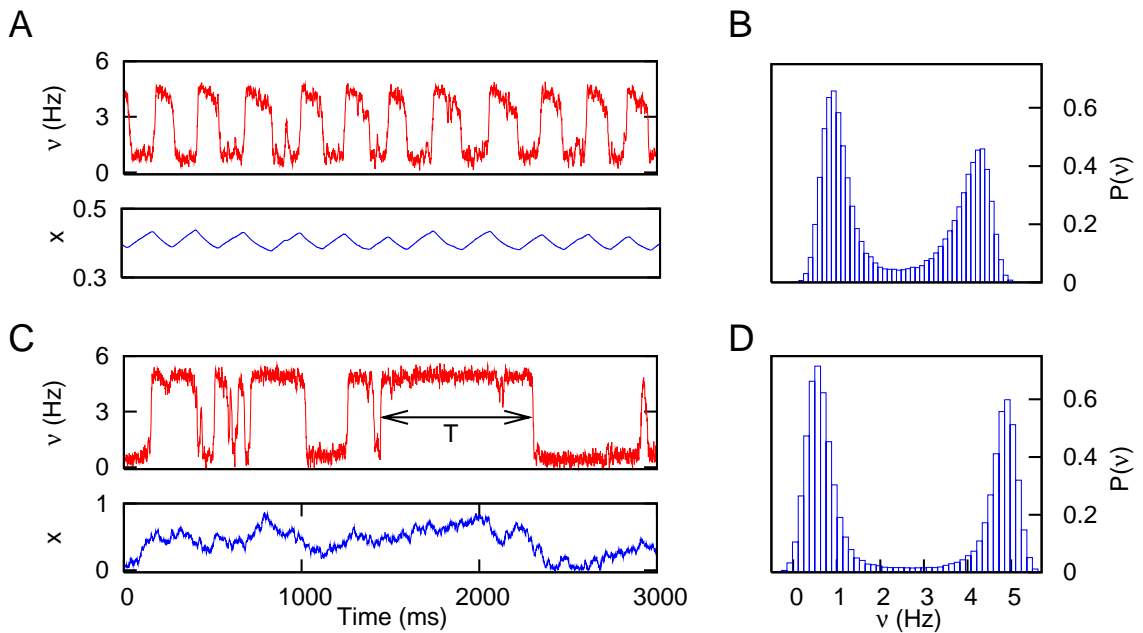


Figure 7.2: (A) Time series of the mean firing rate of the neural population for deterministic depressing synapses. The temporal evolution of the variable  $x$  is also plotted for illustration purposes. (B) Histogram of the mean firing rate, which shows the existence of two well defined states of activity in  $\nu \sim 1 \text{ Hz}$  and  $\nu \sim 5 \text{ Hz}$ , corresponding to the down and up states respectively. The values of the parameters are  $J = 1.2 \text{ mV/Hz}$ ,  $\tau_r = 1000 \text{ ms}$ ,  $u = 0.6$ ,  $D = 0$ ,  $\delta = 0.3 \text{ ms}^{-1/2}$  and  $\nu_{max} = 5 \text{ Hz}$ . (C) Same as (A), but with a certain level of intrinsic stochasticity on the dynamics of the synapses (concretely, we set  $D = 20 \text{ ms}^{1/2}$ ). The two-headed arrow shows a typical interval of permanence in the up state, denoted by  $T$ . (D) Same as (B), but for  $D = 20 \text{ ms}^{1/2}$ . The other parameters take the same values as in (A) and (B).

visual cortex also support these preliminary observations (Lampl et al., 1999). In the next section, we present a theoretical probabilistic approach to explain the emergence of such irregularity in the permanence times and the corresponding *power-law* distributions.

## 7.3 Results

### 7.3.1 Theoretical analysis

The simplifications assumed by our model allows to obtain some analytical derivations for the quantities of interest, and concretely for the probability distributions of permanence times in the up state, denoted by  $P(T)$ . Bistable systems in the presence of different sources of noise have been theoretically studied in detail in many works (Pechukas and Hanggi, 1994; Madureira et al., 1995; Ping, 2006; Dong-Xi et al.,

2008; Tu and Grinstein, 2005). Here, however, we present a probabilistic approach which is very appropriate for the computation of the distribution of permanence times.

#### A. The potential function

In order to compute the potential function  $\Phi(\nu, x)$ , from which one can derive the dynamics of  $\nu$ , one can see that, for realistic values of  $\tau_r$ , the dynamics of  $x$  is very slow compared to that of  $\nu$ . We therefore can write equation (7.1) as

$$\dot{\nu} = -\partial_\nu \Phi(\nu, x) + \zeta(t) \quad (7.3)$$

$$\Phi(\nu, x) = \frac{1}{2}\nu(\nu - \nu_m) - \frac{\nu_m}{2Jx} \log \cosh(Jx\nu - \theta), \quad (7.4)$$

where we have adiabatically eliminated  $x$  from the dynamics of  $\nu$ . The extrema of  $\Phi$  are given then by the solutions of the equation

$$\nu = \frac{1}{2}\nu_m[1 + \tanh(Jx\nu - \theta)] \equiv f(\nu) \quad (7.5)$$

In the following, we choose  $\theta = Jx_0\nu_0$ , with  $\nu_0 \equiv \frac{1}{2}\nu_m$  and  $x_0 \equiv 1/(1 + u\tau_r\nu_0)$ . With this choice, one can easily check from equation (7.4) that the potential becomes symmetric in  $\nu$  around  $\nu_0$  when  $x \simeq x_0$ .

Equation (7.5) may have one or three solutions, depending on the slope of the hyperbolic tangent and on the value of  $\theta$ . In order to obtain three solutions of (7.5) (that is, the bistable regime) the maximal slope of the hyperbolic tangent must be large enough, concretely the condition  $Jx\nu_0 > 1$  must be fulfilled. In addition, the threshold term must be not too small or too large so that  $f(\nu)$  has three crossing points with the straight line  $\nu$ , rather than one. This last condition can be written as  $f(\nu_1) > \nu_1$  and  $f(\nu_2) < \nu_2$ , where  $\nu_{1,2}$  are the values where the curvature of the hyperbolic tangent is maximal and minimal, respectively. The points  $\nu_{1,2}$  can be easily computed from the third derivative of  $f(\nu)$ :

$$f'''(\nu) = -\nu_m J^3 x^3 \frac{1 - 3 \tanh^2(Jx\nu - Jx_0\nu_0)}{\cosh^2(Jx\nu - Jx_0\nu_0)}. \quad (7.6)$$

By setting  $f'''(\nu) = 0$  we obtain

$$\nu_{1,2} = \frac{\nu_0 x_0}{x} \pm \frac{\tanh^{-1}(\sqrt{1/3})}{Jx}. \quad (7.7)$$

Using now these values for  $\nu_{1,2}$ , the conditions  $f(\nu_1) > \nu_1$  and  $f(\nu_2) < \nu_2$  can be written as

$$-\nu_0 \sqrt{1/3} + \frac{1}{Jx} \tanh^{-1}(\sqrt{1/3}) < \frac{\nu_0 x_0}{x} - \nu_0 < \nu_0 \sqrt{1/3} - \frac{1}{Jx} \tanh^{-1}(\sqrt{1/3}), \quad (7.8)$$

which implies that, in order to have one maxima and two minima in  $\Phi(\nu, x)$ , the variable  $x$  must be in the range  $x_1 < x < x_2$ , where

$$x_1 \equiv \frac{\nu_0 x_0 + \frac{1}{J} \tanh^{-1}(\sqrt{1/3})}{\nu_0(1 + \sqrt{1/3})}, \quad x_2 \equiv \frac{\nu_0 x_0 - \frac{1}{J} \tanh^{-1}(\sqrt{1/3})}{\nu_0(1 - \sqrt{1/3})}. \quad (7.9)$$

From equation (7.9), one can see that the range of  $x$  that allows to have three extrema in the potential is

$$\Delta x \equiv x_2 - x_1 = 3 \left( x_0 \sqrt{1/3} - \frac{1}{J\nu_0} \tanh^{-1}(\sqrt{1/3}) \right). \quad (7.10)$$

The condition  $\Delta x > 0$  implies  $Jx_0\nu_0 \gtrsim 1.14$  which is, therefore, a necessary condition to obtain a double well potential<sup>1</sup> for some value of  $x$ . Assuming that this condition is satisfied, three different shapes for the potential function  $\Phi(\nu, x)$  can be found, as the figure 7.3A illustrates. When  $x < x_1$  the potential function presents only one minimum, located around  $\nu \simeq 0$ . Similarly, for  $x_2 < x$  the potential presents also a single minimum, but now located around  $\nu \simeq \nu_m$ . Finally, for  $x_1 < x < x_2$  the potential will take a double well shape, with the maximum being located around  $\nu \simeq \nu_0$  and the minima located around  $\nu \simeq 0$  and  $\nu \simeq \nu_m$ , respectively.

It is worthy to note that moreover  $x_1 < x_0 < x_2$ , with  $x_0$  being the mean value of  $x$ . Due to this, if the range  $\Delta x$  is small compared with the fluctuations of  $x$ , namely  $\sigma_x$ , the potential function will spend most of the time in the regimes  $x < x_1$  and  $x_2 < x$ , with the double well regime appearing only when the system tries to jump from one of these regimes to the other (that is, when  $x \simeq x_0$ ). A direct consequence of this is that the mean firing rate will be basically switching between the up and down states (that is,  $\nu \simeq 0$  and  $\nu \simeq \nu_m$ ), and that this switching will be driven by the dynamics of  $x$ , as it was illustrated in figure 7.2. Therefore, one expects that the distribution of permanence times of  $\nu$  in the up (down) state, becomes approximately equal to the distribution of permanence times of  $x$  in the  $x > x_0$  ( $x < x_0$ ) regime, as long as  $\Delta x \ll \sigma_x$  is satisfied<sup>2</sup>. Due to this equivalence, in order to compute  $P(T)$  we only need to compute the distribution of permanence times of the variable  $x$  in the  $x > x_0$  regime, denoted as  $P_x(T)$ .

---

<sup>1</sup>One can find, however, a small discrepancy between our approximate prediction and the actual properties of  $\Phi(\nu, x)$ . Plotting directly the potential as a function of  $\nu$  reveals that the condition to obtain a double well potential for  $x \simeq x_0$  is  $Jx_0\nu_0 > 1$ , rather than  $Jx_0\nu_0 > 1.14$ .

<sup>2</sup>It should be noted that, since  $x$  is a fraction of available neurotransmitters, its value should be kept within the range  $[0, 1]$ . In practice, this means that the value of  $\sigma_x$  must not be too large, so in order to make  $\Delta x \ll \sigma_x$  one has to restrict to  $\Delta x$  small. In the results presented here,  $x$  remain in its realistic range of values, and imposing *ad hoc* restrictions in such a way that  $x$  is always within the range  $[0, 1]$  does not affect the results obtained here.

*B. Distribution of permanence times*

In order to compute the distribution of permanence times of  $x$  in the  $x > x_0$  (or  $x < x_0$ ) regime, one can assume that the firing rate takes its mean value  $\nu \simeq \nu_0$  in equation (7.2). This is a reasonable approach since  $x$  is much slower than  $\nu$  for realistic values of the parameters. Considering this approach, and after the rescaling  $z \equiv (1 + u\tau_r\nu_0)x - 1$ , equation (7.2) can be written as

$$\frac{dz(t)}{dt} = -\frac{z(t)}{\tau} + \frac{D}{\tau}\xi(t) \quad (7.11)$$

which is the equation of the Ornstein-Uhlenbeck (OU) process (see (van Kampen, 1990) for details), with  $\tau \equiv \tau_r/(1 + u\tau_r\nu_0)$  being the correlation time and  $z_0 \equiv z(x_0) = 0$ . Therefore, computing the distribution of permanence times in the up state for our system is equivalent to obtain the distribution of the so called *ruin times*<sup>3</sup> for the OU process (Chandrasekhar, 1943; Newman, 2005). The strategy employed here to calculate the distribution of ruin times is based on the relation between the ruin time and the *first passage time*, which is the typical time that a stochastic process needs to arrive at a certain threshold value when starting from a certain initial condition (Newman, 2005). Because of the symmetry of the OU process, the distribution of ruin times are equivalent when considering excursions of the variable  $z$  in the  $z < 0$  region or in the  $z > 0$  region. If we consider excursions in the  $z < 0$  region, we can set a small positive threshold  $\epsilon$  near zero (that is,  $0 < \epsilon \ll 1$ ), in such a way that the typical ruin time will be approximately equal to the corresponding first passage time, as the figure 7.3B illustrates. The excursions in the region  $z > 0$  typically lead to very short first passage times (since  $\epsilon$  is too small) which we will not take into account in our calculations by considering only large enough ruin times.

The first passage time for the OU process with a small threshold  $\epsilon$  can be performed by using the relation

$$\mathcal{P}(\epsilon, T|0, 0) = \int_0^T dt \mathcal{P}(\epsilon, T|\epsilon, t) \rho(t), \quad (7.12)$$

where  $\mathcal{P}(a, t_a|b, t_b)$  is the conditional probability distribution of the OU process, and  $\rho(t)$  is the first passage time distribution. This equation can be solved by taking into account the following property of the Laplace transformation

$$f_1(t) = \int_0^t dt' f_2(t-t') f_3(t') \implies \hat{f}_1(s) = \hat{f}_2(s) \hat{f}_3(s), \quad (7.13)$$

---

<sup>3</sup>If we consider a stochastic process  $y(t)$  starting at  $t = t_0$  from  $y = y_0$ , the ruin time is defined as the interval  $t_1 - t_0$ , where  $t_1$  is the time at which  $y(t)$  returns to  $y_0$  for the first time. Since  $y(t)$  is a stochastic process, the ruin times are stochastic quantities which follow a certain probability distribution.

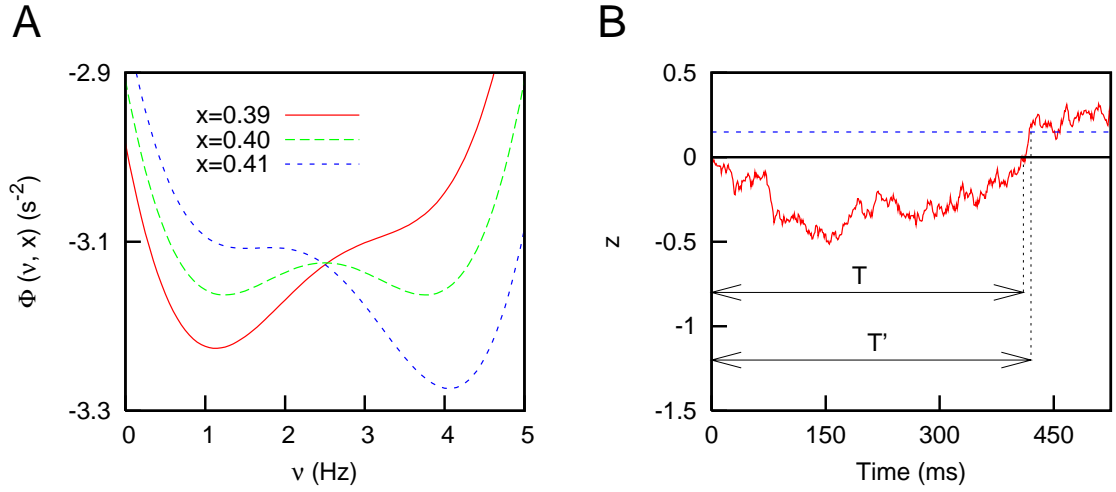


Figure 7.3: (A) Potential function  $\Phi(\nu, x)$ , as a function of the mean firing rate  $\nu$  and for different values of  $x$ . One can appreciate the different regimes explained in the main text. Other parameters are  $J = 1.1 \text{ mV/Hz}$ ,  $\tau_r = 1000 \text{ ms}$ ,  $u = 0.6$  and  $\nu_m = 5 \text{ Hz}$ . (B) An Ornstein-Uhlenbeck (OU) process (see equation (7.11)) with  $\tau = 1000 \text{ ms}$  and  $D = 20 \text{ ms}^{1/2}$ . A typical return event (with return time  $T$ ) and a first passage event (with first passage time  $T'$ ) are indicated for illustrative purposes. For the first passage time, the threshold (depicted as a blue dashed line) was fixed at 0.15.

where  $\hat{f}_i(s)$  is the Laplace transform of  $f_i(t)$ . By solving the Fokker-Planck equation associated with equation (7.11), one can obtain the conditional probability for the OU process

$$\mathcal{P}(z_2, t_2 | z_1, t_1) = \frac{1}{\sqrt{2\pi\sigma_x^2[1 - \exp(-2\Delta t/\tau)]}} \exp \left\{ -\frac{[z_2 - z_1 \exp(-\Delta t/\tau)]^2}{2\sigma_x^2[1 - \exp(-2\Delta t/\tau)]} \right\} \quad (7.14)$$

where  $\Delta t \equiv t_2 - t_1 > 0$ , and  $\sigma_x \equiv D/\sqrt{2\tau}$  being the standard deviation of  $x$ . From expression (7.14), and assuming that  $\tau$  is large enough, one arrives at

$$\mathcal{P}(\epsilon, T | 0, 0) \simeq \frac{1}{\sqrt{4\pi\sigma_x^2 T/\tau}} \exp \left( -\frac{\epsilon^2 \tau}{4\sigma_x^2 T} \right) \quad (7.15)$$

$$\mathcal{P}(\epsilon, T | \epsilon, t') \simeq \frac{1}{\sqrt{4\pi\sigma_x^2 (T-t')/\tau}} \exp \left( -\frac{\epsilon^2 (T-t')}{4\sigma_x^2 \tau} \right).$$

We denote  $f_1(T) \equiv \mathcal{P}(\epsilon, T | 0, 0)$  and  $f_2(T-t') \equiv \mathcal{P}(\epsilon, T | \epsilon, t')$ . Employing the Laplace transformation in  $f_1(T)$  and  $f_2(T-t')$  the following expressions are obtained

$$\hat{f}_1(s) = \sqrt{\frac{\tau}{4s\sigma_x^2}} \exp \left( -\sqrt{\epsilon^2 \tau s / \sigma_x^2} \right) \quad (7.16)$$

$$\hat{f}_2(s) = \tau / \sqrt{\epsilon^2 + 4s\tau\sigma_x^2}.$$

Now, taking into account the property (7.13) in equation (7.12), the expression for  $\hat{\rho}(s)$  is

$$\hat{\rho}(s) = \sqrt{\frac{\epsilon^2 + 4s\tau\sigma_x^2}{4s\tau\sigma_x^2}} \exp\left(-\sqrt{\epsilon^2\tau s/\sigma_x^2}\right). \quad (7.17)$$

Finally, for small  $\epsilon$  one can approximate  $\epsilon^2 + 4s\tau\sigma_x^2 \simeq 4s\tau\sigma_x^2$ . With this approximation, one can easily perform the inverse Laplace transformation to equation (7.17) and obtain the distribution of first passage times for the OU process

$$\rho(T) = \sqrt{\frac{\epsilon^2\tau}{4\pi\sigma_x^2}} T^{-3/2} \exp\left(-\frac{\epsilon^2\tau}{4\sigma_x^2 T}\right). \quad (7.18)$$

In order to obtain now the distribution of ruin times of the OU process, one has to consider large values of  $T$  (as we argue above) and a small (but positive) value of  $\epsilon$ , which leads to  $\rho(T) \sim T^{-3/2}$ . The distribution of ruin times of the variable  $x$ , namely  $P_x(T)$ , and therefore, the distribution of permanence times in the up state, namely  $P(T)$ , for our system are also given by

$$P(T) \sim T^{-3/2}, \quad (7.19)$$

which corresponds to a power-law probability distribution for  $T$ , as we argued above.

### 7.3.2 Statistics of up and down transitions

The above results allow us to analytically compute the probability distributions of the permanence times in the up state, and to study the influence that the different parameters have on these distributions. A first study of interest, for instance, concerns the effect of the synaptic noise strength  $D$  on the dynamics of the neural population. As we have already explained, when deterministic synapses are considered (that is,  $D = 0$ ) the dynamics of the mean firing rate becomes quasi periodic, as it was reported in (Pantic et al., 2002; Holcman and Tsodyks, 2006; Torres et al., 2007), for instance. This type of dynamics naturally leads to exponential distributions for the permanence times<sup>4</sup>. When  $D$  is increased, however, the stochasticity of the synapses leads to the appearance of power-law distributions for the permanence times in the up state, as we have theoretically stated above. This behavior is shown in figure 7.4, where low values of  $D$  corresponds to exponential distributions for

---

<sup>4</sup>More precisely, for  $D = 0$  our model is similar (except for the term  $\zeta(t)$ ) to the one analyzed in (Holcman and Tsodyks, 2006), which shows periodic oscillations of the network mean firing rate. In the case of our model with  $D = 0$ , the term  $\zeta(t)$  introduces certain level of stochasticity which turns these periodic oscillations into quasi-periodic oscillations. This leads to the exponential distributions for the permanence times in the up state.

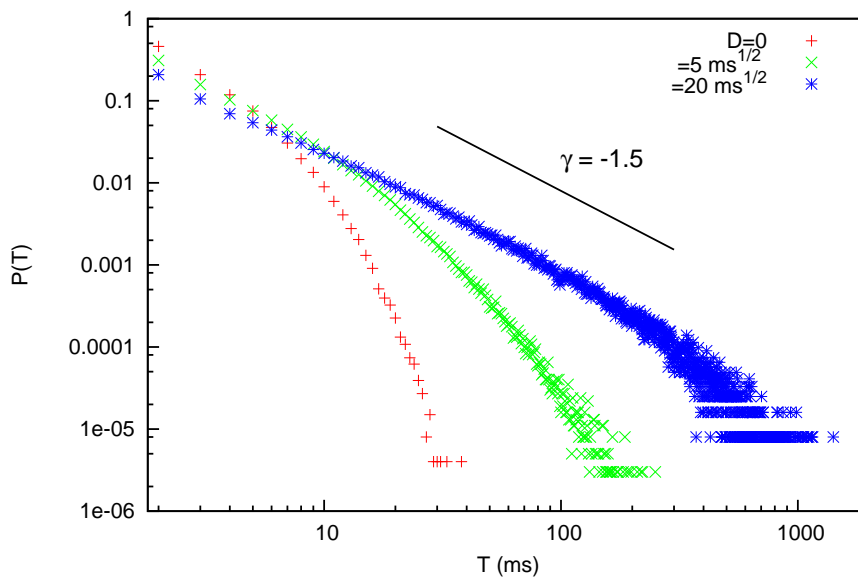


Figure 7.4: Probability distributions of permanence times in the up state, obtained with numerical simulations, for different values of the noise strength  $D$ . One can see that high values of  $D$  lead to the appearance of power-law distributions  $P(T) \sim T^{-\gamma}$  with  $\gamma = 3/2$ , as the mean-field solution predicts. For numerical simulations, we employed time series of  $10^6$  ms and averaged over 100 trials. The values of the other parameters were  $J = 1.1$  mV/Hz,  $u = 0.6$ ,  $\tau_r = 1000$  ms,  $\delta = 0.3$  ms $^{-1/2}$  and  $\nu_m = 5$  Hz. To compute  $P(T)$ , we have considered that the up state has been reached during a period  $T$  (with  $T > 2$  ms) if  $\nu > \eta\nu_m$  during this period. We set  $\eta = 0.8$ .

$P(T)$ , while larger values of  $D$  give  $P(T) \sim T^{-3/2}$  as predicted by our theoretical predictions. Such power-law distributions may explain the high variability of permanence times in the up state (that ranges from 50 ms to 1000 ms), which has been observed in *in vivo* experiments in the cat visual cortex (Lampl et al., 1999). On the contrary, exponential-like distributions, obtained for the case of having  $D = 0$ , are not able to explain this variability. Our predictions also coincide qualitatively well with preliminary experimental studies which find similar power-law dependences for the permanence times in the up state (de Franciscis et al., 2009).

For a better characterization of the dynamics of the system, one can use, for instance, other statistical magnitudes such as the autocorrelation function  $C(t')$  of  $\nu$ , which can be defined as

$$C(t') \equiv \langle \nu(t+t')\nu(t) - \nu(t)\nu(t') \rangle. \quad (7.20)$$

Here,  $\langle \dots \rangle$  indicates a temporal average. The autocorrelation function is depicted in figure 7.5A for the case of deterministic depressing synapses ( $D = 0$ ) and stochastic depressing synapses ( $D = 20$  ms $^{1/2}$ ).  $C(t')$  presents, for  $D = 0$ , two well located peaks at  $t' \simeq \pm 200$  ms, which indicates a strong periodicity of the time series (as can

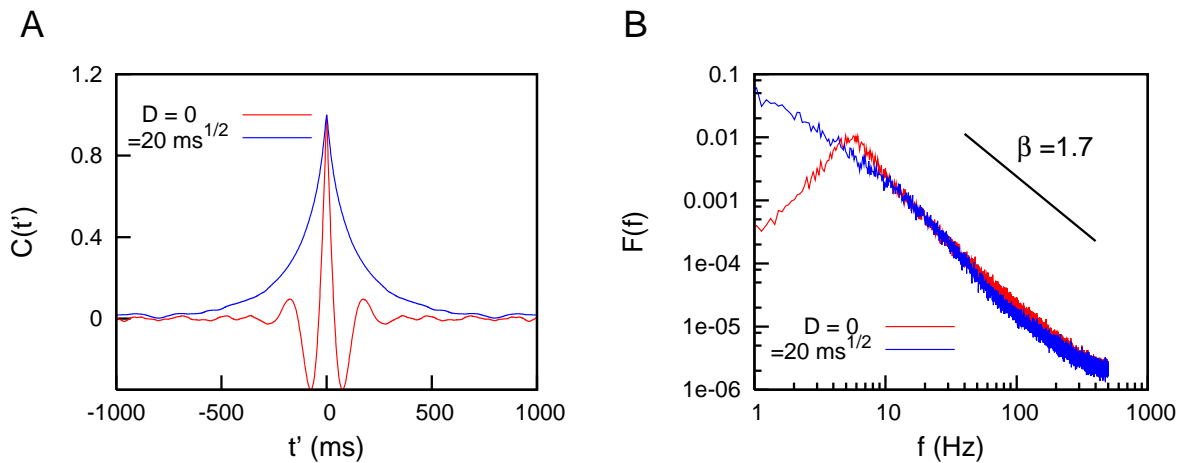


Figure 7.5: (A) Autocorrelation function of the mean firing rate for deterministic ( $D = 0$ ) and stochastic ( $D = 20 \text{ ms}^{1/2}$ ) synapses, in the presence of STD. (B) Power spectra of the mean firing rate for the two cases illustrated in (A). For both panels, we have averaged over  $10^5$  time series of  $10^6 \text{ ms}$  each, and we have fixed  $J = 1.1 \text{ mV/Hz}$ ,  $u = 0.6$ ,  $\tau_r = 1000 \text{ ms}$ ,  $\delta = 0.3 \text{ ms}^{-1/2}$  and  $\nu_m = 5 \text{ Hz}$ .

be seen in figure 7.2A). On the contrary, the inclusion of a certain level of intrinsic stochasticity in the dynamics of  $x$  introduces more pronounced temporal correlations in the dynamics of the system. This fact reflects the existence of long permanence stays in the up state, which occurs with more probability for high enough values of  $D$ , as we have already discussed.

The spectral properties of the dynamics can be analyzed as well, via the power spectrum defined as

$$F(f) \equiv \int C(t') \exp(2\pi i f t) dt. \quad (7.21)$$

As one could expect, the power spectrum of the case  $D = 0$  presents a pronounced peak around a certain frequency, which in the particular case presented in the figure 7.5B is  $f \sim 5 \text{ Hz}$ . The power spectrum for higher values of  $D$  shows however different properties than the case  $D = 0$ . For instance, the figure 7.5B (which considers  $D = 20 \text{ ms}^{1/2}$ ) indicates an approximated power-law behavior for the power spectrum,  $F(f) \sim f^{-\beta}$  with  $\beta \simeq 1.7$ . This scale-free dependence can be understood by considering that, if  $P(T)$  is algebraic with exponent  $\gamma$ , the corresponding power spectrum becomes also algebraic with exponent  $\beta$ , where the equation  $\gamma + \beta = 3$  relates both exponents (Tu and Grinstein, 2005). In our particular case, since  $\gamma \simeq 1.5$ , one obtains a theoretical prediction of  $\beta \simeq 1.5$  for the exponent of the power spectrum. The theoretical relation between  $P(T)$  and  $F(f)$  exposed above, however, is only valid under the so called *single interval approximation*, which implies that the integration variable  $t$  in equation (7.21) is smaller than the permanence time

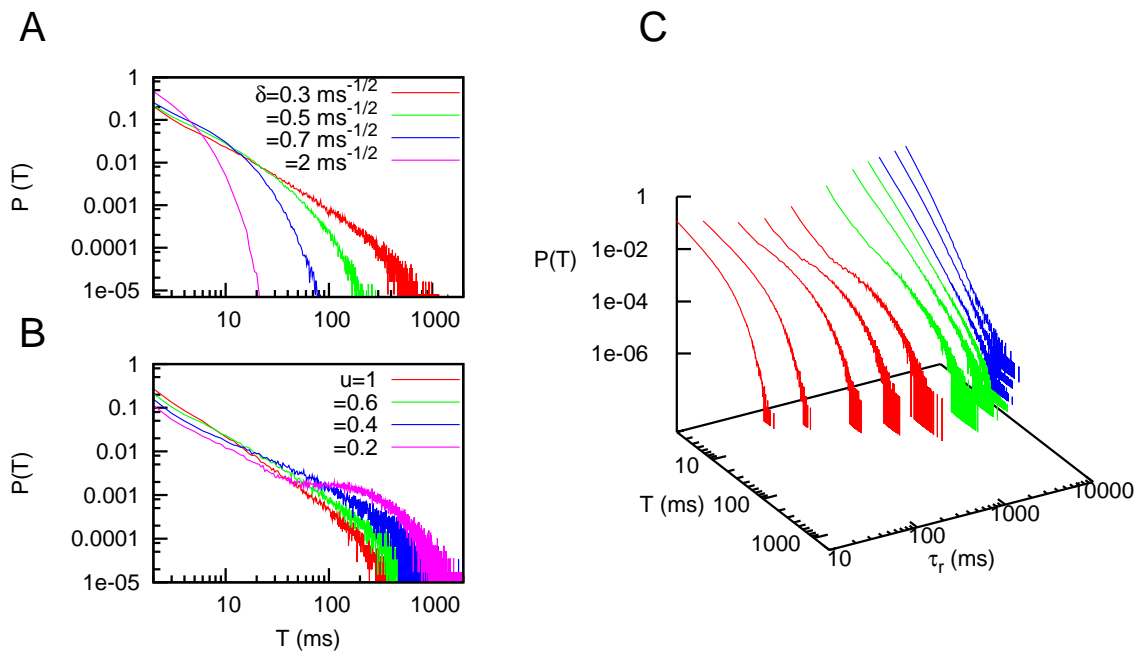


Figure 7.6: (A) Probability distributions of permanence times in the up state, for different values of  $\delta$ . Other parameters are  $J = 1.1 \text{ mV/Hz}$ ,  $u = 0.6$ ,  $\tau_r = 1000 \text{ ms}$ ,  $D = 20 \text{ ms}^{1/2}$  and  $\nu_m = 5 \text{ Hz}$ . (B) Same as in (A), but for different values of  $u$ . The other parameters take the same values as in (A), except for  $\delta = 0.3 \text{ ms}^{-1/2}$ . (C) Probability distribution  $P(T)$  as a function of  $T$  and  $\tau_r$ . The three different regimes are shown with different colors (see main text for details). Other parameters are  $J = 1.1 \text{ mV/Hz}$ ,  $u = 0.6$ ,  $D = 20 \text{ ms}^{1/2}$ ,  $\delta = 0.3 \text{ ms}^{-1/2}$  and  $\nu_m = 5 \text{ Hz}$ . For all panels, we have averaged over 100 times series of  $10^6 \text{ ms}$  each.

$T$  (see (Tu and Grinstein, 2005) for details). This condition does not strictly hold for our system (where  $T$  ranges over several scales), and therefore it may introduce deviations in the theoretically predicted value of  $\beta$  (which is around  $\beta \simeq 1.5$ ) with respect to the value found in simulations (of around  $\beta \simeq 1.7$ ).

Besides the level of synaptic stochasticity, i.e.  $D$ , other parameters of the model could have an important effect on the dynamics as well. The parameter  $\delta$ , for instance, controls the level of stochasticity of the dynamics of  $\nu$ , and therefore one should expect that increasing its value could strongly influence the probability distribution  $P(T)$ . This is shown in figure 7.6A, where an increase of  $\delta$  disrupts the appearance of power-law dependences, and exponential distributions appear instead. This change in  $P(T)$  is due to the fact that high levels of the additive noise  $\delta$  make the system to jump more frequently from one state to the other, and therefore long stays in the up state (and thus distributions with long power-law tails) rarely occur.

The parameters involving the dynamics of  $x$  also affect the probability distributions  $P(T)$ . The parameter  $u$ , for instance, is responsible for the modulation of  $x$

via the mean firing rate  $\nu$  (see equation (7.2)), and therefore it can influence both the dynamics of  $x$  and  $\nu$ . As one may see in figure 7.6B, when  $u$  takes low values a bump in  $P(T)$  emerges for high  $T$ . Such deviation from the power-law dependence indicates that long stays in the up state occur more frequently than in the power-law case. Attending at equation (7.2), one can see that an increase of the mean firing rate  $\nu$  decreases the variable  $x$  via the parameter  $u$ . Therefore, if  $u$  takes lower values the decrement of  $x$  will be smaller. As a consequence, the stays of  $x$  in the  $x_0 \ll x$  regime will last longer, and the stays of the system in the up state will also last longer, causing the observed deviation from the power-law tendency. It should be noted, however, that the values of  $u$  which allow the appearance of power-law dependences in  $P(T)$  for our model agree with the values of  $u$  measured in actual cortical media where up and down transitions are observed (Tsodyks and Markram, 1997).

Finally, the dependence of the dynamics of the system with the STD time constant  $\tau_r$  constitutes also an interesting and relevant issue. In order to clarify this, we have analyzed in detail the effect that varying  $\tau_r$  has on the probability distribution of permanence times. The results are shown in figure 7.6C, where one can distinguish three different regimes as a function of the particular value of  $\tau_r$ . For low  $\tau_r$  (red region in the figure), the probability distributions show an exponential decay for large permanence times. The reason for this decay is that, for low  $\tau_r$ , the variable  $x$  does not perform long excursions in the region  $x_0 \ll x$ , and therefore the probability to have large values of  $T$  decreases and the power law behavior for  $P(T)$  is not obtained. As  $\tau_r$  is increased, long excursions for  $x$  begin to occur, and we obtain a power law behavior  $P(T) \sim T^{-3/2}$  (green region in the figure). Finally, one can appreciate that, for even larger values of  $\tau_r$  (blue region in the figure), the probability distribution of permanence times in the up state presents a power law dependence  $P(T) \sim T^{-\gamma(\tau_r)}$  with  $\gamma(\tau_r) > 3/2$ , being an increasing function of  $\tau_r$ . Such dependence can not be explained by our previous theoretical predictions, based in the assumption that the system is in the bistable regime, and deserves a detailed analysis which will be exposed in the next section.

### 7.3.3 Further analysis

In section 7.3.1, we established several conditions which, in principle, had to be fulfilled in order to obtain power law dependences for  $P(T)$ . In particular, our previous analysis indicates that the condition  $Jx_0\nu_0 > 1$  must hold in order to have a potential function  $\Phi(\nu, x)$  with three extrema (bistable regime). However, as we will see in the following, power law expressions for  $P(T)$  may appear even if the potential function has only one extremum in  $\nu$  (concretely, one minimum).

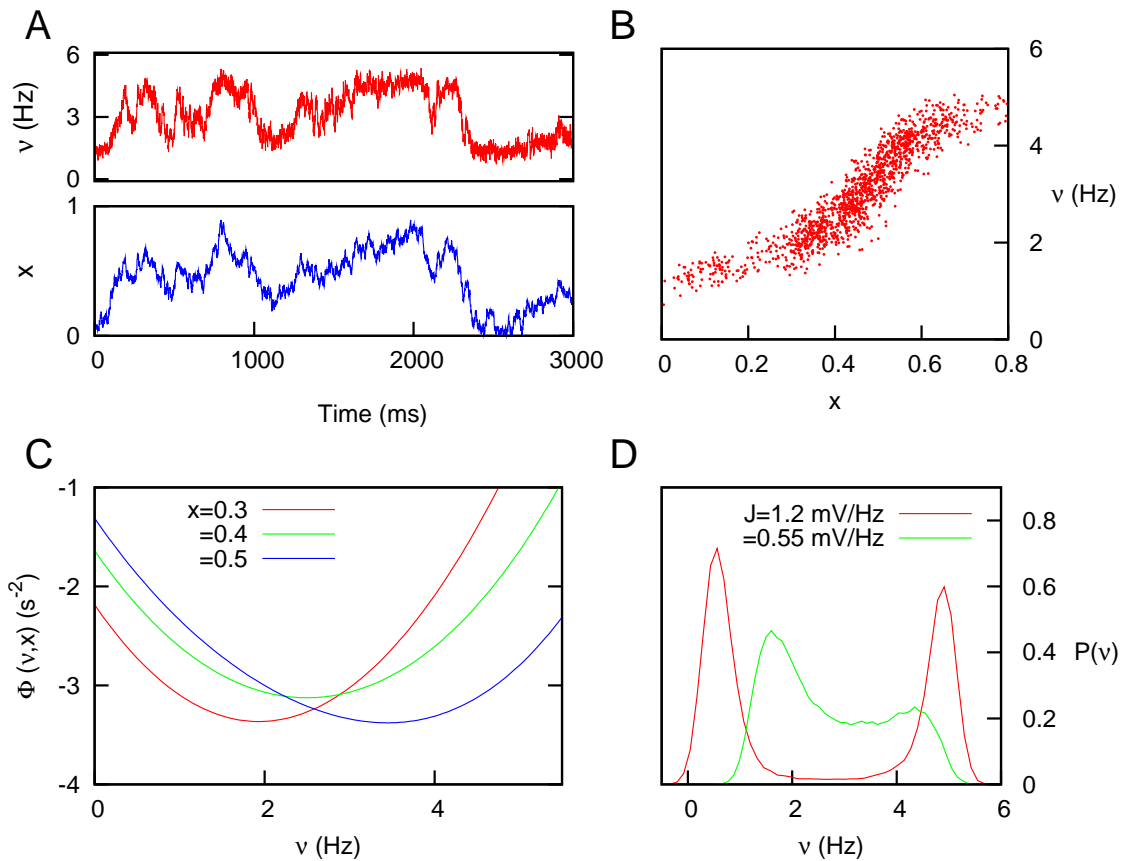


Figure 7.7: Behavior of the system when the condition  $Jx_0\nu_0 < 1$  holds. (A) Time series of the variables  $\nu$  and  $x$ . (B) The same time series, but represented on the  $x - \nu$  plane, illustrates the fact that  $\nu$  is a slave variable of  $x$  (although some level of inner stochasticity on  $\nu$  is still present). (C) The potential function as a function of  $\nu$  for different values of  $x$ . One can appreciate the existence of only one minimum, whose location is controlled by  $x$ . (D) Histograms of the mean firing rate of the system for different values of  $J$ . For the cases showed in this panel, the condition  $Jx_0\nu_0 < 1$  is only satisfied for the case  $J = 0.55$  mV/Hz. For all panels,  $u = 0.6$ ,  $\tau_r = 1000$  ms,  $D = 20$   $\text{ms}^{1/2}$ ,  $\delta = 0.3$   $\text{ms}^{-1/2}$ ,  $\nu_m = 5$  Hz, and  $J = 0.55$  mV/Hz unless specifically specified.

When  $Jx_0\nu_0 < 1$  (which occurs for  $J \ll 1$  or  $\tau_r \gg 1$ , for instance), the potential function  $\Phi(\nu, x)$  has only one minimum in  $\nu$ , whose location strongly depends on  $x$ . An approximated expression for the location of this minimum as a function of  $x$  can be obtained by expanding the hyperbolic tangent in equation (7.5) around its argument (which is small in this limit) up to first order, yielding

$$\nu_{min} = \nu_0 \frac{1 - Jx_0\nu_0}{1 - Jx\nu_0}, \quad (7.22)$$

where  $\nu_{min}$  is the value of  $\nu$  which corresponds to the minimum of the potential function. Therefore as  $x$  varies around  $x_0$ , the location of the minimum of the potential  $\nu_{min}$  also varies in the same way around  $\nu_0$ . The predictions of this expression

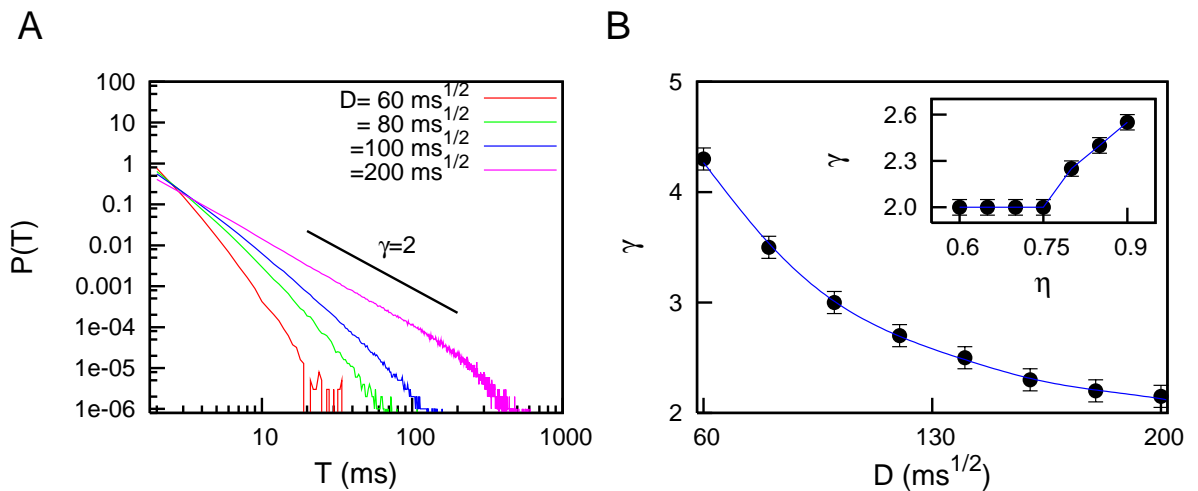


Figure 7.8: (A) Probability distribution of permanence times in the up state in the  $Jx_0\nu_0 < 1$  regime, for  $\eta = 0.75$  and different values of  $D$ . One can see that power law relations  $P(T) \sim T^{-\gamma}$  appear. (B) Dependence of  $\gamma$  with  $D$  for the conditions presented in (A). The inset shows the dependence of  $\gamma$  with the parameter  $\eta$  for the case  $D = 200 \text{ ms}^{1/2}$ . We have averaged over 100 time series of  $10^6 \text{ ms}$  each. Other parameters are  $J = 0.05 \text{ mV/Hz}$ ,  $\tau_r = 1000 \text{ ms}$ ,  $u = 0.6$ ,  $\delta = 0.3 \text{ ms}^{-1/2}$  and  $\nu_m = 5 \text{ Hz}$ .

agree quite well with simulations, as long as the singular value  $x = 1/J\nu_0$  of the above expression is avoided. As an example, time series of both  $\nu$  and  $x$  are shown in figure 7.7A for a given set of parameters which satisfies  $Jx_0\nu_0 < 1$ . In this time series, the variable  $\nu$  fluctuates around the value  $\nu_{min}$ , which is fully determined by  $x$  (that is, the variable  $\nu$  becomes a slave variable of  $x$ ).

Since  $\nu$  behaves now as a stochastic variable which does not present a clear bistable dynamics, the numerical computation of the distribution of the permanence times will depend on the exact value of  $\nu$  above which the system is considered to be in the up state. As we have seen before, this *threshold* value takes the form  $\eta\nu_m$  (see caption of figure 7.4), where usually  $\eta$  may take a value between 0.6 and 0.9. While the results presented for  $Jx_0\nu_0 > 1$  (that is, the bistable regime) are quite robust for different values of  $\eta$ , in the regime  $Jx_0\nu_0 < 1$  this parameter has indeed some effect on  $P(T)$ , which indicates the difficulty to accurately analyze the up and down dynamics in this case.

In figure 7.8A, one observes that the distribution  $P(T)$  shows also a power law behavior  $P(T) \sim T^{-\gamma}$  for  $\eta = 0.75$  and different values of  $D$ , for a set of parameter values which satisfies  $Jx_0\nu_0 < 1$  (that is the monostable regime). The concrete value of  $\gamma$  depends strongly on  $D$  and it has also a weaker dependence with  $\eta$ , as the figure 7.8B illustrates. This type of power-law behavior appearing in the monostable regime corresponds to the blue region in figure 7.6C, as well.

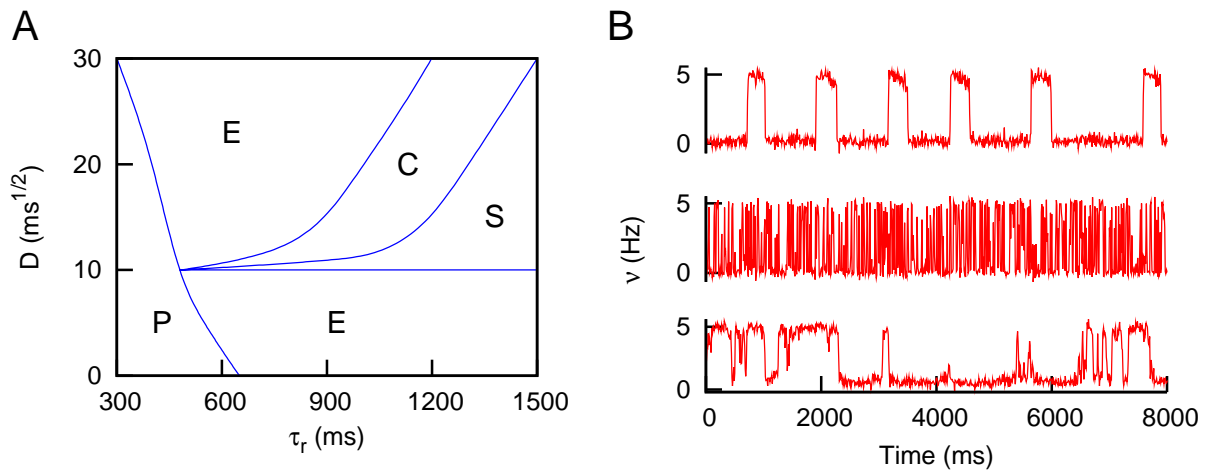


Figure 7.9: (A) Phase plot which shows the different behaviors found in our system. These behaviors corresponds to time series of  $\nu$  for which permanence times in the up state follow an exponential distribution (E), a power-law distribution  $P(T) \sim T^{-\gamma}$  with  $\gamma = 3/2$  (C), or a power-law distribution with  $\gamma > 3/2$  (S). In addition, a phase with a well-defined duration of the up state is found (P). In panel (B) some of these behaviors are depicted. From top to bottom one can see situations P, E and C. Other parameters are  $J = 1.1$  mV/Hz,  $u = 0.6$ ,  $\delta = 0.3$   $ms^{-1/2}$  and  $\nu_m = 5$  Hz.

It is worthy to note that actual recordings of up and down transitions does not present a clear distinction between up and down states, and several nontrivial methods are commonly employed to discriminate between both states (Seamari et al., 2007). Therefore, the results found for the regime  $Jx_0\nu_0 < 1$  could indeed reflect the behavior of actual cortical up-down transitions, showing power law dependences in  $P(T)$  with  $\gamma > 3/2$  and indicating that the concrete nature of the transitions is a synaptic-driven monostable dynamics.

Finally, one can summarize all the observed behaviors in a phase plot such as the one presented in figure 7.9. A total of four different behaviors can be found in the  $(\tau_r, D)$  space. The first one concerns the dynamics of  $\nu$  whose permanence times in the up state follows an exponential distribution (labeled as “E” in the figure). If the noise amplitude  $D$  is sufficiently high, one can increase the value of  $\tau_r$  to reach the regime “C”, in which the dependence  $P(T) \sim T^{-1.5}$  is obtained. By increasing  $\tau_r$  even more, the probability distribution  $P(T)$  takes the form  $\sim T^{-\gamma}$ , with  $\gamma > 1.5$  (regime denoted by “S”), as we have already seen in figure 7.7. Finally, we also observe that when the depression time scale is not large enough (and  $D \lesssim 3$   $ms^{1/2}$ ), a regime of quasi-periodic time series of  $\nu$  is obtained, with a well-defined duration of up states (regime denoted by “P”). It must be clarified, however, that actual up and down cortical transitions probably present a richer repertoire of dynamical

regimes than the one obtained with our simplified model. Therefore, the different behaviors of cortical up-down dynamics, as well as the existence of criticality in such dynamics, deserves further study via detailed computational explorations with more realistic models of neural systems.

## 7.4 Discussion

Many biophysical processes at the subcellular, cellular and network level, can influence the complex collective dynamics that emerges in actual neural systems. An example is the generation of spontaneous transitions between different voltage levels in absence of external stimuli in some cortical areas, that is, the so called up and down transitions. Their origin is still unclear, although different factors that can influence their occurrence have been recently reported. It is known, for instance, that inhibitory GABAergic currents strongly contribute to the temporal coding and spike timing precision of cortical networks during up states of activity (Sanchez-Vives and McCormick, 2000; Hasenstaub et al., 2005). Several modeling studies also show the relevance of inhibitory interneurons in the generation of many types of oscillations in the brain (see for instance (Brunel, 2000)). However, other studies indicate that most of the main features of up and down transitions depends strongly on synaptic plasticity mechanisms, both of long-term and short-term ones (Kang et al., 2008; Holcman and Tsodyks, 2006), and that the transitions appear even in the absence of inhibition (Holcman and Tsodyks, 2006). Following these studies and with the aim to investigate what are the minimal requirements to generate up and down transitions, in this chapter we have not considered inhibition. The presented theory, however, can be easily generalized to include this and other biophysical factors.

Regarding to synaptic characteristics, recent works show that synaptic fluctuations could have an important role in the generation of transitions between up and down states (Cortes et al., 2006; Parga and Abbott, 2007; Johnson et al., 2008). The results presented in this chapter corroborates this hypothesis, and indicates that stochasticity on the synapses may be responsible of the high variability in the duration of the up states. On the other hand, it is known that short-term synaptic mechanisms, such as short-term depression and facilitation, usually play a role in the efficient processing of information. In particular, they may be relevant in many tasks, such as in signal detection and coding (Abbott et al., 1997; Mejias and Torres, 2008, 2009a) or switching between different activity patterns previously stored (Torres et al., 2007; Mejias and Torres, 2009b). However, their role on the transitions between cortical states has been pointed out only very recently (Holcman and Tsodyks, 2006), and their possible effects on the statistics of the transitions have been ignored. To the best of our knowledge, the present study is the first one which

analyzes, even in a simplified manner, the strong effect of synaptic stochasticity and dynamic synapses in the statistics of the up and down transitions. The possible role of other short-term synaptic mechanisms, such as STF, has not been addressed yet and constitutes a interesting issue still open.

The theoretical analysis developed in this chapter serves to highlight what are the mechanisms responsible for the appearance of power-law dependences in  $P(T)$ . However, this theoretical approach may (and should) be improved. For instance, an interesting issue to address could be the theoretical study of the effects of different model parameters. The analytical approach used here is not able, for instance, to quantitatively obtain  $P(T)$  for arbitrary values of  $\tau_r$  (due to the fact that we have assumed a slow dynamics for  $x(t)$ , that is,  $\tau_r \gg 1 \text{ ms}$ ). Similar conclusions are found for  $\delta$  or  $u$ , as well. Therefore, extensions of the theoretical approach introduced in this chapter are needed for a complete understanding of the role of all the different parameters and time scales involved.

We have also tested our main results in different ways. For instance, the election of a differential equation formulation or a discrete map dynamics does not disrupt the emergence of scale-free distributions of permanence times. Different transduction functions preserve the results, as well. This issue is specially relevant because the simple transduction function employed here implies that the probability distribution of permanence times in a stable state is the same for up states and for down states (that is, the system presents up-down symmetry). This is in contradiction with experimental evidences (de Franciscis et al., 2009) which shows that power-law distributions are obtained for permanence times in the up state, while permanence times in the down state are exponentially distributed. However, this discrepancy disappears when one considers a more realistic transduction function which gives an asymmetric potential for the dynamics, and as a consequence the up-down symmetry is broken. More detailed studies considering, for instance, some of the biologically realistic aspects discussed above, should be performed to test our predictions. In particular, a more elaborated study considering realistic neuron models (such as Hodgkin-Huxley model (Hodgkin and Huxley, 1952b)) and stochastic STD models (see (Abbott et al., 1997; de la Rocha and Parga, 2005), for instance) is necessary and it is in preparation.

From a general point of view, evidences of criticality have been recently found in an increasing number of neural systems, such as in the functional connectivity of the living human brain (Eguiluz et al., 2005), in critical avalanches of neuronal activity (Beggs and Plenz, 2003), or in sleep-wake transitions (Lo et al., 2004), to name a few. According to the results presented in this chapter, transitions between up and down cortical states could also present some relevant properties typical of systems at criticality. Some of these properties have been already measured in experiments,

---

such as a high sensitivity of the system to external stimuli (Anderson et al., 2000), or the presence of power-law dependences in the power spectra of the neural dynamics (Hasenstaub et al., 2005). Preliminary results (de Franciscis et al., 2009) also show the presence of power-law distributions of the permanence times in up states in *in vivo* conditions, which properly fits our predictions. Our study shows the importance of some biophysical factors, such as the neurotransmitter recovery time and the inherent synaptic stochasticity for the emergence of this phenomenology. Finally, our results may proportionate a new perspective of the phenomena of up and down transitions that could serve to conciliate the main experimental findings, and that could help for a deep understanding of this complex dynamics of the brain activity.

# Chapter 8

## Conclusions

Mathematical modeling and computer simulations are proving to be two powerful tools to analyse the behavior of neural systems. In this context, an efficient characterization of synaptic properties seems to be crucial to understand many phenomena observed in actual neural media. Long-term plastic modifications of synapses, for instance, play a relevant role in the onset of learning and memory, and have become an important focus of attention for researchers during the last decades (Hopfield, 1982; Hebb, 1949). On the other hand, short-term synaptic plasticity is mainly concerned with the processing and coding/decoding of the information embedded in spike trains (Abbott and Regehr, 2004; Zador and Dobrunz, 1997). These tasks include the access to information previously stored via long-term synaptic mechanisms, and as a consequence short-term synaptic plasticity may have strong implications in memory and retrieval of information as well.

In this thesis we have studied in detail the computational and functional implications of short-term plasticity, and in particular STD and STF, in the performance of different neural systems of interest. This study has been achieved employing numerical simulations, and also analytical treatments when possible. The use of both theoretical and numerical methods constitute a mayor key of the thesis, as the comparison with numerical simulations constitute a reliable method to test our theoretical predictions. A good agreement between theory and simulations also may provide a strong support to our conclusions and results. Moreover, the exploration of the range of validity of some useful theoretical approaches constitute a significative goal itself. At this point, the original contributions presented in this thesis are worthy to be mentioned, since we have analyzed a variety of systems ranging from perceptron-like circuits to large recurrent networks, all of them in the vast framework of time-dependent synaptic connections.

In the following, we will summarize the main results and conclusions of the original contributions of this thesis, paying special attention in possible technological

applications and to future work suggested by such results.

In **chapter 4** we have presented a detailed theoretical and numerical study of how the competition between synaptic facilitation and depression affects the neural detection of temporal correlations between different presynaptic neurons in a background of uncorrelated noise. In particular, we have shown that the transmission of information, codified in spike trains through the synapses, is enhanced in the presence of STF, and the detection of firing rate changes is also improved compared with the case of only depressing synapses. This would lead us to think that STF has a crucial role in the processing of information in actual cortical structures.

We have also seen that it is not essential to have a strong correlation between the different presynaptic afferents to have a good detection of signals, and our results also fulfill for noisy signals. This is of special relevance since it is well known that the intrinsic stochasticity of actual synapses causes fluctuations that disrupt the synchrony between the afferents and produce a highly fluctuating postsynaptic response (Dobrunz and Stevens, 1997). Our results, however, show that the performance of the system with STF is quite robust to synaptic fluctuations.

Facilitation also determines the existence of an optimal frequency which allows good performance for a wide range of neuron firing thresholds. In particular, these results could be important to understand how actual neural systems – where different types of neurons with non-identical firing thresholds are connected in a complex way – can self-organize to efficiently detect and process relevant information (Azouz and Gray, 2000). From a more pragmatical point of view, these findings could be used to design artificial neural systems at the *hardware* level (Saighi et al., 2003; Farquhar and Hasler, 2005). In practice, actual electronic circuits which emulate the behavior of biological neurons do not display exactly the same characteristics (due to errors in the resistors, for instance). For this reason, to find a frequency which optimizes the performance of a highly heterogeneous system seems to be quite relevant in experimental realizations of neuro-inspired electronic circuits.

In order to extend the study presented in chapter 4, in **chapter 5** we have investigated the role of dynamic synapses in the detection of weak signals by neurons embedded in neural networks, via a stochastic resonance formalism. Our analysis reveals a dramatic effect on the stochastic resonance properties of neurons due to the interplay between the dynamical nature of synapses and adaptive threshold mechanisms. Concretely, we have demonstrated that this interplay originates the appearance of bimodal resonances, where the location of the resonances are related with the relevant synaptic parameters. To the best of our knowledge, this is the first time this striking phenomena has been reported to occur in biologically motivated models of neural systems.

Recent studies (Zalanyi et al., 2001; Yasuda et al., 2008) have also suggested a relevant role of STD in neural stochastic resonance, but the emergence of bimodal resonances, which is the crucial point of the study presented in chapter 5, is missed in these works (due to the oversimplified assumptions made in neuron and synapses dynamics). Our main findings are also supported by experimental data taken from (Yasuda et al., 2008). Several questions should be experimentally tested, though. An interesting prediction to test is, for instance, whether STF has the effect on the first resonance peak predicted by our results. This gives an idea of the relevance of residual calcium in the processing of weak signals at spontaneous activity brain states, which are common in cortical areas. In general, the question of how these bimodal resonances can be measured in actual cortical structures, and its effect in the collective dynamics of large cortical neural networks, constitutes an interesting issue that still remains open.

A deeper characterization of these bimodal resonances in more detailed neural systems could be advantageous for the design of electronic sensors which could distinguish a weak signal at different levels of environmental noise. A prominent example of this could be the so called *electronic noses*, that is, electronic devices which are able to detect and classify odors, vapor and gases (Gardner and Bartlett, 1999). Electronic noses with the capacity to detect the weak odor of a certain substance in real conditions (in which different gases and odors usually coexist) could play a major role in defense against chemical weapons, for instance.

After the extensive analysis of the influence of short-term plasticity in simple neural circuits presented in chapters 4 and 5, in **chapter 6** we have focused on large recurrent networks of interconnected neurons. More precisely, we have investigated here the role of the competition between several synaptic activity-dependent mechanisms, such as STD and STF, in the capacity of attractor neural networks to store and retrieve information codified as activity patterns. Previous studies found that depressing synapses drastically reduce the capacity of the network to properly retrieve patterns (Bibitchkov et al., 2002; Torres et al., 2002; Matsumoto et al., 2007). These results highlight the role of depression on the processing of spatio-temporal information at short time scales (which allows for the appearance of dynamical memories), in detriment of its function in stable recall necessary for memory-oriented tasks. We have demonstrated that the consideration of additional potentiating mechanisms, such as synaptic facilitation, turns out to be convenient then for memory recall in these dynamical conditions. This leads to think that synaptic facilitation could have a crucial role in the performance of memory retrieval tasks, while maintaining the well known nonlinear properties of dynamic synapses, convenient for information processing and coding (Abbott and Regehr, 2004).

The novel mean-field theory derived in chapter 6 presents some practical advantages with respect to other theories which may be found in the literature (such as (Shiino and Fukai, 1993; Tsodyks and Feigelman, 1988)). For instance, our mean-field approach considers a certain level of heterogeneity in the firing threshold among all the neurons in the network. In addition, it may constitute a good approximation for high temperatures (i.e., high stochasticity in the dynamics of neurons), as preliminary results show (see appendix C and (Mejias et al., 2009)). Certain features not considered in our study, such as the effect of considering low activity patterns or intrinsically stochastic synapse models, could constitute an interesting extension of our work.

Several technological applications could be derived from the results reported in this chapter. Classical Hopfield networks have been extensively employed so far in pattern recognition and pattern classification tasks, for instance (Cortes et al., 2005). Dynamic synapses, on the other hand, achieves a successful performance in filtering and processing the external information embedded in spike trains, although STD implies a substantial lost of storage capacity as we have discussed previously. By incorporating STF into this picture, both efficient filtering of signals and retrieval properties may be optimally incorporated in artificial neural networks. This could constitute a huge advantage in systems which must filter and/or preprocess images or data before storing them, such as digital cameras or other optoelectronic devices.

Finally, in **chapter 7** we have analyzed the role of stochastic depressing synapses in the generation of spontaneous transitions between different voltage levels observed, in absence of external stimuli, in some cortical areas, that is, the so called up and down transitions. The origin of such collective behavior is still unclear, although different factors that can influence their occurrence have been recently reported. These factors include, for instance, inhibitory GABAergic currents (Sanchez-Vives and McCormick, 2000; Hasenstaub et al., 2005), long-term and short-term synaptic plasticity mechanisms (Kang et al., 2008; Holcman and Tsodyks, 2006), or synaptic fluctuations (Cortes et al., 2006; Parga and Abbott, 2007; Johnson et al., 2008). In the study presented in chapter 7, we have demonstrated that stochastic synaptic transmission, when considered together with STD, may be responsible of the high variability in the duration of the up states observed experimentally *in vivo* (Anderson et al., 2000). The role of STD on up and down transitions has been pointed out very recently (Holcman and Tsodyks, 2006), although its possible effect on the statistics of the transitions has been completely ignored. To the best of our knowledge, the present study is the first one which analyzes, even in a simplified manner, the strong effect of synaptic stochasticity and dynamic synapses in the statistics of the up and down transitions.

The results presented in chapter 7 may proportionate a new perspective of the phenomena of up and down transitions that could serve to conciliate the main experimental findings, and that could help for a deep understanding of this complex dynamics of the brain activity. Concretely, our conclusions expose the importance of some biophysical factors, such as the neurotransmitter recovery time and the inherent synaptic stochasticity for the emergence of this phenomenology. More detailed studies considering, for instance, some biologically realistic aspects (such as the presence of inhibition, the role of STF, or more realistic models of synaptic transmission), should be performed to test our predictions. In particular, a more elaborated study considering realistic neural network models and stochastic STD descriptions is necessary and it is in preparation.

From a general point of view, evidences of criticality have been recently found in an increasing number of neural systems, such as in the functional connectivity of the living human brain (Eguiluz et al., 2005), in critical avalanches of neuronal activity (Beggs and Plenz, 2003), or in sleep-wake transitions (Lo et al., 2004), to name a few. According to our results, transitions between up and down cortical states could also present some relevant properties typical of systems at criticality. Some of these properties have been already measured in experiments, such as a high sensitivity of the system to external stimuli (Anderson et al., 2000), or the presence of power-law dependences in the power spectra of the neural dynamics (Hasenstaub et al., 2005). Preliminary results (de Franciscis et al., 2009) also show the presence of power-law distributions of the permanence times in up states in *in vivo* conditions, which properly fits our predictions. If the irregularity observed in up and down transitions reflects indeed that the cortex is in a critical dynamical state, then the understanding of the mechanisms responsible for such dynamics constitutes a strong assert to the physics of complex systems.

Despite huge efforts of researchers from many different disciplines, the functioning and efficiency of neural systems still remains a vast mystery. The development of detailed simulations of neural structures, as well as theoretical approaches to gain some intuition over the most simple neural circuits, constitutes a striking challenge for physicists, and deserves further study due to its possible future impact on Neuroscience. After all, as the biochemist and novelist Isaac Asimov stated,

*The most exciting phrase to hear in Science, the one that heralds the most discoveries, is not 'Eureka!' (I found it!) but 'That's funny'.*

# Appendix A

## Postsynaptic current with dynamic synapses

An excitatory postsynaptic current (EPSC) may be modulated in a nontrivial manner by synapses which present activity-dependent mechanisms like STD and STF. In particular, such modulation does not depend only on the presynaptic mean firing rate, but also on the precise inter-spike-interval distribution (ISI) (that is, the probability distribution of the interval separating two presynaptic spikes). In this appendix, we calculate the mean EPSC, namely  $I$ , assuming different possible statistics for the presynaptic spike train. To achieve this, we consider a presynaptic population of  $N$  ( $\gg 1$ ) neurons which transmit APs to a postsynaptic neuron, following a perceptron structure. The synapses connecting the presynaptic neurons with the postsynaptic one present short-term plasticity mechanisms. In particular, we use the STD model presented in section 3.3.3 (see also (Tsodyks and Markram, 1997) and chapters 4 and 5), which considers that the dynamical state of a synapse  $i$  is described by

$$\begin{aligned}\frac{dx_i(t)}{dt} &= \frac{z_i(t)}{\tau_{rec}} - u x_i(t) \sum_k \delta(t - t_k) \\ \frac{dy_i(t)}{dt} &= -\frac{y_i(t)}{\tau_{in}} + u x_i(t) \sum_k \delta(t - t_k) \\ \frac{dz_i(t)}{dt} &= \frac{y_i(t)}{\tau_{in}} - \frac{z_i(t)}{\tau_{rec}},\end{aligned}\tag{A.1}$$

with  $u$  being constant. We also consider that the mean EPSC due to a single presynaptic afferent is proportional to the mean fraction of active neurotransmitters, namely  $\bar{y}$ . That is, we consider the dependence  $I = A_{SE}\bar{y}$ , with  $A_{SE}$  being a constant. Concerning the ISI distribution of the presynaptic spike train, we review

here two cases of interest: a periodic spike train and a poissonian spike train.

*a. Periodic spike train*

Our first step is to analyze the behavior of a single presynaptic terminal (in the following, we will omit the subindex  $i$ ). Taking the dynamics of  $x$  in (A.1) and considering that  $z(t) = 1 - x(t) - y(t) \simeq 1 - x(t)$  (which constitutes a good approximation for small  $\tau_{in}$  since  $x(t) \gg y(t)$  most of the time), one can obtain the evolution of  $x(t)$  between two consecutive presynaptic spikes occurring at  $t_n$  and  $t_{n+1}$  respectively, leading to

$$x_{n+1} = 1 - [1 - (1 - u)x_n] \exp(-\Delta t_{n+1}/\tau_{rec}), \quad (\text{A.2})$$

where  $x_n$  is the value of  $x(t)$  just before the  $n$ -th presynaptic spike, and  $\Delta t_{n+1} \equiv t_{n+1} - t_n$ . In steady state conditions one has  $x_{n+1} = x_n \equiv x^-$  and  $\Delta t_n = 1/\nu \forall n$ , where  $\nu$  is the neuron mean firing rate and  $x^-$  is the value of  $x(t)$  just before a spike. Inserting this into equation (A.2) gives

$$x^- = \frac{1 - \exp(-1/\nu\tau_{rec})}{1 - (1 - u) \exp(-1/\nu\tau_{rec})}. \quad (\text{A.3})$$

Similarly, by solving the differential equation of  $y(t)$  in (A.1) between two consecutive spikes occurring at  $t_{n+1}$  and  $t_n$  yields

$$y_{n+1} = (y_n + ux_n) \exp(-\Delta t_{n+1}/\tau_{in}), \quad (\text{A.4})$$

with  $y_n$  being the value of  $y(t)$  just before the  $n$ -th spike. Considering steady state conditions again, one easily arrives at

$$y^- = \frac{ux^- \exp(-1/\nu\tau_{in})}{1 - \exp(-1/\nu\tau_{in})}, \quad (\text{A.5})$$

where  $y^-$  is the value of  $y(t)$  just before a spike in steady state conditions. Finally, we can compute the peak value of  $y(t)$ , namely  $y^+$ , in steady state conditions, using that  $y^+ = y^- + ux^-$  (see equation A.1), which leads to

$$y^+ = \frac{ux^-}{1 - \exp(-1/\nu\tau_{in})}. \quad (\text{A.6})$$

To obtain the mean value of  $y(t)$  at steady state, one also needs to compute the integral of  $y(t)$  between two consecutive spikes. In this interval, one can impose that the first spike arrives at  $t = 0$  and write  $y(t) = y^+ \exp(-t/\tau_{in})$  for  $t > 0$ . This gives

$$\bar{y} = \frac{1}{T} \int_0^T y(t) dt = \frac{1}{T} \int_0^T y^+ \exp(-t/\tau_{in}) dt = \quad (\text{A.7})$$

$$\tau_{in} \nu u \frac{1 - \exp(-1/\nu\tau_{rec})}{1 - (1-u) \exp(-1/\nu\tau_{rec})},$$

with  $T \equiv 1/\nu$  being the mean interspike interval. Finally, the mean EPSC is given by  $I \equiv NA_{SE}\bar{y}$ , and in particular

$$I = NA_{SE}\tau_{in}\nu u \frac{1 - \exp(-1/\nu\tau_{rec})}{1 - (1-u) \exp(-1/\nu\tau_{rec})}, \quad (\text{A.8})$$

which is the expression for the mean EPSC that was employed in section 4.3.1.

*b. Poissonian spike train*

To obtain the mean EPSC for a poissonian presynaptic spike train one may use the general recurrent dynamics (A.2) for  $x(t)$  as well. In this case, there is not a single peak value of  $x(t)$  in the steady state, and therefore the strategy employed above is not valid here. Instead of this, one can average equation (A.2) over the corresponding ISI distribution, namely  $P(t)$ , obtaining

$$\langle x_{n+1} \rangle = 1 - [\langle \exp(-\Delta t_{n+1}/\tau_{rec}) \rangle - (1-u) \langle x_n \exp(-\Delta t_{n+1}/\tau_{rec}) \rangle], \quad (\text{A.9})$$

where the brackets indicate averaging over  $P(t)$  (see also (Romani et al., 2006)). Since  $x_n$  is independent of  $\Delta t_{n+1}$  one may compute

$$\langle \exp(-\Delta t_{n+1}/\tau_{rec}) \rangle = \int_0^\infty \exp(-t/\tau_{rec}) P(t) dt = \tilde{P}(1/\tau_{rec}) \quad (\text{A.10})$$

$$\langle x_n \exp(-\Delta t_{n+1}/\tau_{rec}) \rangle = \langle x_n \rangle \langle \exp(-\Delta t_{n+1}/\tau_{rec}) \rangle = \langle x_n \rangle \tilde{P}(1/\tau_{rec}),$$

where  $\tilde{P}(\cdot)$  is the Laplace transform of  $P(\cdot)$ . Considering steady state conditions in equation (A.9), that is,  $\langle x_{n+1} \rangle = \langle x_n \rangle \equiv \langle x^- \rangle$ , one easily obtains

$$\langle x^- \rangle = \frac{1 - \tilde{P}(1/\tau_{rec})}{1 - (1-u) \tilde{P}(1/\tau_{rec})}. \quad (\text{A.11})$$

where  $\langle x^- \rangle$  is the mean value of  $x(t)$  just before a spike. For the case of a presynaptic poissonian spike train, one has  $\tilde{P}(1/\tau_{rec}) = \tau_{rec}\nu/(1 + \tau_{rec}\nu)$  (Romani et al., 2006), which leads to

$$\langle x^- \rangle = \frac{1}{1 + u\tau_{rec}\nu}. \quad (\text{A.12})$$

Following a similar reasoning for the dynamics of  $y(t)$ , one arrives at

$$\langle y^- \rangle = \frac{u \langle x \rangle \tilde{P}(1/\tau_{in})}{1 - \tilde{P}(1/\tau_{in})}, \quad (\text{A.13})$$

with  $\langle y^- \rangle$  being the mean value of  $y(t)$  just before a spike. The peak value of  $y(t)$  (that is, its mean value just after a spike) may be computed if one employs  $\langle y^+ \rangle = \langle y^- \rangle + u \langle x^- \rangle$ , obtaining

$$\langle y^+ \rangle = \frac{u(1 + \tau_{in}\nu)}{1 + u\tau_{rec}\nu}. \quad (\text{A.14})$$

Finally, employing the same procedure as before (that is, evaluating the integral expression to obtain  $\bar{y}$ ), the expression of the mean EPSC for a presynaptic poissonian spike train is achieved, that is,

$$I = NA_{SE}\tau_{in}\nu u \frac{1 + \tau_{in}\nu}{1 + u\tau_{rec}\nu} [1 - \exp(-1/\nu\tau_{in})]. \quad (\text{A.15})$$

Although the results presented in chapter 4 show that the differences between using expressions (A.8) and (A.15) are minimal when one analyzes the particular system studied there, the concrete presynaptic ISI distribution could be relevant in certain situations not considered in our study, such as for synapses with large values of  $\tau_{in}$  (i.e., NMDA synapses). This and other situations are currently under further study.

# Appendix B

## Mean firing rate of the IF neuron model

The integrate-and-fire (IF) model constitutes one of the simplest mathematical descriptions of neural activity used in the literature. This simplicity allows to derive some analytical results which may help to understand its basic characteristics and functioning. In chapters 4 and 5 of this thesis, we have employed some of this analytical results to describe the behavior of several neural systems of relevance. To complete the theoretical description of these systems, in this appendix we derive the mean firing rate of the IF neuron model for a gaussian noisy input (see also (Tuckwell, 1989; Brunel, 2000; Brunel and Hansel, 2006)). After that, we will consider some limits of interest, such as the low and high mean input current approaches, and their effects in the mean firing rate of the neuron.

We consider a standard IF neuron model (see section 3.2.4 for details), whose dynamics is given by

$$\tau_m \frac{dV(t)}{dt} = -V(t) + RI(t), \quad (\text{B.1})$$

where the variable  $V(t)$  is the membrane potential,  $\tau_m$  is the membrane time constant,  $R$  is the input resistance and  $I(t)$  is the input current. For simplicity, we have considered that the input to the neuron can be written as  $RI(t) = \mu + \sqrt{\tau_m} \sigma \xi(t)$ , where  $\xi(t)$  is a gaussian white noise of mean zero and variance one, and  $\mu$  and  $\sigma$  correspond to the mean and fluctuating part of the input current, respectively. In addition, we consider a threshold membrane  $V_{th}$ , a reset potential  $V_r$ , and an absolute refractory period  $\tau_{ref}$ . In the following we omit the temporal dependences in  $V(t)$ .

Equation (B.1) is a Langevin-type description, which only contains linear terms in  $V$ , and therefore it may be easily transformed into a Fokker-Planck equation (FPE) following a straightforward procedure (van Kampen, 1990). One obtains

$$\tau_m \frac{\partial P(V, t)}{\partial t} = \frac{\sigma^2}{2} \frac{\partial^2 P(V, t)}{\partial V^2} + \frac{\partial}{\partial V} [(V - \mu)P(V, t)], \quad (\text{B.2})$$

where  $P(V, t)$  is the probability of having a value  $V$  for the membrane potential at time  $t$ . This equation can be rewritten as the continuity equation

$$\frac{\partial P(V, t)}{\partial t} = -\frac{\partial S(V, t)}{\partial V}, \quad (\text{B.3})$$

where  $S(V, t)$  is the probability current through  $V$  at time  $t$ . According to equations (B.2-B.3),  $S(V, t)$  is given by

$$S(V, t) = -\frac{\sigma^2}{2\tau_m} \frac{\partial P(V, t)}{\partial V} - \frac{V - \mu}{\tau_m} P(V, t). \quad (\text{B.4})$$

In order to solve equation (B.2), one has to specify the boundary conditions at  $-\infty$ ,  $V_r$  and  $V_{th}$ . The probability current through  $V_{th}$  yields the instantaneous firing rate at time  $t$ , that is,  $\nu(t) = S(V_{th}, t)$  (Brunel, 2000). To obtain a finite value of  $\nu(t)$ , one also needs to impose the absorbing boundary condition  $P(V_{th}, t) = 0$  for all  $t$  (since  $V$  cannot be greater than  $V_{th}$ ). Inserting the latter condition in (B.4) gives

$$\left. \frac{\partial P(V, t)}{\partial V} \right|_{V=V_{th}} = -\frac{2\tau_m \nu(t)}{\sigma^2} \quad (\text{B.5})$$

Similarly,  $P(V, t)$  must be continuous at  $V_r$ , and one has to consider the additional probability current injected in  $V_r$  due to neurons that just finished their absolute refractory period. This can be expressed as  $S(V_r^+, t) - S(V_r^-, t) = \nu(t - \tau_{ref})$ , which leads to

$$\left. \frac{\partial P(V, t)}{\partial V} \right|_{V=V_r^+} - \left. \frac{\partial P(V, t)}{\partial V} \right|_{V=V_r^-} = -\frac{2\tau_m \nu(t - \tau_{ref})}{\sigma^2}. \quad (\text{B.6})$$

On the other hand, the natural boundary condition at  $V \rightarrow -\infty$  is that  $P(V, t)$  should tend sufficiently quickly to zero in order to be integrable

$$\lim_{V \rightarrow -\infty} P(V, t) = 0, \quad \lim_{V \rightarrow -\infty} V P(V, t) = 0. \quad (\text{B.7})$$

Finally, the normalization condition for the probability  $P(V, t)$  can be written as

$$p_r(t) + \int_{-\infty}^{V_{th}} P(V, t) dV = 1, \quad (\text{B.8})$$

$$p_r(t) = \int_{t-\tau_{ref}}^t \nu(z) dz,$$

with  $p_r(t)$  being the probability of the neuron being refractory at time  $t$ .

We are interested here in the steady state properties of the neuron, that is,  $\nu(t) \equiv \nu$ ,  $P(V, t) \equiv P(V)$ ,  $S(V, t) \equiv S(V)$  and  $p_r(t) \equiv p_r$ . In order to compute the steady state probability distribution  $P(V)$ , we can set  $\frac{\partial P(V, t)}{\partial t} = 0$  in equation (B.2) and obtain the following ordinary differential equation for  $P(V)$

$$\frac{\sigma^2}{2} P''(V) + (V - \mu) P'(V) + P(V) = 0, \quad (\text{B.9})$$

where we have used the notation  $\frac{dP(V)}{dV} \equiv P'(V)$ . The solutions of this equation which satisfy the boundary conditions (B.5-B.7) correspond to

$$P(V) = \frac{2\tau_m \nu}{\sigma} \exp\left(-\frac{(V - \mu)^2}{\sigma^2}\right) \int_{\frac{V - \mu}{\sigma}}^{\frac{V_{th} - \mu}{\sigma}} \Theta(z - V_r) \exp(z^2) dz, \quad (\text{B.10})$$

where  $\Theta(z)$  is the Heaviside step function, that is,  $\Theta(z > 0) = 1$  and  $\Theta(z < 0) = 0$ . One can also easily obtain, from equation (B.8), the value  $p_r = \nu \tau_{ref}$  for the probability of the neuron being refractory at any time  $t$ . Finally, considering the normalization condition (B.8) on equation (B.10) one obtains a self-consistent condition that yields the mean firing rate of the IF neuron with a gaussian noisy input,

$$\nu = \left[ \tau_{ref} + \tau_m \int_{y_r}^{y_{th}} f(z) dz \right]^{-1}, \quad (\text{B.11})$$

with  $f(z) = \sqrt{\pi}[1 + \text{erf}(z)] \exp(z^2)$ , and the integration limits given by  $y_{th} \equiv \frac{V_{th} - \mu}{\sigma}$  and  $y_r \equiv \frac{V_r - \mu}{\sigma}$ .

For certain conditions, one may apply some approximations to equation (B.11) to obtain simplified expressions of  $\nu$ . For instance, high firing rates are associated with high values of the mean input current  $\mu$ . If one considers  $\mu \gg V_{th}$ , the integration limits tend to large negative values ( $y_{th, r} \rightarrow -\infty$ ). Taking into account that  $f(z) \rightarrow -1/z$  for large  $z$ , one can easily obtain from equation (B.11) the expression

$$\nu \simeq \left[ \tau_{ref} + \tau_m \log\left(\frac{V_r - \mu}{V_{th} - \mu}\right) \right]^{-1}, \quad (\text{B.12})$$

whose predictions are in good agreement with those of equation (B.11) when the firing rate is high enough (which occurs for  $\mu \gg V_{th}$ , as stated above).

Similarly, one can obtain a simplified expression for situations in which the firing rate takes relatively low values. This occurs for  $V_{th} - \mu \gg \sigma$ , when the mean current is not able to produce strong depolarizations by itself and the spikes are induced by the input fluctuations. In this case, the integral will be dominated by the upper integration limit, which satisfies  $y_{th} \gg 1$ . One can then approximate  $f(z) \simeq 2\sqrt{\pi} \exp(z^2)$  (since  $\text{erf}(z) \simeq 2$  for large  $z$ ), and compute the integral

$$\int_{y_r}^{y_{th}} 2\sqrt{\pi} \exp(-z^2) dz \simeq \pi \operatorname{erfi}(y_{th}). \quad (\text{B.13})$$

with  $\operatorname{erfi}(z)$  being the imaginary error function, namely  $\operatorname{erfi}(z) \equiv -i \operatorname{erf}(iz)$ . Finally, considering the asymptotic expansion of  $\operatorname{erfi}(z)$  up to first order one finally gets

$$\nu \simeq \frac{y_{th}}{\tau_m \sqrt{\pi}} \exp(-y_{th}^2), \quad (\text{B.14})$$

which constitutes a good approximation for low firing rates. Since typical spontaneous activity in the cortex lies on low rates (of around  $\sim 5$  Hz, for instance), this simplified expression is useful to obtain analytical estimates of neuron firing rates in the cortex. One should be careful about its range of validity, though.

# Appendix C

## Stochastic ANN with dynamic synapses

In chapter 6, we have studied the effect of dynamic synapses in some relevant properties of attractor neural networks (ANN) at zero temperature limit ( $T = 0$ ), such as the maximum storage capacity of the network or the size of the basins of attraction of the stored patterns. In particular, we discussed in section 6.3.1 the range of validity of our theoretical calculations, and we demonstrated that the mean-field approach presented there could be applied to situations with low (but greater than zero) temperature, as long as the system reaches a steady state (for instance, a recall, non-recall, or spin-glass state). In this appendix, we employ the mean-field theory developed in chapter 6 to present some theoretical results, together with numerical simulations, for ANN with dynamic synapses and  $T > 0$ .

Attending to the results previously obtained in section 6.3.1, the mean-field equations that describe the steady states of ANN with dynamic synapses at low temperature are

$$m = \left\langle \left\langle \tanh \left[ \hat{\beta} \left( m + z \sqrt{\alpha r + \alpha \left( \frac{1 + \gamma\gamma' - \gamma'}{\gamma'} \right)^2} \right) \right] \right\rangle \right\rangle \quad (\text{C.1})$$

$$q = \left\langle \left\langle \tanh^2 \left[ \hat{\beta} \left( m + z \sqrt{\alpha r + \alpha \left( \frac{1 + \gamma\gamma' - \gamma'}{\gamma'} \right)^2} \right) \right] \right\rangle \right\rangle \quad (\text{C.2})$$

$$r = \frac{q}{\left( 1 - \hat{\beta}(1 - q) \right)^2}. \quad (\text{C.3})$$

This set of equations may be simplified for certain situations of interest. In particular, if one considers a finite number of stored patterns  $P$  (and therefore  $\alpha = \frac{P}{N} \rightarrow 0$  in the thermodynamic limit, that is, for  $N \rightarrow \infty$ ), the mean-field equations are decoupled, and equation (C.1) becomes

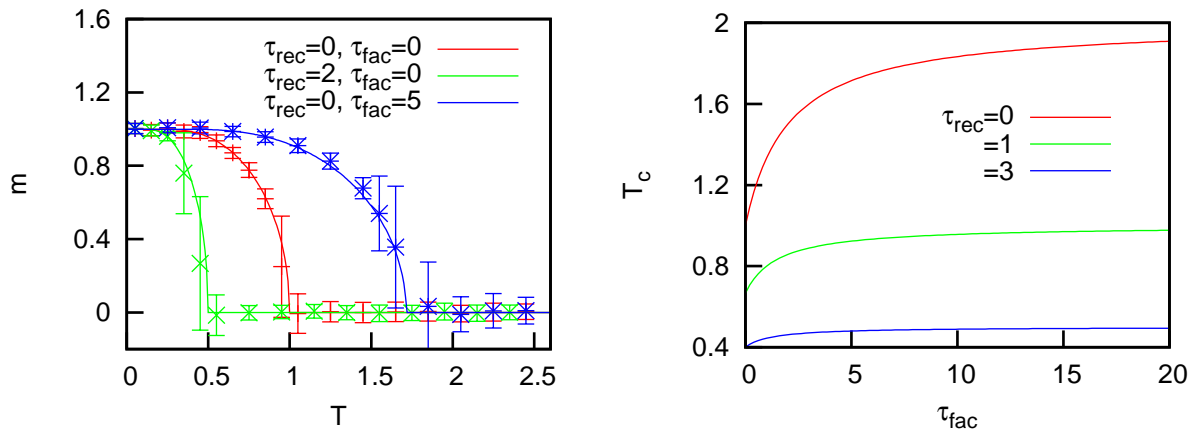


Figure C.1: Left: steady state of the overlap function  $m$  of an ANN, with dynamic synapses and one stored pattern ( $\alpha = 0$ ), as a function of  $T$ . For the case of static synapses, the critical temperature is about  $T_c \simeq 1$ , as one could expect. The inclusion of STD (STF) leads to obtaining lower (higher) values of  $T_c$ . Simulations of an ANN of  $N = 1500$  neurons (points) support our mean-field predictions (lines). Right: critical temperature  $T_c$  as a function of  $\tau_{fac}$ , for different values of  $\tau_{rec}$ . In both panels,  $U_{SE} = 0.5$ .

$$m = \tanh(\widehat{\beta}m), \quad (\text{C.4})$$

with  $\widehat{\beta} = \frac{\gamma'}{1+\gamma\gamma'}\beta$ ,  $\beta = 1/T$ ,  $\gamma \equiv U_{SE}\tau_{rec}$  and  $\gamma' \equiv \frac{1+\tau_{fac}}{1+U_{SE}\tau_{fac}}$ . A relevant issue to consider here is the possible influence of dynamic synapses on the *critical temperature*  $T_c$  for which the system passes from a recall phase to a non-recall phase. In this case, since equations of the type of (C.4) are widely known in the literature (Amit, 1989; Peretto, 1992), the corresponding critical temperature takes the well known value of  $\widehat{\beta}_c = 1$ . This gives the following dependence for the critical temperature,

$$T_c = \frac{\gamma'}{1 + \gamma\gamma'}. \quad (\text{C.5})$$

This dependence of  $T_c$  with the synaptic parameters is only valid for situations in which the system has reached a steady state, as was mentioned above. In addition to this mean-field prediction, the critical temperature  $T_c$  may be evaluated from a numerical point of view by looking the value of  $T$  for which the steady state of the overlap decays to zero (Amit, 1989; Peretto, 1992). This is depicted in left panel of figure C.1, which shows the influence of the synaptic time constants  $\tau_{rec}$  and  $\tau_{fac}$  on the value of  $T_c$ . For the case of static synapses ( $\tau_{rec} = \tau_{fac} = 0$ ), the critical temperature takes the usual value  $T_c = 1$ . When STD is present ( $\tau_{rec} > 0$ ), one observes that lower values of  $T_c$  are obtained (around  $T_c \simeq 0.5$  in the figure). Such result indicates that ANNs with depressing synapses require a low level of intrinsic

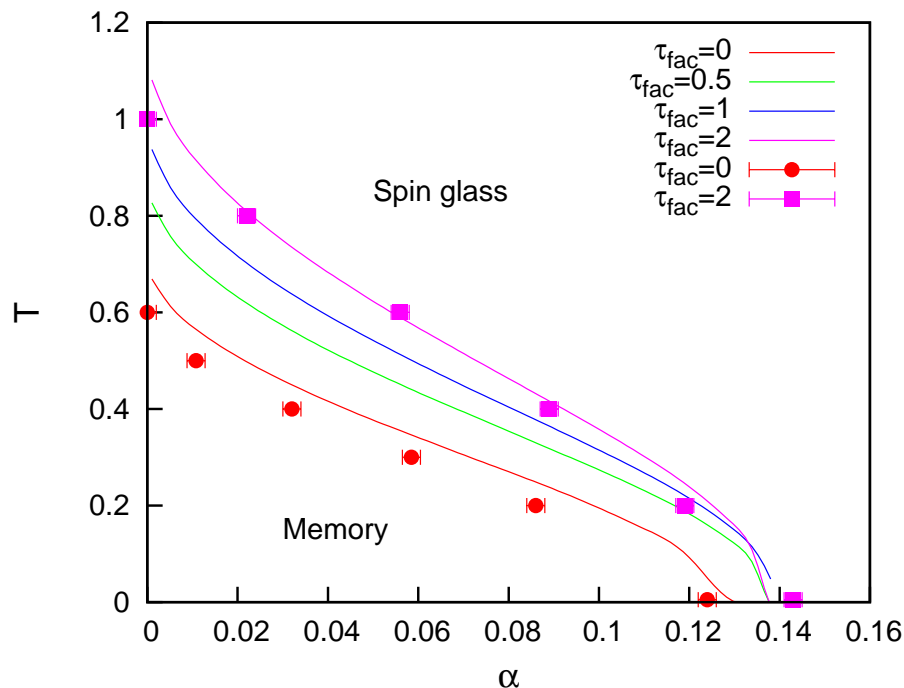


Figure C.2: Critical line  $(T_c, \alpha)$  separating the recall phase (memory phase) and the spin-glass phase for an ANN with dynamic synapses. One can observe that the inclusion of STF extends the area of the recall phase, and decreases the area of the spin-glass phase. The figure also shows that increasing  $\tau_{fac}$  yields larger values of  $T_c$  and  $\alpha_c$ , as we have already discussed in this appendix and in chapter 6. Numerical simulations (points) of an ANN of  $N = 1500$  neurons support our mean-field predictions (lines). Other parameters are  $\tau_{rec} = 2$  and  $U_{SE} = 0.2$ .

stochasticity to perform adequately. On the other hand, the inclusion of STF leads to larger values of  $T_c$ , indicating that an optimal performance in retrieval tasks may be achieved by ANN with facilitating synapses even in the presence of high levels of intrinsic noise. This is also shown in right panel of figure C.1, where one can see that  $T_c$  is a monotonically increasing function of  $\tau_{fac}$ , for different values of the STD time scale.

A detailed theoretical description of the phase diagram of the system may be achieved as well for  $\alpha > 0$ . In order to accomplish this, equations (C.1-C.3) have to be numerically solved (by employing, for instance, a minimization numerical algorithm) to find the steady state values of the variables  $m$ ,  $q$  and  $r$ . Typically, situations in which  $m^\mu \sim O(1)$  for a given pattern  $\mu$  (that is, the pattern  $\mu$  has a *macroscopic* overlap),  $m^\nu \sim O(1/\sqrt{N})$  for  $\nu \neq \mu$  and  $q \sim 1$  corresponds to the recall phase. On the other hand, situations in which several of the patterns have a macroscopic overlap and  $q < 1$  corresponds to the spin-glass phase. In figure C.2 the phase diagram  $(T_c, \alpha)$  for different values of the synaptic parameters is depicted.

For clarity purposes, we have focused only in the critical line separating the recall phase and the spin-glass phase. As one can see, STD and STF time constants have a highly notorious effect on the critical lines of the phase diagram. In particular, the conclusions we obtained previously in this appendix and in chapter 6 are confirmed by this diagram. One can observe, for instance, that the critical temperature for  $\alpha \rightarrow 0$  increases with  $\tau_{fac}$ , as we recently stated. In addition, the increment in the maximum storage capacity  $\alpha_c$  for  $T \rightarrow 0$  with  $\tau_{fac}$ , which was one of the results presented in chapter 6, is also confirmed in the phase diagram, by means of both the mean-field approach and numerical simulations. A more exhaustive analysis of the properties of ANNs with dynamic synapses in general conditions, considering also the non-recall phase which has been, for simplicity, omitted in the diagram presented above, is in preparation (Mejias et al., 2009).

# Appendix D

## Resumen en español

El sistema nervioso es considerado, en la actualidad, como el dispositivo de procesamiento de información más avanzado que se conoce. Incluso los sistemas nerviosos de pequeños invertebrados parecen sobrepasar cómodamente las capacidades de los dispositivos tecnológicos más avanzados, en lo que a asimilación y codificación de información se refiere. Gracias al sistema nervioso, los organismos vivos superiores son capaces de analizar los estímulos procedentes del entorno y responder en consecuencia, incrementando así sus probabilidades de éxito en muchas actividades vitales, como por ejemplo la obtención de alimentos, la reproducción, o escapar de la amenaza de depredadores. A medida que los seres vivos han evolucionado hacia formas más complejas, sus sistemas nerviosos se han vuelto también más sofisticados y han adquirido estructuras altamente jerarquizadas, tanto anatómica como fisiológicamente. La aparición y desarrollo del cerebro, como estructura central del sistema nervioso, ha supuesto un gran avance en las habilidades de los organismos superiores para resolver problemas de alto nivel, e incluso ha conllevado una gran capacidad de aprendizaje en el caso de los mamíferos. El caso particular de la especie humana es quizás el más claro ejemplo de las implicaciones que puede tener tal estructura de procesamiento de información: el lenguaje e interacciones sociales de alto nivel, el pensamiento racional, la Ciencia, la Poesía o la Música son solo algunos de los ejemplos que vienen a la mente.

Algunas de las características de los sistemas nerviosos resultan altamente ventajosas para el procesamiento de información, y han atraído la atención de muchos investigadores, procedentes de distintas áreas de trabajo, durante el siglo pasado. Por ejemplo, los primeros intentos de reproducir dichas características en dispositivos artificiales supuso un gran avance en campos de conocimiento emergentes, como la inteligencia artificial o las ciencias de la computación. Se han desarrollado, en este contexto, un gran número de estrategias computacionales y algoritmos altamente eficientes que conciernen, por ejemplo, a la categorización de imágenes, problemas

de optimización en ciencia e ingeniería, o el diseño de nuevas interfaces hombre-máquina (Cabestany et al., 2009). A pesar de estos avances, nuestro conocimiento acerca de las estrategias que constituyen la clave de la eficiencia de los sistemas neuronales es aún muy primitivo.

En las últimas décadas, sin embargo, se ha realizado un notable esfuerzo para desentrañar las estrategias computacionales que emplea el sistema nervioso. La disciplina científica que emerge de este esfuerzo, conocida como *Neurociencia Computacional*, plantea el estudio de los sistemas neuronales desde un punto de vista funcional, para así identificar algunas de estas estrategias computacionales básicas. Para alcanzar este objetivo, dicha disciplina se basa en el estudio de modelos matemáticos de neuronas, sinapsis y otras estructuras, y de los datos experimentales utilizados para desarrollar tales modelos. En la mayoría de los casos, los estudios experimentales no son suficientes para esclarecer cómo se procesa la información en los sistemas neuronales bajo estudio, dado que dichos sistemas sólo son parcialmente observables con las técnicas experimentales disponibles en la actualidad. Por otra parte, una porción significativa de la fenomenología observada en el cerebro (y asociada a ciertas funciones cerebrales) podría deberse al efecto colectivo de muchos elementos (entorno a  $\sim 10^{10}$ , si consideramos a las neuronas como dichos elementos). Tal situación no podría controlarse experimentalmente, y requeriría de otras formas de abordar el problema. Asimismo, los modelos matemáticos de sistemas neuronales pueden proporcionar al experimentador nuevos enfoques e hipótesis susceptibles de corroboración experimental.

Debido a esta interacción entre experimentos y modelos matemáticos, la Neurociencia Computacional es un campo altamente interdisciplinar, en el que investigadores de ámbitos teóricos y experimentales han contribuido al creciente desarrollo que el campo ha experimentado en los últimos años. Esta metodología se refleja, por ejemplo, en el modelo matemático de neurona presentado por Hodgkin y Huxley en 1952, desarrollado para describir de una forma cuantitativa las propiedades de la membrana celular medidas en experimentos de electrofisiología en el axon gigante del calamar (Hodgkin and Huxley, 1952b). Este modelo es una de las descripciones matemáticas más útiles y representativas en Neurociencia, y constituyó un avance muy significativo en dicho campo. En las últimas décadas, de hecho, se han construido una gran variedad de modelos neuronales para mejorar, extender o simplificar este modelo paradigmático de neurona (véase, como ejemplo, (Izhikevich, 2004)).

El desarrollo de los modelos de redes neuronales atractoras constituye otro ejemplo relevante, desde un punto de vista más teórico, del reciente avance de la Neurociencia Computacional. Dado que muchos sistemas neuronales están constituidos por un ingente número de elementos – las neuronas –, en ocasiones resulta de utilidad adoptar técnicas de Mecánica Estadística para alcanzar una descripción satisfactoria

del sistema a estudiar. Típicamente, la Mecánica Estadística estudia sistemas formados por una gran cantidad de elementos *microscópicos* que interactúan de acuerdo con leyes estocásticas (como gases, sólidos magnéticos, enjambres, vidrios de espín, o vehículos en modelos de tráfico, por ejemplo). Esta disciplina se vale de las leyes que rigen los elementos microscópicos del sistema para describir el comportamiento colectivo emergente del mismo a través de ciertas magnitudes *macroscópicas* (Marro and Dickman, 1999; Cortes, 2005). Bajo ciertas condiciones, los sistemas neuronales pueden ser descritos en este marco teórico. Un ejemplo notable de esto lo constituyen los modelos de redes atractoras, que asumiendo una dinámica relativamente sencilla para las neuronas, estudian la aparición de comportamientos colectivos (como la denominada *memoria asociativa*) que emergen de la interacción entre las neuronas.

En este contexto, se considera que las neuronas son las unidades fundamentales de procesamiento de información, mientras que las sinápsis actúan meramente como conexiones a través de las cuales se comunican las neuronas. Este marco conceptual, sin embargo, parece ser excesivamente simplista a la luz de recientes estudios que indican que las sinápsis participan activamente en el procesamiento de información en el cerebro. En los últimos años, por ejemplo, se ha descubierto que la intensidad con la que las sinápsis transmiten la información entre neuronas puede variar en escalas de tiempo pequeñas, dependiendo de la actividad presináptica (Abbott et al., 1997; Tsodyks and Markram, 1997; Abbott and Regehr, 2004). Tales hallazgos indican que las sinápsis tienen, junto a las neuronas, un papel activo en la codificación y procesamiento de información.

La posibilidad de que ocurran modificaciones sinápticas en escalas de tiempo pequeñas en función de la actividad presináptica se conoce como *plasticidad sináptica de corto alcance* (Zucker and Regehr, 2002; Hempel et al., 2000), y las sinápsis que presentan dicho comportamiento se denominan *sinápsis dinámicas*. De acuerdo con los procesos biofísicos subyacentes, suelen distinguirse dos mecanismos principales responsables de la plasticidad sináptica de corto alcance: la depresión de corto alcance (STD, por sus siglas en inglés) y la facilitación de corto alcance (STF, por sus siglas en inglés). El primero de estos mecanismos es responsable de reducir la intensidad de la respuesta postsináptica bajo una estimulación continuada, mientras que el segundo mecanismo induce un incremento de la respuesta postsináptica bajo el mismo tipo de estímulo.

Las implicaciones funcionales y computacionales de STD y STF no han sido comprendidas en profundidad aún, aunque se sabe que estos mecanismos podrían jugar un papel importante en procesos de transmisión y codificación de la información. Estudios recientes muestran, por ejemplo, que la presencia de STD tiene una enorme influencia en la dinámica de ciertos sistemas neuronales, y que está implicada en el control de ganancia en las sinápsis (Abbott et al., 1997), en el man-

tenimiento de estados de alta actividad en el cortex (Romani et al., 2006), en el almacenamiento de información en redes neuronales atractoras (Bibitchkov et al., 2002; Torres et al., 2002), en la detección de señales coincidentes (Pantic et al., 2003), o en la aparición de “saltos” entre diferentes patrones de actividad en redes de neuronas recurrentes (Pantic et al., 2002; Cortes et al., 2006), que podría estar relacionado con las transiciones espontáneas entre distintos niveles de actividad cortical (Holcman and Tsodyks, 2006). La mayoría de estos estudios, sin embargo, no consideran el posible efecto de STF, que está presente también en muchas de las estructuras neuronales analizadas en estos trabajos. Esta consideración reviste un gran interés, puesto que STD y STF producen, *a priori*, efectos opuestos en la respuesta postsináptica, por lo que ignorar los efectos de STF puede alejar las predicciones de los modelos del comportamiento real de dichos sistemas. Además, considerar estos dos mecanismos simultáneamente en los modelos matemáticos puede revelar nuevos tipos de comportamiento emergente debidos a la *interacción* entre STD y STF. De hecho, esta interacción podría explicar ciertos comportamientos, observados en sistemas neuronales reales, que distan de ser entendidos en su totalidad. Algunos de estos comportamientos son la detección de señales débiles en entornos de actividad neuronal altamente ruidosa (Abbott et al., 1997), la habilidad de los circuitos neuronales para almacenar información mientras procesa la información de manera eficiente (Pantic et al., 2003), o el alto nivel de irregularidad observado incluso en dinámicas neuronales altamente sincronizadas, como por ejemplo la heterogeneidad de la duración de los denominados estados *up* de actividad cortical (Anderson et al., 2000). A pesar de su posible implicación en todos estos fenómenos, el estudio de la interacción entre STD y STF no se ha llevado a cabo aún de manera rigurosa.

**En este contexto, el principal objetivo de esta tesis es investigar el papel e implicaciones de la interacción entre los mecanismos de depresión y facilitación de corto alcance en las propiedades computacionales de sistemas neuronales de interés.**

#### *Objetivos principales de la tesis*

El trabajo presentado en esta tesis persigue, como ya hemos dicho, esclarecer los efectos de la plasticidad sináptica en ciertos sistemas neuronales. En la mayoría de los casos, los análisis se han llevado a cabo a través de simulaciones numéricas y tratamientos teóricos de diversos modelos matemáticos que, por otra parte, comprenden diferentes niveles de detalle en la descripción de las estructuras estudiadas. Concretamente, los principales objetivos de esta tesis han sido:

- Alcanzar un conocimiento más detallado de la influencia de ciertos mecanismos biofísicos sinápticos (como STD y STF) en la capacidad que tienen los

sistemas neuronales típicos para detectar y procesar la información relevante en entornos de actividad ruidosa. Tal objetivo reviste un gran interés puesto que, aunque se conoce el efecto de la plasticidad sináptica de corto alcance en situaciones experimentales controladas, sus efectos en condiciones más realistas distan de ser comprendidas. Asimismo, se sabe que la plasticidad sináptica se halla presente en un gran número de áreas cerebrales, en las que las neuronas operan en un entorno altamente estocástico. Por tanto, sin una caracterización detallada de los efectos de STD y STF, las predicciones e hipótesis que los modelos matemáticos aportaran al conocimiento del funcionamiento del cerebro podrían ser equívocas.

- Investigar el efecto de una posible competición e interacción entre STD y STF (y otros mecanismos de adaptación que puedan presentarse en las estructuras neuronales estudiadas) en el comportamiento emergente de sistemas neuronales. Dicho estudio constituye una parte esencial en la caracterización de los efectos de STD y STF en condiciones realistas, y puede resultar de utilidad para identificar nuevos comportamientos que emerjan de dicha competición entre mecanismos.
- Caracterizar el papel de los mecanismos sinápticos de corto alcance en algunos de los comportamientos colectivos que se dan en el cerebro, como por ejemplo las dinámicas que dan lugar a la memoria asociativa o las transiciones entre estados *up-down* (que implican una alta sincronización entre neuronas). En particular, un estudio del efecto de la plasticidad de corto alcance en estos dos ejemplos mencionados puede arrojar luz sobre aspectos de estos fenómenos que aún están por explicar.

#### *Estructura de la tesis*

El estudio presentado en esta tesis está estructurado como sigue: el capítulo 2 constituye una introducción general básica sobre la biología de los sistemas neuronales. Una vez que dicha introducción ha sido expuesta, el capítulo 3 introduce al lector en el marco de los modelos matemáticos en Neurociencia, con especial énfasis en los modelos de plasticidad sináptica de corto alcance. En los siguientes capítulos se presentan los resultados originales de esta tesis. Más concretamente, en el capítulo 4 se estudia el papel de STD y STF en la detección de señales coincidentes en un entorno de actividad ruidosa. Este análisis se extiende en el capítulo 5, donde se investiga el efecto de la interacción entre STD, STF, y otros mecanismos homeostáticos, en la detección de señales débiles por parte de una neurona. El capítulo 6 expone las implicaciones de considerar plasticidad de corto alcance en las sinapsis

de redes recurrentes de neuronas que presentan propiedades de memoria asociativa. En el capítulo 7 se estudia la dinámica compleja de la actividad de una población de neuronas, resaltando el papel de la plasticidad de corto alcance. Finalmente, en el capítulo 8 se exponen las principales conclusiones de esta tesis, destacando las futuras líneas de investigación que nuestro estudio ha motivado.

Esta tesis está estructurada de manera que se parte de estructuras neuronales simples (por ejemplo, de sistemas de tipo perceptrón en los capítulos 4 y 5) y se avanza hasta modelos de poblaciones neuronales grandes (capítulos 6 y 7). Igualmente, desde el punto de vista de la complejidad de los modelos empleados, la tesis se estructura de mayor a menor complejidad: los capítulos 4 y 5, por ejemplo, presentan modelos realistas (aunque aún muy simplificados) de neuronas y sinapsis. En el capítulo 6 se emplean modelos binarios de neuronas para describir la dinámica de redes de neuronas, y finalmente en el capítulo 7 se trabaja con un modelo que describe directamente la actividad de una población de neuronas, sin detallar las dinámicas de neuronas individuales. Por lo tanto, desde un punto de vista metodológico, cuanto más complejo es el sistema neuronal bajo estudio, más simple es el modelo matemático empleado para su análisis.

A continuación exponemos más detalladamente cada capítulo, incluyendo aquellos que constituyen las aportaciones originales de esta tesis (es decir, los capítulos del 4 al 7):

En el **capítulo 2** presentamos una breve revisión sobre la anatomía y fisiología del sistema nervioso. Dicha revisión incluye los aspectos de biología empleados en los siguientes capítulos, y proporciona algunas descripciones y referencias importantes al lector. El capítulo comienza con una breve exposición de las distintas partes del sistema nervioso central humano, con especial énfasis en el cortex. Después, se describen las características básicas de neuronas y sinapsis, y se detallan los mecanismos biofísicos responsables de la plasticidad de corto alcance.

En el **capítulo 3** se revisan algunos de los modelos matemáticos más relevantes en Neurociencia, para complementar la introducción biológica del capítulo 2. Se describen brevemente algunos modelos neuronales de interés, comenzando por los más detallados (como el modelo de conductancias de Hodgkin y Huxley) y terminando con los más simples (como los modelos binarios de neurona). Tras esta exposición, se detallan algunos modelos de transmisión sináptica, incluyendo algunos comúnmente empleados para describir la plasticidad de corto alcance. Finalmente, se esbozan algunas estrategias usadas para modelar redes de neuronas.

Tras exponer las bases biológicas y metodológicas de nuestro estudio, comenzamos el análisis de los efectos de STD y STF en sistemas neuronales muy simples. En particular, en el **capítulo 4** se estudia la detección de señales correlacionadas

en circuitos neuronales simples, en presencia de plasticidad de corto alcance y en un entorno de actividad ruidosa. Más concretamente, empleando un modelo realista de STD y STF, se estudian las condiciones en las que una neurona postsináptica detecta de forma eficiente los potenciales de acción (AP) coincidentes en el tiempo procedentes de  $N$  neuronas presinápticas que disparan a cierta frecuencia. Un tratamiento analítico y numérico de este sistema muestra que: i) STF mejora la detección de señales correlacionadas procedentes de un subconjunto de neuronas presinápticas excitadoras, y ii) la presencia de STF conlleva una mejora en la detección de cambios en la frecuencia de disparo de las neuronas presinápticas. Se observa también que STF induce la aparición de una frecuencia presináptica óptima que permite una detección eficiente para un amplio (y máximo) rango de valores de los umbrales de disparo neuronales. Esta frecuencia óptima puede ajustarse mediante el valor de los parámetros del modelo de STF. Finalmente, se muestra la robustez de los resultados frente a señales ruidosas y estocasticidad en los modelos de transmisión sináptica.

En el **capítulo 5** se extiende el estudio comenzado en el capítulo 4 mediante el análisis de la detección de señales débiles, por parte de modelos neuronales de tipo integración-y-disparo (IF), en presencia de plasticidad sináptica de corto alcance y un entorno de actividad ruidosa. Empleando tanto técnicas de campo medio como simulaciones numéricas, observamos la existencia de *dos* niveles de ruido que optimizan la transmisión de la señal (en esta tesis, nos referimos a dicho fenómeno con el nombre de *resonancia bimodal*). Este hallazgo contrasta fuertemente con la fenomenología conocida como resonancia estocástica, que es capaz de predecir sólo un nivel de ruido que optimiza la transmisión de señales débiles. El análisis muestra que la interacción entre ciertos mecanismos de adaptación neuronal y la plasticidad sináptica de corto alcance es responsable de la aparición de dicho comportamiento. Nuestros resultados son confirmados mediante el empleo de un modelo más realista de neurona (el modelo de FitzHugh-Nagumo), que presenta mecanismos intrínsecos de adaptación neuronal, así como mediante el uso de señales y modelos de sinápsis más realistas. Por último, se muestran datos experimentales de resonancia estocástica en reflejos táctiles en humanos que corroboran nuestros resultados.

El siguiente paso extiende el estudio a modelos de grandes poblaciones de neuronas. Concretamente, en el **capítulo 6** estudiamos, analíticamente y mediante el empleo de simulaciones Monte Carlo, la influencia de la competición entre STD y STF en las capacidades de almacenamiento de información en redes de neuronas atractoras. Al contrario de lo que ocurre con sinapsis depresoras, con las que la capacidad de almacenamiento de patrones “estáticos” de actividad se ve drásticamente reducida, STF mejora dicha capacidad de almacenamiento en diferentes condiciones. En particular, encontramos valores óptimos de los parámetros del modelo para los que la capacidad de almacenamiento de patrones es máxima y comparable a la

obtenida con sinapsis estáticas (es decir, en ausencia de plasticidad de corto alcance). Concluimos pues que un cierto balance entre los niveles de depresión y facilitación resultan convenientes para un óptimo almacenamiento de información, manteniendo asimismo las características no-lineales de las sinapsis dinámicas que son altamente convenientes para el procesamiento de información.

Tras el análisis de la capacidad de almacenamiento de información en redes neuronales con sinapsis dinámicas (lo cual puede verse como un estudio de propiedades de estado estacionario), nos centramos en el efecto de STD en la dinámica de la actividad de poblaciones de neuronas. En particular, en el **capítulo 7** abordamos el estudio de la dinámica de transiciones de voltaje entre estados up-down observadas en regiones corticales del cerebro, y que constituye un ejemplo de dinámica compleja en sistemas neuronales. Estudiamos esta fenomenología a través de un modelo estocástico biestable simple (concretamente, un modelo de *rate*), en el que la corriente sináptica viene modulada por procesos de plasticidad de corto alcance (en particular, STD) que introducen fluctuaciones y correlaciones temporales en el sistema. Un exhaustivo análisis del modelo, mediante aproximaciones teóricas y simulaciones numéricas, muestra la aparición de transiciones entre estados up-down dirigidas por las fluctuaciones sinápticas, con una distribución de tiempos de permanencia en el estado up que sigue una ley de potencias. Estos resultados concuerdan con observaciones experimentales recientes que indican la aparición de criticalidad en la dinámica de transiciones entre diferentes estados de actividad neuronal.

Finalmente, en el **capítulo 8** se presentan las principales conclusiones de esta tesis, con énfasis en el papel de la interacción entre STD y STF en las propiedades computacionales de sistemas neuronales modelados bajo diferentes niveles de aproximación. Las posibles implicaciones de esta interacción en diferentes fenómenos y comportamientos observados en el cerebro, así como las futuras líneas de investigación que esta tesis propone, son concretadas de igual forma.

# Bibliography

- L. F. Abbott and T. B. Kepler. Model neurons: From hodgkin-huxley to hopfield. *Lectures Notes in Physics*, 368:5–18, 1990.
- L. F. Abbott and S. B. Nelson. Synaptic plasticity: taming the beast. *Nat. Neurosci.*, 3:1178–1183, 2000.
- L. F. Abbott and W. G. Regehr. Synaptic computation. *Nature*, 431:796–803, 2004.
- L. F. Abbott, J. A. Valera, K. Sen, and S. B. Nelson. Synaptic depression and cortical gain control. *Science*, 275(5297):220–224, 1997.
- S. Amari. Characteristics of random nets of analog neuron-like elements. *IEEE Trans. Syst. Man. Cybern.*, 2:643–657, 1972.
- S. Amari. Homogeneous nets of neuron-like elements. *Biol. Cybern.*, 17:211–220, 1975.
- S. Amari. Dynamics of pattern formation in lateral inhibition type neural fields. *Biol. Cybern.*, 27:77–87, 1977.
- D. Amit and M. Tsodyks. Quantitative study of attractor neural networks retrieving at low spike rates. 2. low rate retrieval in symmetrical networks. *Network: Comput. Neural Syst.*, 2(3):275–294, 1991.
- D. J. Amit. *Modeling brain function: the world of attractor neural network*. Cambridge University Press, 1989.
- D. J. Amit, H. Gutfreund, and H. Sompolinsky. Statistical mechanics of neural networks near saturation. *Ann. Phys.*, 173:30–67, 1987.
- J. Anderson, I. Lampl, I. Reichova, M. Carandini, and D. Ferster. Stimulus dependence of two-state fluctuations of membrane potential in cat visual cortex. *Nat. Neurosci.*, 3:617–621, 2000.

- A. Arieli, A. Sterkin, A. Grinvald, and A. Aertsen. Dynamics of ongoing activity: explanation of the large variability in evoked cortical responses. *Science*, 273: 1868–1871, 1996.
- R. Azouz and C. M. Gray. Dynamic spike threshold reveals a mechanism for synaptic coincidence detection in cortical neurons in vivo. *Proc. Natl. Acad. Sci. USA*, 97 (14):8110–8115, 2000.
- R. Azouz and C. M. Gray. Adaptive coincidence detection and dynamic gain control in visual cortical neurons in vivo. *Neuron*, 37:513–523, 2003.
- O. Barak and M. Tsodyks. Persistent activity in neural networks with dynamic synapses. *PLoS Comput. Biol.*, 3(2):323–332, 2007.
- F. Barbieri and N. Brunel. Irregular persistent activity induced by synaptic excitatory feedback. *Front. Comput. Neurosci.*, 1:doi:10.3389/neuro.10.005, 2007.
- M. F. Bear, B. W. Connors, and M. A. Paradiso. *Neuroscience: exploring the brain*, 3rd ed. Lippincott, Philadelphia, 2006.
- M. F. Bear and R. C. Malenka. Synaptic plasticity: LTP and LTD. *Curr. Opin. Neurobiol.*, 4:389–399, 1994.
- J. M. Beggs and D. Plenz. Neuronal avalanches in neocortical circuits. *J. Neurosci.*, 23:11167–11177, 2003.
- R. Bertram, A. Sherman, and E. F. Stanley. Single-domain/bound calcium hypothesis of transmitter release and facilitation. *J. Neurophysiol.*, 75:1919–1931, 1996.
- S. M. Bezrukov and I. Vodyanoy. Noise-induced enhancement of signal-transduction across voltage-dependent ion channels. *Nature*, 378 (6555):362–364, 1995.
- D. Bibitchkov, J. M. Herrmann, and T. Geisel. Pattern storage and processing in attractor networks with short-time synaptic dynamics. *Network: Comput. Neural Syst.*, 13:115–129, 2002.
- T. V. P. Bliss and G. L. Collingridge. A synaptic model of memory: long-term potentiation in the hippocampus. *Nature*, 361:31–39, 1993.
- J. M. Bower and D. Beeman. *The book of GENESIS: exploring realistic neural models with the GEneral NEural SImulator System*. Springer-Verlag, New York, 1994.

- P. C. Bressloff. Traveling fronts and wave propagation failure in an inhomogeneous neural network. *Physica D*, 155:83–100, 2001.
- N. Brunel. Dynamics of sparsely connected networks of excitatory and inhibitory spiking neurons. *J. Comp. Neurosci.*, 8:183–208, 2000.
- N. Brunel and D. Hansel. How noise affects the synchronization properties of recurrent networks of inhibitory neurons. *Neural Comput.*, 18:1066–1110, 2006.
- N. Brunel and M. C. van Rossum. Lapicque’s 1907 paper: from frogs to integrate-and-fire. *Biol. Cybern.*, 97:337–339, 2007.
- C. I. Buia and P. H. E. Tiesinga. Rapid temporal modulation of synchrony in cortical interneuron networks with synaptic plasticity. *Neurocomputing*, 65-66: 809–815, 2005.
- J. Cabestany, F. Sandoval, A. Prieto, and J. M. C. (Eds.). Bio-inspired systems: computational and ambient intelligence. Springer, 2009.
- S. Chandrasekhar. Stochastic problems in physics and astronomy. *Rev. Mod. Phys.*, 15:1–89, 1943.
- F. Chapeau-Blondeau and N. Chambet. Synapse models for neural networks: from ion channel kinetics to multiplicative coefficient  $w_{ij}$ . *Neural Comput.*, 7:713–734, 1995.
- D. C. Chialvo and A. V. Apkarian. Modulated noisy biological dynamics-3 examples. *J. Stat. Phys.*, 70 (1-2):375–391, 1993.
- J. J. Collins, C. C. Chow, and T. T. Imhoff. Aperiodic stochastic resonance in excitable systems. *Phys. Rev. E*, 52(4):3321–3324, 1995.
- A. Compte, C. Constantinidis, J. Tegner, S. Raghavachari, M. Chafee, P. S. Goldman-Rakic, and X. J. Wang. Temporally irregular mnemonic persistent activity in prefrontal neurons of monkeys during a delayed response task. *J. Neurophysiol.*, 90:3441–3454, 2003.
- S. Coombes. Neural fields. *Scholarpedia*, 1:1373, 2006.
- J. Cortes. *Cooperative phenomena in stochastic neural networks with dynamic synapses*. Ph.D. thesis, Universidad de Granada, 2005.
- J. M. Cortes, P. L. Garrido, H. J. Kappen, J. Marro, C. Morillas, D. Navidad, and J. J. Torres. Algorithms for identification and categorization. *AIP Conf. Proc.*, 779:178–184, 2005.

- J. M. Cortes, J. J. Torres, J. Marro, P. L. Garrido, and H. J. Kappen. Effects of fast presynaptic noise in attractor neural networks. *Neural Comput.*, 18:614–633, 2006.
- R. Cossart, D. Aronov, and R. Yuste. Attractor dynamics of network up states in the neocortex. *Nature*, 423:283–288, 2003.
- S. de Franciscis, J. J. Torres, and M. V. Sanchez-Vives. *In preparation*, 2009.
- J. de la Rocha, R. Moreno, and N. Parga. Correlations modulate the non-monotonic response of a neuron with short-term plasticity. *Neurocomp.*, 58-60:313–319, 2004.
- J. de la Rocha and N. Parga. Short-term synaptic depression causes a non-monotonic response to correlated stimuli. *J. Neurosci.*, 25(37):8416–8431, 2005.
- A. Destexhe, Z. F. Mainen, and T. J. Sejnowski. *Kinetic models of synaptic transmission, in Methods in Neural Modelling, C. Koch and I. Segev.* MIT press, Cambridge MA.
- A. Destexhe and E. Marder. Plasticity in single neuron and circuit computations. *Nature*, 431:789–795, 2004.
- L. E. Dobrunz and C. F. Stevens. Heterogeneity of release probability, facilitation, and depletion at central synapses. *Neuron*, 18:995–1008, 1997.
- L. Dong-Xi, X. Wei, G. Yong-Feng, and L. Gao-Jie. Transient properties of a bistable system with delay time driven by non-gaussian and gaussian noises: mean first-passage time. *Commun. Theor. Phys.*, 50:669–673, 2008.
- V. M. Eguiluz, D. R. Chialvo, G. A. Cecchi, M. Baliki, and A. V. Apkarian. Scale-free brain functional networks. *Phys. Rev. Lett.*, 94:018102, 2005.
- G. B. Ermentrout. Type I membranes, phase resetting curves, and synchrony. *Neural Comput.*, 8:979–1001, 1996.
- G. B. Ermentrout and J. D. Cowan. A mathematical theory of visual hallucination patterns. *Biol. Cybern.*, 34:137–150, 1979.
- E. Farquhar and P. Hasler. A bio-physically inspired silicon neuron. *IEEE Trans. Circuits Sys. I*, 52:477–488, 2005.
- S. Fauve and F. Heslot. Stochastic resonance in a bistable system. *Phys. Lett.*, 97A(1-2):5–7, 1983.

- J. M. Fellous, M. Rudolph, A. Destexhe, and T. J. Sejnowski. Synaptic background noise controls the input/output characteristics of single cells in an in vitro model of in vivo activity. *Neurosci.*, 122 (3):811–829, 2003.
- J. Feng. Is the integrate-and-fire model good enough? -a review. *Neural Networks*, 14:955–975, 2001.
- R. FitzHugh. *Mathematical models of excitation and propagation in nerve*. In H. P. Schwan, *Biological Engineering*. McGraw-Hill, New York, 1969.
- D. Fricker, J. H. S. Verheugen, and R. Miles. Cell-attached measurements of firing threshold of rat hippocampal neurons. *J. Physiol.*, 517:791–804, 1999.
- S. Fusi and L. Abbott. Limits on the memory storage capacity of bounded synapses. *Nat. Neurosci.*, 10 (4):485–493, 2007.
- J. M. Fuster. *Memory in the cerebral cortex*. MIT press, Cambridge Mass., 1995.
- L. Gammaitoni, P. Hanggi, P. Jung, and F. Marchesoni. Stochastic resonance. *Rev. Mod. Phys.*, 70:223–287, 1998.
- J. W. Gardner and P. N. Bartlett. *Electronic noses: principles and applications*. Oxford Univ. Press, 1999.
- W. Gerstner. Population dynamics of spiking networks: fast transients, asynchronous states, and locking. *Neural Comput.*, 12:43–89, 2000.
- W. Gerstner and W. Kistler. *Spiking neuron models- Single neurons, population, plasticity*. Cambridge Univ. Press, 2002.
- P. S. Goldman-Rakic. Cellular basis of working memory. *Neuron*, 14:477–485, 1995.
- V. Gomez, A. Kaltenbrunner, V. Lopez, and H. J. Kappen. Self-organization using synaptic plasticity. In *Advances in neural information processing systems*, volume 22, pages 513–520, 2009.
- P. E. Greenwood, L. M. Ward, D. F. Russell, A. Neiman, and F. Moss. Stochastic resonance enhances the electrosensory information available to paddlefish for prey capture. *Phys. Rev. Lett.*, 84(20):4773–4776, 2000.
- A. Gruart, M. D. Munoz, and J. M. Delgado-Garcia. Involvement of the CA3-CA1 synapse in the acquisition of associative learning in behaving mice. *J. Neurosci.*, 26:1077–1087, 2006.

- E. G. A. Harks, J. J. Torres, L. N. Cornelisse, D. L. Ypey, and A. P. R. Theuvenet. Ionic basis for excitability of normal rat kidney (NRK) fibroblasts. *J. Cell. Physiol.*, 196:493–503, 2003.
- A. Hasenstaub, Y. Shu, B. Haider, U. Kraushaar, A. Duque, and D. A. McCormick. Inhibitory postsynaptic potentials carry synchronized frequency information in active cortical networks. *Neuron*, 47:423–435, 2005.
- D. O. Hebb. *The Organization of Behavior: A Neuropsychological Theory*. Wiley, 1949.
- C. M. Hempel, K. H. Hartman, X. J. Wang, G. G. Turrigiano, and S. B. Nelson. Multiple forms of short-term plasticity at excitatory synapses in rat medial prefrontal cortex. *J. Neurophysiol.*, 83:3031–3041, 2000.
- J. Hertz, A. Krogh, and R. Palmer. *Introduction to the theory of neural computation*. Addison-Wesley, 1991.
- M. L. Hines and N. T. Carnevale. The neuron simulation environment. *Neural Comput.*, 9:1179–1209, 1997.
- N. Ho and A. Destexhe. Synaptic background activity enhances the responsiveness of neocortical pyramidal neurons. *J. Neurophysiol.*, 84 (3):1488–1496, 2000.
- A. L. Hodgkin and A. F. Huxley. Action potentials recorded from inside a nerve fibre. *Nature*, 144:710–711, 1939.
- A. L. Hodgkin and A. F. Huxley. The dual effects of membrane potential on sodium conductance in giant axon of loligo. *J. Physiol.*, 116:497–506, 1952a.
- A. L. Hodgkin and A. F. Huxley. A quantitative description of membrane current and its application to conduction and excitation in nerve. *J. Physiol.*, 117:500–544, 1952b.
- D. Holcman and M. Tsodyks. The emergence of up and down states in cortical networks. *PLoS Comput. Biol.*, 2(3):174–181, 2006.
- J. J. Hopfield. Neural networks and physical systems with emergent collective computational abilities. *Proc. Natl. Acad. Sci. USA*, 79(8):2554–2558, 1982.
- D. Horn and M. Usher. Neural networks with dynamical thresholds. *Phys. Rev. A*, 40:1036–1044, 1989.

<http://neuroscience.uth.tmc.edu>.

<http://senselab.med.yale.edu/modeldb>.

- M. Ibanes, J. Garcia-Ojalvo, R. Toral, and J. M. Sancho. Dynamics and scaling of noise-induced domain growth. *Eur. Phys. J. B*, 18:663–673, 2000.
- E. M. Izhikevich. Resonate-and-fire neurons. *Neural Networks*, 14:883–894, 2001.
- E. M. Izhikevich. Which model to use for cortical spiking neurons? *IEEE Trans. Neural Networks*, 15(5):1063–1070, 2004.
- G. G. Izus, R. R. Deza, and H. S. Wio. Exact nonequilibrium potential for the FitzHugh-Nagumo model in the excitable and bistable regimes. *Phys. Rev. E*, 58(1):93–98, 1998.
- S. Johnson, J. Marro, and J. J. Torres. Functional optimization in complex excitable networks. *Europhys. Lett.*, 83:46006(1–6), 2008.
- H. Kamiya and R. S. Zucker. Residual  $\text{Ca}^{2+}$  and short-term synaptic plasticity. *Nature*, 371(6498):603–606, 1994.
- E. R. Kandel, J. H. Schwartz, and T. M. Jessell. *Principles of neural science, 4th ed.* McGraw-Hill, New York, 2000.
- S. Kang, K. Kitano, and T. Fukai. Structure of spontaneous up and down transitions self-organizing in a cortical network model. *PLoS Comput. Biol.*, 4(3):e100022, 2008.
- J. Keener and J. Sneyd. *Mathematical physiology, 2nd ed.* Springer, 2008.
- W. Kistler and J. van Hemmen. Short-term synaptic plasticity and network behavior. *Neural Comput.*, 11:1579–1594, 1999.
- R. Kobayashi, Y. Tsubo, and S. Shinomoto. Made-to-order spiking neuron model equipped with a multi-timescale adaptive threshold. *Front. Comput. Neurosci.*, 3(9):1–11, 2009.
- C. Koch. *Biophysics of Computation: Information Processing in Single Neurons.* Oxford University Press, 1999.
- C. Koch and I. Segev. *Methods in neuronal modeling: from ions to networks, 2nd ed.* MIT press, London, 1998.
- I. Lampl, I. Reichova, and D. Ferster. Synchronous membrane potential fluctuations in neurons of the cat visual cortex. *Neuron*, 22:361–374, 1999.

- L. Lopicque. Recherches quantitatives sur l'excitation électrique des nerfs traitée comme une polarization. *J. Physiol. Pathol. Gen.*, 9:620–635, 1097.
- A. Lazar, G. Pipa, and J. Triesch. Fading memory and time series prediction in recurrent networks with different forms of plasticity. *Neural Networks*, 20:312–322, 2007.
- A. Lazar, G. Pipa, and J. Triesch. SORN: a self-organizing recurrent neural network. *In preparation*, 2009.
- B. Lindner, J. Garcia-Ojalvo, A. Neiman, and L. Schimansky-Geier. Effects of noise in excitable systems. *Phys. Report*, 392:321–424, 2004.
- K. Lingenhohl and E. Friauf. Giant neurons in the rat reticular formation: a sensorimotor interface in the elementary acoustic startle circuit. *J. Neurosci.*, 14(3): 1176–1194, 1994.
- C. C. Lo, T. Chou, T. Penzel, T. E. Scammell, R. E. Strecker, H. E. Stanley, and P. C. Ivanov. Common scale-invariant patterns of sleep-wake transitions across mammalian species. *Proc. Nat. Acad. Sci. USA*, 101:17545–17548, 2004.
- Y. Loewenstein, S. Mahon, P. Chadderton, K. Kitamura, H. Sompolinsky, Y. Yarom, and M. Hausser. Bistability of cerebellar Purkinje cells modulated by sensory stimulation. *Nat. Neurosci.*, 8:202–211, 2005.
- A. Longtin, A. Bulsara, and F. Moss. Time-interval sequences in bistable systems and the noise-induced transmission of information by sensory neurons. *Phys. Rev. Lett.*, 67 (5):656–659, 1991.
- E. Lugo, R. Doti, and J. Faubert. Ubiquitous crossmodal stochastic resonance in humans: auditory noise facilitates tactile, visual and proprioceptive sensations. *PLoS One*, 3(8):1–18, 2008.
- M. A. Lynch. Long-term potentiation and memory. *Physiol. Rev.*, 84:87–136, 2004.
- A. J. R. Madureira, P. Hanggi, V. Buonomano, and W. A. R. Jr. Escape from a fluctuating double well. *Phys. Rev. E*, 51:3849–3861, 1995.
- R. Malenka and R. A. Nicoll. Long-term potentiation: a decade of progress? *Science*, 285:1870–1874, 1999.
- E. Manjarrez, O. Diez-Martinez, I. Mendez, and A. Flores. Stochastic resonance in human electroencephalographic activity elicited by mechanical tactile stimuli. *Neurosci. Lett.*, 324 (3):213–216, 2002.

- H. Markram. The Blue Brain Project. *Nat. Rev. Neurosci.*, 7:153–160, 2004.
- H. Markram, Y. Wang, and M. Tsodyks. Differential signaling via the same axon of neocortical pyramidal neurons. *Proc. Natl. Acad. Sci. USA*, 95(9):5323–5328, 1998.
- J. Marro and R. Dickman. *Nonequilibrium Phase Transitions in Lattice Models*. Cambridge University Press, 1999.
- N. Matsumoto, D. Ide, M. Watanabe, and M. Okada. Retrieval property of attractor network with synaptic depression. *J. Phys. Soc. Japan*, 76(8):084006, 2007.
- V. Matveev and X. J. Wang. Differential short-term synaptic plasticity and transmission of complex spike trains: to depress or to facilitate? *Cerebral Cortex*, 10: 1143–1153, 2000.
- G. Mayor and D. Tank. Persistent neural activity: prevalence and mechanisms. *Curr. Opin. Neurobiol.*, 14:675–684, 2004.
- C. McAdams and J. Maunsell. Effects of attention on orientation-tuning functions of single neurons in macaque cortical area V4. *J. Neurosci.*, 19:431–441, 1999.
- D. A. McCormick. Neuronal networks: flip-flops in the brain. *Curr. Biol.*, 15: R294–R296, 2005.
- P. N. McGraw and M. Menzinger. Topology and computational performance of attractor neural networks. *Phys. Rev. E*, 68(4):047102, 2003.
- B. McNamara and K. Wiesenfeld. Theory of stochastic resonance. *Phys. Rev. A*, 39 (9):4854–4869, 1989.
- B. McNamara, K. Wiesenfeld, and R. Roy. Observation of stochastic resonance in a ring laser. *Phys. Rev. Lett.*, 60:2626–2629, 1988.
- J. F. Mejias, B. Gomez-Hernandez, and J. J. Torres. A general framework for attractor neural networks with dynamic synapses. *In preparation*, 2009.
- J. F. Mejias and J. J. Torres. The role of synaptic facilitation in spike coincidence detection. *J. Comput. Neurosci.*, 24(2):222–234, 2008.
- J. F. Mejias and J. J. Torres. Emergence of resonances in neural systems: the interplay between adaptive threshold and short-term synaptic plasticity. *Submitted*, 2009a.

- J. F. Mejias and J. J. Torres. Maximum memory capacity on neural networks with short-term synaptic depression and facilitation. *Neural Comput.*, 21(3):851–871, 2009b.
- O. Melamed, O. Barak, G. Silberberg, H. Markram, and M. Tsodyks. Slow oscillations in neural networks with facilitating synapses. *J. Comput. Neurosci.*, 25:308–316, 2008.
- G. Mongillo, O. Barak, and M. Tsodyks. Synaptic theory of working memory. *Science*, 319(5869):1543–1546, 2008.
- M. E. J. Newman. Power laws, Pareto distributions and Zipf’s law. *Contemporary Phys.*, 46:323–351, 2005.
- D. Noble. Applications of Hodgkin-Huxley equations to excitable tissues. *Physiol. Rev.*, 46:1–47, 1966.
- G. Palm, A. M. H. J. Aertsen, and G. L. Gerstein. On the significance of correlations among neuronal spike trains. *Biol. Cybern.*, 59:1–1, 1988.
- L. Pantic, J. J. Torres, and H. J. Kappen. Coincidence detection with dynamic synapses. *Network: Comput. Neural Syst.*, 14:17–33, 2003.
- L. Pantic, J. J. Torres, H. J. Kappen, and S. C. A. M. Gielen. Associative memory with dynamic synapses. *Neural Comput.*, 14(12):2903–2923, 2002.
- N. Parga and L. F. Abbott. Network model of spontaneous activity exhibiting synchronous transitions between up and down states. *Front. Neurosci.*, 1:57–66, 2007.
- P. Pechukas and P. Hanggi. Rates of activated processes with fluctuating barriers. *Phys. Rev. Lett.*, 73:2772–2775, 1994.
- P. Peretto. *An Introduction to the modeling of neural networks*. Cambridge University Press, 1992.
- C. C. H. Petersen, T. T. G. Hahn, M. Mehta, A. Grin-vald, and B. Sakmann. Interaction of sensory responses with spontaneous depolarization in layer 2/3 barrel cortex. *Proc. Nat. Acad. Sciences USA*, 100:13638–13643, 2003.
- P. K. D. Pilz and H. U. Schnitzler. Habituation and sensitization of the acoustic startle response in rats: amplitude, threshold, and latency measures. *Neurobiol. Learn. Mem.*, 66(1):67–79, 1996.

- D. Pinault, Y. Smith, and M. Deschenes. Dendrodendritic and axoaxonic synapses in the thalamic reticular nucleus of the adult rat. *J. Neurosci.*, 17:3215–3233, 1997.
- Z. Ping. Dynamical properties of a bistable system driven by cross-correlated additive and multiplicative colored noises. *Chines J. Phys.*, 44:117–126, 2006.
- H. E. Plesser and W. Gerstner. Noise in integrate-and-fire neurons: from stochastic input to escape rates. *Neural Comput.*, 12:367–384, 2000.
- M. I. Rabinovich, J. J. T. ans P. Varona, R. Huerta, and P. Weidman. Origin of coherent structures in a discrete chaotic medium. *Phys. Rev. E*, 60:R1130–R1133, 1999.
- S. Ramon y Cajal. A new concept of the histology of the central nervous system (1892). *Neurological Classics in Modern Translation*. D. A. Rottenberg and F. N. Hochberg (eds.), pages 7–29, 1977.
- A. Renart, R. Moreno-Bote, X. J. Wang, and N. Parga. Mean-driven and fluctuation-driven persistent activity in recurrent networks. *Neural Comput.*, 19:1–46, 2007.
- S. Romani, D. J. Amit, and G. Mongillo. Mean-field analysis of selective persistent activity in presence of short-term synaptic depression. *J. Comput. Neurosci.*, 20: 201–217, 2006.
- A. D. D. Roos, P. H. Willems, P. H. Peters, E. J. van Zoelen, and A. P. Theuvenet. Synchronized  $\text{Ca}^{2+}$  signaling by intercellular propagation of  $\text{Ca}^{2+}$  action potentials in NRK fibroblasts. *Am. J. Physiol.*, 273:C1900–C1907, 1997.
- M. Rudolph and A. Destexhe. Do neocortical pyramidal neurons display stochastic resonance? *J. Comp. Neurosci.*, 11:19–42, 2001.
- S. Saighi, J. Tomas, L. Alvado, Y. Bornat, and S. R.-L. Masson. Silicon integration of biological neurons models. volume ISBN 84-87087-40-X, pages 597–602, 2003.
- M. V. Sanchez-Vives and D. A. McCormick. Cellular and network mechanisms of rhythmic recurrent activity in neocortex. *Nat. Neurosci.*, 3:1027–1034, 2000.
- Y. Seamari, J. A. Narvaez, F. J. Vico, D. Lobo, and M. V. Sanchez-Vives. Robust off- and online separation of intracellularly recorded up and down cortical states. *PLoS One*, 2:e888, 2007.
- M. Shiino and T. Fukai. Self-consistent signal-to-noise analysis of the statistical behavior of analog neural networks and enhancement of the storage capacity. *Phys. Rev. E*, 48(2):867–897, 1993.

- S. Shinomoto, Y. Sakai, and S. Funahashi. The Ornstein-Uhlenbeck process does not reproduce spiking statistics of neurons in prefrontal cortex. *Neural Comput.*, 11:935–951, 1999.
- Y. Shu, A. Hasenstaub, and D. A. McCormick. Turning on and off recurrent balanced cortical activity. *Nature*, 423:288–293, 2003.
- N. S. Simons-Weidenmaier, M. Weber, C. F. Plappert, P. K. D. Pilz, and S. Schmid. Synaptic depression and short-term habituation are located in the sensory part of the mammalian startle pathway. *BMC Neurosci.*, 7:38, 2006.
- W. R. Softky and C. Koch. The highly irregular firing of cortical cells is inconsistent with temporal integration of random EPSPs. *J. Neurosci.*, 13:334–350, 1993.
- S. Song, K. D. Miller, and L. F. Abbott. Competitive hebbian learning through spike-timing dependent synaptic plasticity. *Nat. Neurosci.*, 3:919–926, 2000.
- W. S. Sossin, A. Sweet-Cordero, and R. H. Scheller. Dale’s hypothesis revisited: different neuropeptides derived from a common prohormone are targeted to different processes. *Proc. Nat. Acad. Sci. USA*, 87:4845–4848, 1990.
- W. C. Stancey and D. M. Durand. Stochastic resonance improves signal detection in hippocampal CA1 neurons. *J. Neurophysiol.*, 83 (3):1394–1402, 2000.
- M. Stemmler. A single spike suffices: The simplest form of stochastic resonance in model neurons. *Network: Comput. Neur. Sys.*, 7:687–716, 1996.
- M. Steriade, D. A. McCormick, and T. J. Sejnowski. Thalamocortical oscillations in the sleeping and aroused brain. *Science*, 262:679–685, 1993a.
- M. Steriade, A. Nunez, and F. Amzica. Intracellular analysis of relations between the slow (<1hz) neocortical oscillation and other sleep rhythms of the electroencefalogram. *J. Neurosci.*, 13:3266–3283, 1993b.
- M. Steriade, A. Nunez, and F. Amzica. A novel slow (<1hz) oscillation of neocortical neurons in vivo: depolarizing and hyperpolarizing components. *J. Neurosci.*, 13: 3252–3265, 1993c.
- M. Steriade, I. Timofeev, and F. Grenier. Natural waking and sleep states: a view from inside neocortical neurons. *J. Neurophysiol.*, 85:1969–1985, 2001.
- C. J. Tessone, C. R. Mirasso, R. Toral, and J. D. Gunton. Diversity-induced resonance. *Phys. Rev. Lett.*, 97 (19):194101, 2006.

- A. M. Thomson and J. Deuchars. Temporal and spatial properties of local circuits in neocortex. *Trends Neurosci.*, 17:119–126, 1994.
- J. J. Torres, J. Cortes, J. Marro, and H. Kappen. Competition between synaptic depression and facilitation in attractor neural networks. *Neural Comp.*, 19(10):2739–2755, 2007.
- J. J. Torres, M. A. Munoz, J. Marro, and P. L. Garrido. Influence of topology on a neural network performance. *Neurocomput.*, 58-60:229–234, 2004.
- J. J. Torres, L. Pantic, and H. J. Kappen. Storage capacity of attractor neural networks with depressing synapses. *Phys. Rev. E.*, 66(6):061910, 2002.
- M. Tsodyks and M. Feigelman. The enhanced storage capacity in neural networks with low activity level. *Europhys. Lett.*, 6(2):101–105, 1988.
- M. V. Tsodyks and H. Markram. The neural code between neocortical pyramidal neurons depends on neurotransmitter release probability. *Proc. Natl. Acad. Sci. USA*, 94:719–723, 1997.
- M. V. Tsodyks, K. Pawelzik, and H. Markram. Neural networks with dynamic synapses. *Neural Comput.*, 10:821–835, 1998.
- Y. Tu and G. Grinstein. How white noise generates power-law switching in bacterial flagellar motors. *Phys. Rev. Lett.*, 94:208101, 2005.
- H. C. Tuckwell. *Introduction to theoretical neurobiology. Volume 2: nonlinear and stochastic theories*. Cambridge, 1989.
- C. van den Broeck, J. M. R. Parrondo, and R. Toral. Noise-induced nonequilibrium phase transition. *Phys. Rev. Lett.*, 73:3395–3398, 1994.
- C. van den Broeck, J. M. R. Parrondo, R. Toral, and K. Kawai. Nonequilibrium phase transitions induced by multiplicative noise. *Phys. Rev. E*, 55:4084–4094, 1997.
- N. G. van Kampen. *Stochastic processes in physics and chemistry*. North-Holland, 1990.
- C. van Vreeswijk and H. Sompolinsky. Chaos in neuronal networks with balanced excitatory and inhibitory activity. *Science*, 274:1724–1726, 1996.
- P. Varona, J. J. Torres, R. Huerta, H. D. I. Abarbanel, and M. I. Rabinovich. Regularization mechanisms in the dynamics of spiking-bursting neurons. *Neural Networks*, 14:865–875, 2001.

- E. I. Volkov, E. Ullner, A. A. Zaikin, and J. Kurths. Frequency-dependent stochastic resonance in inhibitory coupled excitable systems. *Phys. Rev. E*, 68:061112, 2003.
- X. J. Wang. Synaptic basis of cortical persistent activity: the importance of NMDA receptors to working memory. *J. Neurosci.*, 19(21):9587–9603, 1999.
- Y. Wang, H. Markram, P. H. Goodman, T. K. Berger, J. Ma, and P. S. Goldman-Rakic. Heterogeneity in the pyramidal network of the medial prefrontal cortex. *Nat. Neurosci.*, 9:534–542, 2006.
- K. Wiesenfeld and F. Moss. Stochastic resonance and the benefits of noise: from ice ages to crayfish and squids. *Nature*, 373:33–36, 1995.
- K. Wiesenfeld, D. Pierson, E. Pantazelou, C. Dames, and F. Moss. Stochastic resonance on a circle. *Phys. Rev. Lett.*, 72:2125–2129, 1994.
- C. Wilson. Up and down states. *Scholarpedia*, 3:1410, 2008.
- H. R. Wilson and J. D. Cowan. Excitatory and inhibitory interactions in localized populations of model neurons. *Biophys. Journal*, 12:1–24, 1972.
- H. R. Wilson and J. D. Cowan. A mathematical theory of the functional dynamics of cortical and thalamic nervous tissue. *Kibernetik*, 13:55–80, 1973.
- M. A. Wilson and J. M. Bower. *The simulation of large-scale neural networks*. Methods in Neural Modelling -From Synapses to Networks, C. Koch and I. Segev (eds.), MIT Press, Cambridge, MA, 1989.
- H. Yasuda, T. Miyaoka, J. Horiguchi, A. Yasuda, P. Hanggi, and Y. Yamamoto. Novel class of neural stochastic resonance and error-free information transfer. *Phys. Rev. Lett.*, 100:118103, 2008.
- A. Zador. Impact of synaptic unreliability on the information transmitted by spiking neurons. *J. Neurophysiol.*, 79:1219–1229, 1998.
- A. M. Zador and L. E. Dobrunz. Dynamic synapses in the cortex. *Neuron*, 19:1–4, 1997.
- L. Zalanayi, F. Bazso, and P. Erdi. The effect of synaptic depression on stochastic resonance. *Neurocomputing*, 38-40:459–465, 2001.
- R. S. Zucker and W. G. Regehr. Short-term synaptic plasticity. *Ann. Rev. Physiol.*, 64:355–405, 2002.

# List of publications

## Journals and book chapters:

1. J. F. Mejias and J. J. Torres, *Improvement of spike coincidence detection with facilitating synapses*. Neurocomputing, 70, 2026-2029, 2007.
2. J. F. Mejias and J. J. Torres, *Signal detection in networks of spiking neurons with dynamical synapses*. AIP Conf. Proc., 887, 83-88, 2007.
3. J. F. Mejias, J. J. Torres and J. Marro, *Modelling neural systems with short-term depression and facilitation*. AIP Conf. Proc., 913, 112-117, 2007.
4. J. F. Mejias and J. J. Torres, *The role of synaptic facilitation in coincidence spike detection*. J. Comp. Neurosci., 24 (2), 222-234, 2008.
5. J. F. Mejias and J. J. Torres, *Maximum memory capacity on neural networks with short-term synaptic depression and facilitation*. Neural Comput., 21 (3), 851-871, 2009.
6. S. Johnson, J. Marro, J. F. Mejias and J. J. Torres, *Development of neural network structure with biological mechanisms*. Lect. Not. Comp. Sci., 5517 (1), 228-235, 2009.
7. J. F. Mejias, J. J. Torres, S. Johnson and H. J. Kappen, *Switching dynamics of neural systems in the presence of multiplicative colored noise*. Lect. Not. Comp. Sci., 5517 (1), 17-23, 2009.
8. J. J. Torres, S. Johnson, J. F. Mejias, S. de Franciscis and J. Marro, *Nonequilibrium Behavior in Neural Networks: Criticality and Optimal Performance*. Accepted in Proceedings of the ICCN'09, 2009.
9. J. F. Mejias and J. J. Torres, *Emergence of resonances in neural systems: the interplay between adaptive threshold and short-term synaptic plasticity*. Submitted, 2009.

10. J. J. Torres, J. F. Mejias and J. Marro, *Stochastic resonance in neural networks with adaptive mechanisms*. Submitted, 2009.
11. J. F. Mejias, H. J. Kappen and J. J. Torres, *Critical dynamics in up and down cortical states*. Submitted, 2009.
12. J. F. Mejias, B. Gomez-Hernandez and J. J. Torres, *A general framework for attractor neural networks with dynamic synapses..* In preparation, 2009.

## Abstracts:

13. J. F. Mejias and J. J. Torres, *Spike detection with dynamic synapses*. Proceedings of the FISES'06 Granada, 2006.
14. J. F. Mejias and J. J. Torres, *Memory and recall of information in neural networks with dynamic synapses*. Proceedings of the FISES'08 Salamanca, 2008.
15. J. J. Torres, J. F. Mejias, J. Marro and H. B. Kappen, *Information processing in neural networks with dynamic synapses*. AIP Conf. Proc., 1091, 295-296, 2009.
16. J. F. Mejias and J. J. Torres, *Memory and pattern storage in neural networks with activity dependent synapses*. AIP Conf. Proc., 1091, 286-286, 2009.